Impact of epigenetic imprinting on the transcriptional profile of colonic epithelial cells and their role in the perpetuation of intestinal inflammation

Thesis

for the degree of

doctor rerum naturalium (Dr. rer. nat.)

approved by the Faculty of Natural Sciences of Otto von Guericke University Magdeburg

by: M.Sc. Elif Gelmez

born on: 04.03.1993 in Gümüshane

Examiner: Prof. Dr. rer. nat. Dunja Bruder

Prof. Dr. rer. nat. Wiebke Hansen

submitted on: 25.10.2022

defended on: 14.02.2023

Preamble

Gelmez E, Lehr K, Kershaw O, Frentzel S, Vilchez-Vargas R, Bank U, Link A, Schüler T, Jeron A, Bruder D. Characterization of Maladaptive Processes in Acute, Chronic and Remission Phases of Experimental Colitis in C57BL/6 Mice. Biomedicines. 2022; 10(8):1903. https://doi.org/10.3390/biomedicines10081903.

Parts of the sections (3.1-3.4, 3.6-3.9, 4.1-4.3, 5.1) were taken directly or were paraphrased from the above mentioned publication.

Contents

Abstract iv
Zusammenfassung v
List of Abbreviations vi
List of Figures ix
Appendix Supplementary Figures xi
List of Tables xii
Appendix Supplementary Tables xiii
1. Introduction 1
1.1 Inflammatory Bowel Disease 1
1.2 Small and Large Intestine and their Epithelial Cell Constituents 3
1.2.1 MHC Class II Molecules and their Functions in IECs 6
1.3 Dextran Sodium Sulfate-induced Colitis as a Mouse Model to Study Different Stages of IBD 8
1.4 Epigenetic Modifications and Related Transcriptomic Changes 9
1.4.1 Basic Concept of Eukaryotic Transcriptional Regulation 10
1.4.2 Epigenetics as a Complementing Layer of Transcriptional Regulation 11
1.4.3 Histones and their Modifications 12
1.4.4 Genome Mapping of H3K27ac and H3K27me3 Histone Marks to Study Epigenetics in IECs 14
1.4.5 Basic Workflow of ChIP-Seq Experiments 15
1.5 Investigating the Immunological and Microbial Alterations in IBD Using the DSS Colitis Model 17
1.5.1 Immunological Changes during Colon Inflammation 18
1.5.2 Dysbiosis during IBD and DSS Colitis 22
1.6 Aims of the Thesis 25
2. Materials 26
2.1 Buffers and Solutions 26
2.2 Antibodies 27
2.3 Consumables 30
2.4 Ethics 31
3. Methods 32
3.1 Establishing and Scoring DSS induced Colitis 33
3.2 Histopathological Evaluation of the Colon 34
3.3 Isolation of Colonic Epithelial Cells and Colonic *Lamina Propria* Leukocytes 34
3.4 Isolation of Splenocytes and Mesenteric Lymph Node Cells 35
3.5 Fluorescence Activated Cell Sorting 35

3.6 Flow Cytometry **36**
3.7 Quantification of Cytokines and Chemokines in Plasma and Colon **40**
3.8 BCA Assay **40**
3.9 Microbioata Analysis **41**
3.10 Isolation of RNA **42**
3.11 Library Preparation, Sequencing and Analysis of RNA-Seq Data **42**
3.12 Chromatin Immunoprecipitation and Reverse Crosslinking **43**
3.13 Library Preparation, Sequencing and Analysis of ChIP-Seq Data **44**
3.14 Statistics **47**
4. Results **48**
4.1 Establishing Consecutive Stages of DSS Colitis **49**
4.2 Characterization of Immunological Changes at Different Stages of Colitis **52**
4.2.1 Changes in Immune Cell Composition during Different Stages of Colitis 52
4.2.2 Changes in Pro-inflammatory Cytokine and Chemokine Levels during Different Stages of Colitis 55
4.2.3 Chronic Stages of Intestinal Inflammation are associated with Systemic Inflammation 57
4.3 Chronification of DSS-Induced Colitis is associated with the Perpetuation of Intestinal Microbiota Dysbiosis **58**
4.4 DSS-induced Intestinal Inflammation Skews Transcriptional CEC Responses towards Antigen Processing and Presentation, T Cell Activation as well as Antimicrobial Humoral Defense **61**
4.5 Transcriptional Consequences of Changes in Epigenetic Histone H3K27me3/H3K27ac Modification Patterns in CECs from all Conditions of the DSS Model **67**
4.5.1 Genome-wide ChIP-read Coverage Correlates with H3K27me3 and H3K27ac Histone Modifications in CECs from all DSS Colitis Conditions 68
4.5.2 Genomic Feature Annotation of High-confidence H3K27me3/H3K27ac ChIP-peaks Reveals Distinct Binding Preferences and DSS Colitis Condition-dependent Patterns 70
4.5.3 Functional KEGG Pathway Annotation of High-confidence H3K27me3/H3K27ac ChIP-peaks in Proximity to TSS 74
4.5.4 Occurrence and Modification-state of Differential H3K27me3/H3K27ac ChIP-peaks Correlates with DSS Colitis Model Conditions and Attributes to MHC-II Gene Loci 79
4.6 Flow Cytometry Verifies Increased Protein Expression of Selected Target Genes Identified in CECs by RNA-Seq during Chronic Stages of the Disease **87**
4.7 Chronification of DSS Colitis is associated with an Accumulation of iTregs in the Colonic *Lamina Propria* **91**
5. Discussion **96**

5.1 Establishment and Comprehensive Immunological Characterization of Consecutive Stages of DSS Colitis **97**
5.2 Understanding Transcriptomic and Epigenetic Adaptations of Colon Epithelial Cells to Chronic Inflammation **100**
5.3 Chronification of DSS Colitis is associated with an Accumulation of iTregs in the Colonic *Lamina Propria* **104**
6. References **109**
7. Appendix **125**
Declaration of Honour **133**

Abstract

Inflammatory bowel diseases (IBD), such as Crohn's disease (CD) and ulcerative colitis (UC), are chronic-relapsing inflammatory disorders of the gastrointestinal tract. Chronic inflammation is associated with disintegration of the intestinal epithelium, ultimately resulting in symptoms such as abdominal pain, diarrhea, bloody stool and weight loss. Next to their key role as intestinal barrier cells, intestinal epithelial cells (IECs) display important immune regulatory functions and contribute to maintenance of intestinal homeostasis. Epigenetic gene regulatory mechanisms act as additional higher-level mechanisms of transcriptional regulation. Epigenetic post-translational histone modifications affect DNA accessibility and thereby influence the transcriptional response of cells. Currently, it is largely elusive if and to what extend histone modifications influence the transcriptional phenotype of IECs and the role this might play for intestinal maladaptation, induced by recurrent inflammatory episodes. To address this, a dextran sodium sulfate (DSS) mouse model for acute and chronic colitis was established, that mimics phases of perpetuating gut inflammation found in IBD patients, as well as interim remission periods. Inflammatory gut immune responses within the DSS model were comprehensively studied and revealed that inflammatory chronification was associated with sustained histopathological changes in the colon. Repeated DSS treatment also resulted in increased numbers of CD4+ and CD8+ T cells as well as B cells in the colonic *lamina propria*, local and systemic cytokine/chemokine dysregulation as well as microbial dysbiosis in feces of mice. Some of these consequences were partially persisting even throughout remission phases. The role of epigenetic imprinting of colon ECs (CECs) in this experimental setup was addressed by chromatin immune precipitation (ChIP) sequencing of H3K27me3 and H3K27ac histone modifications together with CEC transcriptome analysis by RNA-sequencing. Bioinformatic data mining identified several thousands of H3K27me3 and H3K27ac modified genomic regions in CECs at all stages of colitis and remission. H3K27ac regions were preferentially located around transcription start sites (TSS) while most, but not all, H3K27me3 regions were located at distal intergenic regions. At promoters, H3K27me3 and H3K27ac modifications occurred more often in CECs from chronic DSS colitis. Differential transcriptome analysis combined with differential analysis of condition-specific ChIP-enrichment at consensus sites of histone modifications uncovered a set of transcriptionally affected candidate genes whose change in expression correlated with the presence of histone-modified regions at their promoters. Amongst others, in chronic DSS, H3K27me3 hypo-methylation at promoters of the MHC-II-related genes *H2-Ab1* and *H2-DMb1* correlated with their increased expression. Peptide-loaded MHC-II complexes together with T cell co-stimulatory proteins induce CD4+ T cell responses. The frequency of co-stimulation-competent CECs decreased during the chronic remission phase of DSS colitis. Of note, increased MHC-II expression and reduced co-stimulatory capacity of CECs coincided with an accumulation of CD4+ iTregs that may suppress intestinal inflammation in the *lamina propria* and beyond. In summary, the CEC transcriptional program is indeed subjected to inflammation-induced epigenetic changes that differentially affect the expression of disease-associated genes.

Zusammenfassung

Entzündliche Darmerkrankungen wie Morbus Crohn und Colitis ulcerosa sind chronisch-rezidivierende Erkrankungen des Magen-Darm-Trakts, die mit einer Schädigung des Darmepithels und Symptomen wie Bauchschmerzen, Durchfall, blutigem Stuhl und Gewichtsverlust einhergeht. Neben ihrer Schlüsselrolle als Zellen der intestinalen Barriere haben intestinale Epithelzellen (IEZ) wichtige immunregulatorische Funktionen und tragen zur Aufrechterhaltung der intestinalen Homöostase bei. Epigenetische Genregulation umfasst eine Vielzahl an Mechanismen zur Transkriptionsregulation. Epigenetische Histonmodifikationen wirken sich auf die Zugänglichkeit der DNA für Transkriptionsfaktoren aus und beeinflussen so die Transkription in Zellen. Derzeit ist weitgehend unklar, ob und inwieweit Histonmodifikationen das Transkriptionsprofil von IEZ beeinflussen und welche Rolle dies für die durch wiederkehrende Entzündungsepisoden ausgelöste intestinale Maladaptation spielt. Um diese Frage zu klären, wurde ein Dextran-Sodium-Sulfat (DSS) Mausmodell für akute und chronische Kolitis etabliert, das Phasen anhaltender Darmentzündung sowie Remissionsphasen nachahmt. Umfassende Untersuchungen der entzündlichen Reaktionen des Darms ergaben, dass eine Chronifizierung der Entzündung mit anhaltenden histopathologischen Veränderungen im Dickdarm einherging. Eine wiederholte DSS-Behandlung führte zu einer erhöhten Anzahl von CD4+ und CD8+ T-Zellen sowie B-Zellen in der *lamina propria* des Dickdarms, zu einer lokalen und systemischen Dysregulation von Zytokinen/Chemokinen sowie zu einer mikrobiellen Dysbiose der Darmflora. Einige dieser Veränderungen hielten teilweise während der Remissionsphasen an. Die Rolle der epigenetischen Prägung von Colon EZ (CEZ) im DSS-Modell wurde durch Chromatin-Immunpräzipitation (ChIP)-Sequenzierung von H3K27me3 und H3K27ac Histonmodifikationen zusammen mit einer CEZ-Transkriptomanalyse mittels RNA-Sequenzierung untersucht. Durch bioinformatische Analysen wurden mehrere Tausend H3K27me3- und H3K27ac-modifizierte genomische Regionen in CEZ in allen Stadien der Kolitis und Remission identifiziert. H3K27ac-Regionen befanden sich bevorzugt in der Nähe von Transkriptionsstartstellen, während sich die meisten H3K27me3-Regionen in distalen inter-genischen Regionen befanden. H3K27me3 und H3K27ac Modifikationen in Promotoren traten in CEZ aus chronischer DSS verstärkt auf. Eine differenzielle Transkriptomanalyse in Kombination mit einer differenziellen Analyse der ChIP-Anreicherung innerhalb von Konsensus-Regionen mit Histonmodifikationen identifizierte eine Reihe von transkriptionell veränderten Kandidatengenen, deren veränderte Expression in bestimmten Stadien der DSS-Kolitis mit dem Vorhandensein von histonmodifizierten Regionen in ihren Promotoren korrelierte. So konnte in chronischer DSS Kolitis eine H3K27me3-Hypomethylierung von Promotoren der MHC-II Gene *H2-Ab1* und *H2-DMb1* und gleichzeitig deren erhöhte Expression beobachtet werden. Peptid-MHC-II-Komplexe induzieren gemeinsam mit kostimulatorischen Molekülen CD4+ T-Zell-Reaktionen. Der Anteil kostimulationskompetenter CEZ nahm in der chronischen Remissionsphase der DSS-Kolitis ab. Bemerkenswert ist, dass die erhöhte MHC-II-Expression und die verringerte Ko-Stimulationsfähigkeit der CEZ mit einer Zunahme von CD4+ iTregs einherging, welche möglicherweise die Darmentzündung in der *lamina propria* und darüber hinaus supprimieren helfen. Zusammenfassend lässt sich sagen, dass das CEZ-Transkriptionsprofil in der Tat entzündungsbedingten epigenetischen Veränderungen unterworfen ist, die die Expression von krankheitsassoziierten Genen auf unterschiedliche Weise beeinflussen.

List of Abbreviations

% (v/v) volume per volume
% (w/v) weight per volume
% percent
α alpha
AJs adherens junctions
APCs antigen presenting cells
AMPs antimicrobial peptides
β beta
bp base pair(s)
BWA Burrows-Wheeler Aligner
CD Crohn's disease
CD74 invariant chain
CDH1 E-cadherin
CECs colonic epithelial cells
ChIP-on-Chip chromatin immunoprecipitation analyzed by tiling microarray
ChIP-Seq ChIP analyzed by DNA sequencing
CLIP chain-associated peptide
CO_2 carbon dioxide
CPM counts per million reads mapped
DAI disease activity index
DiffBind differential binding analysis of ChIP-Seq peak data
DCs dendritic cells
DMEM Dulbecco's modified Eagle's medium
DN double-negative
DNA desoxyribonucleic acid
DSS dextran sodium sulfate
DTT dithiothreitol
EDTA ethylenediaminetetraacetic acid
EpCAM epithelial cell adhesion molecule
ex vivo latin: "out of the living"
FACS fluorescence activated cell sorting
FC fold change
FCS fetal calf serum
FDR false discovery rate
FFPE formalin fixed paraffin embedded
FMO fluorescence-minus-one
Foxp3 forkhead-box-protein P3
FSC forward scatter
g gram(s)
γ gamma
GI gastrointestinal tract
GM-CSF granulocyte-macrophage colony-stimulating factor
GO Gene Ontology
HBSS Hank's Buffered Saline Solution
H3K27ac histone H3 lysine 27 acetylation
H3K27me3 histone H3 lysine 27 trimethylation

HATs histone acetyltransferases
HDACs histone deacetylases
HDMs histone demethylases
HE hematoxylin and eosin stain
HMTs histone methyltransferases
IBD inflammatory bowel disease
IDR irreproducible discovery rate
Ido1 indoleamine 2,3-dioxygenase 1
IECs intestinal epithelial cells
IFN Interferon
IL interleukin
INR initiator element
in vitro latin: “in the glass”
in vivo latin: “within the living”
IRF interferon regulating factor
ISCs intestinal stem cells
iTregs induced Tregs
kDa dalton (atomic mass)
KEGG Kyoto Encyclopedia of Genes and Genomes
LD live dead
LOD limit of detection
LOQ limit of quantification
Ly6C lymphocyte antigen 6C
Ly6G lymphocyte antigen 6 complex locus G6D
M molar mass
mM millimolar
MACS Model-based Analysis of ChIP-Seq
MAPK mitogen-activated protein kinase
MCFAs medium-chain-length fatty acids
MFI mean fluorescence intensity
µg microgram
MHC major histocompatibility complex
MilliQ purified, deionized water
min minute(s)
mL milliliter
µL microliter
MLNs mesenteric lymph nodes
µm micrometer
MNase micrococcal nuclease
NaCl sodium chloride
ncRNA non-coding RNA-associated gene silencing
n. d. not detectable
NETs neutrophil extracellular traps
NF-κB nuclear factor kappa-light-chain-enhancer of activated B cells
Nrp1 neuropilin-1
nTregs natural Tregs
PBS phosphate buffered saline
PCA principal component analysis

PCR polymerase chain reaction
PCO principal coordinates analysis
PFA paraformaldehyde
RNA ribonucleic acid
ROS reactive oxygen species
rpm rounds per minute
RPMI Roswell Park Memorial Institute
RQN RNA Quality Number
RT room temperature
SIgA secretory IgA molecules
SSC side scatter
TFs transcription factors
Teff effector T cells
TGF transforming growth factor
TJs tight junctions
TLR toll-like receptor
TNBS trinitrobenzenesulfonic acid
TNF tumor necrosis factor
Tregs regulatory T cells
TSS transcription start site
UC ulcerative colitis

List of Figures

Figure 1: Factors responsible for onset and pathogenesis of IBD. 2
Figure 2: Multilayered structure of the intestine. 4
Figure 3: The crypt and mucus layer structure of the small intestine and the colon. 5
Figure 4: Major elements of intestinal barrier. 6
Figure 5: Colonic epithelial cells (CECs) express MHC-II under inflammatory conditions. 8
Figure 6: Regulation of transcription. 11
Figure 7: Chromatin Structure. 13
Figure 8: Basic workflow of ChIP-Seq. 16
Figure 9: Epigenetic, transcriptomic and immunological changes after environmental triggers such as DSS. 18
Figure 10: Types of Tregs: nTregs and iTregs. 20
Figure 11: IBD and microbial dysbiosis. 22
Figure 12: Representative gating strategy used to identify immune cell subsets in the colon. 37
Figure 13: Representative gating strategy used to identify subpopulations of CD4+ T cells in the colon. 39
Figure 14: Representative fragment size distribution of sonicated CEC chromatin. 44
Figure 15: Evaluation of disease activity and histopathological alterations at different stages of DSS colitis. 50
Figure 16: Characterization of innate and adaptive immune cell composition in the colon during consecutive stages of DSS colitis. 53
Figure 17: Quantification of chemokines and cytokines in colon tissue during consecutive stages of colitis. 56
Figure 18: Quantification of IFN-γ and IL-17a in blood plasma during consecutive stages of colitis. .57
Figure 19: Microbiota analysis in feces samples from different stages of DSS-induced colitis. 60
Figure 20: Transcriptional comparison of CECs from all DSS model conditions versus control conditions. 64
Figure 21: Transcriptomic changes during different stages of DSS colitis 66
Figure 22: Clustered Pearson correlations of genome-wide non-normalized binned read counts of ChIP-Seq samples. 69
Figure 23: Genomic feature annotation of high-confidence H3K27me3 and H3K27ac ChIP-peaks. ...72
Figure 24: Distance to TSS of high-confidence H3K27me3 and H3K27ac ChIP-peaks. 73
Figure 25: KEGG pathway enrichment of genes annotated to H3K27me3 high-confidence ChIP-peaks within ± 10 kb range around TSS in CECs from all DSS model conditions. 76
Figure 26: KEGG pathway enrichment of genes annotated to H3K27ac high-confidence ChIP-peaks within ± 10 kb range around TSS in CECs from all DSS model conditions. 78

Figure 27: Occurrence and methylation-state of differential H3K27me3 ChIP-peaks correlates with DSS model conditions. 82
Figure 28: Hypo-methylated ChIP-regions are associated with enhanced gene expression. 83
Figure 29: Occurrence of hyper-acetylated differential H3K27ac ChIP-peaks mainly correlates with acute DSS. 84
Figure 30: Differential H3K27 acetylation is associated with enhanced and reduced gene expression.86
Figure 31: Representative histogram from flow cytometric analysis of selected molecules.....88
Figure 32: Expression level and percentage of CECs expressing selected target molecules. 89
Figure 33: Representative histogram from flow cytometric analysis of CECs. 90
Figure 34: Expression level and percentage of CECs expressing selected target molecules. 91
Figure 35: Characterization of the CD4+ T cell composition in the colon during consecutive stages of DSS colitis. 93
Figure 36: Frequency and absolute cell number of CD4+ T cell subsets during consecutive stages of DSS colitis. 95

Appendix Supplementary Figures

Supplementary Figure 1: Characterization of immune cell subsets in mesenteric lymph nodes during consecutive stages of colitis. 128
Supplementary Figure 2: Characterization of immune cell subsets in the spleen during consecutive stages of colitis. 130
Supplementary Figure 3: ChIP-peak annotation distribution of randomly positioned genomic regions of H3K27me3 and H3K27ac. 131
Supplementary Figure 4: Distance to TSS of randomly shuffled H3K27me3 and H3K27ac ChIP-peaks 132

List of Tables

Table 1: FACS panel used for CECs sorting 27
Table 2: FACS panel used for determination of leukocyte subpopulations 27
Table 3: FACS panel used for determination of T cell subsets 28
Table 4: FACS panel used for determination of protein expression for RNA-Seq identified genes in CECs 29
Table 5: Antibodies used in ChIP-Seq Experiments 29
Table 6: Chemicals 30
Table 7: Kits 31
Table 8: Scoring of DAI in DSS colitis 33
Table 9: Histological scoring 34
Table 10: RQN level of individual RNA-Seq samples 42
Table 11: Numbers of identified IDR determined high-confidence peak regions for H3K27ac and H3K27me3 for each disease conditions and corresponding controls. 71
Table 12: Numbers of identified IDR determined high-confidence peak regions with distances between ± 10 kb around TSS for H3K27ac and H3K27me3 for each disease conditions and corresponding controls. 75

Appendix Supplementary Tables

Supplementary Table 1: Complete representation of Biological Process GO terms differentially expressed genes. 125
Supplementary Table 2: Complete representation of KEGG terms differentially expressed genes.....126

1. Introduction

1.1 Inflammatory Bowel Disease

Inflammation is generally a protective and timely limited response of our body to certain harmful stimuli. Once triggered it can however also lead to aberrant immune responses resulting in manifestation of inflammation and chronification of disease. Inflammatory bowel disease (IBD) encompasses several disorders of the digestive tract including ulcerative colitis (UC) and Crohn's disease (CD) that are characterized by chronic intestinal inflammation (reviewed in (Rubin et al., 2012)). IBD is characterized by diarrhea, abdominal pain, weight loss as well as fever. Mainly young people are affected and disease incidence peaks between the age of 10 and 40 (Carter et al., 2004). IBD is prevalent in industrialized nations such as Scandinavia (Björnsson and Jóhannsson, 2000; Vind et al., 2006), and the United Kingdom (Gunesh et al., 2008) with increasing incidence rates. It is estimated that around three million people in Europe suffer from IBD (reviewed in (Burisch et al., 2013)). Northern Europe and North America have the highest incidence and prevalence of pediatric onset of IBD, while Southern Europe, Asia, and the Middle East have the lowest rates (Kuenzig et al., 2022). However, an increasing incidence rate is also reported in low incidence continents such as Asia (reviewed in (Thia et al., 2008)). Genetic factors (e.g. mutations of NOD2 associated with CD), environmental factors (e.g. lifestyle, smoking, food consumption, stress, appendicectomy, vaccination), microbial factors, immuno-inflammatory factors and nonimmuno-inflammatory factors (e.g. peroxisome proliferator-activated receptors) may cause the disease or contribute to disease progression (reviewed in (Ardizzone and Bianchi Porro, 2002)) (Figure 1). Although, there have been numerous advancements in IBD research, the etiology and pathology of the disease still remains largely elusive.

IBD decreases the quality of life, causes several complications and can require medical therapies or surgery. Conventional therapies such as purine analogues azathioprine and 6-mercaptopurine, and antibiotics or unconventional therapies such as biological therapies, gene therapy, antibody based therapies etc. or nonbiological therapies such as thalidomide reducing TNF-α production, manipulating intestinal microflora by probiotics etc. are possible therapeutic options for the treatment of IBD (reviewed in (Ardizzone and Bianchi Porro, 2002)). However, there is still no permanent cure of the disease existing, therefore, affected individuals will suffer live long. Moreover, when IBD is not treated early after onset, it can cause further complications like colorectal cancer (reviewed in (Kim and Chang, 2014)). Therefore, there is a need for a better understanding of the mechanisms contributing to disease chronification since this is the prerequisite for the development of improved treatments to prevent disease progression or ideally cure the disease.

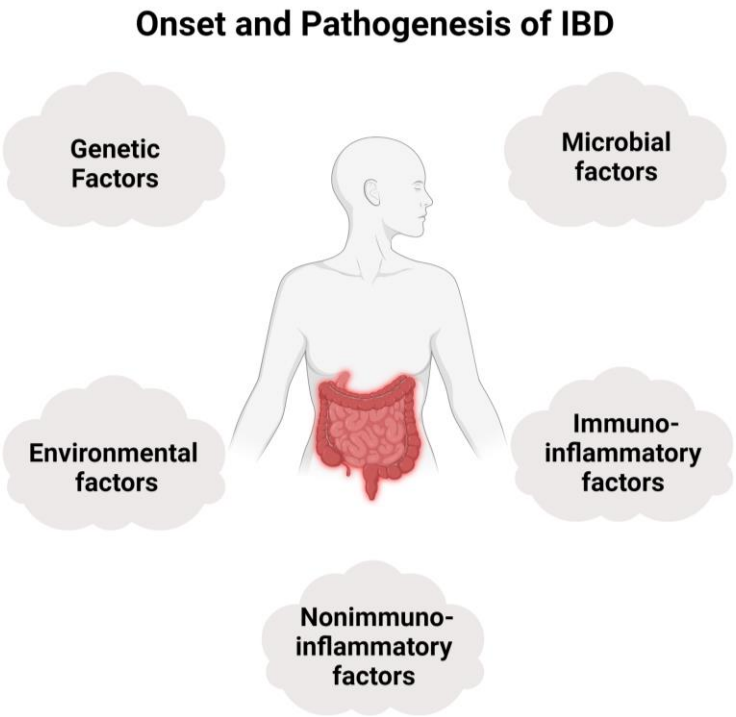

Figure 1: Factors responsible for onset and pathogenesis of IBD. Genetics, microbial, environmental, immuno-inflammatory and nonimmuno-inflammatory factors can contribute to the origination and development of IBD (reviewed in ((Ardizzone and Bianchi Porro, 2002)). The figure was created with BioRender.com (2022).

Atreya et al., concluded in their review article that inflammatory signaling involving the transcription factor NF-κB plays a crucial role in the initiation, progression, and chronification of IBD (reviewed in (Atreya et al., 2008)). In another review by Rogler et al. it was suggested that due to barrier defects bacterial compounds may translocate into the intestinal tissue were they may activate macrophages via binding to CARD15/NOD2. Activation of CARD15/NOD2 can generally lead to activation of the NF-κB pathway, therefore macrophages and intestinal epithelial cells (IECs) may represent key cellular subsets for the initiation of IBD that in concert with secondary T cell activation may contribute to disease progression or chronicity (reviewed in (Rogler, 2004)). Moreover, an impaired axis of IL-22 and its endogenous antagonist, IL-22 binding protein, has been suggested as one of the possible mechanisms that may contribute to the chronification of intestinal inflammation (reviewed in (Kempski et al., 2017)). Bisping et al. showed that epithelial cells had a great capacity for inducing CD8+ T lymphocytes from IBD patients to vigorously express IFN-γ (Bisping et al., 2001). Given the fact that IFN-γ has been demonstrated to play a significant role in the duration of IBD, IFN-γ induction may be crucial for disease chronification (Bisping et al., 2001).

Even though UC and CD are both IBD-related diseases, they are distinct from each other according to the region of disease activity within the intestine. UC mainly affects the colon, while CD affects mainly the last part of the small intestine (ileum) as well as the colon (reviewed in (Macpherson et al., 2012)). Hence these organ compartments are described in more detail in the next section.

1.2 Small and Large Intestine and their Epithelial Cell Constituents

The gastrointestinal tract (GI) spans the region from the mouth to the anus. The upper GI includes mouth, pharynx, esophagus and stomach and the lower GI contains small intestine, large intestine (colon) and anus. Small intestine absorbs nutrients from food and drinks, while the colon absorbs water from wastes, creating stool. There are several structural and functional differences between the small and the large intestine in the context to their cellular composition. Small (0.5-1 mm long) vascularized projections called villi give the mucosa a furry appearance in the small intestine (Chruścik et al., 2021), however, there is no villi structure present in the colon. The number of villi per square millimeter ranges from 20 to 40, greatly expanding the epithelium's surface area (Chruścik et al., 2021). The mucosal epithelium is mostly made up of absorptive cells (Chruścik et al., 2021). Since villi that absorb nutrients increase the small intestine's absorptive surface area, the surface area of the small intestine is roughly 100 times larger (~ 200 m^2) than the skin surface (Chruścik et al., 2021). The small intestine (about 3.05 m long in humans) is around 5 times longer than the colon, however it has a smaller diameter (approximately 2.54 cm) than colon (about 7.62 cm) (Chruścik et al., 2021). Deep fissures each leading into a tubular intestinal gland (crypt of Lieberkühn) in the small intestine are scattered throughout the mucosa in between the villi of the small intestine, in addition to the specialized absorptive features already mentioned above (Chruścik et al., 2021). The colonic epithelium is structured as a flat surface epithelium with crypts of Lieberkühn, which are extremely repetitive invaginations (reviewed in (Snippert, 2016)). Stem cells are located on the bottom of these crypts (reviewed in (Snippert, 2016)). Both, small intestine and colon content (food and microbiota) are separated from tissue by a mucus layer that consists of glycosylated mucin proteins and other hydrated polymers (reviewed in (Herath et al., 2020)).

The intestine contains 4 distinct tissue layers which are mucosa, submucosa, *muscularis propria* and *serosa*. The mucosa includes epithelium (composed of single columnar epithelia cells), *lamina propria* (loose connective tissue), and a muscle layer called *muscularis mucosa* (reviewed in (Siri et al., 2020)). The *lamina propria* is lies beneath the epithelium and harbors multiple innate as well as adaptive immune cells (reviewed in (Turner, 2009)). The second layer, submucosa, is a connective tissue layer containing blood vessels and lymph nodes (reviewed in (Siri et al., 2020)). The third layer, *muscularis propria*, contains an inner circular and longitudinal muscle layer that are important for contraction. Lastly, there is a protective outer *serosa* layer composed of loose connective tissue containing mesothelium (squamous epithelium) (reviewed in (Siri et al., 2020)) (Figure 2).

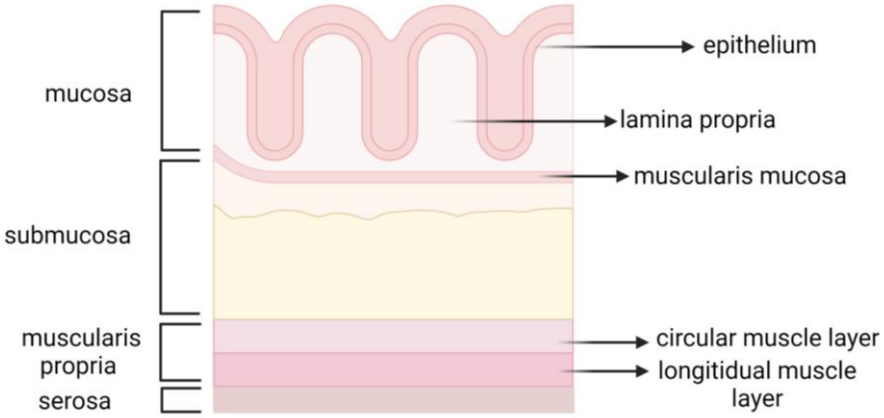

Figure 2: Multilayered structure of the intestine. The intestine consists of 4 distinct tissue layers: mucosa, submucosa, *muscularis propria* and *serosa*. The figure was created with BioRender.com (2022).

There are different subtypes of intestinal epithelial cells, whose occurrence differs according to their localization in the small intestine or large intestine. Both, small and large intestine contain intestinal stem cells, enterocytes, tuft cells, goblet cells and enteroendocrine cells (Figure 3). Paneth cells are found in the intestinal glands and secrete antimicrobial peptides (AMPs) (Cruickshank et al., 2004). While it was initially thought that the large intestine lacks paneth cells, the existence of colonic Paneth-like cells was documented more recently (Sato et al., 2011; Rothenberg et al., 2012; Schewe et al., 2016). Intestinal stem cells (ISCs) are located at the base of intestinal crypts in the small intestine and in the colon. Colonic epithelial cells (CECs) are continuously renewed around every 5-7 days by ISCs (reviewed in (Barker, 2014)). ISCs generate transit amplifying cells which then differentiate into different absorptive or secretory cells like e.g. common enterocytes, goblet cells or enteroendocrine cells (reviewed in (Barker, 2014)). Absorbent enterocytes have a glycocalyx coat that contains digestive enzymes, however, aside from their digestive roles, enterocytes can also contribute to adaptive immune processes by expressing major histocompatibility complex (MHC)-I and MHC-II molecules (reviewed in (Snoeck et al., 2005)). Using taste-chemosensory and succinate receptors to monitor luminal intestinal content and react to a wide variety of chemicals and pathogens, intestinal tuft cells function as a major hub in immunological and regulatory metabolic networks (reviewed in (Hendel et al., 2022)). Enteroendocrine cells produce gut hormones and hormonal signals involving absorption, insulin secretion etc. (reviewed in (Gribble and Reimann, 2019)). In addition to the protective epithelium, the colon exhibits another physical barrier that consists of the mucus layer produced by goblet cells (reviewed in (Birchenough et al., 2015)). While intestinal stem cells can be distinguished from other cells by the expression of the LRG5 marker (Barker et al., 2007), generally epithelial cell adhesion molecule (EpCAM) staining is used to identify all subsets of intestinal epithelial cells for e.g. fluorescence activated cell sorting (FACS) (Gracz et al., 2012; Brügger et al., 2020). However, there are some subset specific properties e.g. SSC high CD24 positive gating strategy can be used to identify Paneth cells by FACS (Sato et al., 2011).

The first line of defense against invading bacteria, food particles, microbial byproducts, and food-associated toxins is the mucus layer that is located on top of the epithelium. This layer serves as a physical defense barrier to bacterial components and other antigenic substances in the lumen, covers the inner surface of the GI tract and lubricates luminal substances (reviewed in (Herath et al., 2020)). The mucus layer takes the form of a sieve-like structure on top of the intestinal epithelium where the immune-sensing and regulatory proteins which are antimicrobial peptides (AMPs) and secretory IgA molecules (sIgA) are secreted (reviewed in ((Vancamelbeke and Vermeire, 2017)). The higher number of goblet cells in the large intestine compared to the small intestine can be attributed to the higher total microbial load. Consequently, the large intestine is covered by a very thick mucus layer (around 150 um thick in mouse) (Malmberg et al., 2006; Johansson et al., 2008). In contrast to the small intestine that is covered by a single mucus layer, the colon surface is protected by two structurally different layers. The outer mucus layer inhabits the microbiota, while the inner layer is largely sterile and firmly attached to epithelium (Johansson et al., 2008) (Figure 3).

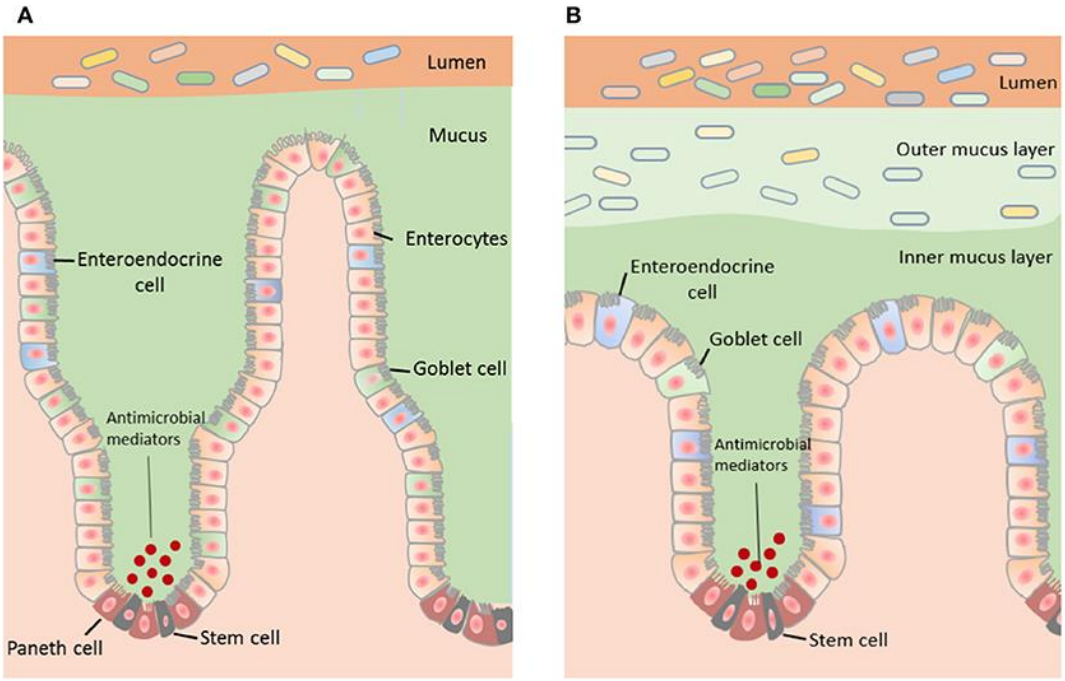

Figure 3: The crypt and mucus layer structure of the small intestine and the colon. Stem cells are located at the bottom of the crypts. Enteroendocrine cells, enterocytes, and goblet cells are found above of the crypts. (A) The small intestine is covered by one layer of mucus which separates luminal bacterial components from the intestinal epithelium. The small intestine contains paneth cells at the bottom of the crypts. Paneth cells secrete AMPs. (B) The distal colon is covered by two different mucus layers. The inner mucus layer is largely sterile while the outer mucus layer contains the intestinal microbiota (taken from (Herath et al., 2020)).

The barrier function of IECs critically depends on tight cell-cell contacts. The junctional complexes (tight junctions (TJs), adherens junctions (AJs), desmosomes) that hold the IECs tightly together help to form a continuous epithelial monolayer. The apical side of the IECs contains the TJs (e.g. claudin, occludin) (reviewed in (Vancamelbeke and Vermeire, 2017)). AJs are located below the TJs and are necessary for their assembly (reviewed in (Vancamelbeke and Vermeire, 2017). Desmosomes act in concert with AJs to form strong adhesive bonds helping to maintain the integrity of the epithelium

(reviewed in (Vancamelbeke and Vermeire, 2017). These junctional complexes control the transport of molecules between IECs (reviewed in (Vancamelbeke and Vermeire, 2017)) (Figure 4).

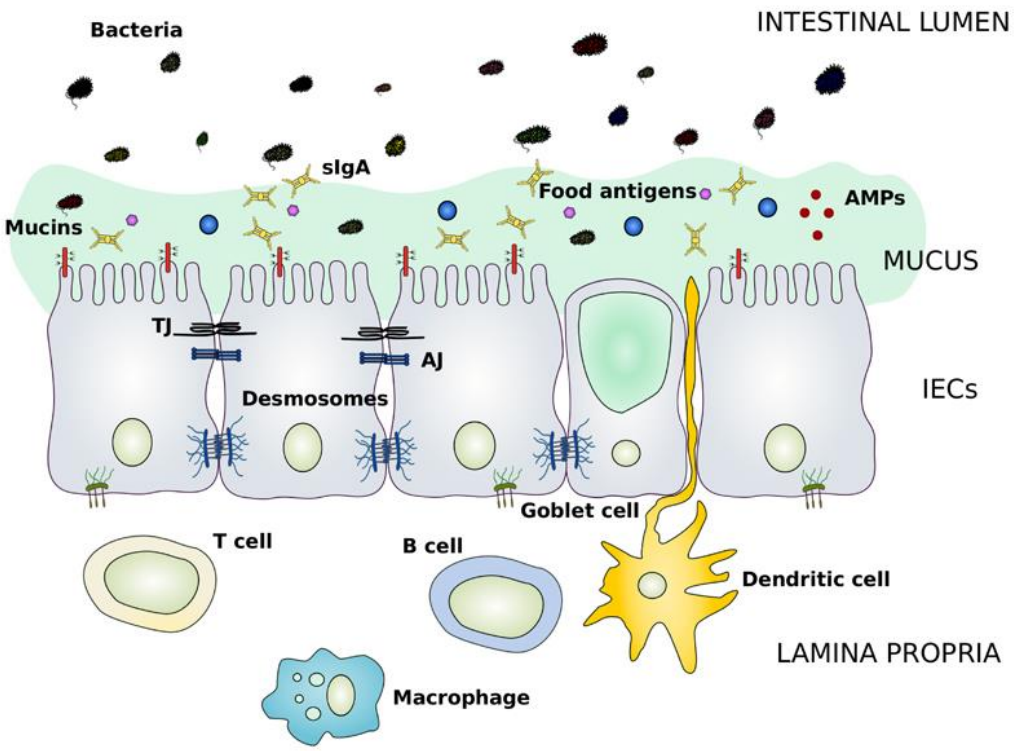

Figure 4: Major elements of intestinal barrier. First element of the intestinal barrier is the mucus layer that contains antimicrobial peptides (AMPs) as well as secretory IgA molecules (sIgA). Second element consist of junctional complexes including tight junctions (TJs), adherens junctions (AJs) and desmosomes which attach IECs to each other. Transportation of small molecules and ions are regulated by TJs. Integrity of intestinal epithelium is provided by AJs and desmosomes. Third element of the intestinal barrier is represented by the *lamina propria* including adaptive and innate immune cells (e.g. T cells, B cells, dendritic cells, macrophages) to provide immune defense (taken from (Vancamelbeke and Vermeire, 2017)).

The integrity of the gastrointestinal tract heavily depends on an intact intestinal barrier for the maintenance of both structural and functional attributes. IBD is associated with extensive barrier breakdown and damage of intestinal barriers which is an important hallmark for IBD onset and chronification. IECs do not only represent a crucial part of the intestinal barrier and modulate crosstalk between luminal microbes and immune cells, but also play active roles in immune regulation by interacting with mucosal T cells. This property of IECs will be described in more detail within the next section.

1.2.1 MHC Class II Molecules and their Functions in IECs

In addition to the before mentioned features, IECs differ in terms of expression of several immunological proteins and factors. Human small IECs express major histocompatibility complex (MHC)-II class molecules (Scott et al., 1980; Chiba et al., 1988; Madrigal et al., 1993), whereas such expression is absent in epithelium of colonic tissues under homeostatic conditions (Scott et al., 1980; Daar et al., 1982;

Selby et al., 1983). However, inflammation such as IBD is associated with increased MHC-II expression in CECs (Selby et al., 1983; Dotan et al., 2007). Moreover, interferon gamma (IFN-γ) was shown to induce MHC-II expression on murine IECs during adoptive transfer colitis (Thelemann et al., 2014) and in a human intestinal epithelial cell line (Colgan et al., 1994).

MHC class II molecules are heterodimeric glycoproteins expressed on the surface of antigen presenting cells (APCs) consisting of α and β chains (reviewed in (KAUFMAN et al., 1984)). Newly synthesized nascent MHC-II α and β chains are located in the endoplasmic reticulum (ER). MHC-II assemble together with the invariant chain (CD74) which prevent premature peptide binding (Roche et al., 1991; Roche and Cresswell, 1991). Invariant chain does not only prevent the peptide binding to nascent MHC-II but also functions as a chaperone by translocating MHC-II molecules to endosomal vesicles (Lamb et al., 1991). After being translocated, the invariant chains within the endosomal compartments get degraded to class II invariant chain-associated peptide (CLIP), that acts as a surrogate ligand and occupies the peptide binding part of MHC-II (Bangia and Watts, 1995; Gautam et al., 1995). Afterward, the non-classical MHC-II molecule HLA-DM removes the CLIP and allows MHC-II to bind to extracellular or cytosolic peptide antigens (Denzin and Cresswell, 1995; Sloan et al., 1995). Then the MHC-II-peptide complex can be transported to the cell surface to interact with CD4+ T cells.

MHC-II expression alone is not sufficient for efficient CD4+ T cells activation and therefore, IECs tend to express additional molecules like CD74, HLA-DM, etc. Moreover, the activation of CD4+ T cells is dependent on the concomitant expression of co-stimulatory molecules such as CD80, CD86, and CD40. B7/BB-1 (CD80 or B7-1) and B70 (CD86 or B7-2) are expressed by APCs to interact with the CD28 receptors on T cells (Linsley et al., 1990; Azuma et al., 1993). However, both costimulatory molecules can also bind to the CTLA-4 receptor on T cells (Azuma et al., 1993; van der Merwe et al., 1997) such as regulatory T cells (Tregs) which constitutively express CTLA-4 (Read et al., 2000). The ligand for CD40 is CD40L (CD154) and is primarily expressed on activated T cells (reviewed in (van Kooten and Banchereau, 2000)). Both *CD80* and *CD86* were detected at the mRNA level in CECs from normal and inflamed mucosa of UC patients (Nakazawa et al., 1999). Although, the costimulatory molecules were detectable at the mRNA level, surface expression of CD80, CD86 and CD40 was not detectable in non-diseased human duodenal epithelial cells (Byrne et al., 2002). Moreover, another study showed that in vivo IFN-γ treatment in mice increased *MHC-II* expression in small IECs but did not change *B7* mRNA level (Sanderson et al., 1993). Also, protein expression of B7 was not detectable in the inflamed colonic epithelium of UC and CD patients (Bloom et al., 1995). Since MHC-II expression in the absence of proper costimulation is known to result in T cell anergy rather than activation (reviewed in (Appleman and Boussiotis, 2003)), IECs might actively contribute to the regulation of T cell responses during intestinal inflammation.

Since the expression of costimulatory molecules in IECs is still controversially discussed, there is still no comprehensible explanation of how the inflammation-induced upregulation of MHC-II expression affects the T cell composition in inflammatory conditions. It is still not clear if the elevated MHC-II levels in CECs would more likely result in improved activation of T effector cells (Teff) further boosting inflammation or the expansion of Tregs counteracting inflammatory processes and providing intestinal homeostasis or result in T cell anergy (Figure 5).

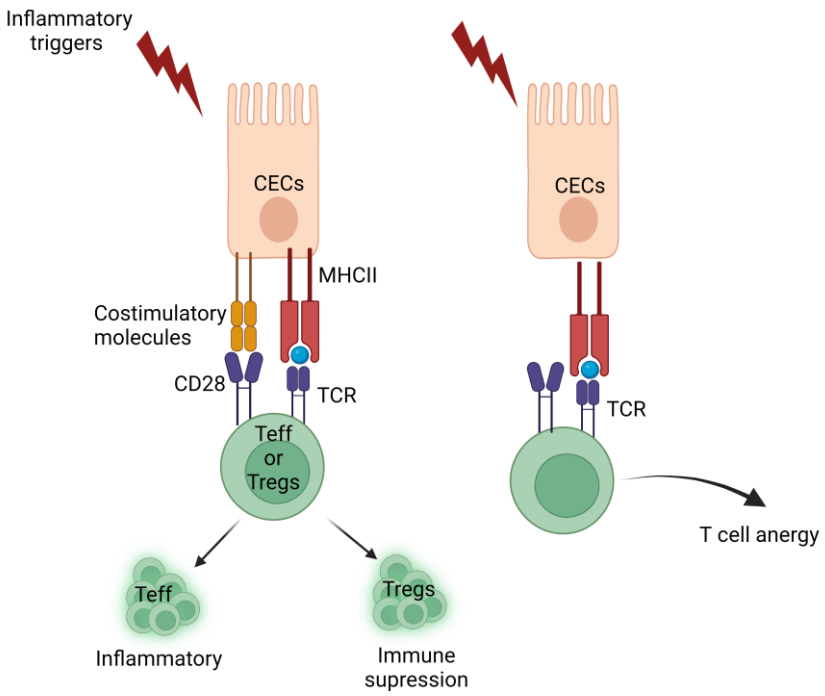

Figure 5: Colonic epithelial cells (CECs) express MHC-II under inflammatory conditions. Inflammatory triggers induce MHC-II expression in CECs. This may support the expansion of Tregs or it may further boost inflammation by activating T effector cells. In the absence of costimulatory molecules, MHC-II recognition by CD4+ T cells may also cause T cell anergy. The figure was created with BioRender.com (2022).

1.3 Dextran Sodium Sulfate-induced Colitis as a Mouse Model to Study Different Stages of IBD

IBD is a multifactorial disease with an unknown etiology, and studying the complex mechanisms underlying its onset and manifestation is not feasible in human subjects. Therefore, murine models are primarily used for mechanistic studies. Frequently used animal models to study disease pathogenesis include chemically induced experimental colitis (Dextran sodium sulfate (DSS)-, trinitrobenzenesulfonic acid (TNBS)- and oxazolone-induced colitis model), adoptive T-cell transfer-induced colitis, genetically engineered models or models based on spontaneous mutation as well as microbiota-induced mouse models (reviewed in (Baydi et al., 2021)). However, none of these animal models can represent each aspect of the disease and each of the individual models has its limitations (reviewed in (Baydi et al., 2021)). The focus of this thesis is the role of CECs in disease progression. One of the most relevant mouse model to study this is the DSS-induced colitis model.

Okayasu I. et al. in 1990 reported that intestinal inflammation resembling acute and chronic UC in humans can be induced in mice by supplementing drinking water with DSS (Okayasu et al., 1990). Depending on the frequency, duration, and dosage of DSS different stages of colitis (acute, chronic, relapsing) can be established (Wirtz et al., 2017).

The exact mechanism behind how DSS reproduces the inflammatory conditions is still unknown. However, it is believed that DSS damages the barrier integrity due to its toxic nature toward CECs. This damaged epithelium and the associated barrier breakdown exposes the colon to bacterial species in the lumen and these bacteria can then translocate into the colon tissue and trigger immune activation. Laroui H. et al. proposed that DSS associates with medium-chain-length fatty acids (MCFAs) in the lumen of the colon before DSS colitis is induced and MCFAs-DSS complexed create ~200 nm nanovesicles that fuse with colonocyte membranes (Laroui et al., 2012). Once in the cytoplasm, these nanovesicles would influence epithelial physiology and decrease epithelial barrier function, ultimately resulting in the activation of inflammatory signaling pathways (Laroui et al., 2012). Since inflammatory signaling cascades are activated in the presence of dextran in the cytoplasm, it was proposed that the dextran moiety is responsible for the inflammatory activity of DSS (Laroui et al., 2012).

In summary, while its mode of action is still not entirely understood, chemically induced DSS colitis in mice is frequently used in IBD research to study the dysfunctional gastrointestinal barrier and subsequent altered immune responses along with the microbiota associated changes. Repeated DSS application with interim remission periods mimics recurrent inflammatory episodes, therefore, it can be used to study IBD-like disease features in acute, chronic and transition phases.

1.4 Epigenetic Modifications and Related Transcriptomic Changes

Additional to the canonical model of eukaryotic transcriptional regulation, research has identified another higher mechanistic level of gene regulation comprising a plethora of mechanisms, summarized under the term epigenetics. Epigenetics means regulation of gene activity without changing the DNA sequence and these modification are transferable to daughter cells (reviewed in (Weinhold, 2006)). There are mainly three types of epigenetic mechanisms that include DNA methylation, non-coding RNA-associated gene silencing (ncRNA) and histone modifications. Aberrant epigenetic changes such as histone modifications have been described in different chronic inflammatory diseases including cardiovascular disease, autoimmune diseases as well as IBD and also in cancer as consequence of chronic inflammation (reviewed in (Lorenzen et al., 2012; Audia and Campbell, 2016; Araki and Mimura, 2017; Lin et al., 2022)). Since the analysis of epigenetic histone modifications in CECs is the major research focus of this thesis, in the following the canonical concept of eukaryotic transcriptional regulation as well as epigenetic histone modifications will be explained in more detail.

1.4.1 Basic Concept of Eukaryotic Transcriptional Regulation

Gene transcription is regulated by regions of non-coding DNA, cis-regulatory elements (e.g. promoters, enhancers, silencers) (reviewed in (Li et al., 2015)). Promoters contain binding sites for additional transcription factors as well as common sequence components like a TATA box and an initiator sequence (INR) that work together to bring the transcriptional machinery to the transcriptional start site (TSS) (reviewed in (Farnham, 2009)). TATA boxes include repeating A and T base pairs and provide binding sites for general transcription factors (TFs) such as TATA binding protein (TBP), one of the main TFs which is responsible for formation of RNA polymerase II. General TFs bind to the core promoter region (Figure 6A) to induce low-basal transcriptional activity (reviewed in (Farnham, 2009)).

Proximal promoter region is the area around 250 base pairs upstream of the TSS. Further specific TFs interact with cis elements in the proximal promoter region to enhance transcriptional activity above the basal level by stabilizing the transcriptional machinery through direct contact (Figure 6B) (reviewed in (Farnham, 2009)).

Optimal transcriptional activity requires additional TFs bound to so-called enhancer and silencer sequences. Enhancers and silencers are remote DNA sequences potentially far away from TSS that nevertheless influence transcriptional activity by interacting with core proximal promoter (reviewed in (Farnham, 2009)). This interaction requires DNA loop structure encompassing TFs bound to the core and/or proximal promoter, TFs bound the enhancers/repressors sites and the patch of DNA between those elements (reviewed in (Farnham, 2009)). TFs bound to enhancers/repressor sites recruit histone-modifying enzymes (e.g. a histone acetyltransferase (HAT) acetylating (Ac) histones) to create a more favorable chromatin structure for the transcriptional machinery, or by attracting a kinase that phosphorylates RNA polymerase II, thereby further enhancing transcriptional activity (Figure 6C, Figure 6D, Figure 6E) (reviewed in (Farnham, 2009)).

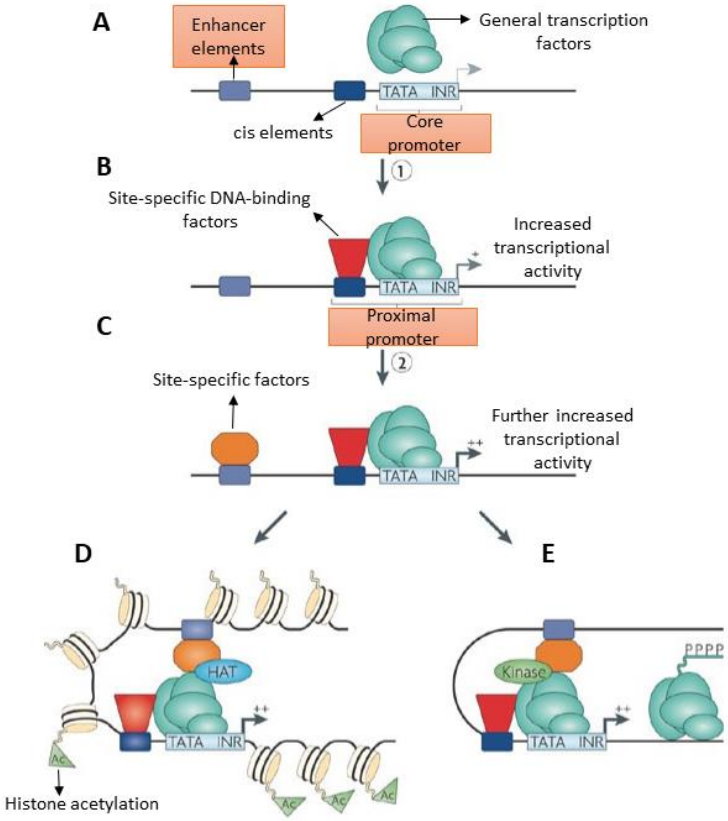

Figure 6: Regulation of transcription. A) General TFs bind to the core promoter region to induce low-basal transcriptional activity. B) Transcriptional activity can be increased by site-specific DNA-binding proteins (TFs) that interact directly with cis elements in the proximal promoter region. C) Further stimulated transcriptional activity is obtained by site specific factors by binding to enhancer elements. D) Increased transcriptional activity can be stimulated by enhancer factors that recruit histone modifying enzymes such as histone acetyltransferase (HAT) to create a more favorable chromatin structure for transcriptional machinery or E) by recruiting a kinase which can phosphorylate RNA polymerase II (adapted from (Farnham, 2009)).

1.4.2 Epigenetics as a Complementing Layer of Transcriptional Regulation

Cell functions are determined by the transcriptional patterns that are defined in response to physiological signals, which are closely regulated by a variety of TFs, epigenetics, and chromatin interactions (reviewed in (Li and Leonard, 2018)). Specifically, regulation of gene expression depends on chromatin accessibility (open or closed), which is regulated by the proper packaging of DNA/nucleosomes (chromatin) within the nucleus (reviewed in (Li and Leonard, 2018)). Binding of specific TFs to their target sites requires accessibility of according DNA regions. In this regard the chromatin state that defines DNA accessibility in term determines the transcriptional activity of gene loci on a higher level than the canonical concept of transcription of regulation (see section 1.4.1).

There are three main epigenetic mechanisms which can regulate chromatin composition and subsequent gene expression: DNA-methylation, ncRNA and histone modifications. DNA methylation entails the direct addition of a methyl group to a cytosine nucleotide within a cytosine-guanine sequence, which is catalyzed by DNA methyltransferase enzymes (Al Aboud et al., 2022). A ncRNA including microRNAs, short interfering RNAs and long non-coding RNAs is transcribed, however it does not translated into

protein. ncRNA can regulate gene transcription by gene silencing (Al Aboud et al., 2022). Lastly, post translational modifications on histone proteins take role in gene activation or silencing by changing chromatin accessibility.

There are some evidence suggesting that epigenetic can take an important role on pathogenesis of IBD. DNA methylations amongst other epigenetic alterations are well known and it has been already shown that after DNA methylation pattern is identified in peripheral blood mononuclear cells of patients, IBD is associated with differentially methylated regions (McDermott et al., 2016). There are also studies which focused on DNA methylation of specific promoter regions. For example, Arasaradnam et al., showed that promoter region of *ESR-1* (oestrogen receptor-1) and *N-33* (tumor suppressor candidate-3) genes were hypermethylated in colorectal mucosal biopsies of UC patients (Arasaradnam et al., 2010). Moreover, Azarschab et al., showed that in contrast to 6% of non-dysplastic biopsies, promoter methylation of the E-cadherin (*CDH1*) was found in 93% of dysplastic biopsy samples from long-standing UC, suggesting that the *CDH1* promoter is subjected to epigenetic regulation in colorectal ulceration (Azarschab et al., 2002). In addition, different studies have shown that the expression of mi-RNAs may be altered in tissue samples (Wu et al., 2010) and blood of IBD patients (Iborra et al., 2013) compared to control groups. Another study discovered that the histone methylation profile at H3K4 changes in IECs of IBD patients and furthermore animal studies showed that alteration of microbiome can be associate with changes in H3K4 profile (Kelly et al., 2018). All these findings clearly indicate that epigenetics have significant impact on the pathogenesis of IBD.

1.4.3 Histones and their Modifications

Histones are positively charged proteins named H1, H2A, H2B, H3, and H4, therefore they can tightly bind to the negatively charged DNA. The basic functional structural unit of chromatin is the nucleosome, containing about 146 base pairs of DNA wrapped around two core histone protein complexes with each consisting of the 4 subunits: H2A, H2B, H3, and H4 (Luger et al., 1997). H1 histone, also known as linker histone H1, is important for nucleosomal stabilization. Cells have a multi-protein machinery that allows post translational histone modification. Most histone modifications occur at the N terminal tail of the amino acid chain but they can also be found in core protein domains (Figure 7). Typically, certain amino acid residues become preferentially modified, with the position and nature of modifications having an important functional meaning. Hence, in the literature there is a common nomenclature that helps to communicate about specific histone modifications.

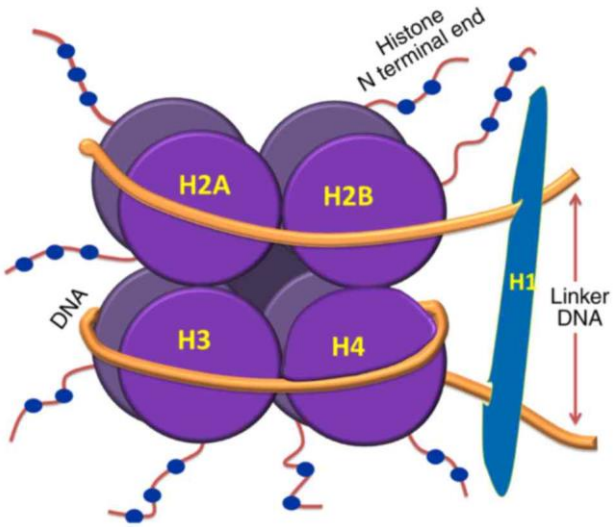

Figure 7: Chromatin Structure. DNA wrapped around two core histone protein complexes. H1 histone protein stabilizes by interacting with the linker DNA. The most of the post translational modifications (PTMs) occur at N terminal of histone (taken from (Thankam et al., 2019)).

Histone modifications can change the chromatin accessibility giving rise to two basic chromatin configurations namely euchromatin and heterochromatin. Euchromatin reflects a loose open state of DNA allowing binding of TFs to their binding sites. On the other site, heterochromatin refers to a compact inaccessible state of the DNA. There are several kinds of histone modifications known, including methylation, acetylation, phosphorylation, ubiquitination, citrullination etc. In the literature there is a common nomenclature that helps to communicate about specific histone modifications. For example, H3K27me3 refers to triple methylation of lysine residue number 27 of the amino acid chain of histone 3. The specific amino acid being modified is stated in amino acid one letter code.

There are whole families of histone modifying enzymes that can be split into 3 categories: writers (addition of new histone modifications), erasers (removal of existing histone modifications), and readers (recognition of histone modification type) (reviewed in (Xu et al., 2017)). Histone acetyltransferases (HATs) and histone deacetylases (HDACs) are examples of enzymes that adds or removes acetyl residues to histones, respectively (reviewed in (Xu et al., 2017)). However, histone methylation is catalyzed by histone methyltransferases (HMTs) and demetylation by histone demethylases (HDMs) (reviewed in (Xu et al., 2017)).

Functionally, there is consent about the fact that histone methylations are partially associated with heterochromatin, whereas histone acetylations are mainly associated with euchromatin. However, there are exceptions from this concept, e.g. where H3K4me3 is associated with an active state of a gene locus (Santos-Rosa et al., 2002).

One mode of action in which histone modification alters chromatin accessibility is by changing the net charge of histones, thereby weakening interaction with DNA (reviewed in (Bannister and Kouzarides, 2011)). Another mode of action involves chromatin-associated factors (reviewed in (Bannister and Kouzarides, 2011)). There is a steadily growing list of such proteins that are capable of recognizing

specific histone modifications and in consequence recruit further histone modifying enzymes (e.g. HATs and HDACs) or promote histone repositioning, thereby e.g. allowing access to previously occluded transcription factor binding sites that in turn contribute to enhance/repressed transcription of adjacent loci via specific TFs (reviewed in (Bannister and Kouzarides, 2011)).

An active field of research deals with the question, how the epigenetic histone modification landscape of a cell's chromatin is propagated to the chromatin of daughter cells during proliferation. A basic model of modification propagation that was suggested by Alabert et al., works as follows: In context of DNA replication modified histones of the parental DNA are locally removed and subsequently re-deposited in a site-specific manner onto both parental and daughter DNA together with new unmodified histone subunits. Thereby, existing histone marks are propagated to the newly synthesized DNA strand in a precise symmetric way, consequently cutting e.g. methylation levels within a patch of DNA into half. To fully restore the original chromatin states the new histones become modified according to their histone neighborhood (Alabert et al., 2020).

That indeed histone modifications and correlated transcriptional alterations in context of an *in vivo* IEC-related mouse model have major impact on intestinal homeostasis has been shown in mouse model with IEC-specific knockout of histone deacetylates 1 (Hdac1) and Hdac2. In this model IECs showed increased proliferation in intestinal crypts, defects in epithelial integrity and signs of chronic inflammation, as identified by altered inflammatory specific gene expression patterns (Turgeon et al., 2013). Further studies from the same research group indicate that conditional IEC-specific Hdac1/Hdac2 loss enhances also sensitivity to DSS induced colitis (Turgeon et al., 2014).

1.4.4 Genome Mapping of H3K27ac and H3K27me3 Histone Marks to Study Epigenetics in IECs

Two antagonizing and thus commonly studied histone modifications (H3K27ac and H3K27me3) are both found at lysine residue 27 of histone 3. H3K27ac correlates with transcription activation, however H3K27me3 correlates with transcription repression. In different studies performed using various cell types, H3K27ac was found at both proximal and distal promoter regions around TSS of expressed genes (Creyghton et al., 2010), however the repressive H3K27me3 mark was found more in the intergenic and intron regions (Yang and Wilson, 2018).

There is also specific knowledge about the two histone modifications in IECs. Chen M et al. identified 56 differentially expressed candidate genes that could be potential targets of differential H3K27ac patterns on certain typical enhancers in a chronic DSS induced colitis model (Chen et al., 2019). Furthermore, Li Y. et al. showed that IL-6/STAT3 pathway regulates intestinal epithelial barrier function by affecting the enrichment of H3K27ac in the promoter regions of intestinal barrier-related Claudin genes (*CLDN1* and *CLDN2*) in the human colon mucosal epithelial cell line NCM460 (Li et al., 2021). In addition to the active histone marks, the repressive histone marks are also associated with DSS

induced colitis. For example, Takeshima et al. showed that DSS induced colitis in mice can cause aberrant H3K27me3 patterns and they suggested that those are involved in cancerization of IECs (Takeshima et al., 2012).

All these findings indicate that H3K27ac and H3K27me3 are two important epigenetic markers having responsibility for IECs function and intestinal homeostasis. Thus, these two histone modifications are worth to be studied in combination with the analysis of *de facto* colitis induced transcriptional alterations in IECs and even more in the context of disease chronification taking place in IBD patients or is mimicked in murine models such as the DSS colitis.

1.4.5 Basic Workflow of ChIP-Seq Experiments

ChIP-on-Chip (Chromatin immunoprecipitation analyzed by tiling microarray) and ChIP-Seq (ChIP analyzed by DNA sequencing) has been proven to be very useful to study positional protein-DNA interactions and histone modifications on a genome-wide scale (Ren et al., 2000; Simon et al., 2001; Barski et al., 2007; Johnson et al., 2007; Robertson et al., 2007). However, ChIP-Seq is superior to ChIP-on-Chip thanks to better signal-to-noise ratios and higher mapping resolution (Ho et al., 2011).

ChIP-Seq analysis is a multi-step experimental procedure (Figure 8). ChIP-Seq protocols start with crosslinking of protein-DNA complexes typically by formaldehyde (Landt et al., 2012). Following the crosslinking, the cells are lysed in an appropriate lysis buffer to make the chromatin, where protein-DNA complexes reside, accessible. Next, the chromatin is fragmented until defined chromatin fragment length distribution is obtained. The fragmentation can be done either enzymatically by micrococcal nuclease (MNase) digestion or by physical fragmentation using sonication (Landt et al., 2012). Defined narrow length distribution is critical for sufficient mapping resolution later in the analysis. In the next step, monoclonal or polyclonal antibodies are used to specifically target the protein or histone modification of interest (in this thesis H3K27ac and H3K27me3) fixed to individual DNA fragments that reflect genomic regions of interest (Landt et al., 2012). During this ChIP procedure, involving agarose or magnetic beads, other proteins and residual chromatin is omitted. Afterwards, obtained antibody-protein-DNA complexes are proteolytically degraded leaving only ChIP-enriched DNA fragments that are finally amplified and sequenced (Landt et al., 2012).

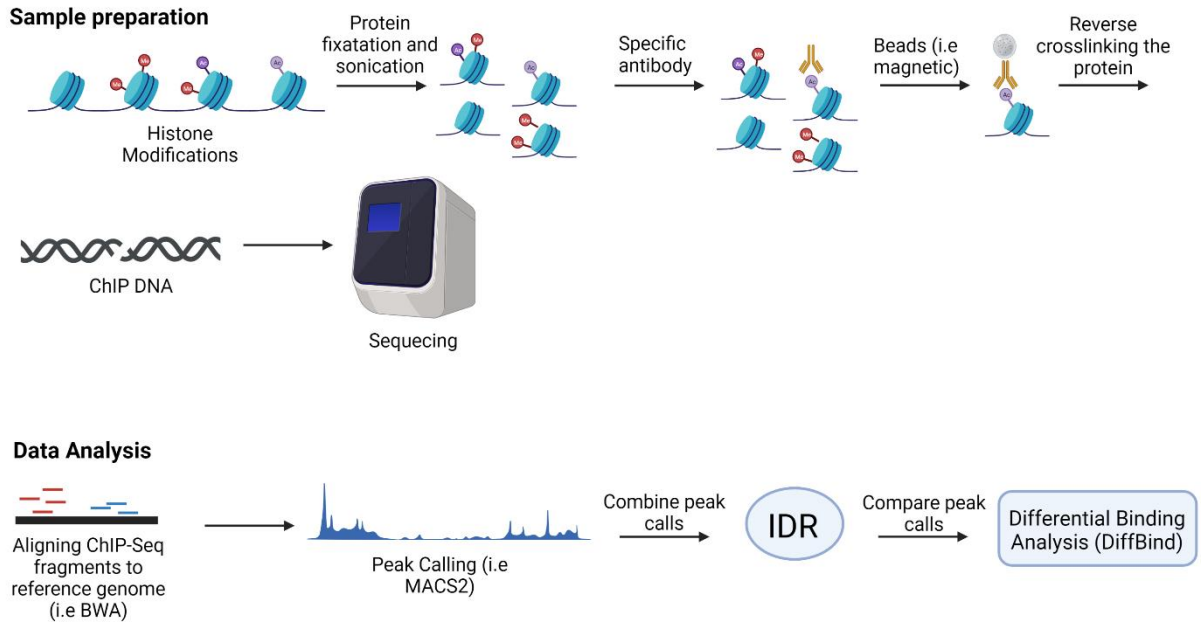

Figure 8: Basic workflow of ChIP-Seq. The figure was created with BioRender.com (2022).

The sequencing reads from the ChIP-DNA fragments (generally in FASTQ format) are mapped to a reference genome by using alignment algorithms such as Bowtie (Langmead et al., 2009), Bowtie2 (Langmead and Salzberg, 2012) and BWA (Li and Durbin, 2009). Genomic sites with high read mapping frequencies are indicative of specific ChIP enrichment and hence indicate sites of protein/histone modification occurrence interpreted as a peak. Next, peak calling steps are performed to determine significantly enriched peak regions across the genome in reference to control samples, e.g. non-ChIP – enriched input DNA. Amongst available peak calling algorithms, Model-based Analysis of ChIP-Seq (MACS) is one of the most used peak caller algorithm (Zhang et al., 2008). It has been shown that most ChIP-Seq signals that come from histone modification marks do not produce point-source transcription-factor-like narrow signals with strong localized ChIP enrichment. Instead, they can have very broadly enriched regions (e.g. H3K27me3) (Barski et al., 2007; Pepke et al., 2009), resembling broad peaks. However, other histone modifications such as H3K27ac can also produce narrow peaks, according to ENCODE statement (Online presence of ENCODE Consortium). Importantly, peak calling algorithms such as MACS2 need to be aware of the expected peak shape in order to work properly.

Integration of biological ChIP-Seq replicates is often performed by calculating an irreproducible discovery rate (IDR) to identify most reproducible peaks with high consistency between replicates (Li et al., 2011). The IDR algorithm uses significance ranking of ChIP regions, e.g. by fold enrichment, to find a transition point in the ChIP enrichment's signal to noise ratios of the biological replicates to identify consistent ChIP-regions in both replicates (Landt et al., 2012). To finally identify genomic regions with differential ChIP enrichment between two experimental conditions an algorithm for differential ChIP enrichments is applied. Differential binding analysis of ChIP-Seq peak data (DiffBind) is a commonly used algorithm for this purpose (Stark R et al., 2011; Ross-Innes et al., 2012). DiffBind

initially finds consensus ChIP-regions that positionally overlap between two experimental conditions and subsequently checks for differential counts of sequencing reads within these regions. To so, elaborate cross-sample normalization of read-counts is performed, in order to compensate for technical variations in ChIP-enrichment and differences in sequencing depth, finally resulting in the calculation of a normalized fold-difference value for differential ChIP-enrichment together with a statistical significance estimation for each individual consensus peak-region.

1.5 Investigating the Immunological and Microbial Alterations in IBD Using the DSS Colitis Model

There is significant crosstalk between CECs and leukocytes in the colon indicating their potential role in immune regulation across the intestinal barrier. In addition to that, CECs are in close contact with bacterial products and their associated signaling mechanisms occurring in the lumen of the colon. Any damage to the epithelial barrier due to a plethora of triggers (e.g. DSS) would result in disruption of its integrity, creating an easy access passage for the luminal microbiome and their antigens causing a subsequent immune response (Figure 9).

Such inflammatory processes are associated with the disruption of microbiota homeostasis due to their imbalanced distribution, also known as dysbiosis. However, it still remains elusive whether dysbiosis is the reason or result of IBD. Since the immunological response to altered microbiota composition and their products contribute to the progression of the disease, it is very important to investigate such changes on a deeper level in order to understand the pathogenesis of IBD and find new therapeutic targets. Correlating these immunological and microbiome changes with epigenetic (specifically H3K27ac and H3K27me3 histone modifications) and transcriptomic alterations in the CECs during different stages of colitis using the DSS colitis model would provide us with the possibility to unravel the complex behavior of our immune system on an interactive pedestal (Figure 9). This would further help us understand whether the commensal antigens play a pro-inflammatory or immunosuppressive role through the interaction between the CECs and activated immune cells.

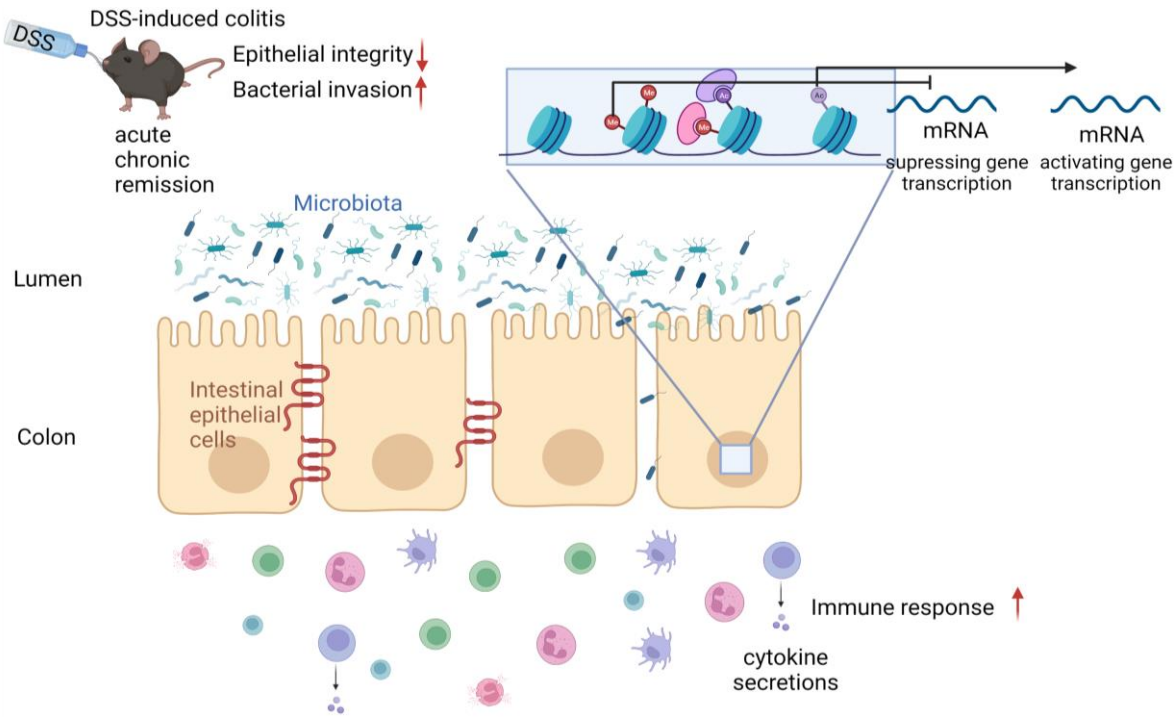

Figure 9: Epigenetic, transcriptomic and immunological changes after environmental triggers such as DSS. DSS damages the intestinal epithelial barrier, and therefore bacteria and their components can translocate into the colon which will activate immune cells. Damage in CECs may induce changes in histone modifications such as H3K27ac (can activate gene transcription) and H3K27me3 (can suppress gene transcription). The figure was created with BioRender.com (2022).

1.5.1 Immunological Changes during Colon Inflammation

By damaging the epithelial integrity, DSS allows the luminal bacteria and their products to enter the colon leading to the triggering of immune cells. These activated immune cells further contribute to the inflammatory environment by producing cytokines and chemokines.

As a first defense mechanism, neutrophils are the first innate immune cells to be recruited to the site of inflammation where they can fight invaded microorganisms by producing reactive oxygen species (ROS) and by releasing neutrophil extracellular traps (NETs) (reviewed in (Rosales et al., 2016)). Neutrophils can have a dual role during inflammation. They can be beneficial through contributions to immune cell recruitment as well as promoting the mucosal healing process by secreting mediators that can help resolution of inflammation (reviewed in (Fournier and Parkos, 2012; Wéra et al., 2016)). On the contrary, when neutrophils are excessively needed and accumulated in the inflamed tissue it can exaggerate IBD conditions by causing extensive tissue injury due to the release of toxic products and extensive transepithelial migration (reviewed in (Fournier and Parkos, 2012)).

Other innate immune cell subsets are eosinophils, which have an important role in fighting parasitic infections. On top of that, they also have functions in autoimmune diseases such as autoimmune myocarditis, primary biliary cirrhosis, IBD, etc. (reviewed in (Diny et al., 2017)). Eotaxin is the selective chemokine for eosinophils (Ponath et al., 1996; Rothenberg et al., 1996) and it is constitutively

expressed (mRNA) in the different human tissues, and it reaches the highest expression levels in the small intestine and colon where the eosinophils reside (Garcia-Zepeda et al., 1996). Matthews AN. et al. showed that eotaxin deficient mice exhibit reduced eosinophil numbers in the jejunum compared to wild-type mice indicating that eotaxin is an important regulator of eosinophils under healthy conditions (Matthews et al., 1998). Eosonophils do not only have immunoregulatory roles by presenting antigens, secreting cytokines etc., but also have effector functions by releasing their granula proteins, lipid mediators etc. (reviewed in (Kita, 2011)). Elevated numbers of eosinophils can be seen in different gastrointestinal disorders such as eosinophilic gastrointestinal diseases, celiac disease, parasitic infections and IBD (reviewed in (Mehta and Furuta, 2015)).

Monocytes, macrophages and dendritic cells are other members of innate immunity. When blood monocytes are recruited in the inflamed tissue, they can differentiate into macrophages or dendritic cells. Macrophages and dendritic cells can distinguish harmful antigens from harmless ones, which is important in the colon mucosal environment inhabiting commensal microbiota and dietary products. Therefore, they have an important role in eliminating pathogenic microorganisms by providing tolerance to harmless antigens. Unlike the macrophages in other tissues, residual mucosal macrophages do not trigger pro-inflammatory responses after getting stimuli to the Toll-like receptor (TLR) in steady state in colon, however TLR responsive proinflammatory macrophages accumulate during DSS colitis (Bain et al., 2013). CD11b+CD103+ dendritic cells can migrate mesenteric lymph nodes (MLNs) to present antigens and therefore regulate T cell response, although (CX3CR1+) *lamina propria* mononuclear phagocytes stay in the mucosa and may maintain Teff and Tregs (reviewed in (Varol et al., 2010)).

The adaptive immune system includes T lymphocytes (CD4+ and CD8+ T cells) and B lymphocytes that compose of the effector cells of cellular and humoral immune responses, respectively (Molnar and Gair, 2015). Naïve T cells further divide into two compartments as CD4+ and CD8+ T cells (Molnar and Gair, 2015). Foreign antigens are presented by APCs to CD4+ cells via MHC-II and to CD8+ cells via MHC-I receptors (Molnar and Gair, 2015). CD4+ T cells are clustered as either Th1 (mainly secrete IFN-γ and express the transcription factor T-BET) or Th2 (mainly secrete IL-4 and express the transcription factor GATA), Th17 (mainly secrete IL-17 and express the transcription factor RORγt), and Tregs (mainly secrete TGF-β and express the transcription factor FOXP3) (reviewed in (Kostic, 2010)).

The role of Tregs during inflammation has shown to be indecipherable due to the high disparity in scientific findings and opinions on the same. Sakaguchi et al. demonstrated that CD4+CD25+ cells limit the immune response to self as well as non-self antigens (Sakaguchi et al., 1995). Later, Itoh et al. showed that these immunosuppressive CD4+CD25+ T cells are generated in the thymus (Itoh et al., 1999). It was later found that Forkhead-Box-Protein P3 transcription factor (*Foxp3*) is necessary for the development and function of CD4+CD25+ T cells (Fontenot et al., 2003). However, some subpopulations of induced Tregs (iTregs) such as Tr1 do not express *Foxp3*, whereas activated CD4+ T

cells in the presence of anti-inflammatory cytokine IL-10 generate Tr1 which have immunosuppressive functions exerted mainly by the released of IL-10 (Groux et al., 1997; Vieira et al., 2004).

According to their origin, Tregs are divided into two subgroups in humans as well as in mice: natural Tregs (nTregs) that develop in the thymus recognizing self-antigens which are presented by MHC-II molecules on APCs and iTregs which peripherally develop from CD4+ T cells in the presence of IL-2, TGF-β and retinoic acid (reviewed in (Ciurkiewicz et al., 2020)). In order to distinguish nTregs from iTregs, Helios expression can be used as a marker (Thornton et al., 2010). Furthermore, nTregs also express a high level of neuropilin-1 (NRP1) (Bruder et al., 2004; Yadav et al., 2012) (Figure 10).

Due to the fact that nTregs and iTregs are generated at different sites, i.e. thymus and periphery, respectively, the antigen repertoire of nTregs is associated with self-peptides (Jordan et al., 2001), and that of iTregs is associated with non-self-specific antigens (Kretschmer et al., 2005). iTregs react to non-self-specific antigens of microbial products in the gut as well as food antigens which is important for maintaining immune tolerance (reviewed in (Cosovanu and Neumann, 2020)).

Due to the very distinctive environment of the intestine, there must be a proper balance between the Teff that fight against the pathogens and the Tregs that tolerate the dietary and commensal antigens. Even though the primary induction of the disease does not require T cells in the DSS colitis model (Dieleman et al., 1994; Axelsson et al., 1996), they are later associated with the chronic stage of disease (Dieleman et al., 1998). Additional to the conventional T cells, atypical γδ+ intraepithelial T lymphocytes are also beneficial to maintaining the colonic epithelium in DSS treated C57BL/6 mice (Chen et al., 2002).

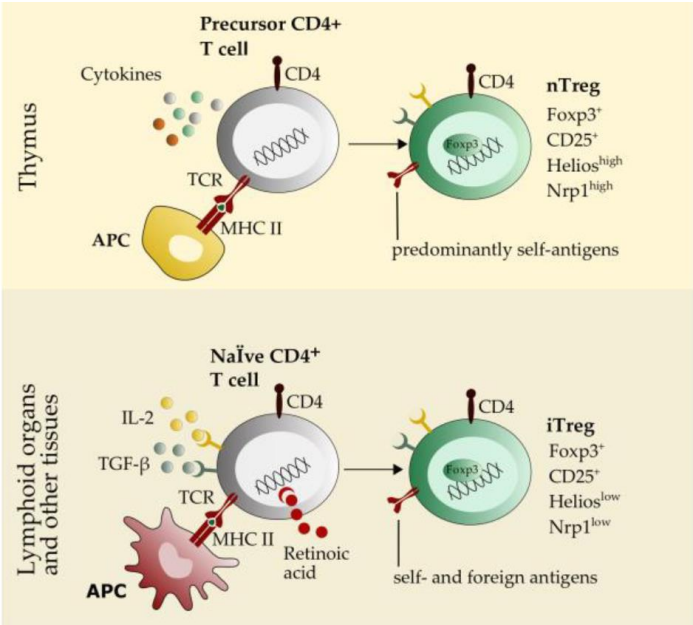

Figure 10: Types of Tregs: nTregs and iTregs. Both types of Tregs express high levels of FOXP3 as well as CD25. nTregs are generally differentiated from iTregs based on their high expression of Helios and NRP1. nTregs are generated in the thymus whereas iTregs are derived from conventional T cells in the presence of IL-2, TGF-β, and retinoic acid in the periphery. nTregs mainly respond to self-antigens and iTregs are responding to both self and foreign antigens (adapted from (Ciurkiewicz et al., 2020)).

Furthermore, the polarization of T cells is associated with the DSS resistance, for instance, BALB/c mice are resistant to DSS colitis due to their Th2/Th17/Treg-polarized immunity while the C57BL/6 mice on the other hand are sensitive to DSS due to Th1 polarization (Yang et al., 2017). Even though CD8+ T cells receive lesser attention than CD4+ T cells in IBD studies, there do exist some contradictory findings that show their protective role in inflammatory bowel disease in mice (Ménager-Marcq et al., 2006; Endharti et al., 2011), as well as some showing their contribution to intestinal inflammatory processes (Nancey et al., 2006; Westendorf et al., 2006).

Although very few is known about the contribution of B cells to IBD, it has been shown that CD11b+ B cells but not CD11b- B cells can ameliorate DSS-induced colitis and they are the main resource of the IgA production (Fu et al., 2021). Moreover, Tregs and B cells are important for the amelioration of DSS induced colitis, and additionally, it was indicated that they can collaborate together (Tregs expansion is promoted by B cells and IgA induction of B cells is supported by Tregs) to suppress DSS colitis and maintain tissue homeostasis (Wang et al., 2015).

Together, all these immune cells secrete many different cytokines and chemokines, dysregulation of which will exaggerate the pro-inflammatory environment. After extracting *lamina propria* CD4+ T cells from IBD patients as well as healthy controls and stimulating them *in vitro*, the Th1 cytokine IFN-γ was increased and the Th2 cytokines IL-4 and IL-5 were decreased in *lamina propria* CD4+ T cells in CD (Fuss et al., 1996). On the other hand, IFN-γ levels stayed normal, IL-4 levels were decreased and IL-5 levels were increased in the *lamina propria* CD4+ T cells for lesional UC compared with control (Fuss et al., 1996). Hence, CD is considered a Th1-related disease and UC is thought to be associated with Th2-type responses (Fuss et al., 1996). Alex et al. showed that acute DSS colitis represented a Th1-Th17 immune response through increased levels of TNF-α, IL-6, IL-17 and KC levels when compared with control groups (Alex et al., 2009). However, compared to acute colitis, chronic the DSS groups demonstrated Th2 immune response by increasing IL-4 and IL-10 and accompanying the decrease in TNF-α, IL-17 and KC levels according to a biometric multiplex assay from the serum of DSS colitis mice (Alex et al., 2009). Therefore, they suggested that Th1/Th17 mediated immune response is seen in acute DSS colitis and it is taken over by Th2 mediated immune response in chronic DSS colitis (Alex et al., 2009).

In summary, both the innate and adaptive immune systems play significant roles in maintaining the homeostasis of the gut tissue. According to different studies, different immune cell subsets associated with disease progression and characterization, therefore detailed studies during different stages of disease are needed to further to enlighten this complex mechanism.

1.5.2 Dysbiosis during IBD and DSS Colitis

While the exact etiology of IBD remains unclear, one of the potential hypotheses proposes that IBD results from an excessive immune response triggered by environmental factors against the altered gut microbiota in a genetically predisposed host. Humans have an estimated 10^{14} microbes in their intestinal tract, and a very big portion of this count resides in the colon. Microbiota alterations/imbalances (known as dysbiosis) are frequently seen in IBD but it is not clear whether dysbiosis is the reason or the result of the disease. Dysbiosis is not only associated with IBD (Frank et al., 2007; Alam et al., 2020), but is also linked with many different systemic diseases such as obesity (Ley et al., 2006), autism (Finegold et al., 2002), type 1 diabetes (Wen et al., 2008) etc. Moreover, microbial diversity decreases in IBD patients compared to healthy controls (Alam et al., 2020) (Figure 11). Antibiotics have been in trend to treat IBD, however broad-spectrum antibiotics lead to several side effects due to their unspecific targeting to beneficial gut bacteria which can metabolize food, produce vitamins and other nutrients for the host, generate anti-microbial substances, support intestinal integrity and homeostasis, reduce and prevent colonization of harmful pathogens.

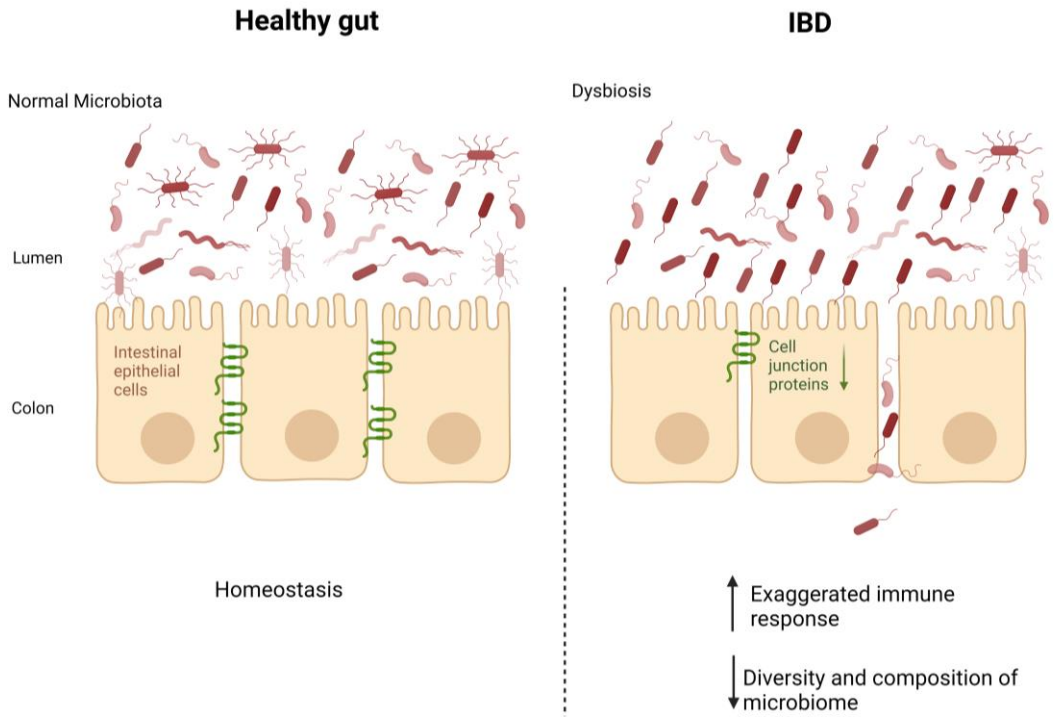

Figure 11: IBD and microbial dysbiosis. IBD is associated with barrier breakdown and microbial dysbiosis. Barrier dysfunction in IBD will facilitate translocation of commensal microbiota into the colonic tissue, which will result in the activation of immune cells, and subsequent exaggerated immune response. Moreover, the diversity and composition of the microbiome will decrease during IBD compared to the healthy gut. The figure was created with BioRender.com (2022).

Even though human and mouse gut microbiome share 90% and 89% similarities in phyla and genera after cut off abundance threshold, respectively (Krych et al., 2013), there are still some differences between human and mouse microbiota. Mouse intestine is rich of several microbial genera such as

Lactobacillus, *Alistipes* and *Turicibacter*, however microbes such as *Prevotella*, *Faecalibacterium* and *Ruminococcus* are more abundant in the human intestine and *Clostridium*, *Bacteroides* and *Blautia* have similar abundance in both the organisms (reviewed in (Nguyen et al., 2015)). Therefore, due to the microbial disparity, findings in animal models may not essentially reflect the entire situation in the human system.

Lactobacillus consists of gram-positive anaerobic bacteria. Exposure of probiotic *Lactobacillus* strain *Lactobacillus kefiri CIDCA 8348* reduced the proliferation of anti-CD3/CD28-activated entero-adhesive *Escherichia coli*-specific *lamina propria* T cells, decreased the pro-inflammatory cytokines (TNF-α, IFN-γ, IL-6 and IL-13) and suppressed the NF-κB pathway (Curciarello et al., 2021). Moreover, beneficial effects of the genus *Lactobacillus* have been shown in strain *Lactobacillus acidophilus* species (*KBL402 and KBL409*) by improving DSS-induced colitis symptoms, downregulating inflammatory cytokines and chemokines, increasing the production of anti-inflammatory IL-10 (by *KBL402*) or Tregs (by *KBL409*) and restoring the diversity of gut microbiota in DSS-induced colitis model (Kim et al., 2021). Mutant *Lactobacillus reuteri F-9-35* decreased the DSS symptoms, decreased the expression of pro-inflammatory cytokines *Tnf*, *Cox-2* and *Il-6* and restored the gut microbiota of DSS colitis treated mice (Sun et al., 2018). Another research used 2 different *Lactobacillus reuteri* strains (rat-derived *R2LC* and human-derived ATCC *PTA 4659* (4659)) to see whether they can protect the mice against DSS induced colitis and they found decreased colitis severity, reduced inflammatory markers and increased mucus thickness showing the protective effect of *Lactobacillus reuteri* strains against DSS colitis (Ahl et al., 2016). *Limosilactobacillus* split from the genus of *Lactobacillus* in 2020 and is now determined as a new genus of lactic acid bacteria (Zheng et al., 2020). Seo H. et al. developed an anti-inflammatory probiotic *Limosilactobacillus reuteri EFEL6901*, and they showed that the administration of this strain to DSS treated mice alleviates DSS symptoms, increases the expression levels of tight junction proteins (E-cadherin and Claudin-3), downregulates the pro-inflammatory cytokines (*Tnf* and *Il-1β*), upregulates the anti-inflammatory cytokines (*Il-10*) and increases the concentration of short chain fatty acids (lactate and butyrate) compared to DSS mice not treated with probiotic, suggesting the therapeutic potential of *EFEL6901* for treating IBD (Seo et al., 2021). All these results clearly demonstrated the beneficial effects of the *Lactobacillus* and *Limosilactobacillus* genus on gut health.

Another gram-positive bacteria *Turicibacter*, mostly found in the animal gut was recently shown as a possible target microorganism that is positively correlated to the development of colitis (Shang et al., 2021). Moreover, DSS decreased the diversity of the microbiome and caused dysbiosis, and one of the many microorganisms identified, *Turicibacter*, was positively correlated with the acute DSS group in fecal and colonic samples of mice (Munyaka et al., 2016).

Prevotella is a genus of gram negative bacteria. It is abundant in fecal microbiota of non-Western *versus* Western populations (Clemente et al., 2015). Since *Prevotella* is highly abundant in the human gut, it

might indicate that it is beneficial in nature, however many studies have conflicting thoughts on this assumption. Different studies showed that different species of *Prevotella* can be associated with exaggeration of DSS colitis symptoms (Dziarski et al., 2016; Iljazovic et al., 2021). Moreover, *Prevotella* is one of the many genera that shows a significant increase in UC patients as compared to the control group (Gryaznova et al., 2021).

In summary, the gut microbiome includes many beneficial bacteria such as *Lactobacillus* and *Limosilactobacillus* which are important for maintaining and protecting mucosal integrity. Even though it is unknown whether dysbiosis is causing IBD or it is the consequences of the disease, the diversity and composition of the microbiome have a very crucial role in the prevention and treatment of the disease. Some bacteria such as *Turicibacter* and *Prevotella* are associated with colitis. Therefore, they may represent interesting targets to specifically regain gut microbiome composition and subsequent gut homeostasis.

1.6 Aims of the Thesis

Intestinal inflammation and epithelial barrier breakdown are associated with broad changes in the gene expression profile of CECs. There is evidence that at least part of these transcriptional alterations are the consequence of epigenetic changes involving histone modifications. The impact of posttranslational histone modification on maladaptive processes during chronic inflammatory conditions at the intestinal barrier remains largely unknown. We hypothesize that inflammation-induced epigenetic imprinting in CECs would promote perturbation rather than resolution of intestinal inflammation. In order to test this hypothesis, five specific aims were addressed within this thesis:

Aim 1: to assess inflammation-induced histone modification in the intestinal epithelium at different disease states the DSS colitis model had to be established and comprehensively characterized. This model would enable us to reflect different disease stages in mice: acute colitis, chronic colitis and the according remission phases. Characterization of the model comprised next to determination of the disease activity index and the histopathological score a detailed characterization of the innate and adaptive immune cell compartment in the colonic *lamina propria*, the colonic cytokine and chemokine profile as well as the intestinal microbiota composition at different stages of DSS induced colitis.

Aim 2: to isolate CECs from mice at different stages of DSS colitis to perform bulk RNA-seq analysis.

Aim 3: to use the same CEC pool for the generation of genome-wide maps for the two specific histone modifications Histone H3 Lysine 27 acetylation (H3K27ac) and Histone H3 Lysine 27 trimethylation (H3K27me3) by ChIP-Seq analysis.

Aim 4: to apply comprehensive bioinformatic data mining to correlate genome-wide histone modifications (H3K27me3 and H3K27ac) with the transcriptional profile of CECs at different stages of DSS colitis.

Aim 5: to validate selected target genes that were identified in aim 2 by flow cytometry and to correlate their epigenetic modification / expression (aim 5) with disease-specific immunological alterations in the inflamed tissue.

2. Materials

2.1 Buffers and Solutions

FACS Buffer
PBS (Ph=7.4), 2 % (v/v) FCS, 2 mM EDTA

cOmplete™, Mini Protease Inhibitor Cocktail
1 tablet resolve in 7 ml NP40 cell lysis buffer

0.2 % NaCl and 1.6 % NaCl
MilliQ

1.5 M NaCl
87.66 g NaCl (M=58.44 g/mol) in 1000 ml MilliQ

0.15 M NaCl
1:10 dilution of 1.5 M NaCl

DMEM Complete
10 % FCS (v/v)

RPMI 1640 Medium, GlutaMax Complete
2 % FCS (v/v), 100 U/ml penicillin and streptomycin

HBSS, No Calcium, No Magnesium Complete
10 mM HEPES

Predigestion Solution
HBSS (no Ca^{+2}, Mg^{+2}, 10 mM HEPES) containing 5 mM EDTA, 5 % FCS, 1 mM DTT freshly before each preparation

HBSS with Calcium and Magnesium Complete
10 mM HEPES

Digestion Solution
HBSS (with Ca^{+2}, Mg^{+2}, 10 mM HEPES) containing 5 % FCS freshly before each preparation

PB buffer Complete
PBS, pH=7.2 containing 0.5 % FCS

2.2 Antibodies

Used antibodies are shown below. All antibodies were diluted according to their dilution factors that are determined by titration experiments before usage. Fixable viability dyes were used for flow cytometry to exclude death cells.

Fixable viability dyes used for experiments

Fixable Viability Dye eFlour® 780, eBioscience
Fixable Viability Dye eFlour® 506, eBioscience
Zombie Aqua™ Fixable Viability Kit, BioLegend
Zombie NIR™ Fixable Viability Kit, Biolegend

Table 1: FACS panel used for CECs sorting

Surface Antibodies:

Antibody	Conjugation	Clone	Manufacturer
EpCAM (CD326)	BV421	G8.8	BioLegend
CD45	PerCP-Cy5.5	30-F11	BioLegend
CD31	APC	390	BioLegend

Table 2: FACS panel used for determination of leukocyte subpopulations

Surface Antibodies:

Antibody	Conjugation	Clone	Manufacturer
CD170	FITC	S17007L	BioLegend
Ly6C	PerCP-Cy5.5	HK1.4	BioLegend
CD24	PE	M1/69	BioLegend
CD8a	PE-Cy5	53-6.7	BioLegend
CD4	PE-Cy7	RM4-5	BioLegend
CD11c	APC	N418	BioLegend
Ly6G	AlexaFluor 700	1A8	BioLegend
CD11b	APC-Cy7	M1/70	BioLegend
CD64	BV421	X54-5/7.1	BioLegend
CD45	BV605	30-F11	BioLegend
I-A/I-E	BV711	M5/114.15.2	BioLegend

Table 3: FACS panel used for determination of T cell subsets

Surface Antibodies:

Antibody	Conjugation	Clone	Manufacturer
CD45	PE/Fire™ 640	30-F11	Biolegend
CD3	APC/Fire™ 810	17A2	Biolegend
TCR γ/δ	BV711	GL3	BD Biosciences
CD4	Spark YG™ 593	GK1.5	Biolegend
CD8a	AF700	53-6.7	Biolegend
CD25	Vio Bright V423	REA568	Miltenyi
CD44	BV605	IM7	Biolegend
CD62L	PE-Cy7	MEL-14	Biolegend
CD45R/B220	Biotin	RA3-6B2	Biolegend
NK1.1		PK136	Biolegend
CD11b		M1/70	Biolegend
CD11c		N418	Biolegend

Anti-Biotin Antibodies:

Antibody	Conjugation	Clone	Manufacturer
Anti-Biotin	VioGreen	REA746	Miltenyi

Intracellular Antibodies:

Antibody	Conjugation	Clone	Manufacturer
FOXP3	Vio R667	REA788	Miltenyi
KI67	AF532	SolA15	ThermoFisher Scientific
HELIOS	PE-Vio 615	REA829	Miltenyi
RORγt	BV650	Q31-378	BD Biosciences
T-BET	KIRAVIA Blue 520	4B10	Biolegend
GATA3	PE	16E10A23	Biolegend

Table 4: FACS panel used for determination of protein expression for RNA-Seq identified genes in CECs

Panel 1 Surface Antibodies

Antibody	Conjugation	Clone	Manufacturer
EpCAM	BV421	G8.8	Biolegend
CD31	AF488	390	Biolegend
CD45	PerCp-Cy5.5	30-F11	Biolegend
I-A/I-E (MHCII)	BV650	M5/114.15.2	Biolegend
I-Ak (MHCII)	APC	REA610	Miltenyi
CD177	AF700	1171A	R&D Systems
H-2Kb/H-2Db (MHCI)	PE-Cy7	28-8-6	Biolegend

Panel 1 Intracellular Antibodies

Antibody	Conjugation	Clone	Manufacturer
IDO1	PE	mIDO-48	Invitrogen

Panel 2 Surface Antibodies

Antibody	Conjugation	Clone	Manufacturer
EpCAM	BV421	G8.8	Biolegend
CD45	BV750	30-F11	Biolegend
CD31	AF488	390	Biolegend
CD80	PE	16-10A1	Biolegend
CD86	APC-Cy7	GL-1	Biolegend
CD40	PE-Cy5	3/23	Biolegend

Panel 2 Intracellular Antibodies

Antibody	Conjugation	Clone	Manufacturer
iNOS	PE-Cy7	CXNFT	Invitrogen
CD74	AF647	In1/CD74	Biolegend

Table 5: Antibodies used in ChIP-Seq Experiments

Antibody	Clonality	Manufacturer
Anti-histone H3 (acetyl k27) antibody	Polyclonal	Abcam
Histone H3K27me3 antibody	Polyclonal	Active Motif

2.3 Consumables

Table 6: Chemicals

Product	Catalog Number	Manufacturer
16 % Formaldehyde, Methanol Free	12606	Cell Signalling
BD FACS™ Clean	340345	BD Bioscience
BD FACS™ Flow	342003	BD Bioscience
BD FACS™ Rinse	340346	BD Bioscience
BD FACS™ Shutdown	334224	BD Bioscience
BD Horizon™ Brilliant Stain Buffer	563794	BD Bioscience
BD™ CompBead Plus Negative Control	51-9006227	BD Bioscience
Brilliant Stain Buffer	563794	BD Bioscience
cOmplete™, Mini Protease Inhibitor Cocktail	11836153001	Roche
DL-Dithiothreitol (DTT)	D0632	Sigma-Aldrich
DMEM	41965-039	Gibco
EDTA	E6758-500G	Sigma-Aldrich
Ethanol, 100 %	8025	Baker
Ethanol, absolute	2246.1000	CHEMSOLUTE®
FCS	P4047500	PAN Biotech
HBSS	14025-050	Gibco
HBSS, no calcium, no magnesium	14170-088	Gibco
hemoCARE	005031	CAREdiagnostica
HEPES (1M)	15630080	Gibco
IMDM	31980-022	Gibco
Linear Acrylamide	AM9520	Invitrogen
Lysing Matrix D	116913100	MP Biomedicals
MilliQ	_	_
NaCl	3975.2	Carl Roth
NH_4OAc	A2706-100ml	Sigma-Aldrich
NP40 Cell Lysis Buffer	FNN0021	Invitrogen
Paraformaldehyde	252549-1L	Sigma-Aldrich
PBS	14190-094	Gibco
PBS Tablets	18912-014	Gibco
PBS, pH=7.2	20012027	Gibco
Penicillin-Streptomycin	15070-063	Gibco
Penicillin-Streptomycin	15070-063	Gibco/Invitrogen
Percoll	17-0891-01	GE Healthcare
RLT Buffer	79214	Qiagen
RNA*later*™ Stabilization Solution	AM7024	Invitrogen
RNase*Zap*™ RNase Decontamination Solution	AM9780	Invitrogen
RPMI 1640,GlutaMAX™ Supplement	61870036	Gibco
ß-Mercaptoethanol	1001090202	Sigma-Aldrich
Trypan blue	15250-061	Gibco
UltraComp eBeads™ Compensation Beads	01-2222-41	Invitrogen

Table 7: Kits

Product	Catalog Number	Manufacturer
MAGnify™ Chromatin Immunoprecipitation System	492024	Invitrogen
RNeasy Mini kit	74104	Qiagen
DNA-*free*™ DNA Removal Kit	AM1906	Invitrogen
Lamina Propria Dissociation Kit, mouse	130-097-410	Miltenyi Biotec
MinElute PCR Purification Kit	28004	Qiagen
LEGENDplex™ Mouse Inflammation Panel (13-plex)	740446	BioLegend
LEGENDplex™ Mouse Proinflammatory Chemokine Panel (13-plex)	740451	BioLegend
Foxp3/Transcription Factor Staining Buffer Set	00-5523-00	eBioscience
Pierce™ BCA Protein Assay Kit	23225	Thermo Fischer
Pierce™ Bovine Serum Albumin Standard Ampules	23209	Thermo Fisher

2.4 Ethics

Experiments were performed according to institutional regulation license (Landesamt für Verbraucherschutz, Sachsen-Anhalt; file ID: AZ 42502-2-1521 UniMD and 42502-2-1691 UniMD). Mice were sacrificed by CO_2 or isoflurane inhalation.

3. Methods

Note: Parts of the method section (3.1-3.4, 3.6-3.9) were taken directly or were paraphrased from the below mentioned publication:

Gelmez E, Lehr K, Kershaw O, Frentzel S, Vilchez-Vargas R, Bank U, Link A, Schüler T, Jeron A, Bruder D. Characterization of Maladaptive Processes in Acute, Chronic and Remission Phases of Experimental Colitis in C57BL/6 Mice. Biomedicines. 2022; 10(8):1903. https://doi.org/10.3390/biomedicines10081903.

3.1 Establishing and Scoring DSS induced Colitis

11-13 weeks old female C57BL/6JRj mice obtained from the same vendor (Janvier) and the same breeding barrier (U02) were used for the animal experiments. Pathogen-free conditions were provided for all experimental mice at the central animal facility of the Medical Faculty of the Otto-von-Guericke-University, Magdeburg. Animal experiments were approved by the local authorities (Landesamt für Verbraucherschutz, Sachsen-Anhalt) under license ID AZ 42502-2-1521 UniMD or 42502-2-1691 UniMD. Mice were sacrificed by CO_2 inhalation or isoflurane inhalation. Mice received *ad libitum* 2 % (w/v) DSS (36-50 kDa, MP Biomedicals) in their drinking water for 6 days to establish acute and acute remission (recovery phase of acute) experimental groups. Subsequently, remission group received normal drinking water for further 19 days to recover. To establish chronic phase and chronic remission (recovery phase of chronic) stage of disease, mice were provided *ad libitum* with 1.7 % (w/v) DSS for 6 days a total of three cycles, containing 14 days recovery period with normal drinking water in the first 2 DSS cycle. After completion of the third DSS cycle, chronic remission mouse group received normal drinking water for additional 21 days for recovery. Acute control and chronic control mice received normal drinking water during all experimental period. Body weight of mice was determined on experimental day 0 and this specific weight was used as a reference to determine relative body weight loss. Relative weight loss was monitored regularly. Combination of relative weight loss, consistency of stool and presence of blood in stool was used to determine disease activity index (DAI). When blood was not macroscopically detectable, presence of the blood in the stool was determined by hemoCARE kit (CARE diagnostica, Germany). DAI scoring details can be found below in Table 8. After slightly stretching the colon and cecum tissue on a tissue paper to align the colon and the cecum in a right angle, colon and cecum length were measured by ruler. After removing the cecum part and cleaning the colon from feces with ice cold PBS and drying it with tissue paper, weight of colon was measured by an analytical balance.

Table 8: Scoring of DAI in DSS colitis

DAI	Weight Loss	Stool Consistency	Bleed in Feces
0	0-5 %	Normal stool	Normal stool/ hemoCARE test (-)
1	5-10 %	Slightly loose stool	Blood is not detectable macroscopically/ hemoCARE test (+)/ occult blood +
2	10-15 %	Loose stool but still shaped	Blood is not detectable macroscopically/ hemoCARE test (+)/ occult blood ++
3	15-20 %	Loose stool, not shaped	Blood is detectable macroscopically/occult blood +++
4	20-25 %	Mucus only	Blood is detectable macroscopically/gross bleeding

3.2 Histopathological Evaluation of the Colon

Dr. Olivia Kershaw (Freie Universität Berlin) performed histopathological analysis. Shortly, after mice were sacrificed, intact colon and cecum tissues were placed together in histology cassettes. Subsequently, histology cassettes were kept in 4 % PFA at the 4 °C until they were transferred to Dr. Olivia Kershaw. Formalin fixed paraffin embedded (FFPE) tissue slices, were stained with hematoxylin and eosin (HE). To determine histopathological tissue damage, the following criteria were used: infiltration of immune cells (Chelakkot et al., 2017), epithelial damage (Chinen et al., 2011; Chelakkot et al., 2017), extent of damage (Dieleman et al., 1998), percentage of tissue exhibiting inflammation (Dieleman et al., 1998). Details of scoring criteria can be found in Table 9 below. Since terminal region of the rectum and anorectal junction can exhibit inflammation due to the expected diarrhea, these areas were excluded from the histopathological analysis.

Table 9: Histological scoring

Histological changes	Score: 0	Score: 1	Score: 2	Score: 3	Score: 4
Infiltration of immune cells	no inflammation	around crypt base	into mucosa	extensive mucosal infiltration and oedema	into submucosa
Epithelial damage and loss of goblet cells	intact	slight loss of goblet cells	considerable loss of goblet cells and slight loss of intestinal crypts	extensive loss of intestinal crypts	
Extent	none	mucosa	mucosa and submucosa	transmural	
Percent involvement		1-25 %	26-50 %	51-75 %	76-100 %

This table were already represented in submitted manuscript (Gelmez et al., 2022).

3.3 Isolation of Colonic Epithelial Cells and Colonic *Lamina Propria* Leukocytes

CECs were isolated according to the recommendations given in the protocol of the Lamina Propria Dissociation Kit (Miltenyi Biotec), which allows to isolate intraepithelial lymphocytes with few modifications. Shortly, feces were washed away with ice cold PBS. Afterwards, colon was cut longitudinally and then cut into ~0.5-1 cm pieces. Incubation period was performed in a heated (37 °C) incubator with sample agitation. Tissue pieces were incubated for 20 min at 37 °C with shaking at ~200 rpm in 20 ml pre-digestion solution which was prepared according to Lamina Propria Dissociation kit protocol. Afterwards, tubes were vortexed for ~10 seconds and subsequently cells were passed through a 100 µm cell strainer. Cells were kept on ice, and tissue pieces were incubated, vortexed and filtered one more time. Filtered cell suspensions were pooled, centrifuged. Cells were stained with antibodies

listed in Table 1 to perform RNA-Seq and ChIP-Seq experiments or they were stained with antibodies listed in Table 4 to validate RNA-Seq results.

The remaining colon tissues were enzymatically digested according to the protocol provided with the Lamina Propria dissociation kit from Miltenyi Biotec, which is designed to isolate *lamina propria* leukocytes from the colon. Total leukocytes from digested colon samples were obtained by density gradient centrifugation (20 min, 1800 rpm, room temperature, without rotor brake) using Percoll™ (GE Healthcare, Sweden) (density: ~1,041 g/ml). Then, supernatant was discarded; the leukocyte pellet was washed once with ice cold PBS in order to get rid off the remaining Percoll artifacts. Approximately half of the volume of the isolated leukocyte suspension was used for following FACS analysis of leukocyte panel (Table 2) or approximately entire of the volume of isolated leucocyte suspension was used for FACS analysis of T cell panel (Table 3).

3.4 Isolation of Splenocytes and Mesenteric Lymph Node Cells

Spleens were weighted on an analytical balance and either the complete or an approximately 50 % of balanced fraction of the spleen was used for isolation of splenocytes. Afterwards, spleen was placed in a 100 µm cell strainer and meshed through the strainer using a syringe plunge into 6-well plate including ice cold sterile PBS. Cell suspension was transferred into a 15 ml falcon tube, the tube was centrifuged (10 min, 1200 rpm, 4 °C) and supernatant was discarded. Next, erythrocyte lysis was performed by resuspending cell pellet with 5 ml 0.2 % NaCl for 15-30 seconds. Subsequently, 5 ml 1.6 % NaCl was added to stop the reaction by providing physiological osmolarity. Next, cells were passed through a 70 µm cell strainer and centrifuged (10 min, 1200 rpm, 4 °C). Supernatant was discarded, pellet was resuspended in ice-cold FACS buffer and aliquot was stained with FACS antibodies (Table 2).

Mesenteric lymph nodes (MLNs) were placed in a 70 µm cell strainer and meshed through the strainer using a syringe plunge into 6-well plate including ice-cold sterile PBS to release leukocytes. Next, cell suspension was transferred into 15 ml falcon tube and the tube was centrifuged (10 min, 1200 rpm, 4 °C). Supernatant was discarded; pellet was resuspended in ice-cold FACS buffer and and aliquot was stained with FACS antibodies (Table 2).

3.5 Fluorescence Activated Cell Sorting

For sequencing of CECs, cells which were obtained according to section 3.3 were incubated with Fixable Viability Dye eFluor 780 (eBioscience) and TruStain FcX (anti-mouse CD16/32) antibody (Biolegend) to block the unspecific binding of antibody to the Fc receptors which are expressed by B cells, monocytes, macrophages, dendritic cells etc. for 10 min at 4 °C in the dark. Next, cells were split into two parts to be used for ChIP-Seq and RNA-Seq experiments and thereafter, centrifuged (1200 rpm, 10 min, 4 °C). Cells reserved for the ChIP-Seq experiments were treated with PBS containing methanol-

free formaldehyde (1 %) for 10 minutes at room temperature (RT) by occasionally inverting the tube for fixation of the cells. Subsequently, glycine (0.125 M) was added on top and the tube was inverted occasionally for 5 min at RT to stop the formaldehyde activity. Then, cells were centrifuged (1200 rpm, 10 min, 4 °C) and were stained with surface antibodies (Table 1) diluted in FACS buffer for 10 minutes at 4 °C in the dark. After cells were washed, cells were suspended in DMEM (10 % FCS) medium to increase survival of CECs during sorting period. Next, cell suspension was pass through a 30 µM cell strainer and cells were sorted in DMEM containing medium. Then, cell number was manually determined by Neubauer hemocytometer additional to cell number determined by the cell sorter. Afterwards, cell suspension was centrifuged and supernatant was discarded carefully. Next, ~50 µl lysis buffer containing protease inhibitor (Magnify™ Chromatin Immunoprecipitation System, Invitrogen) were added to the cell pellet for every 10^6 cells. If less than 10^6 cells were obtained, ~50 µl lysis buffer containing protease inhibitor was added to the cell pellet. Finally, cells were vortexed, kept around 5 min on ice and were stored at -80 °C until further use.

After live-death and Fc block incubation, cells reserved for RNA-Seq experiments were stained with surface staining antibodies (Table 1) without any fixation. After cells were washed, cells were suspended in DMEM (10 % FCS) medium and were pass through a 30 µM cell strainer. Then, cells were sorted in DMEM containing medium. After sorting, cells were centrifuged and supernatant were discarded. Next, cell pellet was resuspended in 350 µl RLT buffer and were stored at -80 °C until further use.

For cell sorting BD FACSAria™ III Cell Sorter was used. UltraComp eBeads™ Compensation Beads (Invitrogen) or splenocytes were used for compensation parameters for single stainings.

3.6 Flow Cytometry

For FACS staining of leukocytes, cells isolated according to section 3.3 and 3.4 were transferred into in a 96-well round (U) bottom plate. Cells were pre-treated with TruStain FcX Antibody and Fixable Viability Dye eFluor 506 (eBioscience) or equivalent Zombie Aqua Fixable Viability dye (BioLegend). CompBead Plus Negative Control beads (BD Biosciences) were used to determine absolute cell number of colon leukocytes. A suspension of CompBeads was prepared in PBS and Neubauer hemocytometer was used to determine bead concentration. 20,000 CompBeads/well were added to each colon leukocyte sample and cells were incubated with TruStain FcX blocking and viability staining for 10 min at 4 °C in the dark. Cells were washed once with FACS buffer (centrifugation: 1200 rpm, 5 min, 4 °C).

Next, cells were incubated with surface antibodies (Table 2) diluted in FACS buffer for 10 min at 4 °C in the dark. Afterwards, cells were fixed with 2 % paraformaldehyde (in PBS) for ~20 min at 4 °C in the dark, centrifuged (1200 rpm, 5 min, 4°C), resuspended with 200 µl FACS buffer and finally analyzed on an Attunue NxT flow cytometer (Thermo Fisher). UltraComp eBeads™ Compensation Beads were used for single staining for compensation. Splenocytes were used for single staining for the viability

dye. FlowJo (version 9.9.6) software was used to analyze Flow cytometry data. Marker choice and gating strategy is based on a published research paper by Yu Y.R. et al. (Yu et al., 2016). Details on the gating strategy for all compartments can be found in the figure below for colon (Figure 12) and in the Supplementary Figure 1 and Supplementary Figure 2 for MLN and spleen.

Details of gating strategy according to published paper (Yu et al., 2016) as well as according to our few modifications for colon is described below (Figure 12).

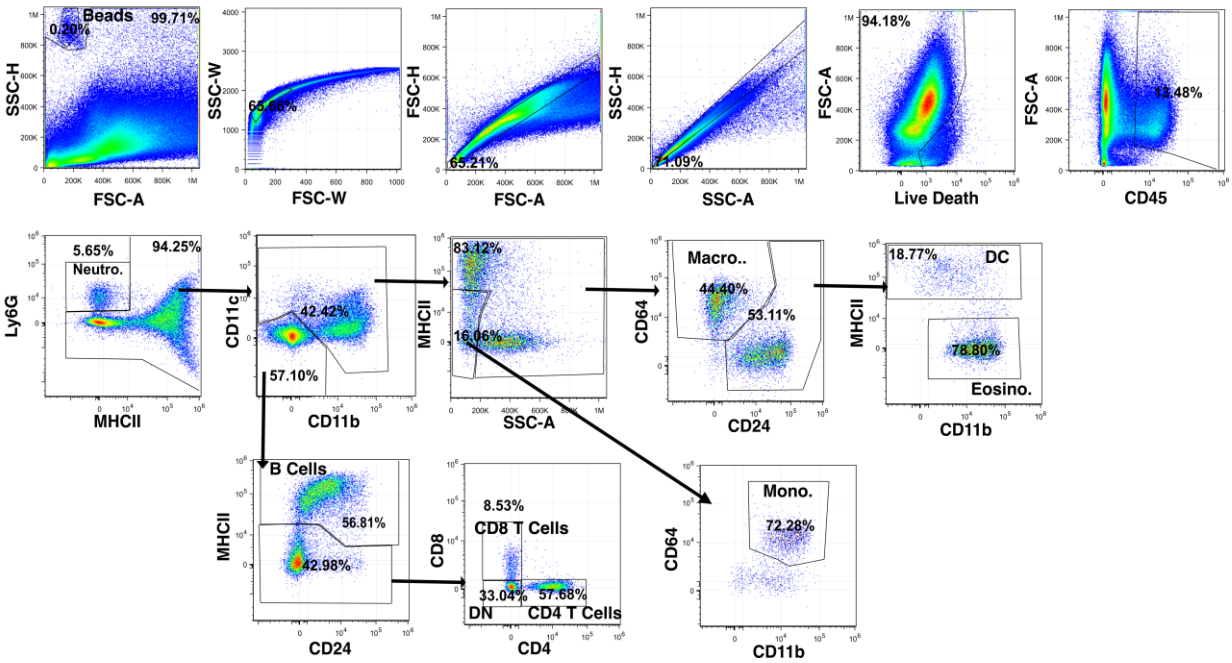

Figure 12: Representative gating strategy used to identify immune cell subsets in the colon. Gating for colon leukocytes was performed according to a research paper published in 2016 by Yu et al. with few modifications (Yu et al., 2016). Counting beads were excluded by SSC-H/FSC-A gating. Cell debris and doublets were eliminated by sequential gating on FSC/SSC parameters (SSC-W vs FSC-W, FSC-H vs FSC-A, SSC-H vs SSC-A). Dead cells were excluded and viable leukocytes were identified by CD45 staining. Neutrophils were identified by Ly6G expression. CD11b and CD11c staining was used to differentiate the myeloid cells from CD11b-CD11c- lymphoid immune cells. B and T lymphocyte subsets were determined by B cell-specific surface markers (MHCII and CD24). Next, CD4+ and CD8+ T cells were determined by gating on CD4 and CD8 cell surface markers. Lymphoid cells negative for CD4 and CD8 lineage markers were considered as double negative (DN) lymphoid cells. MHCII expression and SSC characteristics were used to further subdivide myeloid cell populations. MHCII- and SSC low populations include monocytes (CD11b+CD64+). Macrophages (CD64+CD24-) were separated from MHCII and SSC high populations. Finally, eosinophils (MHCII-CD11b+) were separated from dendritic cells. Figure and figure legend have already been published in (Gelmez et al., 2022).

For FACS staining of T cells, leukocytes isolated according to section 3.3 were transferred into in a 96-well round (U) bottom plate together with CompBead Plus Negative Control beads (BD Biosciences). A suspension of CompBeads was prepared in PBS and Neubauer hemocytometer was used to determine bead concentration (20,000 Compbeads/well). Next, cells were pre-treated with TruStain FcX Antibody and Zombie NIR™ Fixable Viability Kit (BioLegend) for 10 min at 4 °C in the dark. Cells were washed once with FACS buffer (centrifugation: 1200 rpm, 5 min, 4 °C). Then, cells were incubated (10 min at 4 °C in the dark) with surface antibodies (Table 3) diluted in FACS buffer and appropriate amount of

Brilliant Stain Buffer from BD Biosciences (50 µl for each well) to prevent fluorescent dye interactions which can result with staining artifacts. Next, cells were washed once with FACS buffer (centrifugation: 1200 rpm, 5 min, 4 °C) and then cells were incubated with anti-biotin (Table 3) antibody diluted in FACS buffer for 10 minutes at 4 ° C in the dark. Afterwards, cells were washed with FACS buffer. Next, the Invitrogen™ eBioscience™ Foxp3/Transcription Factor Staining Buffer Set protocol was followed for intracellular staining. Shortly, 100 µl Foxp3 Fixation/Permeabilization solution were added to each well for around 30 min at 4 °C in the dark. Afterwards, cells were washed by 1X Permeabilization buffer (centrifugation: 1200 rpm, 5 min, 4 °C). Next, cells were incubated with intracellular antibodies (Table 3) diluted in 1X Permeabilization buffer for around 1 hour at 4 °C in the dark. Then, cells were washed 2 times with 1X Permeabilization buffer (centrifugation: 1200 rpm, 5 min, 4 °C). Finally, cell pellet was resuspended in ice-cold FACS buffer and measured on an ID7000™ Spectral Cell Analyzer (Sony). In case of T-BET, GATA-3, RORγt, negative cells were defined with the corresponding fluorescence-minus-one (FMO) controls. UltraComp eBeads™ Compensation Beads or cells were used for single stainings. FlowJo (version 10) software was used to analyze Flow cytometry data.

The identification of different T cell subsets started with gating the counting beads to use them later to determine absolute cell number of individual immune cell subtypes. Next, cell debris and cell doublets were excluded by different gating strategies (FSC-H vs FSC-A, SSC-H vs SSC-A), afterwards dead cells and lineage positive cells (NK.1.1+, CD11b+, CD11c+, CD45R/B220+) were excluded and live leukocytes were determined by CD45 staining. CD3+ cells were gated from live dead- lineage- CD45+ cell population. Afterwards, CD4+ and CD8+ T lymphocytes were identified within the CD3+ T cells according to their unique CD4 and CD8 expression, respectively. Next, TCRγδ-CD4+ T cells were gated according to FOXP3 expression. FOXP3+HELIOS- iTregs and FOXP3+HELIOS+ nTregs were identified and excluded from conventional T cells and subsequently analysed for KI67 expression. Afterwards, remaining conventional T cells were further gated to determine different conventional T cell subsets according to expression of T-BET (Th1), GATA-3 (Th2) and RORγt (Th17) and to identify protein expression of KI67 (Figure 13).

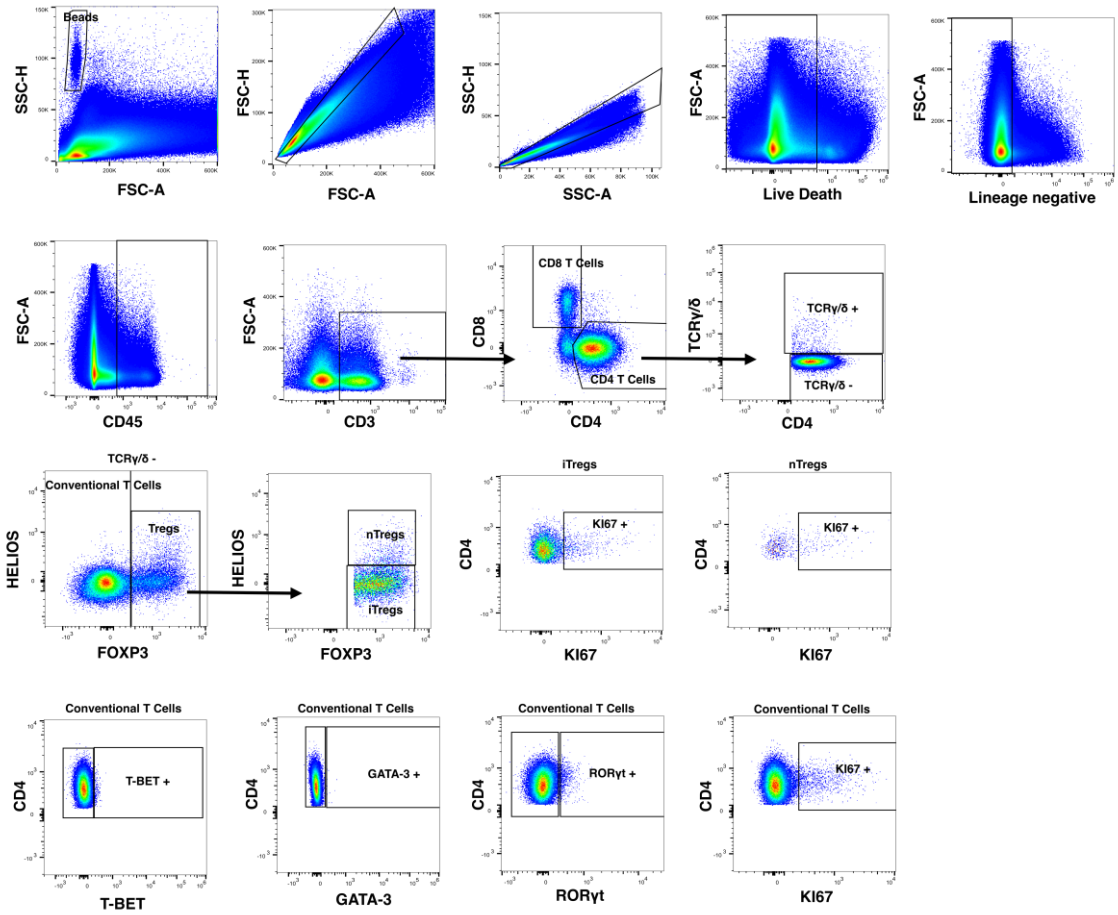

Figure 13: Representative gating strategy used to identify subpopulations of CD4+ T cells in the colon. Details of gating strategy can be found in text above.

To determine protein expression of genes identified by RNA-Seq in CECs, CECs isolated according to section 3.3 and were transferred into in a 96-well round (U) bottom plates. Next, cells were pre-treated with TruStain FcX Antibody and Zombie Aqua Fixable Viability Kit (BioLegend) for 10 min at 4 °C in the dark. Cells were washed once with FACS buffer (centrifugation: 1200 rpm, 5 min, 4 °C). Then, cells were incubated (10 min at 4 ° C in the dark) with surface antibodies (Table 4) diluted in FACS buffer. Next, cells were washed once with FACS and above described intracellular staining protocols were followed using intracellular antibodies depicted in Table 4. FACS analysis was performed using an ID7000™ Spectral Cell Analyzer (Sony). In case of I-A/I-E, I-Ak, CD177, IDO1, CD80, CD86, CD40, iNOS and CD74 negative cells were defined with the corresponding FMO controls. Small intestinal epithelial cells and LPS treated splenocytes were analyzed by using the same FACS panel too. UltraComp eBeads™ Compensation Beads or splenocytes were used for compensation parameters for single stainings. FlowJo (version 10) software was used to analyze Flow cytometry data.

Absolute cell count for colon samples was calculated as follows: (V/v) · s · (B/b), with V: total volume of FACS buffer used to resuspend the cell pellet, v: partial volume used for FACS staining, s: events obtained for a given immune cell population, B: added CompBeads number (20,000 beads/well), b: acquired effective CompBeads number. In case an immune cell population was counted with less than

100 events per sample, this population was excluded from calculations of absolute cell number calculation and frequency of CD45+ cells. In case a sample had less than 2000 events of CD45-positive cells, the sample was completely discarded from the calculation of absolute cell numbers and frequency.

3.7 Quantification of Cytokines and Chemokines in Plasma and Colon

Blood samples were collected from the mice by cardiac puncture and were filled into 20 µl EDTA (0.5 M) including Eppendorf tubes which were centrifuged for 10 min at 500 x g at 4 °C to obtain platelet-free plasma. Next, supernatants were transferred into new Eppendorf tubes. Afterwards, samples were centrifuged one more time at maximum speed at 4 °C. Then, supernatant were transferred into new Eppendorf tubes and stored at -80 °C until further use.

To determine cytokine and chemokine concentrations in the colon, colons were first cleaned from feces and were washed with ice-cold PBS. Next, colons were opened longitudinally, and were cut into small tissue pieces which were mingled and split into four approximately equal portions. One of this portion was put into lysis Matrix Tubes D (MP Biomedical) including 500 µl NP40 Cell lysis buffer (Thermo Fischer) with protease inhibitors (cOmplete™ Mini Protease Inhibitor Tablets, Roche, one tablet for 7 ml extraction buffer). Afterwards, tissues were homogenized by a FastPrep instrument (MP Biomedical) with setup of 40 seconds at a speed of 6.0 m/s. Homogenized samples were centrifuged at 10,000 x g for 10 min at 4 °C and supernatant was collected and transferred into new Eppendorf tubes. Samples were stored at -80 °C until further use. Remaining colon tissue portions were frozen at -80 °C as a backup material.

To standardize subsequent cytokine/chemokine detection in colon tissue samples, total protein concentration of samples was determined by BCA assay (see below).

To determine cytokine concentrations in blood plasma, and to determine cytokine and chemokine concentrations in tissue homogenates, LEGENDplex mouse inflammation panel (IL-23, IL-1α, IFN-γ, TNF-α, MCP-1, IL-12p70, IL-1β, IL-10, IL-6, IL-27, IL-17A, IFN-b, GM-CSF) and LEGENDplex Mouse Proinflammatory Chemokine Panel (RANTES, MCP-1, IP-10, Eotaxin, TARC, MIP-1α, MIP-1β, MIG, MIP-3α, LIX, KC, BLC, MDC) (both from BioLegend) were used following the manufacturer's recommendation. LegendPlex assays were measured on Attune NxT flow cytometer (Thermo Fisher). Data were analyzed using Biolegend's cloud bases LEGENDplex analysis software (version 2021.07.01). Cytokine and chemokine levels were normalized to total protein concentration obtained from BCA assay.

3.8 BCA Assay

Pierce™ BCA Protein Assay Kit (ThermoFischer) was used to identify total protein concentration of colon tissue homogenates. Pierce™ Bovine Serum Albumin Standard Ampules (Thermo Fisher) was

used to create standard curves. Isotonic saline 0.9 % (Fresenius Kabi GmbH) were used to dilute the standards and samples (Dilution factor: 1:5).

3.9 Microbioata Analysis

Feces samples were collected at day 0, 6, 20, 26, 40, 47, 56 from control chronic mice and 0, 6, 20, 26, 40, 47, 67 from chronic remission mice. Feces samples were stored at -80 °C until DNA extractions. DNA extraction as well as data analysis were performed in collaboration with Prof. Dr. Alexander Link, Ramiro Vilchez-Vargas and Konrad Lehr, Department of Gastroenterology, Hepatology and Infectious Diseases, OVGU, Magdeburg. DNA was extracted from feces samples using QIAamp Fast DNA Stool Mini Kit (Qiagen). Amplicon libraries were generated by amplifying the V1-V2 region of the 16S rRNA gene after 20 cycles PCR reaction using the 27F and 338R primers and sequencing on an Illumina MiSeq (2×250 bp, Illumina, Hayward, California, USA) (Camarinha-Silva et al., 2014; Chaves-Moreno et al., 2015).

All fastQ files, generated after sequencing and demultiplexing, were analyzed using dada2 package version 1.14.1 in R (Callahan et al., 2016). Resulting in a unique table containing all samples with the sequence reads (Phylotype) and their abundance. 69 samples were resampled to equal the smallest library size of 11414 reads using the phyloseq package version 1.30.0 in R (McMurdie and Holmes, 2013). Sequences reads were taxonomical annotated with the ribosomal database project (Maidak et al., 1997), based on the naïve Bayerisian classification (Wang et al., 2007) with a pseudo-bootstrap threshold of 80%. In addition, the first 100 more abundant phylotypes in the cohort were manually annotated with the NCBI database using the Blast-Algorithm (Altschul et al., 1990; Database resources of the National Center for Biotechnology Information, 2016). Microbial community were analyzed at the taxonomic rank of genus in relative abundances (expressed as percentages). The complete list of identified taxa is available in the online supplement of the published paper by (Gelmez et al., 2022).

PCO clustering and multivariate tests (Anosim and Permanova) were performed in Primer 7, based on a Bray-Curtis resemblance measurement at the taxonomic rank of genus (Clarke, 1993; Anderson, 2001; Clarke and Gorley, 2015). Differences in the distribution of genera between the following experimental days of each group were calculated by the Mann-Whitney U unpaired test with 95 % confidence interval, by using the ExactRankTest package version 0.8-29 in R. The resulting p values were corrected by applying the Benjamini-Hochberg false-discovery rate correction (desired FDR = 5 %) (Hochberg and Benjamini, 1990).

3.10 Isolation of RNA

RNA for RNA-Seq experiments was isolated from CECs (CECs were isolated according to section 3.3) using the RNeasy Mini Kit from Qiagen following the manufacturer's recommendations. At the end of the protocol, RNA was eluted with 100 µl RNase free water. Afterwards, ethanol precipitation was performed to concentrate RNA. For precipitation, 2 µl linear polyacrylamide (LPA), 50 µl 7.5 M ammonium acetate and 375 µl absolute ethanol (pre-cooled to -20 °C) was added to the eluted RNA. RNA was precipitated for a minimum of 2 hours or over night at -80 °C followed by centrifugation at 17.000xg for 30 min at 4 °C. Next, supernatant was discarded carefully, washed twice with 80 % ethanol (pre-cooled to -20 °C), and finally the pellet was dried at 37 °C. Pellet was reconstituted in RNase free water. Potential DNA contaminations within isolated RNA were digested with DNA-free™ Removal Kit from ThermoFisher according to manufacturer's protocol. Afterwards, RNA concentrations were photometrically quantified by Nanodrop (ThermoFisher). Additionally, quality and integrity of RNA-Seq samples (RNA Quality Number, RQN) was validated with Agilent Technologies 2100 Bioanalyzer (Agilent Technologies; Waldbronn, Germany). Samples with RQN > 6.2 were used in RNA-Seq experiments. RQN of each sample is depicted in Table 10.

Table 10: RQN level of individual RNA-Seq samples

Conditions	RQN level
Control Acute 1	7.1
Control Acute 2	7.2
Acute 1	7.7
Acute 2	8.1
Acute Remission 1	6.7
Acute Remission 2	7.3
Control Chronic 1	7
Control Chronic 2	7.3
Chronic 1	6.3
Chronic 2	8.2
Chronic Remission 1	7.3
Chronic Remission 2	6.8

3.11 Library Preparation, Sequencing and Analysis of RNA-Seq Data

Library preparation and sequencing were performed in the Genome Analytics Group at the Helmholtz Center for Infection Research (HZI) in Braunschweig. Basic data analysis was performed by Dr. Robert Geffers. Shortly, RNA sequencing library was generated from NEBNext Single Cell/Low Input RNA Library Prep (New England BioLabs) according to the manufacture's protocols. The libraries were sequenced on Illumina NovaSeq 6000 using NovaSeq 6000 S2 Reagent Kit (100 cycles, paired end run)

with an average of 5 x10^7 reads per RNA sample. Each FASTQ file got a quality report generated by FASTQC tool (Andrews S. 2010). Before alignment to reference genome each sequence in the raw FASTQ files was trimmed on base call quality and sequencing adapter contamination using Trim Galore! wrapper tool (Krueger F. 2012). Reads shorter than 20 bp were removed from FASTQ file. Trimmed reads were aligned to the reference genome (mm10) using open source short read aligner STAR (Dobin et al., 2013) (https://code.google.com/p/rna-star/) with settings according to log file. Feature counts (Liao et al., 2014) were determined using R package "Rsubread". Only genes showing counts greater 5 at least two times across all samples were considered for further analysis (data cleansing). Gene annotation was done by R package "bioMaRt" (Durinck et al., 2005). Before starting the statistical analysis steps, expression data was $\log_2$ transformed and TMM normalized (edgeR). Differential gene expression was calculated by R package "edgeR" (Robinson et al., 2010). PCA plots were created by using $\log_2$ counts per million reads mapped (CPM) values. To create volcano plots, each DSS model group was individually compared with its corresponding control. Transcripts with log2 CPM values < 1 in at least one of the 2 replicates were excluded. Transcripts not fulfilling the CPM criterion in all conditions were excluded as well. Transcripts with a fold change (FC) in gene expression of $|\log_2 FC| > 1$ and a false discovery rate (FDR) of FDR < 0.05 in a pair-wise generalized linear model quasi-likelihood F test (glmQLFTest), implemented in edgeR, were considered significantly regulated. To identify differentially expressed (DE) genes between all DSS conditions, compared with their corresponding controls, global generalized linear model quasi-likelihood F test (glmQLFtest) was performed. Filtering details for DE genes were: Genes with $\log_2$ CPM < 1 in all 12 samples were excluded. Finally, only genes with $|\log_2 FC| > 1$ in at least one experimental condition and FDR < 0.05 were kept. Hierarchically clustered heatmap graph of differentially expressed genes was prepared using Genesis software (Sturn et al., 2002) based on z-scores of $\log_2$ CPM data. Finally, KEGG pathway and gene ontology enrichment of gene symbols of DE genes was performed using Cytoscape software with ClueGO plugin (Bindea et al., 2009) v2.5.8.

3.12 Chromatin Immunoprecipitation and Reverse Crosslinking

Immunoprecipitation was performed using the Magnify™ Chromatin Immunoprecipitation System (Invitrogen) following the manufacturer's recommendations. Shortly, sorted CECs (section 3.5) were fixed in PBS with 1 % formaldehyde (methanol-free) for 10 min at room temperature, formaldehyde was quenched with Glycin solution, cells were washed with PBS and lysed in lysis buffer (provided in the kit) containing protease inhibitors at a cell density of one million cells per 50 µl. Released chromatin (~50 µl sample) was fragmented with Bioruptor Plus sonication device (Diagenode) for 16 cycles with sonication on for 30 seconds and 30 seconds off at 4 °C.

A proper, reproducible and narrow chromatin fragment-size distribution after sonication is crucial in order to ensure sufficient mapping resolution of IP'd DNA fragments after next-generation sequencing.

Following sonication, chromatin had fragment-sizes between 200 and 600 bp, as recommended for ChIP experiments (Komar et al., 2016; He et al., 2021). Chromatin fragment-size distribution was controlled using a fragment analyzer (Genome Analytics Group, HZI in Braunschweig), before continuing with the ChIP procedure. A representative result for the fragment analysis of chromatin samples is shown below (Figure 14).

For ChIP of histone modifications two different antibodies were used: Histone H3K27me3 antibody (Active Motif) and Anti-histone H3 (acetyl k27) antibody (Abcam). 4.5-5 µg ChIP-antibody per IP was used. ChIP was performed according to the Magnify™ Chromatin Immunoprecipitation Kit (ThermoFisher) protocol. Per sample and per histone modification type, two IP's with ~100,000 cells each were prepared and pooled together at the final DNA purification step of the protocol, to yield ChIP-DNA from a total of ~200,000 cells per IP. For negative controls, input-DNA samples, containing 1/10 of the chromatin amount of the actual ChIP-samples, were saved. ChIP-DNA was reverse-crosslinked according to the Magnify Kit and purified using the MinElute PCR Purifcation Kit from Qiagen according to manufacturer's recommendations.

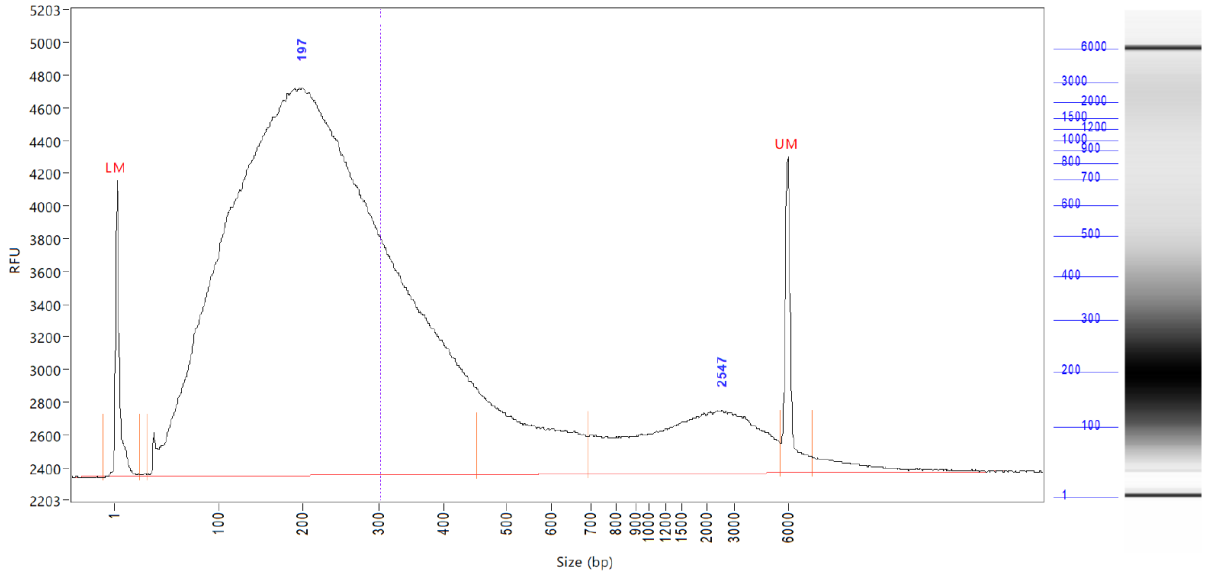

Figure 14: Representative fragment size distribution of sonicated CEC chromatin. Sonicated, reverse-crosslinked, purified chromatin DNA from CECs of untreated mice were analyzed on a Fragment Analyzer (Agilent Biotechnologies). Left: X-axis represents DNA fragment size (in bp), y-axis represents relative fluorescence units (RFU). LM: lower marker (1 bp), UM: upper marker (6000 bp). Blue numbers indicate estimates of most frequent fragment sizes in the distribution. Right: Sub-figure represents a color-coded (black/white) version of the fragment size distribution. Reference fragment sizes are stated in blue. Typically, fragment sizes were between 100 – 300 bp Note: In cooperation with Dr. Robert Geffers (Helmholtz Centre for Infection Research in Braunschweig, Genome Analytics Group).

3.13 Library Preparation, Sequencing and Analysis of ChIP-Seq Data

Library preparation and sequencing were performed by the Genome Analytics Group at the Helmholtz Center for Infection Research (HZI) in Braunschweig. Data analysis for FastQ, FastQC (before and after adaptor trimming for quality control), read alignment and bam file generation were performed by Dr.

Robert Geffers, HZI Braunschweig. Scripts for MACS2 and DiffBind were established by Dr. Robert Geffers as well.

Shortly, DNA sequencing libraries were generated from immunoprecipitated DNA using NEBNext Ultra II DNA Library according to the manufacture's protocols without size selection. The final DNA sequencing library was purified, size controlled by Agilent Technologies 2100 Bioanalyzer (High Sensitivity DNA ChIP) and prepared for sequencing according to the manufacture's protocol (Illumina). The libraries were sequenced on Illumina NovaSeq 6000 using NovaSeq 6000 S2 Reagent Kit (100 cycles, paired end run) with an average of 5 x10^7 reads per sample.

Each FASTQ file got a quality report generated by FASTQC tool. Before alignment to mm10 reference genome each sequence in the raw FASTQ files was trimmed based on base call quality and sequencing adapter contamination using Trim Galore! wrapper tool. Trimmed FASTQ files were aligned to mouse reference genome mm10 using BWA aligner.

From BAM files, binned read coverages across the mouse genome were calculated by the multiBamSummary function of deeptools version 3.3.2 (Ramírez et al., 2016) and visualization was performed by deeptool's plotCorrelation function that calculates Pearson correlation coefficients between binned read coverages of all samples. Analysis parameters were: multiBamSummary bins --*bamfiles* (required bam files) --outFileName --*labels* --*numberOfProcessors* max/2 –*outRawCounts* --*ignoreDuplicates* --*scalingFactors* –*centerReads* --*verbose* followed by plotCorrelation --*corData* --*corMethod* (pearson was chosen) --*whatToPlot* (heatmap was chosen) --*plotFile* --skipZeros --*plotFileFormat* svg --*removeOutliers* --*labels* --*outFileCorMatrix* --*plotNumbers*.

Next, peak calling was performed using the MACS algorithm (Model-Based Analysis of ChIP-Seq) (Zhang et al., 2008; Feng et al., 2012) in version MACS 2.2.7.1. H3K27me3 is a broad histone mark (Online presence of ENCODE Consortium) , therefore MACS peak caller algorithm was used with choosing these parameters: macs2 callpeak *-t -c -f* (BAMPE was chosen) *-g* (mm was chosen) *-n --broad -q 0.05 --outdir*, and for narrow histone mark H3K27ac (Online presence of ENCODE Consortium), these parameters were used: macs2 callpeak *-t -c -f* (BAMPE was chosen) *-g* (mm was chosen) *-n --call summits -q 0.05 --outdir*.

Next, the Irreproducible Discovery Rate (IDR) algorithm in version 2.0.4.2 (Li et al., 2011) was used to achieve peak consistency between ChIP-sample replicates (parameters: idr --*samples* --*input-file-type* (broadPeak for H3K27me3 and narrowPeak for H3K27ac) --*output-file* --*output-file-type* (bed was chosen) --*plot* --*idr-threshold 0.05* --*verbose*).

Afterwards, genomic locations of high confidence IDR peaks were annotated in terms of genomic features by using annotatePeak function of ChIPseeker (Yu et al., 2015) package and annotated peaks were visualized by plotAnnoBar and plotDistToTSS functions of ChIPseeker package. ChIPseeker gives

priority to annotations in the following order: promoters, 5' UTR, 3' UTR, exon, intron, downstream and intergenic. Promoters regions were defined as ranging from ±3 kb around TSS.

Moreover, to prove that ChIP region annotations are meaningful and did not occur by chance, randomized non-overlapping versions of high confidence ChIP-region sets were generated with keeping region count per chromosome and region length distribution consistent to experimentally derived ChIP-region sets. This was calculated using the Galaxy repository and it's bedtools ShuffleBed tool (Quinlan and Hall, 2010; Gruening, 2014). Afterwards, bar plots for feature distribution and TSS distances were also created for these shuffled region files.

Before functional term-enrichment analysis, peak sets and corresponding gene symbol annotations were limited to have distances to TSS not more than ± 10 kb. Remaining lists of gene symbols from all DSS model conditions were analyzed by Cytoscape software and the ClueGo plugin (Bindea et al., 2009) to perform KEGG-term over-representation analysis.

To identify differentially histone modified ChIP-regions, the DiffBind algorithm (Stark R et al., 2011; Ross-Innes et al., 2012) in version 3.2.5 in R (version 4.1.0) (R Core Team 2021) was applied. Diffbind needs a target file including the information of sample name, sample assignment to DSS conditions and biological replicates, bam files of ChIP samples and input controls, bed files of IDR high-confindence ChIP regions.

Shortly, DiffBind workflow was as follows:

```
DBA<- dba.blacklist (DBA,blacklist=T, greylist=F)

DBA <- dba.count(DBA, summits = F, bParallel = F, minOverlap=2)

DBA<- dba.normalize (DBA, method=DBA_DESEQ2, normalize=DBA_NORM_LIB, library=DBA_LIBSIZE_FULL)
```

DBA contrast was created for each DSS condition versus it's corresponding control (e.g. in below):

```
DBA <- dba.contrast(DBA,minMembers = 2, group1 = DBA$masks$a_DSS, group2 = DBA$masks$a_healthy,  name1 = "acute",  name2 = "ctr_young")

DBA <-dba.analyze(DBA,method=DBA_DESEQ2, bBlacklist = F,bGreylist = F, bParallel=F)
```

Annotation of significant Diffbind regions was done by using annotatePeakInBatch function of ChIPpeakAnno package (Zhu et al., 2010; Zhu, 2013; Zhu et al., 2017). Below, the main code used for ChIP annotation is stated:

```
annoData <- toGRanges (data = TxDb.Mmusculus.UCSC.mm10.knownGene)

bindingRegion = c(-10000,10000)

c <- annotatePeakInBatch(dba.report(DBA,contrast = i, DataType=DBA_DATA_GRANGES), bindingType="startSite",  bindingRegion = bindingRegion,  AnnotationData = annoData, output= "both", multiple=F , PeakLocForDistance="middle", FeatureLocForDistance="TSS", select="all")

 c <- addGeneIDs(annotatedPeak=c, orgAnn="org.Mm.eg.db", feature_id_type="entrez_id", IDs2Add="symbol")
```

3.14 Statistics

Visualization and statistical analyses were performed by GraphPad Prism Software version 8 or 9.2 (GraphPad Software, Inc., La Jolla, USA), if otherwise not indicated. $P < 0.05$ was considered statistically significant.

4. Results

Note: Parts of the results section (4.1 - 4.3) were taken directly or were paraphrased from the following publication:

Gelmez E, Lehr K, Kershaw O, Frentzel S, Vilchez-Vargas R, Bank U, Link A, Schüler T, Jeron A, Bruder D. Characterization of Maladaptive Processes in Acute, Chronic and Remission Phases of Experimental Colitis in C57BL/6 Mice. Biomedicines. 2022; 10(8):1903. https://doi.org/10.3390/biomedicines10081903.

4.1 Establishing Consecutive Stages of DSS Colitis

This thesis aimed to gain a better understanding regarding the epigenetic and transcriptomic changes in CECs during different stages of the colitis and its contribution to the progression or resolution of intestinal inflammation. Therefore, the initial aim was to set up and extensively characterize the murine DSS colitis model in our laboratory. Since many factors such as sex, age, genetic background, and the hygiene conditions at the distributing vendor can affect the experimental results, 11-13 weeks old female C57BL/JRj mice purchased from the same vendor and the same breeding barrier were used for the experiments.

Mice received 2 % DSS in drinking water for 6 days to induce acute DSS colitis. Then the animals received normal drinking water for the next 19 days to allow them to recover and to establish the remission stage for the acute colitis. Chronic DSS colitis was induced by administrating 1.7 % DSS thrice for 6 days interrupted by 14 days provision of normal drinking water after each cycle. At the end of the third DSS cycle the mice were allowed to recover for the next 21 days by giving them normal drinking water in order to establish the remission phase for the chronic stage of the disease (Figure 15A). Since due to the experimental set up there was an age difference between mice with acute and chronic DSS colitis, two different age-matched control groups, namely control acute and control chronic, were used, respectively. To monitor disease progression, the mice were scored according to relative body weight and disease activity index (DAI). DAI was determined according to weight loss, the softness of stool, and blood in stool.

In Figure 15A, the experimental design of consecutive stages of DSS colitis is represented. As expected, weight loss occurred during each DSS cycle and it continued for several days after termination of DSS treatment. The animals regained their initial weight each time during the water phase. Control mice showed an expected increase in body weight during the duration of the experiment (Figure 15B, Figure 15D). In line with the loss in body weight, DAI increased during each DSS cycle and normalized within a few days after termination of the DSS cycle. However, while mice that experienced three DSS treatment cycles, including the final remission period, were able to compensate their body weight loss, the DAI remained slightly elevated due to persistent alterations in stool consistency, indicative of low-grade residual colon inflammation (Figure 15D, Figure 15E).

As expected, colons became significantly shorter (about 2 cm) during acute and chronic stages of DSS colitis compared to the control groups. Even though colon length largely normalized during the recovery phases, it did not reach the colon length of control animals (Figure 15F), which is in line with the previously mentioned residual DAI score at this time point. Colon inflammation was associated with the accumulation of *lamina propria* leukocytes and the subsequent increase of specific colon tissue weight. Mice with chronic inflammation and both acute and chronic remission stages exhibited a significantly increased colon weight compared to control groups (Figure 15G). In line with this, also the weight of

the spleen increased significantly during chronic inflammation and the according remission stage, indicative of persistent low-level systemic inflammation (Figure 15H).

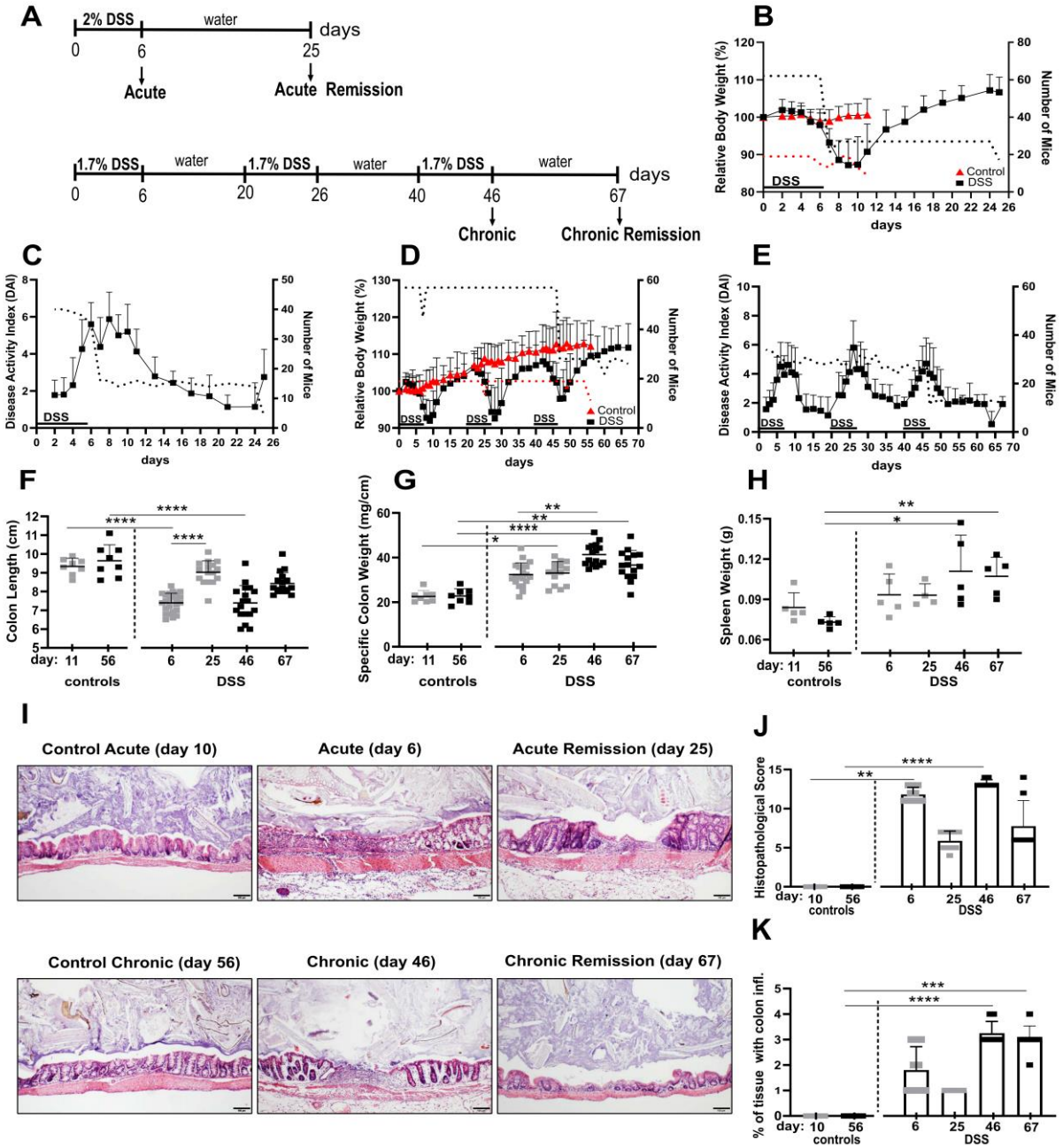

Figure 15: Evaluation of disease activity and histopathological alterations at different stages of DSS colitis. A) Experimental design to induce consecutive stages of DSS colitis. (B,C) Relative body weight (n = 17–62 mice, pooled from 3–5 independent experiments) and disease activity index (DAI; n = 4–40 mice from 1–3 independent experiments) of mice after a single treatment with 2% DSS water for 6 days (acute and acute remission) and relative body weight (n = 9–19 mice pooled from 2–4 independent experiments) of mice for control acute group. D,E) Relative body weight (n = 22–57 mice from 3–4 independent experiments) and DAI (n = 11–34 mice from 1–2 independent experiments) of mice that received three consecutive cycles of 1.7% DSS water (chronic and chronic remission) and relative body weight (n = 11–19 mice pooled from 2–4 independent experiment) of mice for control chronic group. F–H) Colon length, specific colon weight and spleen weight for all mouse groups. Colon length was obtained from 2 independent experiments (n = 8–18 mice) except for the acute DSS colitis group which contains data from 3 independent experiments (n = 24 mice). Specific colon weight was obtained from two independent experiments (n = 8–

16 mice) except for the acute DSS group which contains data from 3 independent experiments (n = 20 mice). Spleen weight was obtained from one experiment (n = 4–5 mice). I) Representative histological pictures of the colons taken after hematoxylin and eosin staining (scale bar: 100 µm). J,K) Histopathological score and percent of tissue exhibiting colon inflammation during different stages of colitis. Histology results were obtained from 2 independent experiments for all mouse groups (n = 8 mice) except for the acute DSS colitis group which contains data from 3 independent experiments (n = 10 mice). Data for control groups are from one experiment (n = 6). (B-E) Dotted lines represent the number of mice for each stated time point. F-H,J,K) Grey squares represent control acute, acute and acute remission conditions and black squares represent control chronic, chronic and chronic remission groups. Data represent mean with error bars indicating standard deviation. Significance was calculated by Kruskal–Wallis test. All groups were compared with each other, significance is indicated only for relevant groups. **** $p < 0.0001$, *** $p < 0,001$, ** $p < 0.01$, * $p < 0.05$. Note: Histology results were obtained in cooperation with Dr. Olivia Kershaw (Freie University Berlin, Institute of Animal Pathology). Figure and figure legend have already been published in reference (Gelmez et al., 2022).

Additional to macroscopic changes, alterations at the microscopic level were also determined (Figure 15I). In the control groups, regardless of their age, neither epithelial inflammation nor damage was observed. Immune cells infiltrated into the submucosa in the acute and chronic DSS colitis stages. However, infiltration of immune cells was restricted to remission stages and immune cells mostly infiltrated into the crypt base or mucosa during recovery periods of DSS. Moreover, acute and chronic DSS colitis was associated with extensive loss of intestinal crypts, and damage was transmural. However, during remission phases, generally slight loss of goblet cells or considerable loss of goblet cells and slight loss of intestinal crypts were detected. Moreover, damage was mostly restricted to the mucosa or both mucosa and sub mucosa (Figure 15I). The total histology score reached the maximum level during chronic and acute stages of intestinal inflammation. The severity of inflammation decreased during remission phases but notably, inflammation did not fully resolve (Figure 15J). In addition, when the percentage of colon tissue exhibiting inflammation was evaluated, the histological score for chronic colitis and the according remission stage was determined as ~3, indicating that 51-75 % of the colon tissue was inflamed. In contrast, while during the acute stage, the score was around ~2, indicating that 26-50 % of the colon was inflamed, the histological score of the acute remission phase was determined as 1, indicating that at this stage only 1-25 % of the colon was still inflamed (Figure 15K). Here, the affected area became significantly larger after the third DSS cycle and remained increased in the according remission phase 3 weeks later.

In summary, different stages of DSS induced colitis were successfully established in our laboratory. As expected, parameters indicating active colitis such as the DAI score, macroscopic as well as microscopic intestinal damage increased during the acute and especially during the chronic phase of colitis. Interestingly, despite full recovery of body weight and partial restoration of other disease parameters during the remission periods, tissue homeostasis was not fully restored within the given observation time. These findings support the initial hypothesis that repeated periods of colon inflammation are associated with the establishment of maladaptive processes that prevent the resolution of intestinal inflammation and support progression of inflammation to chronic disease.

4.2 Characterization of Immunological Changes at Different Stages of Colitis

4.2.1 Changes in Immune Cell Composition during Different Stages of Colitis

Since the histology results and disease parameters including colon length and weight clearly indicated that there is local inflammation and immune cell infiltration during each stage of DSS colitis, we next investigated whether disease progression would be associated with distinct changes in the immune cell composition in the colon.

Different stages of colitis were induced according to Figure 15A and total *lamina propria* leukocytes were isolated from enzymatically digested colon at indicated time points. Subsequently, FACS analysis was performed to quantify major immune cell subsets (B cells, lineage negative (lin^-) lymphocytes, macrophages, CD4+ and CD8+ T cells, eosinophils, dendritic cells, monocytes and neutrophils) at consecutive stages of the disease. Details about the gating strategy are provided in the methods section 3.6. Similar event counts from analyzed colon samples per condition were merged in silico and lineage marker expression was used for t-distributed stochastic neighbor embedding (t-SNE) of cell subsets. Subset identification was performed by manual gating according to section 3.6. Cell subset identity in t-SNE plots was color-coded accordingly.

The qualitative visual overview obtained from t-SNE plots uncovered remarkable changes in the cell composition at different stages of DSS colitis. One of the most obvious change was the rapid infiltration of neutrophils. Neutrophils were not detectable in both control groups, but their proportion increased during acute colitis and remained elevated during chronic intestinal inflammation (Figure 16A). In addition, the CD4+ T cell population increased during the remission phase after acute DSS colitis and stayed persistently high during the chronic disease stages. Unexpectedly, eosinophils represented the biggest portion within the t-SNE plot during acute DSS colitis when compared to other disease stages (Figure 16A). Percentage of eosinophils reached around 20 % of total CD45+ cells exclusively in the acute stage of the disease, suggesting eosinophils to be good predictors to differentiate the acute from other disease stages (Figure 16B).

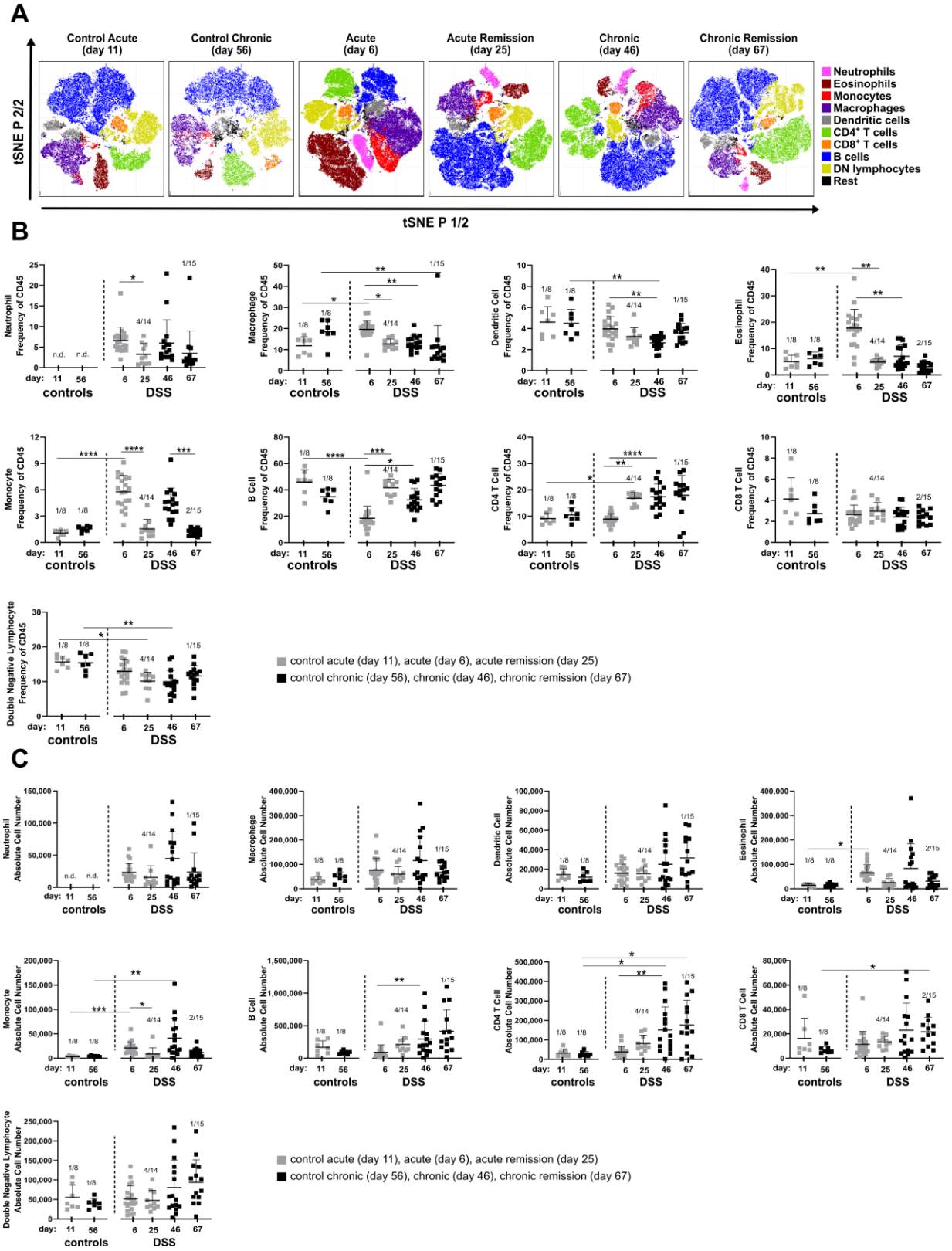

Figure 16: Characterization of innate and adaptive immune cell composition in the colon during consecutive stages of DSS colitis. DSS colitis and respective remission stages were induced as indicated in Figure 15A. At indicated time points, mice were sacrificed and colonic leukocytes were isolated followed by antibody staining and flow cytometry analysis. Unsupervised clustering of immune cell subsets was performed by t-distributed stochastic neighbor embedding (t-SNE) and cell subsets were identified and color-coded based on manual gating. A) Representative t-SNE plots. B) Frequency of indicated immune cell subsets within the CD45+ cell pool. C) Absolute numbers of the

indicated immune cell types. Data were obtained from 2 independent experiments (n = 8–16 mice), except for acute DSS colitis for which data were obtained from 3 independent experiments (n = 20 mice). Data represent mean with error bars indicating standard deviation. n.d.: not detectable. Number of excluded samples is indicated on top of each condition (number of excluded sample/total sample number). Significance was calculated by Kruskal–Wallis test. All groups were compared with each other, significance is indicated only for relevant groups. **** $p < 0.0001$, *** $p < 0.001$, ** $p < 0.01$, * $p < 0.05$. Figure and figure legend have already been published in (Gelmez et al., 2022).

As already observed in the t-SNE plots, neutrophils were recruited to the colon early after onset of DSS-induced inflammation (day 6) and remained clearly increased in frequency and absolute cell number in all other disease stages (Figure 16B, Figure 16C). While percentage and absolute cell number of eosinophils mainly increased in the acute stage, other myeloid cells such as monocytes were increased in both acute and chronic stages of colitis but returned to normal levels during the remission phases (Figure 16B, Figure 16C). Both, absolute cell number and percentage of adaptive immune cell subsets such as CD4+ T cells and B cells increased after the first DSS cycle and the absolute cell number reached the maximum at the chronic phase and remained increased through the according remission phase. Although the percentage of CD8+ T cells did not change, absolute cell number significantly increased in the chronic remission stage. Despite obvious changes in their frequencies, no significant alterations in absolute cell numbers was observed for double negative lymphoid cells, dendritic cells and macrophages at different stages of DSS colitis (Figure 16B, Figure 16C).

Next to local changes in cellularity within the colonic tissue itself, the draining mesenteric lymph nodes (MLNs) similarly showed elevated frequencies of B cells in acute remission and during chronic inflammation. Moreover, frequencies of lymph node dendritic cells were elevated in chronic inflammation and the according chronic remission phase of DSS colitis (Supplementary Figure 1).

Immune cell composition in the spleen, indicative for the systemic inflammatory response, also showed adaptations to repeated DSS episodes. Here, e.g. the neutrophil frequency was particularly elevated in the chronic DSS colitis phase (Supplementary Figure 2).

Together these results show that the number of inflammatory immune cells remains increased in the colon, especially during the remission period following chronic colitis. Therefore, it is evident that full recovery and restoration of tissue homeostasis is not achieved up to 3 weeks after termination of DSS treatment despite full recovery of body weight and a largely normalized DAI. Interestingly, the increase in eosinophil numbers was restricted to the acute stage of colitis, while accumulation of adaptive immune cells such as CD4+ T cell, CD8+ T cell as well as B cells occurred mainly during disease chronification.

4.2.2 Changes in Pro-inflammatory Cytokine and Chemokine Levels during Different Stages of Colitis

Since different stages of colitis were characterized by distinct changes in immune cell composition, we next quantified pro-inflammatory cytokines and chemokines typically produced by tissue-resident cells or activated immune cells. Characterization of the local cytokine milieu at consecutive stages of colitis was performed to better understand how locally produced cytokines and chemokines might contribute to long-lasting cellular dysbalances. To this end, selected inflammation-related cytokines and chemokines were quantified in supernatants of colon homogenates using a bead-based multiplex assay.

Regardless of the generally increased protein levels of many cytokines and chemokines in the acute and chronic colitis phases (KC, MCP-1, MIG, IP-10, MIP-1α, IL-1α, IFN-γ, IL-6, TNF- α), some were more abundant in the chronic phase (MIP-3α, BLC, IL-17A, IL-1β), suggesting a specific local adaptation of the colonic milieu to repeated episodes of the inflammation. From this point of view, the expression of the chemokine MDC is particularly interesting, as it shows an increased expression especially in the chronic DSS colitis phase as well as three weeks after termination of DSS treatment in the late remission phase. Moreover, the colonic IL-17A concentration was as well slightly elevated in the chronic remission phase (Figure 17A, Figure 17B).

Eotaxin is an eosinophil chemotattractant protein that was slightly increased in the colon during the acute stage of DSS colitis which is well in line with the increased numbers of eosinophils in the colonic *lamina propria* (Figure 16, Figure 17A). There was a significant decline in the protein levels of cytokines and chemokines during the remission stages. However, the levels generally did not return to baseline and were still significantly elevated in the chronic remission phase in case of MDC and IL-17A and, even though not significant, as well for MIP-1α, IL-1α, KC, MIP-3α, MCP-1, MIG, IP-10, IL-1β and TNF- α.

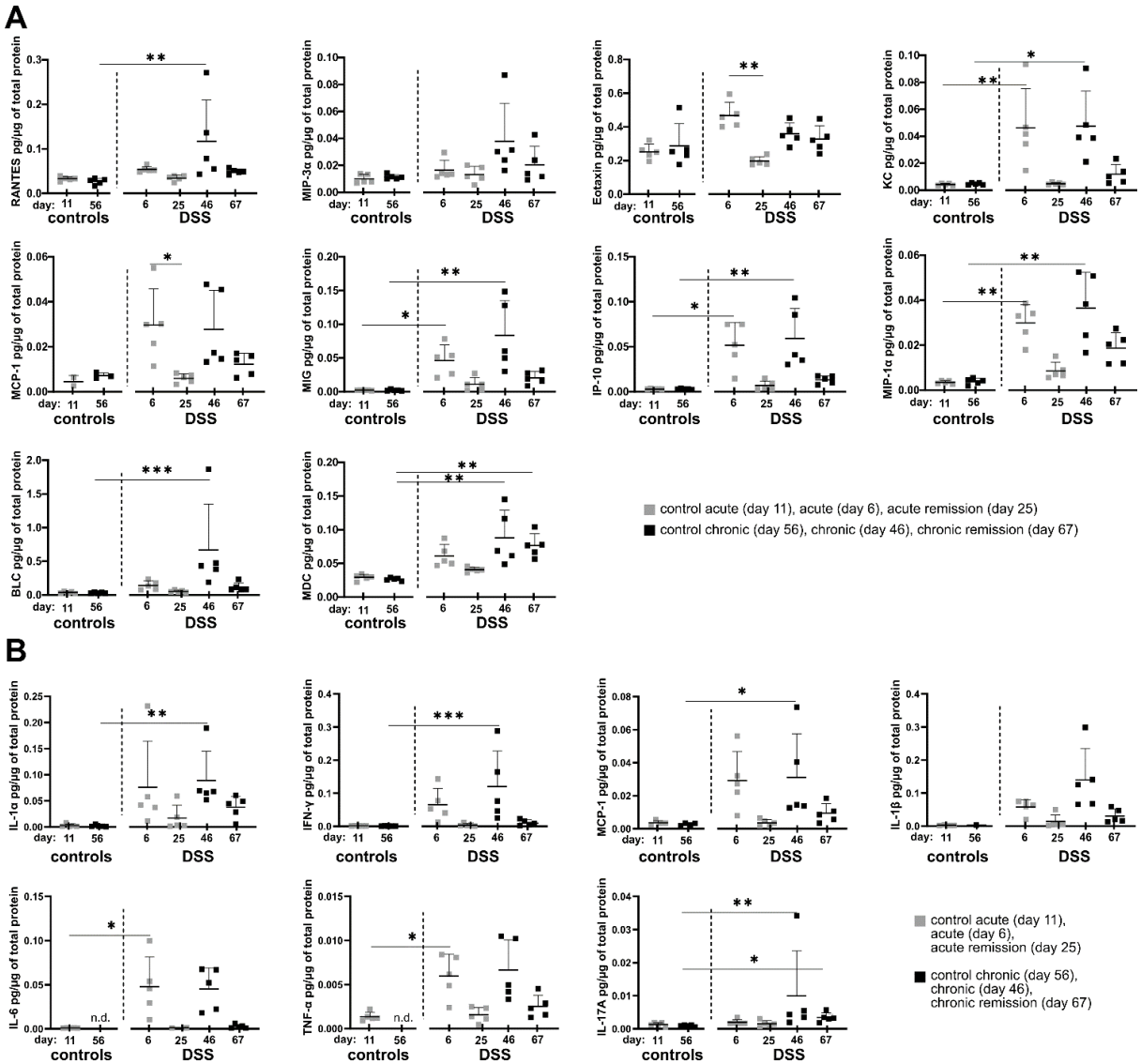

Figure 17: Quantification of chemokines and cytokines in colon tissue during consecutive stages of colitis. Dextran sulfate sodium (DSS) colitis and respective remission stages were induced as indicated in Figure 15A. At indicated time points, mice were sacrificed, and chemokine and cytokine levels were determined in colon homogenates and normalized to total protein amount. Depicted data match the following criteria: cytokine/chemokine concentration is above the limit of quantification (LOQ) in at least 4 out of 5 samples (80 %) in at least one condition. Samples with final concentrations that were under the limit of detection (LOD) in at least one out of two technical replicates were excluded. (A) Chemokine levels (n = 5 per group). (B) Cytokine levels (n = 5 per group). Data represent mean with error bars indicating standard deviation. n.d.: not detectable. Significance was calculated by Kruskal–Wallis test. All groups were compared with each other, significance is indicated only for relevant groups. *** $p < 0.001$, ** $p < 0.01$, * $p < 0.05$. Figure and figure legend have already been published in (Gelmez et al., 2022).

Taken together, levels of pro-inflammatory cytokines and chemokines were significantly altered at different stages of DSS colitis. Even though most of the cytokine and chemokine concentrations decreased during remission phases, they usually did not drop down to baseline levels. Thus, well in line with the observed alterations in immune cell composition, chronification of DSS-induced colitis is associated with a sustained dysbalance in the colonic cytokine and chemokine milieu.

4.2.3 Chronic Stages of Intestinal Inflammation are associated with Systemic Inflammation

According to histology, large areas of the colon were inflamed especially during chronic stages of colitis (Figure 15K). As shown before, spleen weight was significantly increased during the chronic stages of colon inflammation (Figure 15H), and in addition, the percentage of neutrophils in the spleen was significantly increased in the chronic stage of disease (Supplementary Figure 2). These results suggest that chronification of intestinal inflammation is associated with the establishment of systemic inflammation. In order to experimentally prove this, pro-inflammatory cytokines were quantified in blood plasma obtained from mice at different stages of DSS colitis using the LEGENDplex mouse inflammation panel (IL-23, IL-1α, IFN-γ, TNF-α, MCP-1, IL-12p70, IL-1β, IL-10, IL-6, IL-27, IL-17A, IFN-b, GM-CSF). While concentration of most of the analyzed cytokines were under the limit of quantification (LOQ), plasma IFN-γ and IL-17A were detectable by this approach.

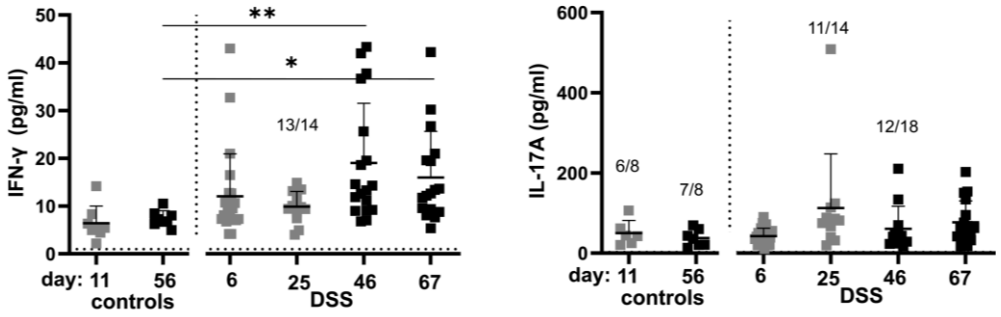

Figure 18: Quantification of IFN-γ and IL-17a in blood plasma during consecutive stages of colitis. DSS colitis and respective remission stages were induced as indicated in the Figure 15A. At indicated time points, blood samples were collected, and cytokine levels were determined in plasma. Depicted data matched the following criteria: concentration of the cytokines was above the limit of quantification (LOQ) in at least 71 samples out of 89 samples from all conditions (80 %). Samples with final concentrations that were under the limit of detection (LOD) in at least one out of two technical replicates were excluded from data. Detectable sample numbers out of total samples are indicated in the figure. LOD is indicated by the horizontal dotted line. Data are from n = 8 - 24 mice per group. Grey squares represent control acute (day 11), acute (day 6) and acute remission (day 25) conditions and black squares represent control chronic (day 56), chronic (day 46) and chronic remission (day 67) groups. Data represent mean with error bars indicating standard deviation. Significance was calculated by Kruskal-Wallis test. All groups were compared with each other, significance is indicated only for relevant groups. ** $p < 0.01$, * $p < 0.05$. Figure and figure legend have already been published in (Gelmez et al., 2022).

Even though IL-17A concentration was significantly increased in the colon in chronic disease stages (Figure 17B), the IL-17A levels in plasma did not show any significant differences between the DSS conditions and controls (Figure 18). In contrast, systemic IFN-γ levels were significantly elevated in the chronic phases of inflammation, indicating that chronification of colitis is indeed associated with systemic inflammation (Figure 18).

In summary, increased spleen weight, increased number of neutrophils in the spleen, and significantly increased IFN-γ levels in blood plasma during chronic stages of the disease confirmed the hypothesis that chronic colitis induced by repeated DSS treatment i) does not resolve during the remission phase

and ii) is associated with persistent low-level systemic inflammation even during remission. Moreover, plasma IFN-γ might represent a good indicator for systemic maladaptation as its concentration was increased in blood plasma exclusively during chronic DSS colitis as well as in the chronic remission phase.

4.3 Chronification of DSS-Induced Colitis is associated with the Perpetuation of Intestinal Microbiota Dysbiosis

It has been shown before that acute DSS colitis is associated with reduced diversity of bacterial species as well as marked changes in the intestinal microbiota composition (Munyaka et al., 2016). However, the sustainability of intestinal dysbiosis and/or its potential gradual consolidation during colitis chronification are only poorly understood to date. To experimentally address these issues, time-resolved rRNA-gene-based microbiota analysis were performed of feces from the same mouse individuals at consecutive stages of the disease model—after the first cycle of DSS treatment (day 6), after the second (day 26) and after the third (day 47) DSS cycle and the respective recovery stages (day 20, 40 and 67, respectively).

The analysis of microbiome data obtained from this cohort showed that the intestinal microbial community consists of 89 different genera and 20 taxa not classified to genus level. The complete list of identified taxa is available in the online supplement of the published paper by (Gelmez et al., 2022).

Principle component (PCO) cluster analysis revealed that DSS treatment and the resulting colitis clearly affects the intestinal microbiome in a cumulative fashion. In the PCO-plot (black symbols: DSS dosage, gray symbols: after DSS remission phase, red symbols: water control) this becomes evident by the fact that only microbiomes from feces of mice before receiving DSS and microbiomes of mice that are in the first remission phase (day 20, gray triangles) cluster together with the microbiomes of drinking water control mice (Figure 19A). Microbiomes of the two later (day 40 and 56) remission phases (gray plus symbols and gray squares) remain, however, positioned in between microbiomes of control and DSS consuming mice (day 6, 26 and 47) in the PCO plot mice (Figure 19A), thereby indicating overall perpetual microbial inflammatory adaptation, which takes hold from the second DSS episode on.

Evolving maladaptation of the microbial community with an increasing number of DSS treatments and chronicity of colitis was further supported by multivariate Anosim and Permanova tests, which statistically confirmed, firstly, microbial adaptation during each DSS dosing period (compared with water-only controls) and, secondly, impairment of the microbiome's ability to restore the initial composition of the gut flora in the last remission phase (day 67) after three DSS cycles (Figure 19B). In more detail, this analysis revealed that while classified intestinal microbial genera in control animals remained largely stable (except around day 20, Figure 19B,C upper panel), significant differences were detectable in the DSS cohort at any time point analyzed. In general, on the genus level, the most

significant microbial adaptations occurred at the end of DSS dosing periods, e.g., accompanied by a reduction of *Lactobacillus* and outgrowth of *Prevotella* species (Figure 19C). In principle, microbiome composition normalized to some extent during a 2-week interim remission period. However, the ability of the microbiome to return to the initial gut flora composition during remission phases decreased with each of the three DSS periods applied, as evidenced, for example, by a persistently reduced proportion of *Lactobacilli* after the last remission phase on day 67 (Figure 19C).

Amongst classified bacterial genera, the most dynamic DSS-induced changes in the microbiome composition attributed to *Lactobacillus*, *Prevotella*, *Limosilactobacillus* and *Turicibacter* (Figure 19C and Figure 19D). The relative abundance of *Lactobacillus* and *Limosilactobacillus* followed a pattern of highest abundance in healthy mice and in the recovery phases, respectively, with a failure in re-establishing initial abundancies after the third DSS cycle (Figure 19D). Abundance of the genus *Prevotella* followed the same course as the disease activity index (Figure 15E), with high abundance in stages of DSS-dosage and a decline back to normal in the recovery phases (Figure 19D). The *Turicibacter* genus was largely undetectable in healthy animals but, strikingly, its abundance in the active stages of colitis steadily increased with each DSS cycle applied but normalized during the recovery phases (Figure 19D).

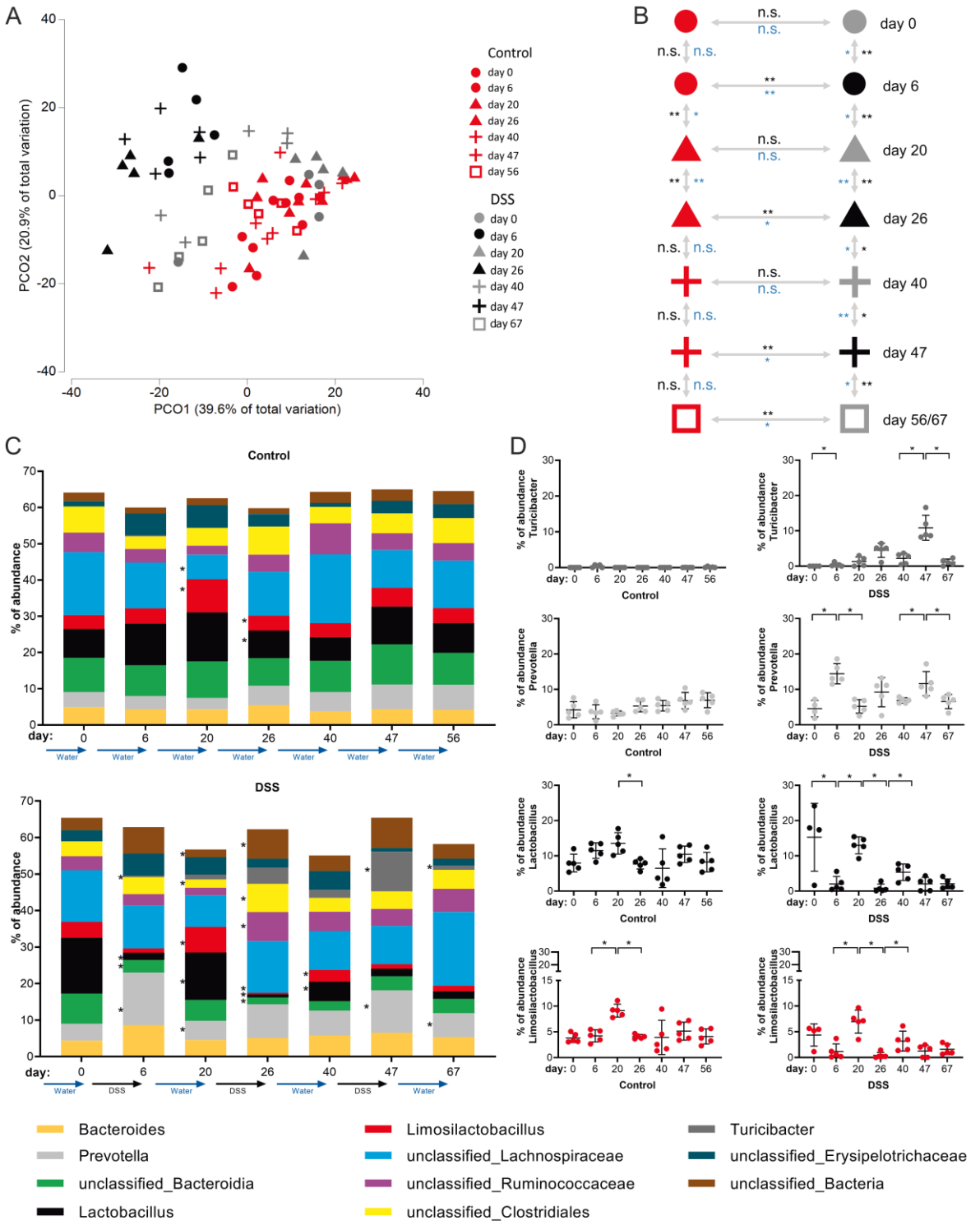

Figure 19: Microbiota analysis in feces samples from different stages of DSS-induced colitis. DSS colitis was induced as indicated in Figure 15A (lower time-line). Control mice received normal drinking water. At indicated time points (see above text), feces were collected and subjected to Illumina MiSeq sequencing. (A) Principle component clustering of all feces samples. (B) Results of multivariate Anosim (black) and Permanova (blue) tests between the control group (normal drinking water) and the different DSS groups for each experimental day, based on a Bray–Curtis-resemblance measurement at the taxonomic rank of genus. n.s.: not significant. (C) Relative abundance of the global bacterial community at the taxonomic rank genus and (D) relative abundance of selected genera for each mouse. Data are from n = 5 mice per group. Statistical significance indicated by * $p < 0.05$ and ** $p < 0.01$. Note: Microbiota data were generated in cooperation with Prof. Dr. Alexander Link, Konrad Lehr and Dr. Ramiro Vilchez-Vargas (OVGU, Department of Gastroenterology, Hepatology and Infectious Diseases). Figure and figure legend have already been published in (Gelmez et al., 2022).

Together, intestinal dysbiosis is clearly initialized by active periods of DSS-dosage in which each period has a cumulative progressive impact on microbiota composition, leading to dysbiosis in the chronic remission phase.

4.4 DSS-induced Intestinal Inflammation Skews Transcriptional CEC Responses towards Antigen Processing and Presentation, T Cell Activation as well as Antimicrobial Humoral Defense

The characteristics of the DSS colitis model described so far provide strong evidence of pathological, immunological and microbial alterations of the intestinal milieu in all four stages of DSS colitis investigated. IECs in general and CECs in particular are at the forefront of the intestinal barrier (see section 1.2) and are physiologically intimately involved in the observed inflammatory processes of DSS colitis. Restoration of intestinal barrier function is necessarily linked to IEC cellular activities and their return to a normal physiological state. As DSS colitis mainly affects the colon, the DSS model, comprehensively described above, is excellently suited to investigate cellular activities of CECs from the corresponding DSS stages in more detail. Methodologically, transcriptome analysis is suitable for this purpose, e.g. by means of RNA-Seq, which allows to describe cellular transcriptional changes and their temporal stability and to draw corresponding conclusions about cellular inflammatory reactions and their association with immune cell responses as well as microbial dysbiosis.

To this end, sufficient numbers of vital CECs had to be isolated from colon tissue of mice. There are established protocols to roughly detach and separate the luminal layer of CECs from colon tissue by resolving the mucus with the reducing chemical reagent DTT and by using EDTA for cell detachment (see section 3.3). The obtained cell fraction not only contained CECs but also e.g. fibroblasts and intraepithelial leukocytes. As CECs are fragile short-lived cells, a major fraction of CECs in this approach was typically apoptotic or dead cells. Thus, to obtain highly pure vital CEC cell samples, a FACS-sorting strategy was applied. This involved fluorescence labeling of dead cells (LD) and staining with the general leukocyte marker CD45 as well as the fibroblast marker CD31 for lineage exclusion, respectively. For general restriction to the epithelial cell lineage EpCAM marker (CD326) was used. Finally, CECs were sorted as LD-CD45-CD31-EpCAM+ cells. It is important to note that the sorted CECs are likely a mixture of the different epithelial subtypes commonly found in the colon (see section 1.2), and that the exact composition of epithelial cell subsets is unknown and may vary in each DSS condition. Thus, bulk RNA-Seq transcriptomics of sorted CECs represents the average mRNA content of the epithelial EpCAM+ compartment. Of note, sorted CECs were split and used for both RNA-Seq and later ChIP-Seq analysis (see section 4.5).

For each control/DSS condition (control acute, control chronic, acute, acute remission, chronic and chronic remission) CECs from 4-8 identically treated mice were pooled together to obtain sufficient

material. Two independent biological replicates per experimental condition were generated, such that in total 12 CEC samples were available for RNA-Seq. DNA-free RNA was isolated from sorted CECs (see section 3.10). RNA integrity was evaluated on a fragment analyzer and RNA Quality Number (RQN) was on average 7.3 indicating minimal RNA degradation. Library preparation, 50 bp paired-end-sequencing and initial data analysis was performed as described in section 3.11.

Initially, principal component analysis (PCA) of $\log_2$ CPM data of all identified transcripts and all conditions was performed to identify global similarities between control/DSS groups. The two major principal component dimensions are plotted in Figure 20A. Interestingly, both untreated control groups (green symbols), that deviate from one another only in the age of the used mice, cluster together in the PCA-plot and are set apart from all DSS conditions. Thus, the PCA analysis indicates a negligible impact of the age of the mice on CEC transcription patterns if mice were left untreated. Moreover, PCA-analysis reveals that DSS-induced intestinal inflammation had a clear impact on the gene expression patterns of CECs, as all DSS conditions clearly cluster apart from the untreated mouse groups. Of note, both samples of the remission conditions (acute remission and chronic remission) still cluster together with those of the acute and chronic conditions which on a first glace indicates that the remission periods (normal drinking water) were not sufficient to restore the steady-state transcriptional profile of CECs in these mice.

Next, all DSS conditions (acute, acute remission, chronic, chronic remission) were individually compared with their corresponding control condition to identify condition-specific differentially expressed genes. To limit the analysis-impact of lowly transcribed genes, whose CPM counts typically have large variances, transcripts with $\log_2$ CPM values < 1 in at least one of the 2 replicates were excluded. Transcripts not fulfilling the CPM criterion in all conditions were excluded as well. Differential gene expression between pairwise condition comparisons were calculated using a pair-wise generalized linear model quasi-likelihood F test (glmQLFTest), implemented in the EdgeR package. Transcripts with a fold change (FC) in gene expression of $|\log_2 FC| > 1$ and a false discovery rate (FDR) of $FDR < 0.05$ were considered significantly regulated. A volcano plot for each pair-wise comparison was generated showing statistical significance (FDR value) versus magnitude of differential gene expression (Figure 20B).

The “chronic DSS vs. control chronic” comparison clearly showed highest numbers of up/down-regulated genes (down: 40, up: 62; Figure 20B) followed by the “acute DSS vs. control acute” comparison (down: 19, up: 15; Figure 20B). Interestingly, when comparing the acute remission condition with the control acute condition, no significant differential gene expression could be observed. Comparison of the chronic remission condition with the control chronic condition resulted in only three significantly up-regulated transcripts (*Iigp1*, *Duoxa2* and *H2-Ab1*; Figure 20B).

When comparing the three lists of differentially expressed genes from the four comparisons by means of a Venn diagram, it becomes clear that many regulated genes (24) in CECs from acute DSS are also regulated in the chronic stage of the disease (Figure 20C). The majority of regulated genes (75) is however specifically associated only with the chronic DSS condition (Figure 20C). Only 3 transcripts were regulated in the acute, chronic as well as the chronic remission condition (Figure 20C). Numeric characteristics of the CEC transcriptome data analysis so far drive the notion that CECs from acute DSS show surprisingly few transcriptional adaptations to acute intestinal inflammation, and that they return to their initial transcriptional state after the first remission period. However, transcriptional adaptations become more numerous after three DSS cycles and tend to be slightly more stable after the final remission period.

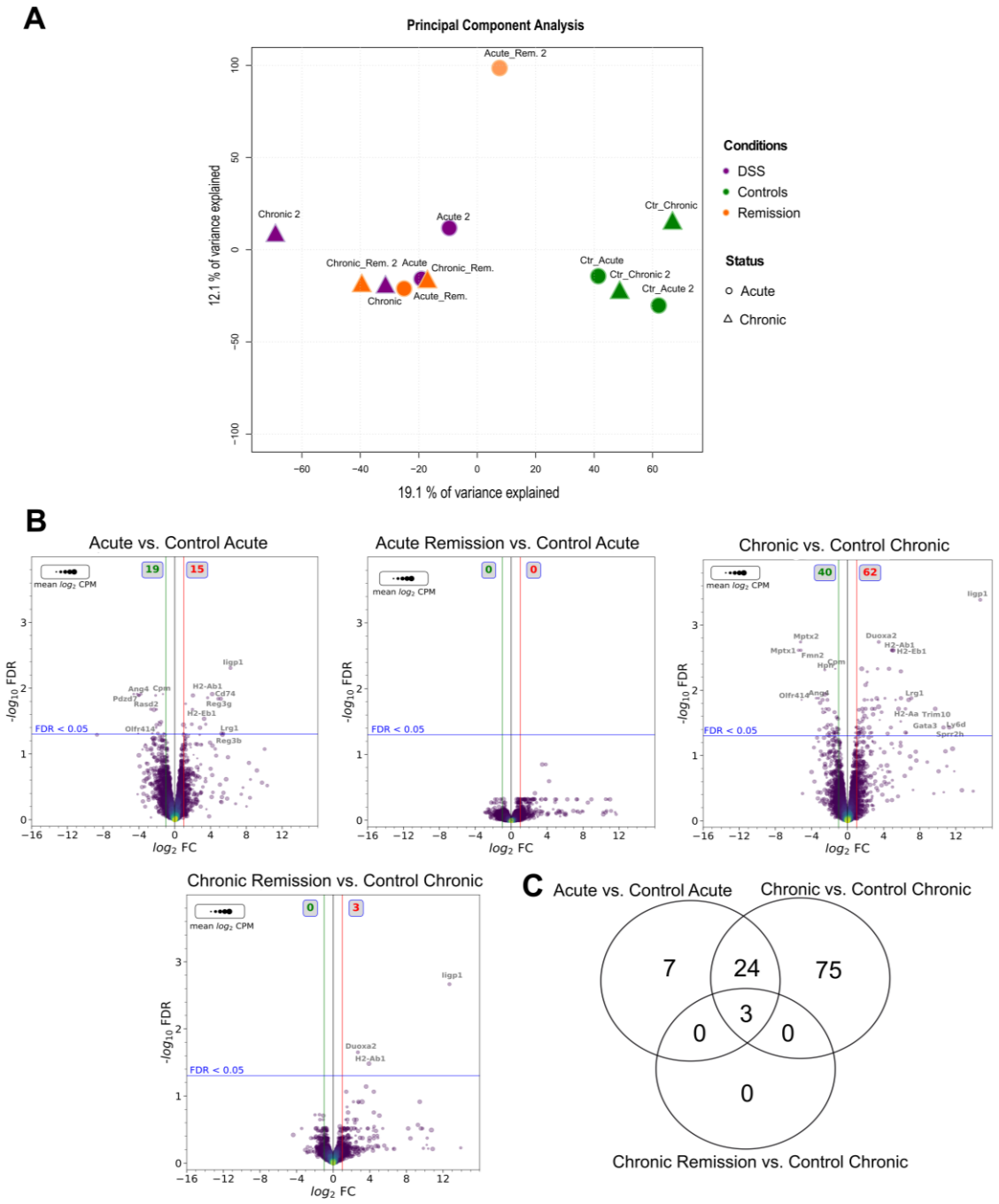

Figure 20: Transcriptional comparison of CECs from all DSS model conditions versus control conditions. FACS-sorted LD-CD45-CD31-EpCAM+ CECs from 4 to 8 mice per experimental condition were pooled and a portion of each cell pool was used for total-RNA isolation and paired-end RNA-Seq. Basic data analysis was performed as described in section 3.11. Sequencing and basic data analysis was performed in cooperation with Dr. Robert Geffers (Helmholtz Centre for Infection Research, Braunschweig, Genome Analytics Group). Data represent two independent mouse experiments per condition. A) Principal component analysis (PCA) of log2 CPM values of all identified transcripts from all control/colitis conditions. Figure only shows the first two principal component dimensions with % explained data variance stated on x and y axes. Acute DSS and the according control condition are represented by circles. Chronic DSS and the according control condition are represented by triangles. Purple, green, and orange colors are representing DSS, remission stages, and control groups, respectively. B) Volcano plots (-log10 FDR vs. log2 FC) for stated individual condition comparisons using pair-wise generalized linear model quasi-likelihood F test (glmQLFTest), EdgeR. Transcripts with log2 CPM < 1 in all replicates from both compared conditions were excluded. The numbers of downregulated (green) and upregulated (red) genes with FDR < 0.05 and |log2FC| > 1 are stated. Point size represents the log2 CPM value. Point color reflects point density (yellow: high, purple: low). Vertical green (FC < -2) and red (FC > 2) lines indicate applied fold change criteria. Horizontal blue line indicates FDR criterion (FDR < 0.05). C) Venn diagram comparing differentially expressed genes identified in B.

To compare differential gene expression across all experimental conditions, rather than relying only on pairwise comparisons, next a generalized linear model quasi-likelihood Ftest (glmQLFtest) implemented in the edgeR library was applied to the RNA-Seq data. Within this statistical model, DSS conditions were compared with their corresponding control group and their combined effect on all conditions versus according controls was analyzed. Transcripts with $\log_2$ CPM < 1 in at least one of the 2 replicates and with $\log_2$ CPM < 1 in all conditions were excluded. Transcripts with $|\log_2 FC| > 1$ (two-fold difference) in at least one comparison and FDR < 0.05 were considered significantly regulated. In total, 52 differentially expressed genes (out of 17168 genes in total) were identified. Z-score transformed $\log_2$ CPM values of the 52 genes were hierarchically clustered and color-coded to visualize their gene expression (Figure 21A). Cluster analysis suggests partitioning of the 52 differentially expressed genes into two main sub-clusters. The first one consists of 20 genes that are steadily expressed in both untreated control groups, implying genuine importance for CEC steady-state cellular functions. Importantly, all 20 genes become down-regulated upon acute and chronic DSS colitis with their expression only partially being restored after the according remission phases. The remaining 32 genes make up the second cluster in Figure 21A. In principle, they show an inverted expression pattern, compared to the first cluster. Thus, their expression is low in steady-state and becomes up-regulated in periods of DSS consumption. Their expression patterns after remission phases are non-uniform, with few genes almost returning back to the initial level, but with most genes keeping an expression level that lies between the level of untreated controls and acute/chronic DSS conditions. Of note, the genes *Cd177* and *Ubd* show a somewhat unique expression pattern within the second cluster, as their expression only enhances during the acute remission phase of the DSS model, becomes even more enhanced in the chronic condition and clearly remains elevated in the chronic remission phase. Thus, *Cd177* and *Ubd* seem to be associated with the chronic phase of the DSS model.

Together, especially two remission conditions provide valuable indications for as to which extend colitis-induced transcriptional responses of CECs, upon tissue recovery, are stable or depend on an acute

inflammatory milieu. According to Figure 21A, most differentially expressed genes from both sub-clusters do not return to their initial expression levels within the chosen remission periods, thereby suggesting at least semi-stable inflammation-driven transcriptional adaptations of CECs.

Next, to give a detailed functional interpretation of identified differential expression patterns amongst the 52 genes, Gene Ontology (GO) and Kyoto Encyclopedia of Genes and Genomes (KEGG) pathway term enrichment analyses were performed. To this end, the list of 52 gene symbols was analyzed with the ClueGO plugin of the Cytoscape software (Bindea et al., 2009) GO/pathway terms with FDR < 0.05 in a right-sided hypergeometric test were considered meaningful (Figure 21B).

According to GO-term enrichment of the GO-category "Biological Process", enriched genes were associated with terms like humoral or antimicrobial immune response, antigen processing and presentation of exogenous peptide antigen via MHC-II, and negative regulation of T cell proliferation as well as their activation (Figure 21B, upper panel). Moreover, KEGG-term analysis suggested involvement of enriched genes in antigen presentation and T cell differentiation (Figure 21B, lower panel). Detailed GO-term and KEGG-pathway enrichment results can be found in the Supplementary Table 1 and Supplementary Table 2, respectively.

Combining GO/KEGG term analyses with the expression patterns of the 52 differentially expressed genes indicates that CECs after colitis-induction respond with clear induction of genes related to MHC-II dependent antigen-presentation (*Cd74*, *H2-Aa*, *H2-Ab1*, *H2-Eb1*, *H2-DMb1*, *H2-DMa*), that is most pronounced in the chronic phase of the DSS model. This is remarkable, since the only naturally interacting ligand to peptide-loaded MHC-II complexes are T cell receptors of the CD4+ T cell compartment. The latter was found to be expanded in the *lamina propria* compartment (compare section 4.2.1) of conditions where the RNA-Seq analysis of CECs showed enhanced expression of MHCII-related genes. In line with this, interferon regulatory factor-1 (*Irf1*), a known key transcriptional regulator of MHC-I and MHC-II complexes (Hobart et al., 1997) was upregulated especially in the chronic DSS condition, too (Figure 21A). Moreover, the expression of the indoleamine 2,3-dioxygenase 1 (*Ido1*) from the first DSS cycle on was enhanced in CECs, with IDO playing a role in compromising T cell proliferation and activation (Munn et al., 1999; Hwu et al., 2000; Mellor et al., 2002).

Further interpretations of observed CECs expression patterns in acute/chronic DSS colitis conditions can be concluded by the increased expression levels of *Reg3γ* and *Reg3β* as well as the decreased expression level of *Ang4*. Their expression levels are known to be regulated by pathogenic gut microbes or bacterial activity (Hooper et al., 2003; Cash et al., 2006; Stelter et al., 2011). This may relate to the previously identified changes in microbiota composition in periods of DSS dosage (compare Figure 19).

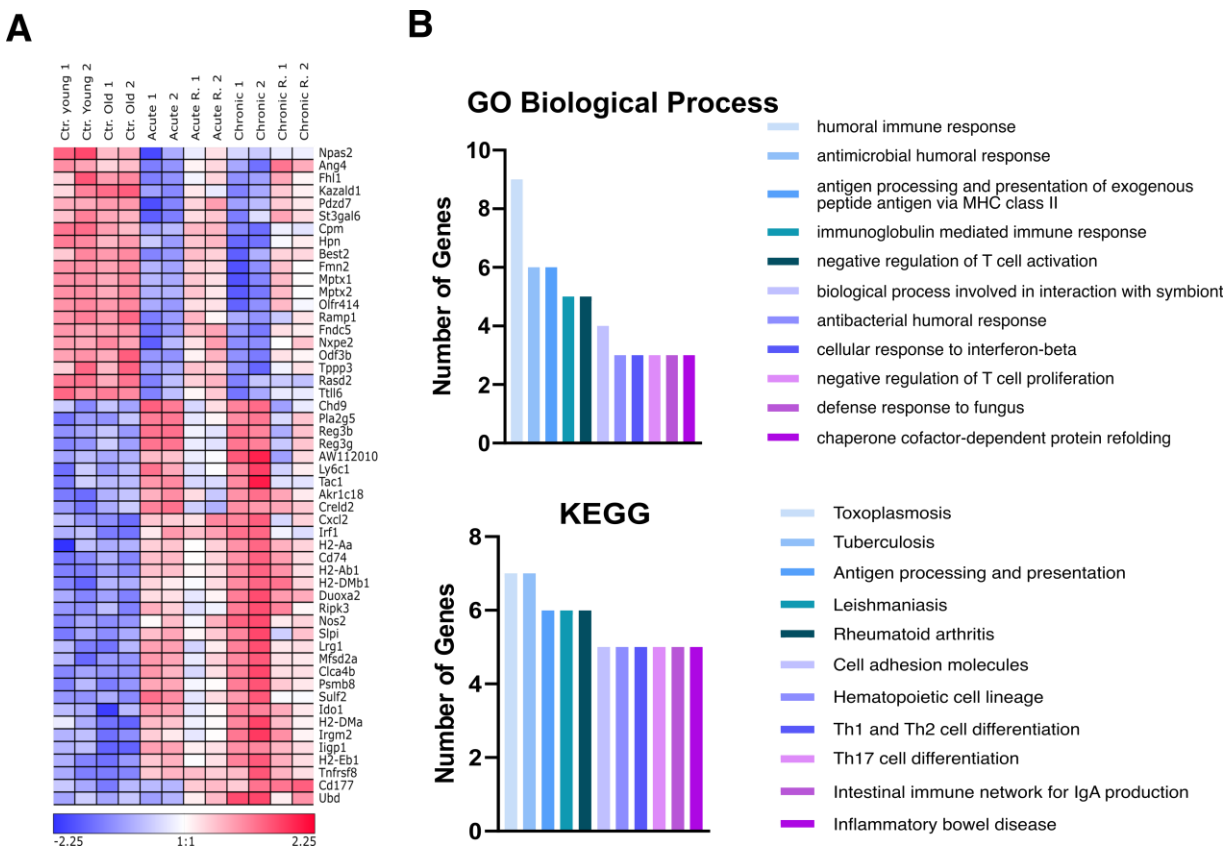

Figure 21: Transcriptomic changes during different stages of DSS colitis. Differential expression within RNA-Seq data was analyzed by a generalized linear model quasi-likelihood F test (glmQLFtest, edgeR) model, representing the combined effect of all experimental conditions versus their corresponding control groups. Basic data analysis was performed in cooperation with Dr. Robert Geffers (Helmholtz Centre for Infection Research, Braunschweig, Genome Analytics Group). Genes with log2 CPM < 1 in all 12 samples were excluded. 52 genes with |log2 FC| > 1 (in at least one comparison) and FDR < 0.05 were identified, out of 17168 expressed genes in total. A) Hierarchical clustering and heatmap of z-score transformed log2 CPM values of the 52 identified genes. Color code represents z-score of log2 CPM, columns represent individual RNA-Seq replicates from stated conditions. B) GO (Biological Process) and KEGG term enrichment analysis of genes in A, using Cytoscape/ClueGO software and a right-sided hypergeometric test with Bonferroni step-down p-value correction (FDR < 0.05). As reference gene set for enrichment statistics, gene symbols of the 17168 genes were used. GO hierarchy-levels were constrained to a minimum of 3 and a maximum of 16. Data represent number of genes per significantly enriched GO/KEGG term. Bar colors correspond to the color-coded terms on the right.

In summary, transcriptome analyses proofs that CECs, conditioned in the DSS colitis milieu, transcriptionally respond in multiple functional aspects like antigen presentation, antimicrobial and antibacterial humoral response. Importantly, transcription patterns of MHC-II-related genes strongly imply cell-cell interaction with CD4+ T cells, likely residing in the intra-epithelial or *lamina propria* space. Their transcriptional response is most pronounced in the chronic and less pronounced in the acute inflammatory condition. Expression patterns of MHC-II-related genes normalize to some extend but do not fully reach the steady-state niveau after any of the remission periods. Although in the individual comparison of the chronic remission condition versus the chronic control only one MHC-II gene (*H2-Ab1*) is still significantly up-regulated, the overall expression pattern of the entire MHC-II-related group of genes demands closer investigation of the CEC/CD4+ T cell axis in the DSS model.

4.5 Transcriptional Consequences of Changes in Epigenetic Histone H3K27me3/H3K27ac Modification Patterns in CECs from all Conditions of the DSS Model

RNA-Seq analysis of CECs showed dedicated transcriptional adaptations of CECs in particular in the chronic DSS colitis condition. At this stage, mice underwent three consecutive periods of DSS treatment with two interim remission phases (compare Figure 15A). Compared to the acute DSS condition with just one DSS treatment period, CECs from the chronic DSS condition clearly show more versatile transcriptional responses. Thus, it is tempting to speculate about underlying influential factors for this transcriptional enhancement in CECs. Next to a boosted and likely more influential inflammatory environment in the colon that immediately impacts CEC transcriptional responses, an evolved CEC-intrinsic re-programming of the inflammation-triggered CEC transcriptional response might have occurred over time, thus providing another possible explanation for the observed RNA-Seq-based CEC characteristics.

The concept of epigenetics provides several conceivable mechanisms that may be involved in transcriptional re-programming of CECs upon inflammation, additionally influencing the basal canonical gene regulatory machinery. The epigenetic concept of histone modifications is known to impact IECs in many aspects. Amongst the plethora of known histone modifications, H3K27me3 and H3K27ac are best studied in general and within IECs in particular (compare section 1.4.4). Taken together, the above arguments justify the hypothesis that epigenetic histone modifications, such as H3K27me3 and H3K27ac, may have a relevant impact on the transcriptional profile of CECs in the DSS model, possibly contributing to the perpetuation and chronification of intestinal inflammation.

To experimentally approach this hypothesis, ChIP-Seq analyses of immunoprecipitated CECs chromatin fragments harboring patches of accordingly modified histones can be used as a state-of-the-art technique. Genome-wide mapping of epigenetic histone modifications are functionally most enlightening when combined with RNA-Seq data from the very same cell batch, as only that way meaningful synchronous molecular correlations between epigenetics and *de facto* transcriptional activity of a given locus can be assumed. For this reason, ChIP-Seq experiments were performed from the same isolated CECs pools that have already been used in the RNA-Seq experiments (see section 4.4).

In short, formaldehyde (1 %) fixed LD-CD45-CD31-EpCAM+ CECs were FACS-sorted and lysed to release the chromatin. For each DSS model condition, two independent biological replicates were generated, with each replicate integrating pooled CECs from 4-8 identically treated mice (compare section 4.4). In total 12 chromatin samples were generated. After chromatin fragmentation by sonication, for each sample two chromatin immunoprecipitations were performed with antibodies specific for H3K27me3 and H3K27ac histone modifications, respectively. As sample-specific negative controls, input-DNA samples containing 1/10 of the chromatin amount of the actual ChIP-samples were used.

Resulting ChIP-DNA and input-DNA samples (in total 36 samples) were applied to ChIP-Seq-library preparation and were sequenced by means of 50 bp paired-end sequencing. The anticipated sequencing-depth was 50 x 10^6 reads/sample.

To ultimately elucidate transcriptional consequences of epigenetic changes in CECs from the DSS model, in the following first results of the ChIP-Seq data will be presented and subsequently matched with the RNA-Seq data of the previous chapters.

4.5.1 Genome-wide ChIP-read Coverage Correlates with H3K27me3 and H3K27ac Histone Modifications in CECs from all DSS Colitis Conditions

Initial data analysis of CECs H3K27me3 and H3K27ac ChIP-Seq data involved amongst other things adapter-primer-trimming and quality control of raw FASTQ files (for details, see section 3.13). ChIP-read sequences were aligned to the mouse reference genome (mm10) using the Burrows-Wheeler Aligner (BWA), finally resulting in sorted BAM files. Initial data analysis performed by Dr. Robert Geffers (Helmholtz Centre for Infection Research, Braunschweig, Genome Analytics Group).

To globally compare and cross-check validity of the total ChIP-Seq data set, the 36 sorted BAM files were analyzed with the deeptools library and its “multiBamSummary” functionality (Ramírez et al., 2016). Briefly, this tool tiles the mouse genome in adjacent 10 kb bins across all chromosomes and calculates the number of mapped reads within each bin. Of note, this initial analysis was performed without cross-sample normalization of read counts, which also allows evaluation of possible batch effects, introduced by e.g. variances in cell isolation, ChIP-efficiency, library amplification, library size and sequencing depth. Binned read coverage data from all samples are used to calculate Pearson correlation coefficients between the samples that are then used to visualize sample similarities following hierarchical clustering. Thus, ChIP/input-DNA samples with sufficiently correlated non-normalized binned read coverages along the genome are placed next to each other in Figure 22. This approach allows to check global reproducibility of biological replicates and is supposed to result in clearly separated clustered sample groups, defined by the sample kind (H3K27ac, H3K27me3 or input control) as, by design, each of them can be expected to have distinct genomic ChIP-read distributions.

As expected, in Figure 22 ChIP-samples of the same kind cluster together into three major sample groups, corresponding to the three sample types. Since the input controls represent crosslinked and fragmented chromatin but without immunoprecipitation (IP) they all homogeneously cover the entire mouse genome. Thus, expectedly they show very high similarities (Pearson correlation coefficients around 1), independent of the DSS/control condition the samples where derived from. Even though the biological replicates in many cases do not cluster exactly adjacent to each other, still the overall Pearson coefficients per histone modification type are typically > 0.9, suggesting specificity of the two histone modification IP types. In line with this, the Pearson correlation coefficients typically decrease to about

0.7 (or lower), when different IP types or input controls are compared with each other. Importantly, this global correlation-based analysis approach is inadequate to derive condition-specific differences within a given sample type (e.g. comparison of H3K27me3 in acute DSS vs. H3K27me3 in chronic DSS), as such differences are more likely to have a locally constrained character, rather than affecting the entire genome-wide histone modification landscape. Thus, variations in the Pearson correlation between samples of the same sample type likely reflect batch effects of some kind (see above). Examples of this are observable in H3K27ac samples from acute, acute remission and chronic DSS colitis conditions (Figure 22).

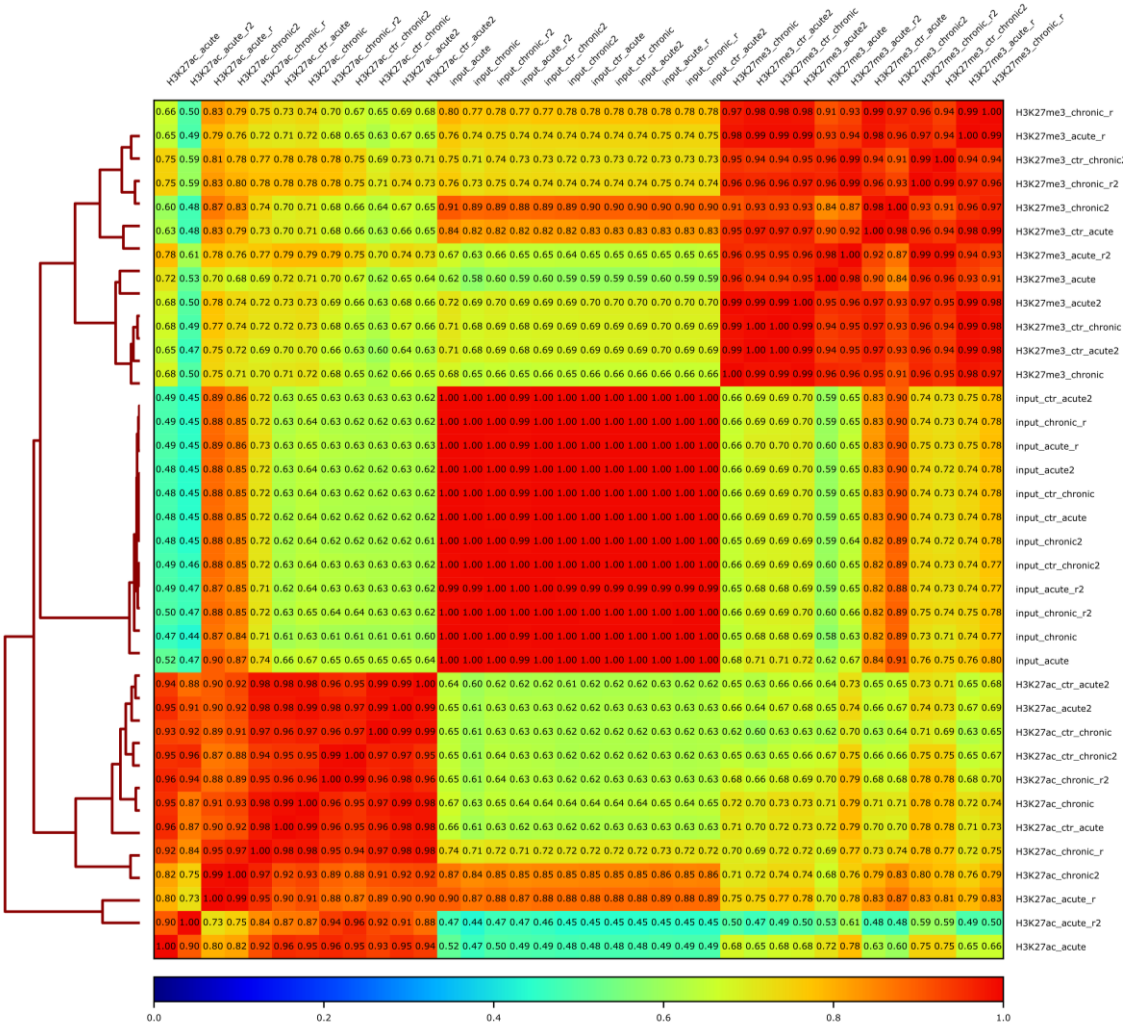

Figure 22: Clustered Pearson correlations of genome-wide non-normalized binned read counts of ChIP-Seq samples. FACS-sorted colon LD-CD45-CD31-EpCAM+ CECs from 4 to 8 mice per DSS model condition were pooled and analyzed by ChIP-Seq for epigenetic H3K27me3 and H3K27ac histone modifications together with IP input controls. Two independent biological replicates per condition were generated. Genome-wide non-normalized binned (10 kb) read coverage from 36 sorted BAM files was calculated by multiBamSummary function. Pearson correlation coefficients between read coverage data were computed using plotCorrelation function. Both multiBamSummary and plotCorrelation are part the deepTools analysis package (Ramírez et al., 2016). Color code represents Pearson correlation coefficients. "_ctr_acute": untreated young mice, "_ctr_chronic": untreated old mice, "_acute": one DSS cycle, "_chronic": three DSS cycles, "_acute_r": acute remission, "_chronic_r": chronic remission. Sample names ending with the number "2" represent the second biological replicate.

In summary, high read coverage correlations between the same histone modifications suggest global modification-specific genome-wide epigenetic patterns in CECs that are clearly distinct from their input controls. However, there are some indications of sample batch effects that require a careful normalization strategy for further quantitative condition-specific analyses.

4.5.2 Genomic Feature Annotation of High-confidence H3K27me3/H3K27ac ChIP-peaks Reveals Distinct Binding Preferences and DSS Colitis Condition-dependent Patterns

The primary read-out of histone modification ChIP-Seq analysis per sample is a list of genomic regions, defined by genomic start and end coordinates, that comprise statistically sufficient numbers of accordingly modified nucleosomes in immunoprecipitated fragments of the fixed chromatin sample. Indirectly, this primary read-out is derived from the local ChIP-fragment counts, accessible through the sorted BAM files. As statistical background model, sample-individual ChIP input control samples are used, that typically (apart from e.g. black-listed genome regions and alignment artifacts) show homogeneous ChIP-fragment densities across the genome. Genomic regions with significantly higher ChIP-fragment counts compared to the matching input control sample can be interpreted as enriched ChIP-regions of a given histone modification. Computationally, this procedure is termed “peak calling”, resulting in identification of so called "ChIP-peaks”. ChIP-peaks are the bases for the further ChIP-seq analysis pipeline.

Peak calling for all 12 individual H3K27me3 and H3K27ac ChIP-Seq samples, in relation to their corresponding input DNA sample, was calculated with the “Model-based Analysis of ChIP-Seq" (MACS version 2.2.7.1) algorithm (Zhang et al., 2008). Only ChIP-enriched peak-regions with $p < 0.05$ were considered relevant. Of note, the MACS2 algorithm also calculates IP fold-enrichment values for each called peak-region. Depending on the kind of histone modification, the overall shape of ChIP-peaks can be sharp (a few hundred bp long), broad (up to several thousand bp long), or a mixture of both. The MACS2 peak caller however needs a pre-assumption of the expected shape of the ChIP-peaks that is to be provided by the user. According to the ENCODE consortium, H3K27ac ChIP-regions cumulatively create sharp (narrow) and H3K27me3 ChIP-regions tend to create broad ChIP-peaks (Online presence of ENCODE Consortium). Therefore, MACS2 peak-calling was performed in narrow peak mode for H3K27ac and broad peak mode for H3K27me3.

The next step in the ChIP-seq analysis was the integration of ChIP-peak data of the biological replicates. The ChIP-peak positioning between ChIP-seq replicates was subjected to biological and technical variances that need to be considered. To this end, the ENCODE consortium recommends the calculation of an “Irreproducibility Discovery Rate” (IDR), which aims at the identification of reproducible ChIP-peak regions within two individual replicate sets of peak-regions (Li et al., 2011). The algorithm finds positional overlapping peak regions between the replicates and makes use of their previously MACS2-

calculated ChIP fold-enrichment values together with a robust rank-based test-statistic. Replicate peak-regions with IDR < 0.05 were considered significantly reproducible. This approach resulted in final sets of highly reproducible H3K27ac/H3K27me3 peak-regions from CECs from each condition of the DSS model (Table 11).

Conditions	Numbers of high-confidence peak-regions for H3K27ac	Numbers of high-confidence peak-regions for H3K27me3
Control acute	25045	38724
Acute	40053	56345
Acute Remission	14518	61339
Control chronic	33653	56119
Chronic	13848	27599
Chronic Remission	27511	48875

Table 11: Numbers of identified IDR determined high-confidence peak regions for H3K27ac and H3K27me3 for each disease conditions and corresponding controls.

After peak-calling and replicate integration, the goal was to derive biological meaning from the genomic positioning of identified high-confidence peak-regions in relation to known genomic features and gene annotation, potentially correlating to the DSS model conditions. To this end, identified peak locations were annotated in terms of genomic features by using the ChIPseeker software package (Yu et al., 2015). The “Annotatepeak” function of ChIPSeeker was used with defining promoter regions as ranging from ±3 kb around TSS. If a ChIP region is adjacent to more than one gene locus the reported annotation only accounts for the closest one, with the following prioritization of genomic annotation: promoter, 5’ UTR, 3’ UTR, exon, intron, downstream, and intergenic regions by default (in this order of importance).

Figure 23 represents relative frequencies of genomic feature annotations for high-confidence ChIP-peaks of both histone marks across the genomes of CECs from all conditions of the DSS model. Independent of the DSS condition, the majority of H3K27me3 peaks (on average about 40 %) were identified in distal intergenic regions, whereas H3K27ac peaks were mostly present in the ±1 kb promoter range around TSS (between 40 and 59 %). This underlines genuine differences in terms of positional preferences of histone H3K27me3 and H3K27ac modifications for CECs in general. The H3K27ac preference for proximal promoter regions together with the known tendency of H3K27ac to be rather associated with open chromatin structures (see section 1.4.4) may imply an enhanced likelihood for active transcription of loci with H3K27ac-regions in their promoters. Of note, around 15 to 22 % of H3K27me3-peaks are also annotating to the “Promoter ≤ 1 kb” feature category, with the 22 % only observable in the chronic DSS colitis condition. This shows that histone triple-methylation in principle also occurs at proximal promoters and might even have meaningful implications for DSS-condition-specific epigenetic influences. Similarly, H3K27ac peak-annotation show condition-specific variations as well. Here, the fraction of H3K27ac-peaks within the proximal promoter range (Promoter ≤ 1 kb) clearly enhances in the acute remission and chronic DSS colitis condition (both > 50 %). Taken together, the combined H3K27me3 and H3K27ac ChIP-peak feature annotation drives the notion that

based on relative numeric changes within the annotation distributions, the chronic DSS colitis condition shows promising epigenetic alterations in histone modification compared to all other conditions. Interestingly, in CECs from chronic DSS colitis, H3K27me3 and H3K27ac modified ChIP-peaks are both more frequently positioned in proximal promoter regions, compared to most other conditions (except: H3K27ac in acute remission). This is also in line with the comparably larger number of differentially regulated genes within the RNA-seq analysis of the same condition (compare Figure 20B).

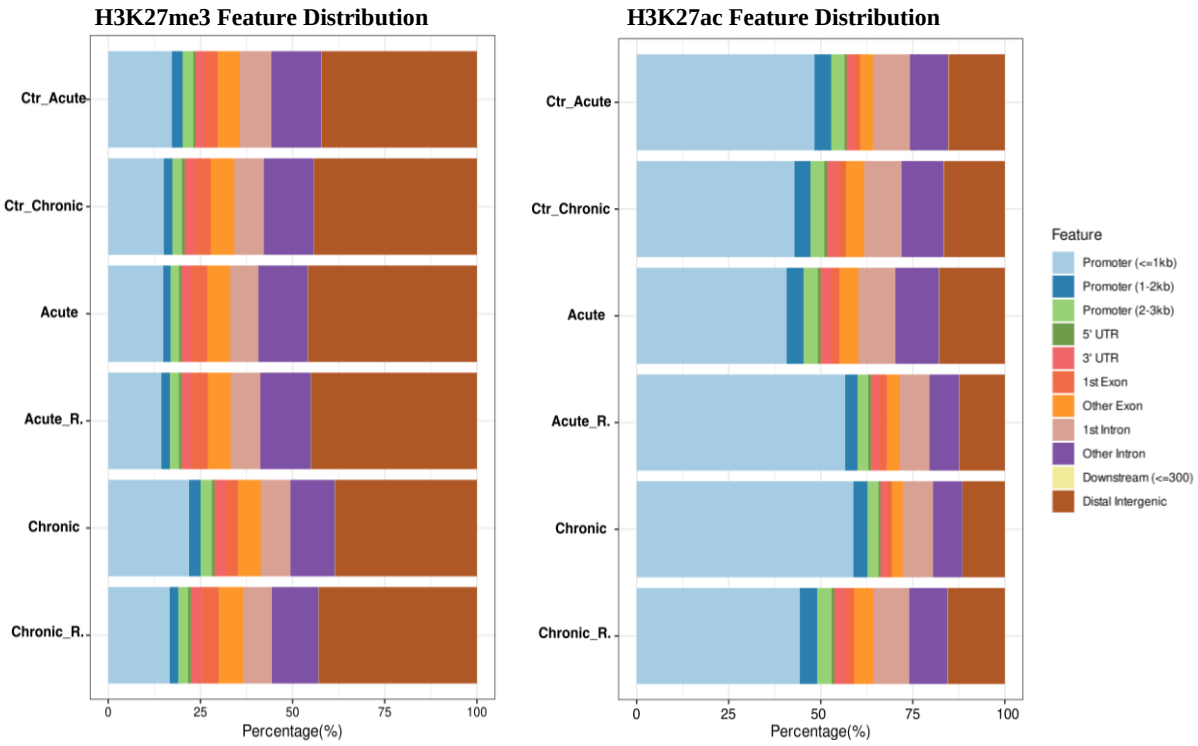

Figure 23: Genomic feature annotation of high-confidence H3K27me3 and H3K27ac ChIP-peaks. High-confidence H3K27me3/H3K27ac ChIP-peaks from all DSS model conditions were determined by MACS2 peak-calling and IDR calculation as described in the text. Genomic locations of Chip-peaks were annotated in terms of genomic features using the ChIPseeker package. Data represent relative abundances of stated genomic features, visualized with ChIPseeker's plotAnnoBar function. Promoter regions were defined as ranging from ±3 kb around TSS. If a ChIP region is adjacent to more than one gene locus the reported annotation only accounts for the closest one, with the following prioritization of genomic annotation: promoter region, 5' UTR, 3' UTR, exon, intron, downstream and intergenic. Ctr_Acute: untreated young mice, Ctr_Chronic: untreated old mice, Acute: one DSS cycle, Chronic: three DSS cycles, Acute_R: acute remission, Chronic_R: chronic remission.

To prove the significance of the observed annotational differences by checking the possibility to obtaining similar ChIP-peak annotation distributions with randomly positioned genomic regions, randomized surrogate ChIP-peak data sets were generated and annotated with ChIPseeker. For each set of experimentally derived high-confidence H3K27me3/H3K27ac ChIP-peaks from each DSS condition, a positional randomized version was generated, while maintaining the exact numbers and length-distributions of ChIP-peaks per chromosome as in the original ChIP-peak data sets without allowing shuffled regions to overlap. ChIP-region permutation was performed using the "ShuffleBed" function within the bedtool library, implemented in the online version of the Galaxy software suite (Quinlan and

Hall, 2010; Gruening, 2014). Supplementary Figure 3 shows that indeed randomly shuffled ChIP-peaks do not result in any feature-distribution differences between H3K27ac and H3K27me3 modifications nor between DSS disease conditions. Generally, randomized ChIP-regions had a higher tendency to annotate to distal intergenic regions compared to any of the experimentally determined sets of IDR-peaks (Supplementary Figure 3).

In summary, random-peak annotation clearly contradicts the annotation results of the experimentally derived ChIP-peak data sets, thus underlining validity and biological meaning of the experimentally generated ChIP-peak data sets.

As epigenetic histone modifications around TSS are most meaningful to interpret for consequences of transcriptional activity of a given locus, next the distances of identified high-confidence ChIP-peaks to known TSS were analyzed in more detail. Using the annotatePeak function of ChIPseeker (Yu et al., 2015), the closest TSS to each ChIP-peak was reported and its distance to the ChIP-region start was calculated. In Figure 24 , results of this approach are visualized (plotDistToTSS function), representing relative abundance of ChIP-peaks within a certain distance range from TSS for all DSS model conditions.

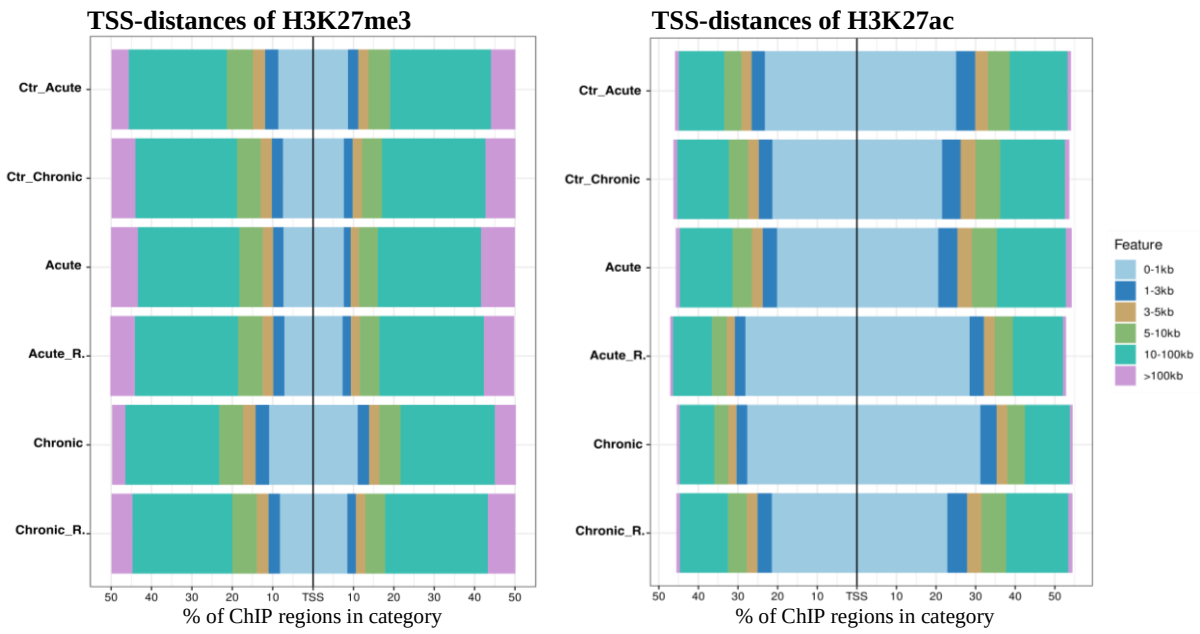

Figure 24: Distance to TSS of high-confidence H3K27me3 and H3K27ac ChIP-peaks. High-confidence H3K27me3/H3K27ac ChIP-peaks from all DSS model conditions were determined by MACS2 peak-calling and IDR calculation as described in the text. ChIP-peak positioning in reference to TSS was analyzed by ChIPseeker's annotatePeak function. For each ChIP-peak only the closest TSS was reported. Distance to TSS was calculated in reference to peak start. Distances were plotted using the plotDistToTSS function. X-axis represents the percentage of ChIP-regions having a TSS-distance falling into one of the stated and color-coded distance categories. Ctr_Acute: untreated young mice, Ctr_Chronic: untreated old mice, Acute: one DSS cycle, Chronic: three DSS cycles, Acute_R: acute remission, Chronic_R: chronic remission.

Since based on Figure 23, around 40 % of H3K27me3 peaks were to be expected in distal intergenic regions, it is not surprising that a large percentage of H3K27me3 peaks were indeed positioned far away at 10 - 100 kb from the TSS (Figure 24, left). Only about 20 % of the H3K27me3 peaks were narrowly positioned within the range of ±1 kb from TSS (Figure 24, left). In contrast, more than 40 % of H3K27ac peaks were found in the same range (±1 kb from TSS, Figure 24, right), again underlining H3K27ac preference for proximal promoter regions. Similar to Figure 23, abundance of H3K27ac and H3K27me3 ChIP-peaks in the proximal promoter range (±1 kb from TSS) was relatively increased in the chronic DSS colitis condition (Figure 24). The same holds true for H3K27ac-peaks in the acute remission condition (Figure 24, right).

TSS-distances of the randomly shuffled ChIP-peaks mostly fell into the range of 10 - 100 kb or > 100 kb and they did not show any distribution differences between H3K27ac and H3K27me3 ChIP-peaks. Correspondingly, no such differences were seen among the different disease conditions (Supplementary Figure 4), again indicating validity of experimentally generated ChIP-peaks.

Taken together, positional and genomic feature annotations of high-confidence ChIP-peaks revealed distribution patterns, specific for the type of histone modification. This underlines different epigenetic functions of H3K27me3 and H3K27ac, requiring according positional preferences in relation to genomic features. Though the feature distribution patterns of H3K27me3 and H3K27ac are largely similar between the DSS colitis conditions, still in acute remission and chronic DSS colitis conditions remarkable deviations from the average feature distribution patterns became evident. Especially, CECs from chronic DSS colitis show an enhanced association of both H3K27me3 and H3K27ac in proximal promoter regions, that is ±1 kb around TSS. This in turn maybe interpreted as the epigenetic aftermath of the three DSS cycles with their inflammatory episodes the CECs were exposed to. How this change in histone mark positioning around TSS in the chronic DSS colitis condition is functionally related to an adapted transcriptional CEC phenotype and *de facto* altered transcriptional activity of according loci was the next logical question to ask. Hence, a closer look on the functional association of gene loci harboring H3K27me3 and H3K27ac marks might give further clues in this regard.

4.5.3 Functional KEGG Pathway Annotation of High-confidence H3K27me3/H3K27ac ChIP-peaks in Proximity to TSS

By positional and genomic feature annotation of high-confidence ChIP-peaks from all DSS model conditions, identified gene symbols became associated with one or several ChIP-peaks with the according gene symbol locus being in proximity to the peak position. The resulting lists of unique gene symbols represent gene loci whose expression is possibly affected by epigenetic histone modifications. Kyoto Encyclopedia of Genes and Genomes (KEGG, (Kanehisa et al., 2004)) pathway enrichment analysis is a commonly used bioinformatic tool that helps to gain insights into functional aspects of a

set of genes that has been identified by an experimental approach by finding statistically over-represented descriptive terms. Overrepresented terms indicate that certain genes in the list of input gene symbols may be functionally important for the experimental condition from which the input list was compiled from and provide important clues as to which cellular aspects may be affected.

Functional KEGG annotation of ChIP-peaks can be expected to be more relevant when limited to a narrow annotation frame around TSS, thereby ignoring uncertain long-distance ChIP-peak/TSS associations and improving interpretability. Hence, only ChIP-peaks with distances between ± 10 kb around TSS were retained (Table 12). The distance restriction limited the ChIP-peaks to a fraction of the total set of high-confidence H3K27me3 ChIP-peaks: control acute: 40 %, control chronic: 36 %, acute DSS: 34 %, acute remission: 35 %, chronic DSS: 45 %, chronic remission: 38 %.

Conditions	Numbers of high-confidence ChIP-peaks with distances between ± 10 kb around TSS for H3K27ac	Numbers of high-confidence ChIP-peaks with distances between ± 10 kb around TSS for H3K27me3
Control acute	18052	15668
Acute	26744	19314
Acute Remission	11035	21444
Control chronic	23060	20153
Chronic	10862	12394
Chronic Remission	19330	18495

Table 12: Numbers of identified IDR determined high-confidence peak regions with distances between ± 10 kb around TSS for H3K27ac and H3K27me3 for each disease conditions and corresponding controls.

Unique lists of gene symbols annotated to above ChIP regions were analyzed for KEGG term enrichment by ClueGO (Bindea et al., 2009). Only KEGG terms with FDR < 0.05 in a right-sided hypergeometric test were considered relevant and for each significant term, the relative term coverage was calculated. That means to which percentage the entire list of gene symbols of a given KEGG term could be also found in the gene symbol set of an annotated (± 10 kb around TSS) high-confidence ChIP-peak list from a DSS model condition. To some extent, this measure may provide an association strength between genes involved in a certain functional category and the presence of at least one high-confidence H3K27me3 and/or H3K27ac ChIP-peak within a 20 kb range around TSS. Of note, such associations must not be expected to necessarily affect *de facto* transcriptional activity.

Figure 25 shows the KEGG enrichment results for H3K27me3 high-confidence ChIP-regions. At a first glance, it becomes obvious that most of the 25 KEGG terms have term coverages of at least 62 % or higher and are stably enriched, regardless of the DSS model condition. This is at least in part a statistical consequence of the large numbers of identified H3K27me3 ChIP-regions within the CEC chromatin that despite the restriction by TSS-distance in total annotate to most genes in the murine genome. On the other hand, this also may imply that the overall set of genes whose TSS are in proximity to at least one of the identified ChIP-peaks is remarkably stable. In the chronic DSS colitis condition, many KEGG terms showed smaller term coverages compared to all other conditions. This is likely due to a smaller list of unique gene symbols resulting from the ChIP annotation of regions from this condition.

Of note, core pathway-associated KEGG terms are most insightful for functional interpretation as they encompass elaborate biochemical knowledge about protein interactions and regulatory networks. Amongst enriched core KEGG pathway models, terms like “Calcium signaling pathway”, “cAMP signaling pathway”, “PI3K-Akt signaling pathway”, “MAPK signaling pathway”, “Wnt signaling pathway”, “Pathways in cancer” and “Phospholipase D signaling pathway” can be found. In context of CECs, Wnt-signaling (109 enriched gene symbols from in total 169 in this term) is particularly interesting, as this pathway is known to regulate IEC differentiation from epithelial stem cells (reviewed in (Mah et al., 2016)).

The most significantly enriched KEGG term was “neuroactive ligand-receptor interaction” referring to 286 genes. However, “Pathways in cancer” was the KEGG term with the largest number of enriched genes found (303). Interestingly, also the KEGG term “Inflammatory bowel disease” was significantly over-represented (47 enriched genes). Found genes in this term mostly refer to cytokines, transcription factors and antigen presentation.

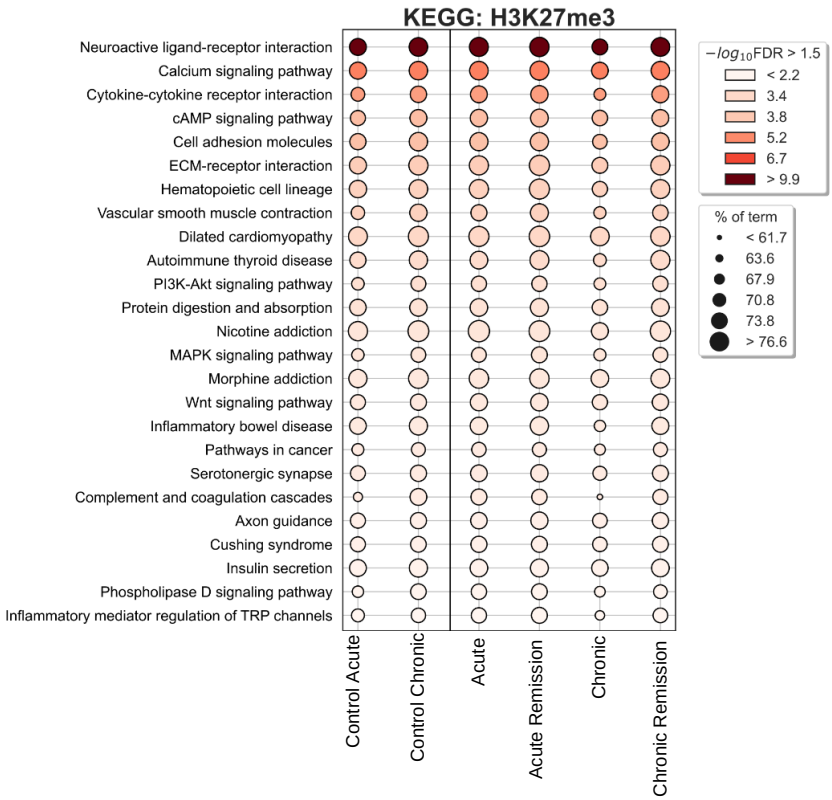

Figure 25: KEGG pathway enrichment of genes annotated to H3K27me3 high-confidence ChIP-peaks within ± 10 kb range around TSS in CECs from all DSS model conditions. High-confidence H3K27me3 ChIP-peaks from all DSS model conditions with TSS-distances of ± 10 kb were annotated to adjacent gene loci using ChIPseeker package. Lists of unique gene symbols per condition were analyzed by KEGG pathway term enrichment using ClueGO addon for the Cytoscape software. Statistical over-representation was calculated using a right-sided hypergeometric test with Bonferroni step-down p-value correction. Only overview terms from a GO-term grouping process with FDR < 0.05 were considered significant. Data represent color-coded -log10 FDR values and circle-sizes reflecting the relative term coverage. Terms are descendingly sorted by the average -log10 FDR value across all conditions.

The same kind of analysis was performed for high-confidence H3K27ac ChIP-peaks, too. Restriction to the narrow annotation frame of ± 10 kb around TSS reduced the numbers of relevant H3K27ac ChIP-peaks to some extend: control acute: 72 %, control chronic: 69 %, acute DSS: 67 %, acute remission: 76 %, chronic DSS: 78 %, chronic remission: 70 %.

H3K27ac ChIP-peaks were mainly close to TSS, compared to most H3K27me3 ChIP-peaks (Figure 24). Hence, H3K27ac ChIP-peaks annotated to even more gene loci than the H3K27me3 peak-annotation and, not surprisingly, attributed to even more (in total 65) enriched KEGG pathway terms (Figure 26). Most over-represented H3K27ac KEGG terms have coverages of at least 80 % or higher, even exceeding those found in the H3K27me3-peak KEGG annotation. Interestingly though, the acute remission and chronic DSS colitis conditions both show systematically reduced term coverages compared to all other conditions. This is again likely due to the smaller lists of unique gene symbols resulting from the ChIP annotation of regions from these conditions.

Overall, the top 10 most significantly enriched KEGG core signaling pathway terms for the H3K27ac-peaks were: “MAPK”, “Rap1”, “Insulin”, “Ras”, “Neurotrophin”, “Hippo”, “mTOR”, “Thyroid hormone”, “ErbB” and “AMPK signaling pathways”. Like the H3K27me3-peak KEGG annotation, in the H3K27ac annotation also the term “Pathways in cancer” contains the most enriched genes (439 from 543 total genes in that term). In comparison, only 9 KEGG terms were found to be enriched in both, H3K27ac and H3K27me3 peak annotations (“PI3K-Akt”, “MAPK”, “Calcium”, “cAMP”, “Wnt” and “Phospholipase D signaling pathway” as well as “Axon guidance” and “Cushing syndrome”).

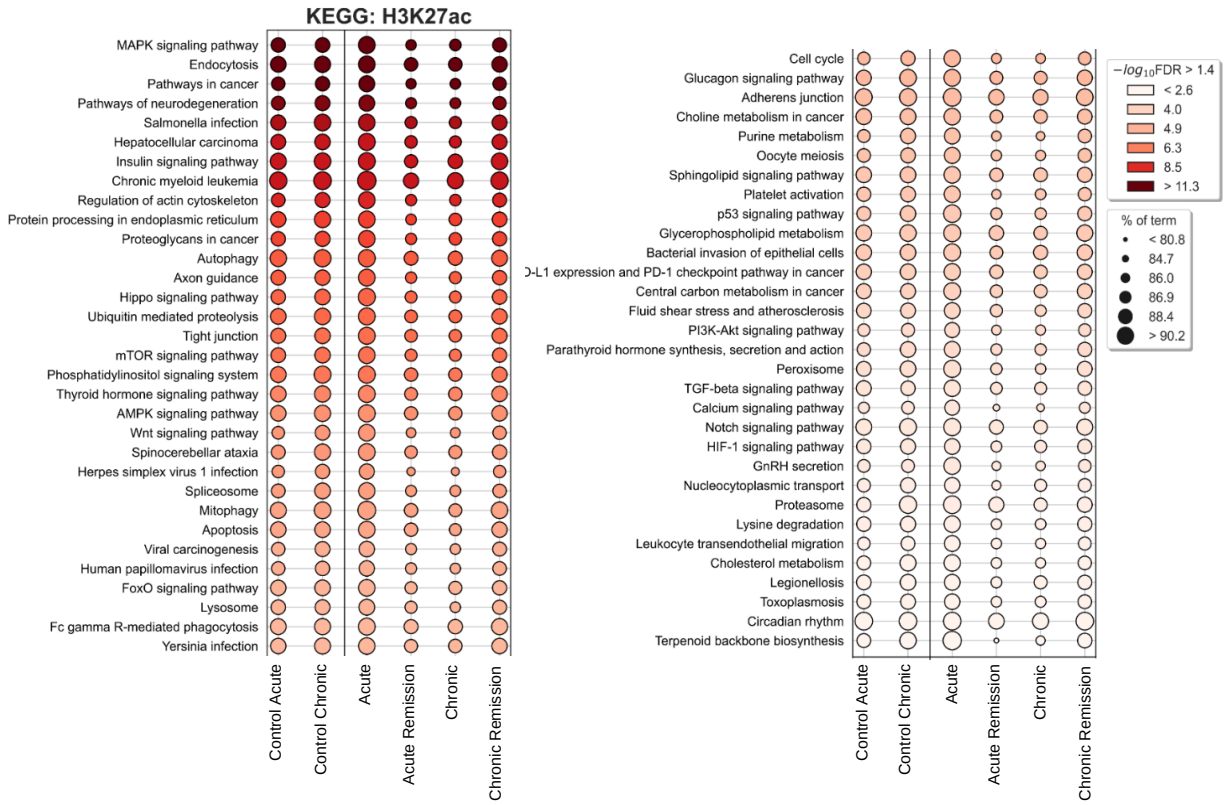

Figure 26: KEGG pathway enrichment of genes annotated to H3K27ac high-confidence ChIP-peaks within ± 10 kb range around TSS in CECs from all DSS model conditions. High-confidence H3K27ac ChIP-peaks from all DSS model conditions with TSS-distances of ± 10 kb were annotated to adjacent gene loci using ChIPseeker package. Lists of unique gene symbols per condition were analyzed by KEGG pathway term enrichment using ClueGO addon for the Cytoscape software. Statistical over-representation was calculated using a right-sided hypergeometric test with Bonferroni step-down p-value correction. Only overview terms from a GO-term grouping process with FDR < 0.05 were considered significant. Data represent color-coded -$\log_{10}$ FDR values and circle-sizes reflecting the relative term coverage. Terms are descendingly sorted by the average -$\log_{10}$ FDR value across all conditions.

Taken together, the KEGG annotation approach sheds some light on the overall potential functional involvement of TSS-proximal high-confidence H3K27me3/H3K27ac histone modifications in CECs, based on the mere proximity of according ChIP-peaks to TSS. This is of course an over-simplification of the involvement of the two histone modifications in transcriptional regulation, which must be further cross-checked with the above CEC RNA-seq data.

The relatively small KEGG term-overlap between H3K27me3- and H3K27ac-peak annotations again stresses the deviating characters of H3K27me3 and H3K27ac histone modifications that has been described already for the positional and genomic feature ChIP-peak annotations.

Strikingly, KEGG term coverages of H3K27ac-peaks in acute DSS and chronic DSS colitis conditions as well as those of H3K27me3-peaks in the chronic condition show systematically reduced term coverage values, compared to all other conditions. This is noteworthy, as these conditions already proofed most interesting in the RNA-Seq analysis (compare section 4.4).

Still it remains difficult to derive concise conclusions about differences in functional ChIP-peak annotations between the DSS model conditions. Here, a differential peak set analysis that first compares the extend of H3K27me3 and H3K27ac modifications between the DSS model conditions and then annotates sites of differential histone modifications seems promising as the next step in the ChIP-seq analysis pipeline.

4.5.4 Occurrence and Modification-state of Differential H3K27me3/H3K27ac ChIP-peaks Correlates with DSS Colitis Model Conditions and Attributes to MHC-II Gene Loci

The ChIP-seq analysis pipeline outlined so far gave an overview as to where in CEC chromatin from the different DSS model conditions genomic patches of H3K27me3 and H3K27ac histone modification reproducibly occur in principle. Moreover, positional and genomic feature annotation as well as functional KEGG annotation gave insights to overall genome-wide differences in histone modification patterns, lacking however position-specific information.

Importantly, an IP fold-enrichment value of each identified ChIP-peak was calculated in reference to the sample-specific input control during the peak-calling process, but so far was only used during the IDR calculation. The IP fold-enrichment in reference to the sample's input DNA control is an important indicator of the number of modified histone entities within a given ChIP-region, but also reflects the IP-efficiency. However, IP fold-enrichment values of ChIP-regions cannot only be calculated for a given IP-sample versus its input control, but instead can be also used to compare ChIP-seq samples from different experimental conditions. Thereby it is possible to directly compare the extent of histone modification between positionally overlapping ChIP-regions derived from e.g. the DSS-treated model conditions versus their untreated counterparts. This approach identifies specific genomic regions that deviate in the extent of histone modification, which can be interpreted as a change in epigenetic control of that given genomic position and the possible change in transcriptional regulation of adjacent loci.

A major goal of this thesis was to identify alterations in the epigenetic control of CEC transcriptional responses following DSS-induced colitis. Thus, the final analysis step in the ChIP-seq analysis pipeline is differential ChIP-seq analyses of CEC ChIP-seq samples from acute DSS, acute remission, chronic DSS and chronic remission conditions versus their respective untreated control conditions.

To this end, ChIP-Seq data were analyzed with the DiffBind (Stark et al., 2011; Ross-Innes et al., 2012) software package which determines genomic regions with statistically significant condition-specific H3K27me3/H3K27ac ChIP-enrichment. DiffBind integrates read-count data from all sorted bam-files, genomic coordinates of MACS2 peak-called IDR high-confidence ChIP-regions, exclusion of black-listed genomic regions as well as the experimental design matrix. To compensate for technical variance in IP-efficiency, library preparation and effective sequencing depth, DiffBind performs elaborate cross-

sample normalization calculations and performs comparative statistics of ChIP-regions from desired experimental contrasts.

Diffbind results provide information about the fold-difference and significance of histone hypo/hyper-methylation and hypo/hyper-acetylation of consensus ChIP-regions. Relevant differentially histone-modified genomic regions between two experimental conditions were ultimately identified by application of a cutoff for statistical significance (FDR ≤ 0.05). Resulting differential ChIP-regions were annotated by the annotatePeakInBatch function of the ChIPpeakAnno software package (Zhu et al., 2010; Zhu, 2013; Zhu et al., 2017) within an annotation range of ± 10 kb around TSS. Peak distance calculation were done based on distance to TSS in reference to middle of peak. Associated gene symbols were further analyzed for KEGG-term enrichment to give a conclusive functional interpretation of identified differential histone epigenetic marks.

Figure 27 shows the result of H3K27me3 differential ChIP-analyses. To give an overview, on the above-mentioned four condition comparisons, Figure 27A presents for each of them a volcano plot that correlates statistical significance of differential methylation of according consensus ChIP-regions with the according $\log_2$ fold-difference of ChIP-enrichment. In the plots, each point represents a consensus ChIP-region, with significant ones (FDR ≤ 0.05) colored in purple. In reference to the untreated control conditions, CECs from acute DSS colitis condition had 133 significantly different histone-modified genomic sites, with most of them being hyper-methylated and only 9 being hypo-methylated. In the acute remission condition, still 153 differential genomic sites were identified, with again most sites being hyper- and only 5 sites hypo-methylated. Strikingly, CECs from chronic DSS colitis condition had 339 mostly hypo-methylated differential genomic sites, thereby presenting an opposing pattern to the acute DSS colitis condition. Interestingly, CECs from chronic remission condition only showed a single hyper-methylated site, suggesting a complete restauration of the initial H3K27me3 modification landscape during the final 3-week remission phase.

Positional annotation of differential H3K27me3 ChIP-regions within an annotation range of ± 10 kb around TSS reduced the number of relevant ChIP-regions and resulted in 4 gene symbol lists that were compared with one another in a Venn diagram (Figure 27B). Surprisingly, TSS-proximal differential H3K27me3 ChIP-regions from the 4 comparisons annotated to more or less unique sets of gene symbols, suggesting mostly condition-specific H3K27me3 epigenetic adaptation. In acute DSS colitis, 51 condition-specific gene loci had at least one differential ChIP-region adjacent to their TSS. 44 gene loci were shared with the acute remission condition and again 51 gene loci were specific for the latter condition as well. 156 gene symbols were unique for the chronic condition. 3 gene symbols were shared amongst acute DSS colitis, acute remission and chronic DSS colitis. Only one gene symbol was shared between acute remission and chronic DSS colitis as well as chronic DSS colitis and chronic remission, respectively. All in all these findings allow the conclusion that the H3K27me3 modification landscape

strongly deviates over time from the acute to the chronic DSS colitis condition. Not only the acute DSS and chronic DSS colitis conditions hardly share any gene loci with differential ChIP-regions proximal to TSS, but even more the overall state of H3K27me3 modifications turn from mostly hyper-methylated in acute DSS colitis to mostly hypo-methylated in chronic DSS colitis. This clearly drives the notion of CEC epigenetic adaptations caused by repeated episodes of colonic inflammation.

Given the large total number of initially identified H3K27me3-regions, it is noteworthy that the number of differentially modified H3K27me3 ChIP-regions is generally rather small. This might indicate that indeed the CEC genomic H3K27me3 modification landscape is rather stable and only changes to some extend within comparatively few, but specific H3K27me3-sites.

KEGG-term enrichment of the gene symbols incorporated within the Venn diagram in Figure 27B allowed further functional interpretation of differential H3K27me3 patterns (Figure 27C). Here, the most significant KEGG term was “Inflammatory bowel disease”, and it was mainly associated with the chronic DSS colitis condition and to a minor extend with acute DSS colitis. Enriched genes within the term “Inflammatory bowel disease” were *H2-Ab1*, *H2-DMb1*, *H2-DMb2*, *H2-Eb2* and *Il4ra*. Interestingly, four genes in this list encode for MHC-II variant proteins. Of note, several MHC-II variant genes were already observed in RNA-Seq analysis (compare section 4.4). Moreover, all four MHC-II genes in the chronic colitis condition had hypo-methylated ChIP-regions next to their TSS (data not shown) which might, indicate enhanced transcriptional activity of these MHC-II loci. The KEGG-term “Pyruvate metabolism” was over-represented in acute DSS colitis, acute remission and chronic DSS colitis, thereby suggesting an epigenetic H3K27me3 impact on this glycolysis-related core-metabolic pathway. The KEGG-terms “Tyroid hormone synthesis” and “Arginine and proline metabolism” includes genes like *Duox2* and *Nos2* which are related to reactive oxygen and nitrogen species. Both genes were also found in the RNA-seq analysis. Overall, most over-represented KEGG-terms accounted for the chronic DSS colitis condition, matching the relative large number of genes with differential H3K27me3 ChIP-regions in this condition.

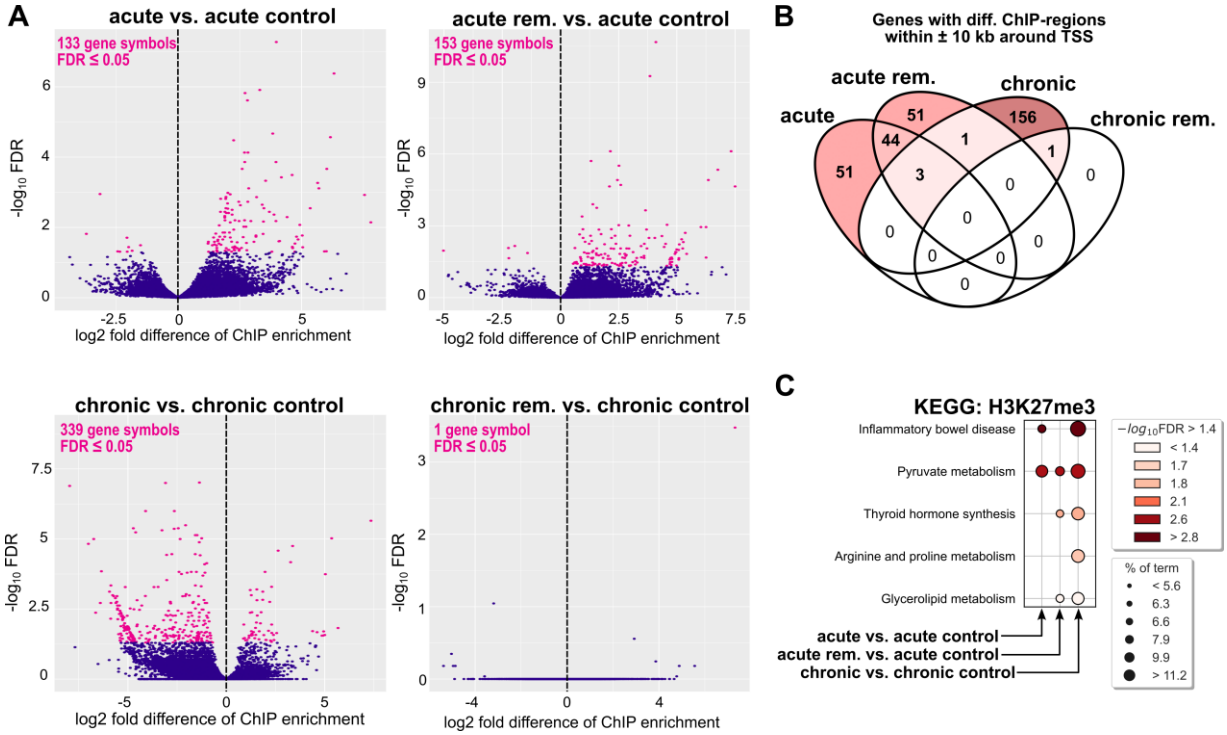

Figure 27: Occurrence and methylation-state of differential H3K27me3 ChIP-peaks correlates with DSS model conditions. Differential H3K27me3 ChIP-enrichment of DSS model conditions versus their control conditions was calculated by DiffBind algorithm for consensus high-confidence ChIP-regions – see text for details. A) Volcano plots representing -$\log_{10}$ FDR and $\log_2$ fold-difference of ChIP-regions from indicated comparisons. Pink dots represent differential ChIP-regions with FDR ≤ 0.05. Numbers of statistically significant sites are stated in upper left corners. B) Venn Diagram comparing gene symbols of genomic loci with at least one differential ChIP-region in indicated comparisons within ± 10 kb around TSS. C) KEGG-term enrichment analysis of genes symbol lists from B) using ClueGO software with right-sided hypergeometric test and Bonferroni step-down p-value correction. Only overview terms from a GO-term grouping process with FDR < 0.05 were considered significant. Circle-color and size represents -$\log_{10}$ FDR and relative term coverage, respectively.

The analysis of differential ChIP-enrichment for DSS model conditions (versus untreated controls) effectively narrowed down the epigenetic focus on surprisingly few dedicated ChIP-regions in a condition-specific fashion. TSS-proximal annotation led to the identification of promising candidate genes whose transcriptional activity are possibly influenced by differential H3K27me3 ChIP-regions. If these ChIP-seq-based candidate genes indeed are differentially expressed in the according experimental condition, can be ultimately validated by cross-checking with the matched RNA-seq-based expression analysis, described in section 4.4. Indeed, amongst the H3K27me3-associated candidate genes, 10 were significantly expressed. Figure 28 correlates the RNA-seq-based $\log_2$ FC of these genes with the ChIP-seq-based $\log_2$ fold-difference of ChIP-regions adjacent to their TSS (within ± 10 kb). In the acute DSS colitis condition, down-regulation of *Odf3b* (Outer Dense Fiber Of Sperm Tails 3B) and *St3gal6* (ST3 Beta-Galactoside Alpha-2,3-Sialyltransferase 6) correlates with hyper-methylation of TSS-proximal H3K27me3 ChIP-regions (Figure 28, left). In the chronic DSS condition, hyper-methylation of TSS-proximal H3K27me3 ChIP-regions correlated with the down-regulation of *Cpm* (Carboxypeptidase M) and *Soat1* (Sterol O-Acyltransferase 1). Inversely, at the same time, up-regulation of *Duoxa2* (Dual Oxidase Maturation Factor 2), *Duox2* (Dual Oxidase 2), *Nos2* (Nitric Oxide Synthase 2), *Ido1*

(Indoleamine 2,3-Dioxygenase 1), *H2-DMb1* (Major Histocompatibility Complex, Class II, DM Beta) and *H2-Ab1* (Histocompatibility 2, class II antigen A, beta 1) was clearly correlated with hypo-methylation of adjacent H3K27me3 ChIP-regions (Figure 28, right). Thus, the combined RNA/ChIP-seq data clearly show the *de facto* transcriptional activity of all 10 genes to depend on the H3K27 methylation status of genomic regions that are within a range of ± 10 kb from the locus TSS.

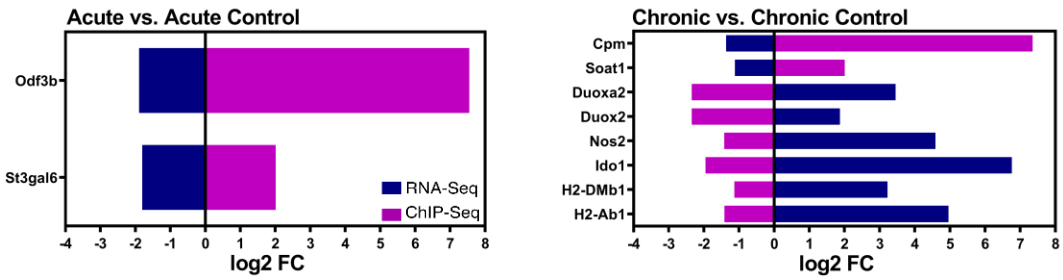

Figure 28: Hypo-methylated ChIP-regions are associated with enhanced gene expression. Gene symbols attributing to annotated differential H3K27me3 ChIP-regions from stated condition comparisons were matched with results from differential RNA-seq analysis. Only significantly regulated genes with at least one significant differential H3K27me3 ChIP-region within ± 10 kb from TSS are shown. Data represent $\log_2$ FC of differential transcriptional activity (blue bars) and $\log_2$ fold-difference in H3K27me3 ChIP-enrichment (pink bars).

The differential ChIP-seq approach as described for H3K27me3 was also performed for H3K27ac histone modifications (Figure 29). Figure 29A shows the respective volcano plots. Interestingly, for differential H3K27ac in both remission conditions no significant differential ChIP-regions were found.

There were 10789 significant differentially acetylated regions in the acute DSS colitis condition compared to the acute control condition (Figure 29A, left) with basically almost all of them being hyper-acetylated. The chronic versus chronic control comparison resulted in 212 significantly altered ChIP-regions (Figure 29A, right) that all were hypo-acetylated. Thus, similar to the findings for differential H3K27me3 ChIP-regions, differential H3K27ac ChIP-regions also show an inversion of modification states comparing the acute with the chronic DSS colitis condition.

The Venn diagram of TSS-proximal (± 10 kb) gene loci annotating to at least one differential H3K27ac ChIP-region shows that only 135 genes were identified in both, acute and chronic DSS conditions (Figure 29B). The vast majority of genes (10113) with differential H3K27ac ChIP-regions were however clearly specific for the acute DSS colitis condition. This indicates major epigenetic changes in the CEC genomic H3K27ac landscape after an acute DSS dosage period with many gene loci becoming likely more accessible due to hyper-acetylation. Interestingly, hyper-acetylation of all sites disappears after three cycles of DSS dosage (chronic DSS colitis condition), and histone acetylation then even becomes reduced at few genomic sites. This in turn implies the existence of some unknown factors drastically affecting epigenetic histone modifications in CECs after the end of the first and the end of the third DSS dosage period.

Figure 29C, shows functional KEGG-term enrichment of genes with differential H3K27ac ChIP-regions within ± 10 kb around TSS. Given the over 10000 associated genes from the acute DSS condition, it may not surprise that KEGG-enriched terms are dominated by this set of genes. The most significant KEGG-term was “Protein processing in endoplasmic reticulum” with 134 enriched genes. Amongst core KEGG pathways terms like MAPK, mTOR, Wnt, Insulin, Hippo, FoxO, Sphingolipid, Thyroid hormone, Glucagon, p53 signaling pathways were found. “Endocytosis” had most enriched genes (178 of 272 in that term) amongst cell function related terms. Moreover, differential H3K27 acetylation was also correlated with terms like “Cell cycle”, "Tight junction”, “Colorectal cancer” and “Bacterial invasion of epithelial cells”. Since most differential H3K27ac ChIP-regions showed hyper-acetylation in acute DSS colitis, a substantial number of associated proximal genes might have patches of accessible DNA in their gene bodies and/or promoter regions.

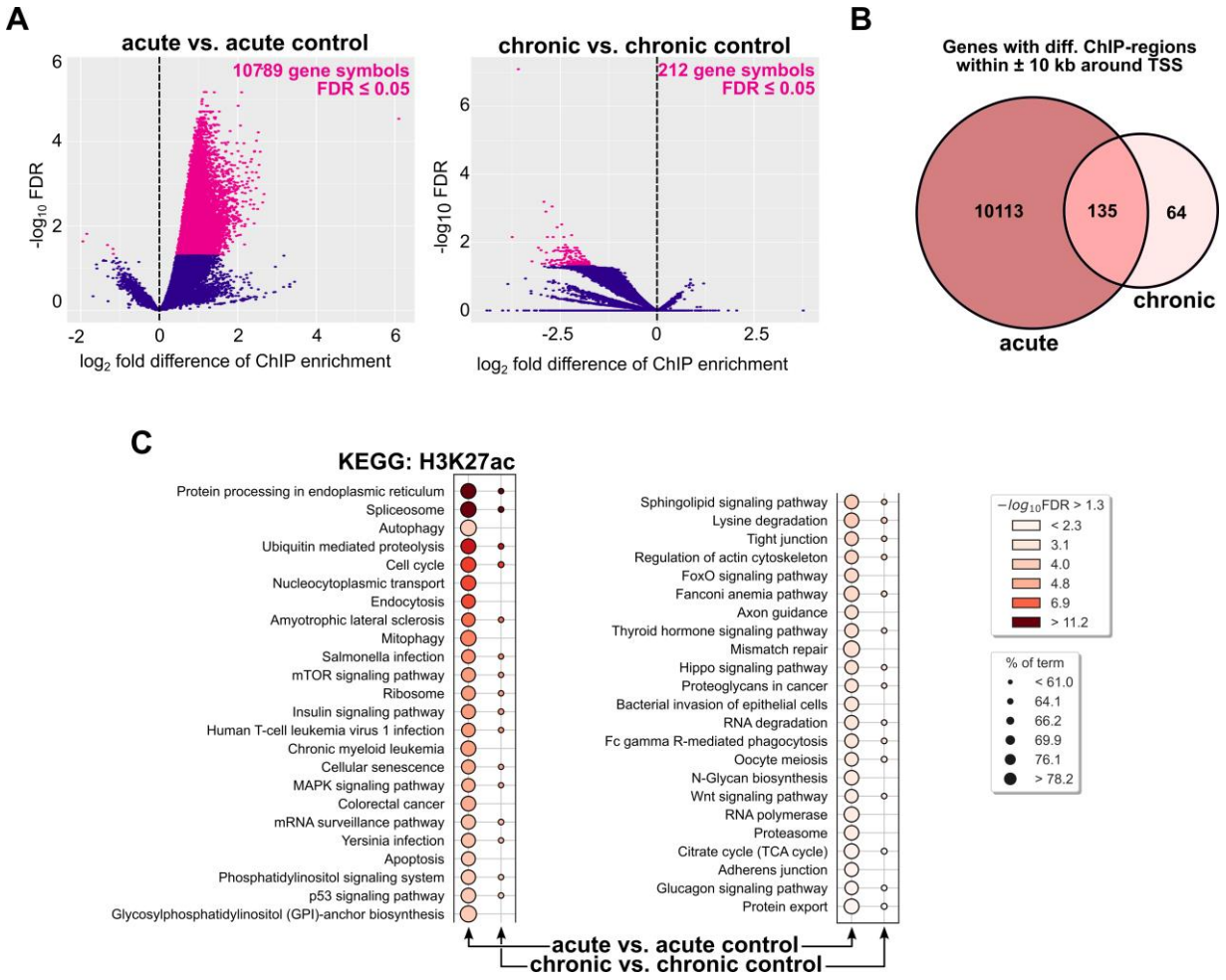

Figure 29: Occurrence of hyper-acetylated differential H3K27ac ChIP-peaks mainly correlates with acute DSS. Differential H3K27ac ChIP-enrichment of DSS model conditions versus their control conditions was calculated by DiffBind algorithm for consensus high-confidence ChIP-regions – see text for details. A) Volcano plots representing -$\log_{10}$ FDR and $\log_2$ fold-difference of ChIP-regions from indicated comparisons. Pink dots represent differential ChIP-regions with FDR ≤ 0.05. Numbers of statistically significant sites are stated in upper right corners B) Venn diagram comparing gene symbols of genomic loci with at least one differential ChIP-region in indicated comparisons within ± 10 kb around TSS. C) KEGG-term enrichment analysis of genes symbol lists from B) using ClueGO software with right-sided hypergeometric test and Bonferroni step-down p-value correction. Only overview terms from a GO-term grouping process with FDR < 0.05 were considered significant. Circle-color and size represents -$\log_{10}$ FDR and relative term coverage, respectively.

To check this, results from the DiffBind analysis of H3K27ac was compared to the RNA-seq results by matching lists of significant differentially expressed genes (compare section 4.4) with those from the ChIP-region annotation. Since different peak regions can be associated with the same gene symbol, some gene names are represented more than once. For matching genes, $\log_2$ fold differences of H3K27ac enrichment and transcript $\log_2$ fold changes from the RNA-Seq data were plotted together (Figure 30). For unexpectedly few genes a match between the two data sets were found.

In the acute DSS colitis condition, H3K27ac hyper-acetylation was not always correlated with increased gene expression. This was the case for genes like: *Cpm* (Carboxypeptidase M), *Retreg1* (Reticulophagy Regulator 1), *St3gal6* (ST3 Beta-Galactoside Alpha-2,3-Sialyltransferase 6), *Hpn* (Hepsin), *Rasd2* (RASD Family Member 2), *Fbxo32* (F-Box Protein 32), *Fam189a2* (family with sequence similarity 189, member A2), *Npas2* (Neuronal PAS Domain Protein 2), which were down-regulated despite association with hyper-acetylated ChIP-regions (Figure 30, left). Thus, these genes represent examples for cases in which enhanced gene expression is not positively correlated with locus hyper-acetylation. Other than that, hyper-acetylation of the MHC-II related protein *H2-Eb1* (histocompatibility 2, class II antigen E beta) was associated with increased gene expression as expected (Figure 30, left). Genes like *Lrg1* (Leucine Rich Alpha-2-Glycoprotein 1), *Creld2* (Cysteine Rich With EGF Like Domains 2), *Sulf2* (Sulfatase 2), *Duoxa2* (Dual Oxidase Maturation Factor 2) *Hspa8* (Heat Shock Protein Family A (Hsp70) Member 8) and *Ccnd1* (Cyclin D1) also show the expected correlation between hyper-acetylation and enhanced expression (Figure 30, left). Still there does not seem to exist a numeric 1:1 correlation between the extent of H3K27ac modification represented by the $\log_2$ fold-difference and the effective fold change of transcript expression.

Within the chronic DSS colitis conditon there were only two matches between H3K27ac ChIP-seq and RNA-seq data: *Ttll6* (Tubulin Tyrosine Ligase Like 6) and *Chd9* (Chromodomain Helicase DNA Binding Protein 9). Here, hypo-acetylation was correlated with a decrease in gene expression of *Ttl6* and an increase in expression of *Chd9* (Figure 30, right).

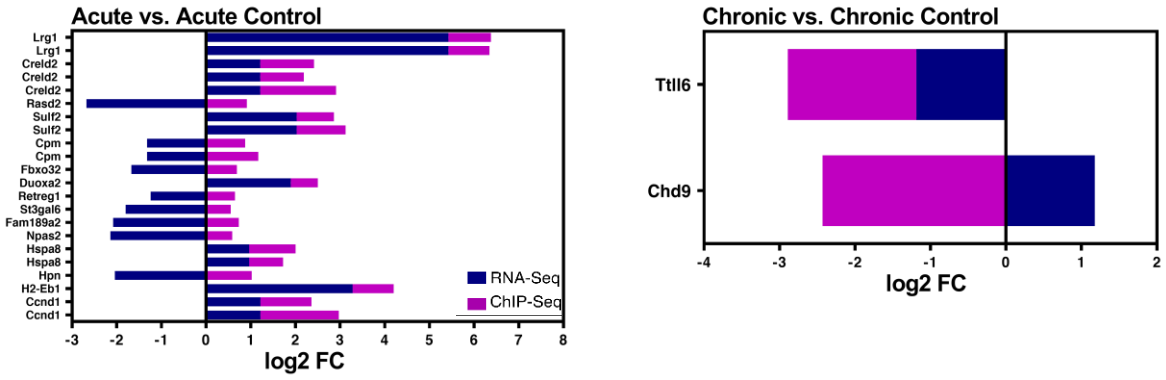

Figure 30: Differential H3K27 acetylation is associated with enhanced and reduced gene expression. Gene symbols attributing to annotated differential H3K27ac ChIP-regions from stated condition comparisons were matched with results from differential RNA-seq analysis. Only significantly regulated genes with at least one significant differential H3K27ac ChIP-region within ± 10 kb from TSS are shown. Bars from RNA-Seq and ChIP-Seq is stacked. Data represent $\log_2$ FC of differential transcriptional activity (blue bars) and $\log_2$ fold-difference in H3K27ac ChIP-enrichment (pink bars).

In summary, epigenetic TSS-proximal and differential H3K27me3/H3K27ac changes that can be correlated with *de facto* altered transcript expression could only be detected in the acute and chronic DSS colitis conditions, with according observations being clearly more frequent in CECs from acute DSS colitis.

Interestingly, in acute DSS colitis the gene "ST3 Beta-Galactoside Alpha-2,3-Sialyltransferase 6" (*St3gal6*) has both, associations with hyper-methylated ChIP-regions as well as hyper-acetylated ChIP-regions (Figure 28, left and Figure 30, left) and is down-regulated in reference to CECs from untreated mice.

Duoxa2 (Dual Oxidase Maturation Factor 2) is transcriptionally up-regulated in acute and chronic DSS colitis but has hyper-acetylated H3K27ac ChIP-regions only in acute DSS colitis and only H3K27 hypo-methylated regions in the chronic DSS colitis condition (Figure 30, left and Figure 28, right). This may hint at distinct epigenetically altered regulatory sites in this locus, that act independently to ensure enhanced expression of *Duoxa2* encoding for a protein that is responsible for proper cellular localization and maturation of the dual oxidase 2 enzyme that in turn is part of a peroxide generating enzyme complex (Grasberger and Refetoff, 2006).

A similar observation can be made for the "Carboxypeptidase M" (*Cpm*), a membrane-bound arginine/lysine carboxypeptidase, that is transcriptionally down-regulated in acute and chronic DSS colitis conditions but only has associated hyper-acetylated H3K27ac ChIP-regions in acute DSS colitis and hyper-methylated H3K27me3 ChIP-regions in chronic DSS colitis in proximity to its TSS (Figure 30, left and Figure 28, right). Again, this may hint at distinct epigenetic influences leading to, in this case, consistent down-regulation of *Cpm* in CECs during episodes of DSS consumption of mice.

Furthermore, in total three genes related to MHC class II antigen presentation, *H2-Ab1* (Histocompatibility 2, class II antigen A, beta 1), *H2-DMb1* (histocompatibility 2, class II, locus Mb1) and *H2-Eb1* (Histocompatibility 2, class II antigen E beta) were amongst correlating ChIP-seq/RNA-seq candidates. All three genes are up-regulated particularly in the chronic DSS colitis condition and to some extend in CECs from acute DSS colitis. However, loci of *H2-Ab1* and *H2-DMb1* both harbor differential H3K27me3 hypo-methylated ChIP-regions only in chronic DSS colitis and the *H2-Eb1* locus only contains differential H3K27ac hyper-acetylated ChIP-regions in acute DSS colitis adjacent to their respective TSS (Figure 28, right and Figure 30, left).

Taken together, the elaborate transcriptional and epigenetic analysis of CECs, especially in acute and chronic DSS colitis, revealed conceivable candidate genes that are highly relevant for inflammatory involvement of CECs in the context of colitis. Expression of these genes may be influenced by condition-specific H3K27me3/H3K27ac histone modifications that render according genomic sites more/less accessibility for the core transcription machinery. Thus, the above-mentioned candidate genes and their encoded proteins have also the potential to give new clues for understanding the role of CECs for inflammatory perpetuation of colitis in the DSS-model and may also spawn transferable knowledge that helps to better understand inflammatory conditions in IBD patients.

4.6 Flow Cytometry Verifies Increased Protein Expression of Selected Target Genes Identified in CECs by RNA-Seq during Chronic Stages of the Disease

We next aimed to verify the expression of selected target genes identified by RNA-Seq and/or the combined ChIP-Seq/RNA-Seq approach on the protein level. Among the candidate genes, MHC-II related molecules appeared to be of special interest. The rationale behind this was that well in line with RNA-Seq data that indicated increased expression of MHC-II related genes during DSS colitis (Figure 21), CD4+ T cells accumulated in the *lamina propria* in the chronic stages of the disease (Figure 16). Moreover, on the molecular level, increased MHC-II gene expression was most likely the result of hypomethylation of MHC-II related genes in the chronic stage of disease (Figure 28, right). Other interesting candidate genes that were identified to be overexpressed in CECs in chronic disease stages were *Cd177*, *Ido1* and *Nos2 (iNOS)*. So far, increased expression of the MHC-II related genes *Cd74*, *H2-Aa*, *H2-Ab1* as well as *CD177*, *Ido1* and *Nos2* was exclusively identified on the mRNA levels. However, since gene expression not always positively correlates with protein expression due to the potential action of various post-transcriptional mechanisms, protein level of the selected candidate genes was next determined by flow cytometry. Since most pronounced effect in gene expression were observed in the chronic stage of disease and the accumulation of CD4+ T cells in the *lamina propria* was especially evident in chronic and chronic remission stages, only these experimental conditions were analyzed. While costimulatory molecules (*Cd80*, *Cd86*, *Cd40*) were only weakly expressed in CECs according to RNA-Seq data (data not shown), they are of crucial importance in shaping the CD4+ T cell

pool in inflammatory settings. More specifically, while MHC-II+ costimulation-competent CECs may favor the expansion of Teff cells further boosting inflammation or may favor the expansion of Tregs, CD4+ T cell stimulation by MHC-II+ CECs in the absence of sufficient costimulation may favor the induction of T cell anergy. Therefore, in order to determine costimulatory capacity of CECs in the chronically inflamed intestine, flow cytometric quantification of CD80, CD86 and CD40 on CECs was included in the survey.

CECs were isolated and analyzed for marker expression using two different antibody staining panels: panel one included CD177, I-Ak (MHC-II), I-A/I-E (MHC-II) and IDO1; panel two included CD74 (invariant chain), iNOS, CD86, CD80 and CD40. Since epithelial cells from the small intestine are known to express MHC-II molecules in the steady state, and activated splenocytes do express costimulatory proteins, IECs from small intestine and LPS-treated splenocytes were used as positive controls for both panels.

Figure 31 shows representative histograms of CD177+, IDO1+, I-Ak+ and I-A/I-E+ CECs, respectively, as well as expression of these molecules on LPS-treated splenocytes and epithelial cells from the small intestine as controls.

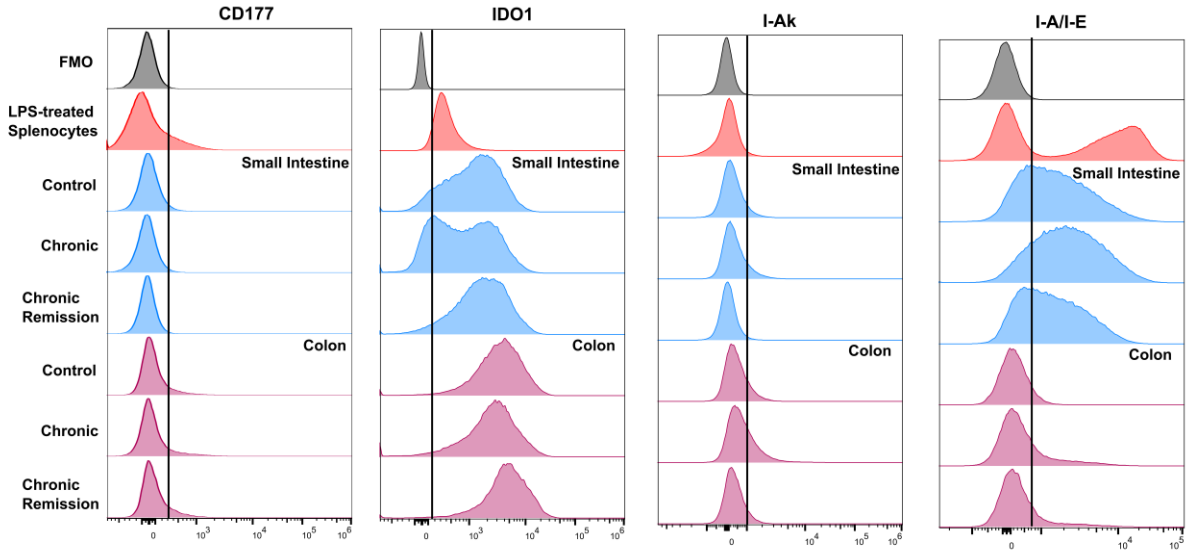

Figure 31: Representative histogram from flow cytometric analysis of selected molecules. LD-CD45-CD31-EpCAM+ CECs were downsampled 10,000 events in the colon for each condition, if possible and subsequently concanated to create a summary file for each condition. FMOs were used as negative controls. LPS-treated splenocytes and epithelial cells from the small intestine were used as positive controls. Gray color represents each individual FMO, red color represents LPS-treated splenocytes, blue colors represent IECs from small intestine, and pink colors represent CECs in chronic stages of disease and corresponding control. For the spleen, CD45+ cells or myeloid compartment of CD45+ cells were gated after excluding singlets and dead cells. Modal mode was chosen to scale histograms.

Figure 32 shows the MFI and frequency of CECs according to their expression of CD177, IDO1, I-Ak and I-A/I-E for individual colon samples. The percentage of CD177+ cells within the CEC population significantly increased in the chronic stage and remained slightly elevated in the chronic remission phase, while the overall low level of CD177 expression did not change upon inflammation. In contrast,

while virtually all CECs were IDO1+ independent of intestinal inflammation, the level of IDO1 expression by CECs was particularly high in the chronic remission phase. Protein expression level of MHC-II molecules was significantly increased in the chronic stage of disease followed by decline during the remission phase compared to control. The same pattern was observed for the frequency of MHC-II+ CECs, although only in case of I-A/I-E the differences were statistically significant (Figure 32).

Taken together, most protein expression data correlated well with alterations on the transcriptional level (Figure 20, Figure 21A). Moreover, FACS analysis provided additional information regarding the relative abundance of cells within the entire CEC pool being positive for the analyzed marker and the level of marker expression by individual CECs. Of note, compared to the positive controls, i.e. LPS-treated splenocytes, only a small population of CECs expressed MHC-II (Figure 31).

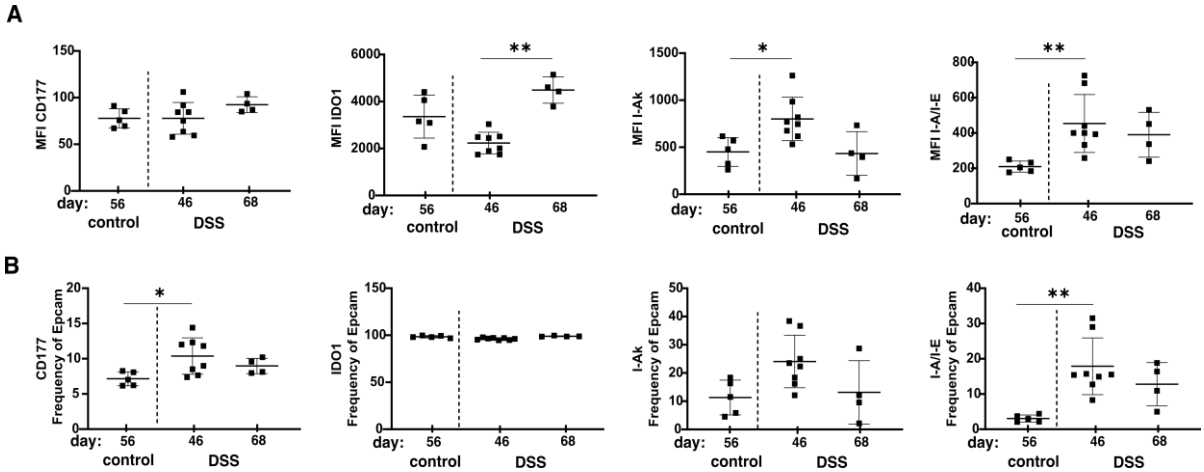

Figure 32: Expression level and percentage of CECs expressing selected target molecules. CECs were isloated from control (day 56), chronic (day 46) and chronic remission group (day 68). After excluding singlets, live-dead, CD45+ and CD31+ cells; EpCAM+ cells were used to determine the geometric mean of MFI for targeted proteins. CECs were gated for CD177, IDO1, I-Ak and I-A/I-E to determine percentages of positive cells. FMOs were used to determine positive gates A) MFI of EpCAM positive CECs (n=4-8) B) Frequency of indicated marker expression within the EpCAM positive CEC pool (n=4-8). Data represent mean with error bars indicating standard deviation. Significance calculated by Kruskal-Wallis test where applicable. ** $p < 0.01$, * $p < 0.05$.

Next, protein expression of the MHC-II related protein CD74, iNOS and the costimulatory molecules CD86, CD80 and CD40 was analysed based on the second staining panel. Figure 33 represents histograms of CD74+, CD86+, CD80+, CD40+ and iNOS+ CECs, respectively. Again, LPS-treated splenocytes and epithelial cells from the small intestine were used as controls.

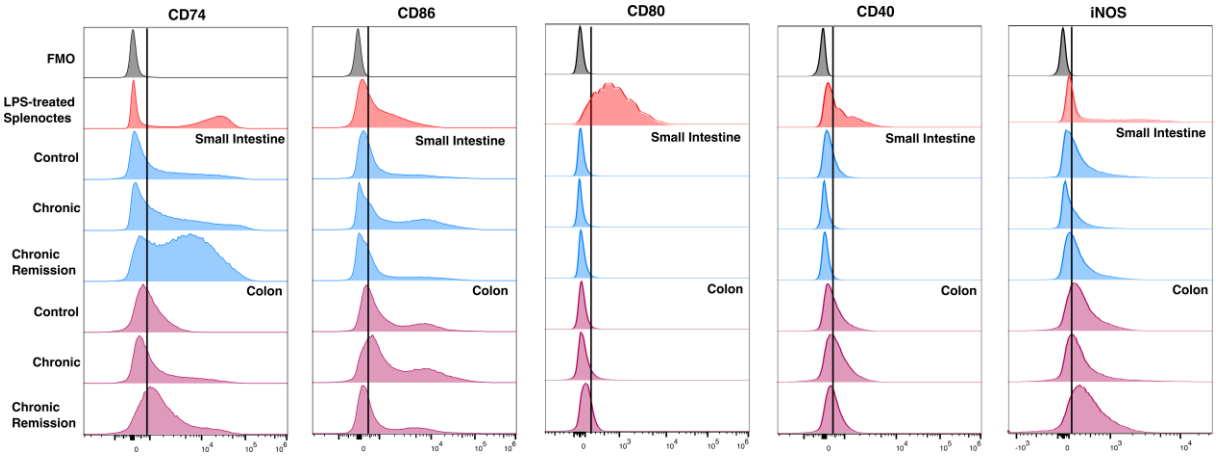

Figure 33: Representative histogram from flow cytometric analysis of CECs. LD-CD45-CD31-EpCAM+ CECs were downsampled 10,000 events in colon for each condition, if possible and subsequently concanated to create a summary file for each individual condition. FMOs were used as negative controls. LPS-treated splenocyte and epithelial cells from the small intestine were used as positive controls. Gray color represents each individual FMO, red color represents LPS-treated splenocytes, blue colors represent IECs from small intestine, and pink colors represent CECs in chronic stages of disease and corresponding control. For the spleen, CD45+ cells or myeloid compartment of CD45+ cells were gated after excluding singlets and dead cells. Modal mode was chosen to scale histograms.

Figure 34 summarizes the MFI and frequency of CECs according to their expression of CD74, iNOS, CD86, CD80 and CD40 for individual colon samples. Both, intensity of CD74 expression on CECs and percentage of CD74+ CECs significantly increased in the chronic remission stage. iNOS protein expression followed a different pattern as it first slightly decreased during chronic DSS colitis before significantly increasing in the remission state. With regard to the costimulatory molecules, several interesting observations were made. Among the costimulatory molecules, CD80 was expressed only by a minor population of CECs in the steady state (< 5%). Although the percentage of CD80+ CECs transiently increased upon inflammation and as well the CD80 expression level on CECs significantly increased upon inflammation, the relatively low abundance of CD80+ CECs and the overall low protein expression level suggested that CD80+ CECs might by negligible for the MHC-II-dependent interaction with CD4+ T cells in the colon. Interestingly, CECs expressed considerable levels of CD86 and especially CD40 already in homeostatic conditions (Figure 33). Strikingly though, both the percentage of CD86+ and CD40+ cells within the CEC pool as well as the level of CD86 and CD40 expression remained largely unaffected during chronic DSS colitis, but considerably dropped down during the chronic remission stage (Figure 34). Thus, while in line with gene expression data CECs transiently upregulate the expression of MHC-II related molecules, they do this without the concomitant upregulation of costimulatory molecules and even a significant loss of costimulatory capacity became evident in the chronic remission state (Figure 34).

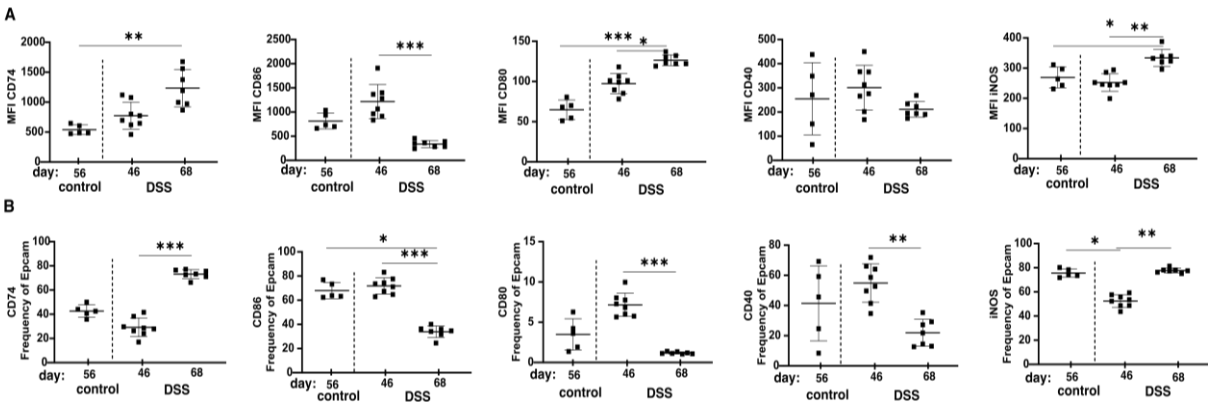

Figure 34: Expression level and percentage of CECs expressing selected target molecules. CECs were isloated from control (day 56), chronic (day 46) and chronic remission group (day 68). After excluding singlets, live-death, CD45+ and CD31+ cells, EpCAM+ CECs were used to determine the geometric mean of MFI for targeted proteins. CECs were gated for CD74, CD86, CD80, CD40 and iNOS to determine percentage changes. FMOs were used to determine positive gates. A) MFI of EpCAM positive CECs (n=4-8) B) Frequency of indicated marker expression within the EpCAM positive pool (n=4-8). Data represent mean with error bars indicating standard deviation. Significance calculated by Kruskal-Wallis test. *** $p < 0.001$, ** $p < 0.01$, * $p < 0.05$.

In summary, a relatively small population of CECs expressed MHC-II molecules in the steady state. Both, the frequency and the expression level of the analyzed MHC-II related proteins I-Ak and I-A/I-E increased in the chronic stage of disease which is well in line with RNA-Seq data (Figure 20, Figure 21A). The frequency of CD177+ CECs as well correlated with RNA-Seq data. However, the overall low level of CD177 protein expression did not change upon inflammation. *Cd74* gene expression was significantly increased in chronic stages of disease and remained slightly high during the remission phase. However, on the protein level CD74 was only expressed significantly in the chronic remission phase. In case of iNOS and IDO1, transcriptomic data could not be verified at the protein level, suggesting possible post-translational modifications. Additional analysis of costimulatory molecule expression by CECs revealed very low level expression of CD80 but decent CD86 and CD40 expression already in the healthy gut. Strikingly, while MHC-II expression level and frequency of MHC-II+ CECs increased during the chronic disease stage, the opposite was found for CD86 and CD40. Here, no obvious changes occurred during chronic DSS colitis, but both frequency and expression level considerably decreased in the chronic remission stage. This obvious discrepancy between MHC-II expression and the expression of costimulatory molecules prompted us to have a closer look to the CD4+ T cell pool in the *lamina propria*.

4.7 Chronification of DSS Colitis is associated with an Accumulation of iTregs in the Colonic *Lamina Propria*

As described above, CD4+ T cell numbers in the *lamina propria* steadily increased during disease chronification (Figure 16). Moreover, GO/KEGG term analyses identified CECs to respond to colitis with the clear induction of genes related to MHC-II dependent antigen-presentation (Figure 21) and in addition, hypo-methylation of adjacent H3K27me3 ChIP-regions in the stage of chronic DSS colitis

correlated with up-regulation of MHC-II related genes (Figure 28, right). Dependent on the presence or absence of costimulatory molecules, the interaction of CD4+ T cells with MHC-II-expressing CECs may result in expansion of Teff cells further boosting inflammation, in expansion of Tregs subsequently counteracting inflammatory processes or in T cell anergy induction, respectively. Given these facts, the next question to be addressed was if and how increased expression of MHC-II related genes in the absence of an accompanying upregulation of costimulatory molecules would affect the composition of the CD4+ T cell pool in the *lamina propria*.

To experimentally address this, total *lamina propria* leukocytes were isolated from the colon at consecutive stages of the disease and CD4+ T cells were analyzed by FACS. FOXP3 and HELIOS staining was done to allow the identification of the three major CD4+ T cells subsets (conventional CD4+ T cells (FOXP3-HELIOS-), iTreg cells (FOXP3+HELIOS-) and nTreg cells (FOXP3+ HELIOS+). As additional markers, the high-affinity IL-2 receptor CD25 and the proliferation marker KI67 were included. Moreover, conventional CD4+ T cells were further subtyped according to expression of the transcription factors T-BET (Th1), GATA-3 (Th2) and RORγt (Th17). For details regarding the gating used to distinguish the T cell subsets, please refer to section 3.6.

First, for t-SNE embedding of cell subsets, similar event counts from analyzed colon samples per condition were merged *in silico* and expression of CD4, FOXP3, HELIOS, CD25 and KI67 was analysed. This qualitative visual overview showed remarkable changes in the CD4+ T cell composition at different disease stages that were partially sustained during the recovery phase of chronic DSS colitis (Figure 35).

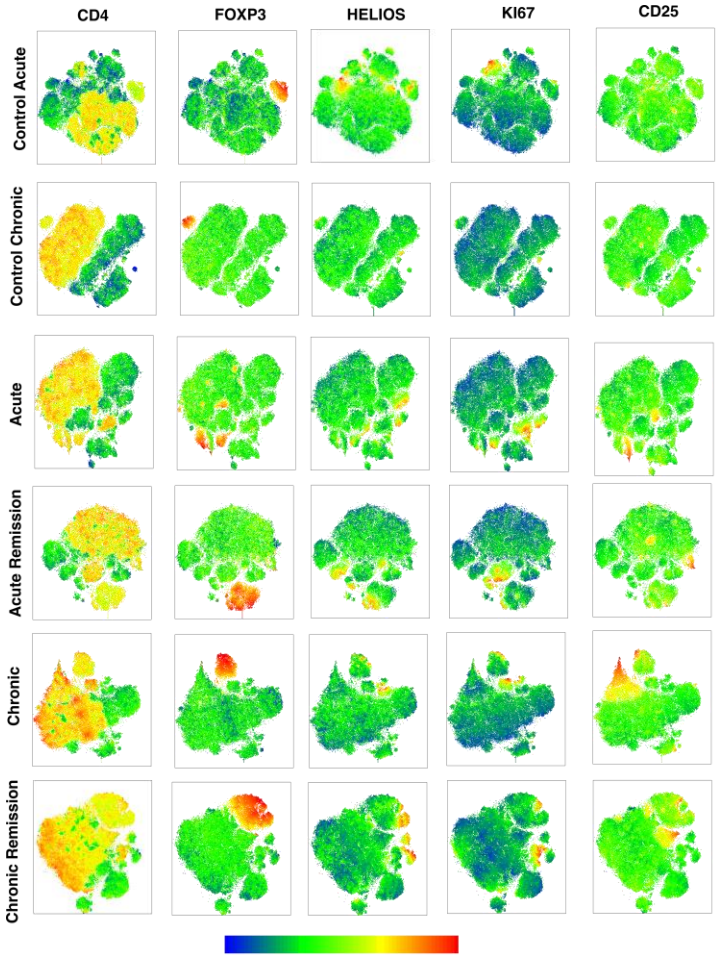

Figure 35: Characterization of the CD4+ T cell composition in the colon during consecutive stages of DSS colitis. FACS data was cleaned from debris, doublets, dead cells and lineage positive cells (NK.1.1+, CD11b+, CD11c+, CD45R/B220+). Then, CD45+CD3+ were downsampled to 20,000 events from each sample, if possible and then concanated to one summary file per disease conditions. These summary files were used to create unsupervised clustering by t-SNE to visualize expression of CD4, FOXP3, HELIOS, KI67 and CD25, respectively. Expression strength were represented by the colors in ascending order of blue, green, yellow, orange and red.

Well in line with data in Figure 16, t-SNE plots showed that the proportion of CD4+ T cells increased already after the first cycle of DSS treatment compared to the control groups. Interestingly, increase in CD4+ T cells was accompanied with an increase in the proportion of cells expressing FOXP3 and, to a lesser extent, CD25. More specifically, according to the t-SNE plots, CD4+FOXP3+ Tregs were CD25-. Moreover, CD4+FOXP3+ Tregs were mostly HELIOS-, indicating that most Tregs in the colon were in fact iTregs. The proportion of CD4+FOXP3+ Tregs increased during DSS, and it reached a maximum in chronic remission phase. This is well in line with a slight increase of KI67 expression during DSS periods indicating proliferation of Tregs in the colon (Figure 35).

t-SNE-based analyses were complemented by analysis of mouse-individual CD4+ T cell subset frequencies and quantification of absolute cell numbers belonging to the different subsets (Figure 36). As already observed in the t-SNE plots, iTregs comprised roughly 15 % of the total CD4+ T cell population and nTregs around 4 % of the total CD4+ T cell population during colitis, respectively. The

percentage of iTregs gradually increased during the different stages of colitis and the iTreg population was significantly enriched within the CD4+ T cell pool in the chronic remission phase. Even though not reaching the level of statistical significance, a similar trend was seen for the absolute cell numbers of iTregs (Figure 36). In line with the expansion of the iTreg pool, the frequency of iTregs expressing the the proliferation marker KI67 was significantly increased in the chronic disease stage, before dropping back to baseline level during the chronic remission stage (Figure 36). The percentage of nTregs in the CD4+ T cell pool and their absolute numbers in the *lamina propria* were in general lower than that of iTregs. While both parameters slightly increased during DSS treatment and expansion of nTregs was associated with increased KI67 expression, this effect was not significant (Figure 36). Together, these findings clearly document the expansion of iTregs during disease chronification. Among the conventional CD4+ T cells, the frequency and number of RORγt+ Th17 cells was highest. Interestingly, while DSS colitis was not associated with significant changes in the proportion and numbers of Th1 and Th2 cells, the frequency of Th17 cells was increased during the chronic remission state and therefore follows a similar pattern observed for the iTregs (Figure 36).

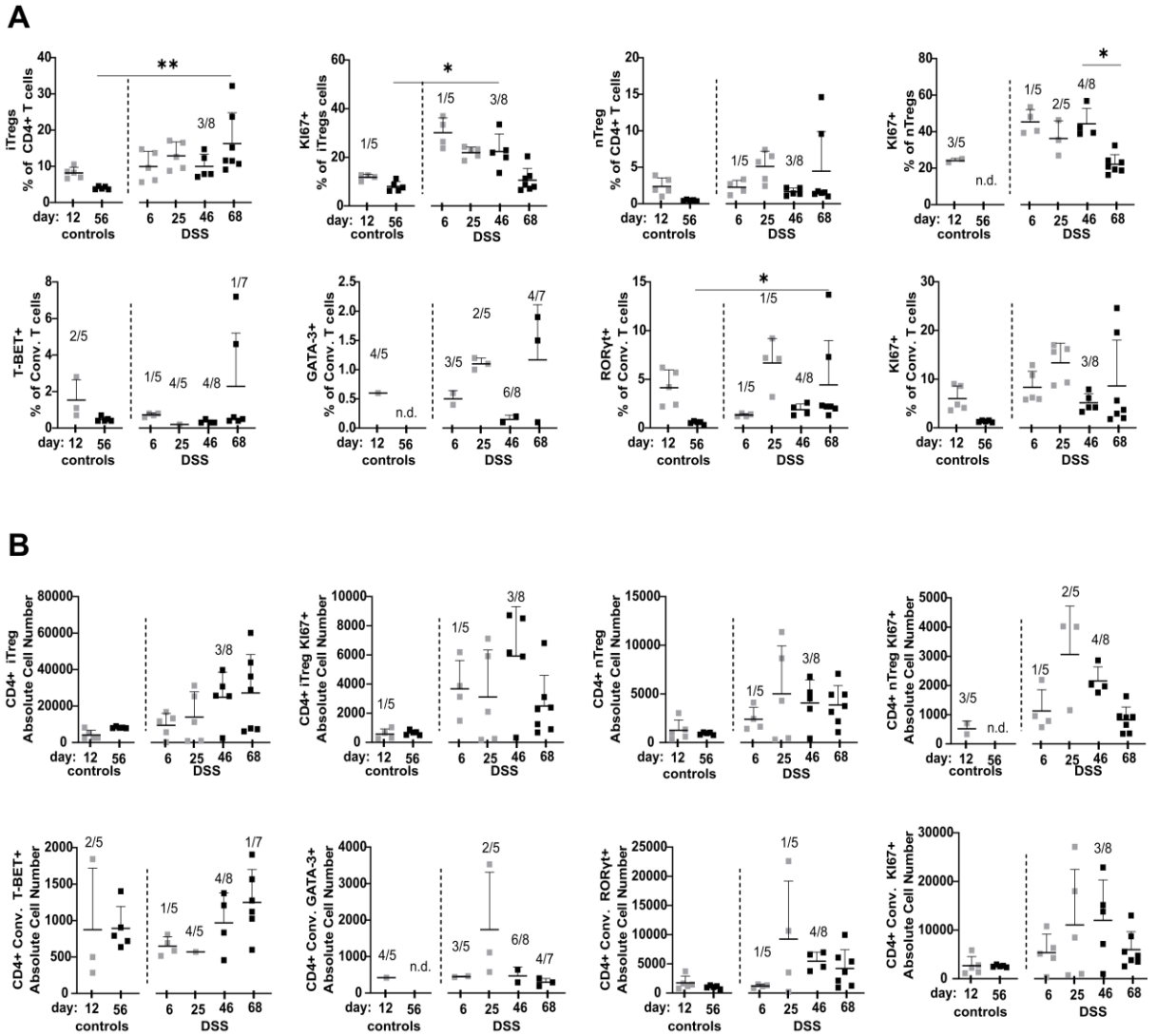

Figure 36: Frequency and absolute cell number of CD4+ T cell subsets during consecutive stages of DSS colitis. FACS data was cleaned from debris, doublets, dead cells and lineage positive cells (NK.1.1+, CD11b+, CD11c+, CD45R/B220+). CD45+CD3+ were further gated to CD4+ and CD8+ T lymphocytes. After excluding TCRγδ- cells, FOXP3+ HELIOS- iTregs and FOXP3+ HELIOS+ nTregs were identified and gated for their KI67 expression. Afterwards, remaining conventional T cells were further gated to determine different subsets according to the expression of T-BET (Th1), GATA-3 (Th2) and RORγt (Th17) and to identify the protein expression of KI67. A) Frequency of indicated Tregs cell subset within the total CD4+ T cells, frequency of their KI67 expression within the iTregs and nTregs and frequency of T-BET, GATA-3, RORγt, KI67 expression within conventional T cells (CD4+TCRγδ-Tregs-). B) The absolute number of indicated immune cell subtypes. Data represent the mean with error bars indicating standard deviation. Number of excluded samples is indicated on top of each condition (number of excluded sample/total sample number). n.d.: not detectable. Significance was calculated by Kruskal-Wallis test. All groups were compared with each other, significance is indicated only for relevant groups. ** $p < 0.01$, * $p < 0.05$.

Taken together, combining ChIP-Seq with RNA-Seq of CECs from different stages of DSS induced colitis uncovered amongst others the epigenetic regulation of MHC-II related gene expression during chronic stages of the disease. Increased MHC-II expression was confirmed by flow cytometry and additional analyses revealed the lack of concomitant induction and even a decrease of costimulatory function in CECs during chronic remission stage. Chronic intestinal inflammation is characterized by accumulation of CD4+ T cells in the *lamina propria*. While potentially disease-driving Th17 cells are increased within this pool, a significant expansion of iTregs was observed as well. The induction of Tregs during disease chronification might be the consequence of MHC-II-dependent CD4+ T cell interaction with CECs within the inflammatory milieu of the colon and might be part of an immune regulatory network to counteract uncontrolled tissue destruction and disease progression.

5. Discussion

Note: Parts of the discussion section (5.1) were taken directly or were paraphrased from the following publication:

Gelmez E, Lehr K, Kershaw O, Frentzel S, Vilchez-Vargas R, Bank U, Link A, Schüler T, Jeron A, Bruder D. Characterization of Maladaptive Processes in Acute, Chronic and Remission Phases of Experimental Colitis in C57BL/6 Mice. Biomedicines. 2022; 10(8):1903. https://doi.org/10.3390/biomedicines10081903.

5.1 Establishment and Comprehensive Immunological Characterization of Consecutive Stages of DSS Colitis

None of the existing mouse models reproduces all aspects of disease onset, progression and resolution, however, the chemically induced DSS colitis model is highly reproducible and allows generation of different stages of inflammation (e.g. acute, chronic, relapsing) by varying frequency and amount of DSS in drinking water (Wirtz et al., 2017). From the immunological point of view, in DSS colitis studies there is dissenting usage of terminology and meaning of the concepts of “acute” and “chronic” inflammation as well as “remission phase”. Melgar and Hall et al. proposed that one DSS cycle is sufficient for establishing acute and chronic stages of intestinal inflammation in C57BL/6 mice (Melgar et al., 2005; Hall et al., 2011). They defined an early acute stage of the disease as ranging from day 1 to 8, based on neutrophil influx into the colon (Melgar et al., 2005; Hall et al., 2011). Moreover, they defined a late stage of acute DSS colitis from day 12 on, based on neutrophil decline and increased numbers of adaptive immune cells. From day 25 on, the chronic stage of DSS colitis is reached, encompassing significant numbers of B and T cells in colonic tissue (Melgar et al., 2005; Hall et al., 2011).

However, other studies described one cycle of DSS to induce acute DSS colitis and repeated cycles of DSS to induce chronic DSS colitis in mice (Okayasu et al., 1990; Kim et al., 2013; Oh et al., 2014; Bank et al., 2020; Xu et al., 2021). Also we do not consider a single DSS treatment period to be sufficient to fully represent the recurrent inflammatory episodes that occur in IBD patients and therefore use the term “chronic inflammation” in this thesis exclusively in the context of cyclically repeated episodes of inflammation and the term “acute inflammation” in the context of a single, short-term DSS episode. Similarly, the term “remission phase” is not used in a standardized way in studies involving the DSS colitis model and is not linked to clear criteria. Remission period generally defines periods following DSS dosage, although a reduction of most colitis symptoms does not occur immediately after the termination of DSS dosage. In this respect and in the context of DSS colitis model in this thesis, we understand “remission” in the sense of an ongoing homeostatic process with still ongoing but declining inflammatory signatures and less as an achieved terminal state.

Weight loss and DAI parameters show similar trajectories regardless of the number of DSS periods undergone. Differences in this aspect only become apparent with other inflammatory parameters such as specific colon weight, inflammatory affected histological colon area, and spleen weight. In the chronic remission phase, all three parameters are comparatively elevated after three cycles of DSS compared with the remission phase after a single acute DSS period. These maladaptive developments only occurred upon chronification of the disease. Spleen weight was significantly increased only in the chronic stage and chronic remission stage of the disease, suggesting disease chronification to be associated with low-grade systemic inflammation (Figure 15).

In line with the histopathological observations, the number of immune cells increased during acute and chronic DSS phases compared to their corresponding controls. As expected, adaptive immune cells such as CD4+, CD8+ T cells and B cells are naturally linked to the evolving colonic mucosal immune response upon repeated cycles of DSS administration. It is clearly shown in this study that the absolute cell counts of CD4+ and CD8+ T cells as well as B cells within the colonic *lamina propria* increase dependent on the number of DSS cycles applied (Figure 16C). Most probably, this is due to their repeated exposure to microbial antigens, leading to initial expansion and re-activation of specific T and B cell clones (Kullberg et al., 2003; Boland et al., 2020). Since the DSS colitis model works a well in SCID mice lacking T and B cells (Dieleman et al., 1994; Axelsson et al., 1996), the induction of DSS colitis obviously does not depend on the presence of these cells, i.e. however, T cells do play a role in chronic DSS colitis with clear contributions of mixed Th1/Th2 cell responses (Dieleman et al., 1998). Moreover, CD11b+ IgA-secreting B cells were reported to ameliorate DSS colitis in mice (Fu et al., 2021). However, when experimentally restricted to the analysis of relative frequencies, e.g., from mouse colon tissue biopsies, only CD4+ T cell frequencies of around ~20 % (in reference to total CD45+ *lamina propria* leukocytes) seem to be a clear indicator of repeated DSS episodes in C57BL/6 mice (Figure 16B).

Neutrophils become a permanent colon immune cell subset from the first DSS cycle on and are present even throughout remission phases. Colonic neutrophils are important for sufficient immunothrombosis and thereby help to reduce rectal bleeding (Leppkes et al., 2021). Interestingly, elevated neutrophil frequencies were demonstrated in the spleen, especially in the chronic DSS condition (> 5 % of CD45+ leukocytes) (Supplementary Figure 2C). Similar observations were made in blood and colon biopsies of IBD patients (Zhou et al., 2018b). CD177+ neutrophils were reported to be a beneficial phenotypic adaptation in IBD colitis, with CD177-deficient mice developing more severe DSS colitis (Zhou et al., 2018a; Zhou et al., 2018b). Since the expression of CD177 on neutrophils were not determined in this study, it remains unclear whether the frequency of CD177+ neutrophils would be an even more specific indicator of chronic DSS effects in our DSS model that would be potentially assessable also by blood sampling of DSS treated mice.

Chronic gut inflammation by no means triggers only a locally restricted immune response. Patients with CD, but not UC, exhibit significantly elevated levels of serum IFN-γ (Korolkova et al., 2015). Similarly, increased protein levels of IFN-γ were found in blood plasma samples of mice from the late stages of DSS colitis, i.e. the chronic and chronic remission conditions (Figure 18). IFN-γ is causatively linked to DSS colitis as in a model of acute DSS colitis, IFN-$\gamma^{-/-}$ mice are largely protected (Ito et al., 2006). As notable colonic IFN-γ expression was only found in active periods of DSS dosage, the plasma IFN-γ level rather than the local colon IFN-γ level may be a good marker for an adaptation to, or the consequence of, repeated DSS episodes.

Among the soluble mediators produced within colon tissue we found the chemokines BLC (also known as CXCL13) and MDC (also known as CCL22) to have a meaningful expression pattern, with the latter being especially prominent in the chronic remission phase. B lymphocyte chemoattractant (BLC) is already in focus in basic and clinical IBD research. In a mouse model with BLC overexpression in intestinal epithelial cells during inflammatory conditions, influx of B cells, lymphoid tissue inducer cells and NK cells with immunomodulatory and repair functions was described (Marchesi et al., 2009). Similarly, enhanced expression of the human homologue of BLC, BCA-1 was reported in colon specimens from UC patients (Carlsen et al., 2002). The fact that BLC expression in colonic tissue was found to be particularly high only after three DSS cycles (Figure 17A) renders this chemokine a good indicator of inflammatory adaptation in our DSS model and moreover, is a mechanistic link to the high numbers of B cells at the same point in time. Moreover, particularly high and stable expression of Macrophage-derived chemokine (MDC, or CCL22) was found in the chronic and chronic remission conditions (Figure 17A), which is a criterion for a DSS-cycle-dependent inflammatory indicator. In mice, CD11c+ dendritic cells require T cell-derived GM-CSF to become the main producers of MDC in secondary lymphatic organs during homeostasis (Piseddu et al., 2020). Under inflammatory conditions, MDC is a potent T cell chemoattractant also produced by colon epithelial cells, e.g., in response to pro-inflammatory cytokines or infection with enteroinvasive bacteria (Berin et al., 2001). Recently, the CCL22/CCR4 axis was identified as an immune checkpoint controlling intestinal T cell and Treg cell immunity with CCL22-deficient mice being more susceptible to DSS inflammation (Rapp et al., 2019). Hence, MDC in colonic tissue provides a mechanistic link to the likewise elevated *lamina propria* T cell counts in chronic and chronic remission phases of our colitis model.

An analysis of the microbial composition allows further insights into consequences of repeated DSS cycles for the gut commensals. Beneficial *Lactobacilli* and *Limosilactobacilli* steadily reduced with each further DSS cycle and were not able to regain their initial level. In turn, harmful species belonging to the *Turicibacter* genus continuously expanded in frequency in each DSS consumption period (Figure 19D). Thus, the prevalence of *Lactobacilli* and *Turicibacter* species are easy-to-access feces-indicators of colon adaptation to consecutive inflammatory episodes. Similar results have been reported previously (Liu et al., 2020) and further studies have been successfully undertaken to, e.g., complement the DSS colitis-shaped microbiome with probiotic *Lactobacillus acidophilus XY27* (Kim et al., 2021) or *Limosilactobacillus reuteri EFEL6901*, resulting in decreased expression of pro-inflammatory cytokines *Tnf* and *Il-1β,* and higher levels of anti-inflammatory *Il-10* in the colon (Seo et al., 2021). Furthermore, *Lactobacillus* species are related to many other beneficial host/microbiome interactions taking place at the epithelial barrier including, e.g., the enhancement of mucus production, the enhanced release of anti-microbial peptides and a higher prevalence of luminal secretory immunoglobulin A, as intensively reviewed by Dempsey and Corr (Dempsey and Corr, 2022). However, little is known about actual microbial mechanisms leading to the perpetuating decrease of *Lactobacilli* during DSS colitis. Still, it

is conceivable that many of the known beneficial contributions of this bacterial genus might be critically missing within the inflamed colon and thus justify further elaborate research in this regard.

In conclusion, results of first part of the study point out indicators of disease progression in experimental ulcerative colon inflammation and provide clues to major immunological characteristics in different stages of the DSS model and their transition. Based on the data, colonic maladaptation requires two or more DSS periods. Thus, this study may help to improve experimental IBD animal models to enhance their clinical relevance, as well as to identify novel therapeutic targets to prevent disease progression and chronification of colitis in IBD patients.

5.2 Understanding Transcriptomic and Epigenetic Adaptations of Colon Epithelial Cells to Chronic Inflammation

The concept of inflammatory tissue memory encompasses concepts and mechanisms that enable tissues to remember inflammatory states. Ordovas-Montanes et al. proposed six main components to conceptualize how tissues can store inflammatory memories (Ordovas-Montanes et al., 2020):

1.) Specificity:	How an initiating inflammatory stimulus is recognized (e.g. unique recognition, sensing of a context or unspecific detection).
2.) Quantity:	Frequency of responding cells.
3.) Quality:	Polarization of responding cells into specified cellular subsets.
4.) Durability:	Time period with increased quality/quantity of response.
5.) Distribution:	Spatial tissue localization of cell lineages and subsets with intrinsic alterations in points 1 to 4.
6.) Cooperativity:	Importance of interaction and communication between cells for inflammatory tissue memory and recall.

Some but not all aspects of this concept have been addressed in this thesis to find indications for gut tissue memory and accompanying maladaptations using DSS-induced colitis as a trigger of the inflammatory state. Especially, points 2, 3, 4 and to some extend point 6 of the above list have been experimentally addressed with a focus on intestinal epithelial cells of the colon. Given that CECs are rather short-lived cells that can be expected to be replenished in high turn-over rates, it is interesting to wonder if the experimentally observed transcriptional CEC responses necessarily only are the mere result of cellular sensing of the current colon inflammation state at the given moment of cell isolation, completely lacking any inflammatory memory induced in previous DSS episodes? If this should however not be the case, a consequent question is why CECs should then need to “remember” previous inflammatory episodes in the first place? Moreover, if there is indeed a biological need for “inflammatory memory” of CECs, it is important to understand how such a memory is passed over to replenished CECs? This thesis tried to give some answers to the above questions having epigenetic

histone modifications in focus as an obvious mechanism by which CECs integrate and intrinsically may propagate inflammatory memory.

After initially studying immune responses and microbiota composition, both defining the colon inflammatory environment in DSS colitis, next the focus was on CECs and their integration within this environment. For this purpose, state-of-the-art RNA sequencing techniques were used to foster understanding of the CEC transcriptomic phenotype within all DSS model conditions. Importantly, the CECs used for bulk RNA-seq were pure and vital EpCAM+ epithelial cells, but of course still may be an unknown mixture of colonic epithelial cell subsets. These facts are important to keep in mind when trying to interpret transcriptional profiles of CECs, especially from acute and chronic DSS model conditions with clearly observable tissue damage and barrier destruction. Pair-wise data analysis (in reference to untreated mice) showed surprisingly resilient transcriptional phenotypes of CECs as not too many differentially expressed genes were observed in the acute and chronic conditions. Resilience and/or strong regenerative capacities of CEC transcriptional responses became also clear by the fact that after remission phases transcription profiles were almost normal again.

On the other hand, PCA analysis of RNA-seq data indicated overall alterations in condition-specific gene profiles. RNA-seq data of untreated control groups were clearly separated from all DSS groups and even data from the remission conditions did not seem to have regained a gene expression profile comparable to that of untreated controls, indicating an incomplete remission of the transcriptional CEC phenotype (Figure 20). For remission of a single acute DSS episode, similar observations were made by Czarnewski and co-authors. They performed RNA-seq of total colon tissue from DSS treated mice. They observed that a 7 day remission period following 7 days of acute DSS dosage was also not sufficient to re-establish the initial expression profile of day 0 samples (Czarnewski et al., 2019).

The multi-condition comparison approach of RNA-seq data showed that along the timeline of the DSS model differentially expressed genes followed basically two distinct patterns. Either the genes were upregulated during the acute but even stronger in the chronic condition and had again reduced expression in the remission conditions or they were downregulated in the acute and chronic DSS conditions with almost regaining their initial expression in remission conditions. However, gene expression of *Cd177* and *Ubd* did not exactly follow either pattern. Both genes became upregulated during remission of acute DSS with reaching the peak expression in chronic DSS and kept this level throughout the chronic remission phase (Figure 21).

It has been shown in active IBD patients and in a murine model of chronic colitis, induced by microbiota antigen-specific T cells, that CD177 expression as well as the frequency of CD177+ neutrophils are elevated (Zhou et al., 2018b). Even though, CD177 is known as a neutrophil-related protein, Kluz et al., demonstrated that CD177 is also expressed by breast cancer epithelial cells, and that its expression is associated with a good survival prognosis (Kluz et al., 2020). Mechanistically, CD177 seems to be

involved in the Wnt/β-catenin signaling pathway as CD177-deficiency leads to increased Wnt/β-catenin signaling (Kluz et al., 2020). Therefore, the increase of CD177 expression in CECs might have a protective function during colon inflammation with Wnt/β-catenin signaling being important for CEC differentiation and proliferation. However, this hypothesis was not further investigated in this thesis.

Ubiquitin D (UBD) is a ubiquitin-like protein-modifier involved in proteasomal degradation of accordingly tagged proteins. Expression of *Ubd* in intestinal tissues from IBD patients was shown to have an interesting spatial distribution pattern. Without inflammation, UBD expression is limited to CECs at the crypt bottom, whereas in inflamed tissues UBD is expressed throughout the crypt (Kawamoto et al., 2019). This might also explain the observed upregulation of *Ubd* in bulk RNA-seq CEC samples from chronic and chronic remission conditions, as it is conceivable that more cells across colonic crypts express *Ubd*. Interestingly, expression of UBD in a human intestinal epithelial cell line can be strongly induced by triggering Notch-signaling in presence of TNF-α (Kawamoto et al., 2019). This matches with the high levels of TNF-α found in colon tissue homogenates especially in the chronic DSS condition (Figure 17B) and provides a further mechanistic clue to *Ubd*-induction in murine CECs.

In the chronic DSS condition, generally RNA-seq analysis identified more genes to be differentially regulated compared to acute DSS. Together, this could be carefully interpreted as a sign or the consequence of inflammatory memory of some kind, as experimentally the only difference between those two states was the number of inflammatory DSS-episodes the mice had undergone. However, most of the differentially regulated genes normalized their expression during the final remission phase. Few genes however, still had clearly altered expression at this point in time. This was especially the case for *Iigp1*, *Duoxa2* and *H2-Ab1* genes, which remained significantly upregulated after the chronic remission phase (Figure 20), thereby reflecting strong evidence of an inflammatory adaptation of CECs. Thus, in the following it is important to interpret the expression of *Iigp1*, *Duoxa2* and *H2-Ab1* and set them into the right context.

“Interferon gamma inducible GTPase 1” (*Iigp1*) belongs to the super-family of IFN-Inducible GTPases and in more detail to the sub-family of Immunity-Related GTPases (IRGs) that take part in cell-autonomous immunity of cells. Although many IFN-inducible GTPases are shared across vertebrate species, there seems to be no human homologue of murine *Iigp1* (Kim et al., 2012). *Iigp1* showed the highest fold-induction value of all genes found to be differentially regulated in CECs. Hence, it must be of utter importance for CEC autonomous immunity. Indeed, *Iigp1* is highly expressed in distal and proximal colon tissue upon treatment of mice with 3 % DSS in drinking water for 7 days (Asad et al., 2021). Functionally, *Iigp1* was shown to be important for limiting intracellular pathogens like *Toxoplasma gondii* by disrupting parasitophorous vacuoles that contain the parasite (Martens et al., 2005). Type I and type II IFNs were found to be the main inducers of *Iigp1* expression (Zerrahn et al., 2002). Recently, importance of IIGP1 was demonstrated also for viral infections. Overexpression of

IIGP1 in cell lines limits Rabies virus replication, and in a mouse model with forced expression of IIGP1 viral load and pathogenicity of Rabies virus in the brain was reduced (Tian et al., 2020). *Iigp1* was not amongst the differentially expressed genes in whose promoter also differential epigenetic histone marks were found. Hence, it is likely, that *Iigp1* expression depends on the IFN-γ presence in the colon tissue.

DUOXA2 is a maturation factor for the thyroid H_2O_2 generator DUOX2 (Grasberger and Refetoff, 2006) also detectable in human colons. DUOX2 is a source for NADPH oxidase-derived reactive oxygen species in the gut (El Hassani et al., 2005). MacFie et al., also showed that gene expression of *Duox* as well as *Duoax2* was elevated during active UC in human mucosal biopsies (MacFie et al., 2014). Expression of DUOX2 has been already described to be induced in scenarios involving chronic inflammation and microbial dysbiosis to boost release of epithelial-driven H_2O_2 as a potent anti-microbial compound (Burgueño et al., 2019). Accordingly, transfer of disturbed microbiota from IBD patients into germ-free mice resulted in increased H_2O_2 production (Burgueño et al., 2019), which matches microbial dysbiosis found in the DSS model (Figure 19). In the chronic DSS condition, at promoters of *Duoxa2* and *Duox2* differential hypo-methylated H3K27me3 regions were found (Figure 28, right), suggesting that this inflammatory adaptation of CECs at least in part depends on epigenetic gene regulation. This also matches with the observation of hyper-acetylated regions at the *Duoax2* promoter in the acute DSS condition (Figure 30, left). Together, the ability to produce anti-microbial H_2O_2 seems to be a cellular feature of CECs that is enhanced over the course of the DSS colitis model and that maybe "memorized" by means of epigenetic histone marks at *Duoxa2* and *Duox2* promoters that contribute to efficient transcription of these genes.

H2-Ab1 (Histocompatibility 2, class II antigen A, beta 1) is a gene encoding for an MHC-II variant protein. Sæterstad et al., showed also by RNA-seq analysis of monolayer IECs from biopsies of IBD patients (both UC and CD) increased gene expression of human MHC-II related genes (e.g. *HLA-DPA1*, *HLA-DPB1*, *HLA-DRA*), important for antigen presentation to adaptive T and B cells (Sæterstad et al., 2022). In short-time DSS-treated wildtype mice, CECs were also shown to upregulate MHC-II related genes (e.g., *H2-DMb1, H2-Ab1, H2-Aa, H2-Eb1, Cd74*) as well as IFN-γ induced transcription factors (e.g., *Irf1, Irf7,* and *Irf9*) as early as 4 days after DSS dosage had been started (Muzaki et al., 2016). This matches also the RNA-seq data in section 4.4, that show as well equally induced expression of not only *H2-Ab1* but also further MHC class II related genes (e.g. *Cd74, H2-Aa, H2-Eb1, H2-DMb1, H2-DMa*) as well as transcription factor *Irf1* in acute and even more in chronic DSS conditions (Figure 21). IFN-γ is known to enhance MHC-II protein expression in CECs. Hershberg et al. concluded that IFN-γ enhances MHC class II dependent antigen presentation on the surface of human colonic IEC-like cell lines based on induced expression of "Invariant polypeptide of major histocompatibility complex, class II antigen-associated" (CD74) and HLA-DM (Hershberg et al., 1997). They also showed that in the absence of IFN-γ, IECs make use of a distinct MHC-II protein which requires high antigen concentrations (Hershberg et al., 1997). Since locally IFN-γ was increased in the colon mainly during

the acute and chronic stage of the DSS model (Figure 17) and the increased gene expression of MHC-II related genes in the RNA-seq data was observed in the same conditions (Figure 20, Figure 21), this is conceivably a consequence of IFN-γ sensing by CECs. Moreover, it has been shown in lymphocytes, treated with IFN-γ, that the promoter region of the MHC-II variant gene *H2-Ab1* becomes hypo-methylated in terms of H3K27me3 histone modifications (Robbins et al., 2012), demonstrating epigenetic involvement in MHC-II gene regulation also in cells other than CECs. In the CEC ChIP-seq analysis of H3K27me3 and H3K27ac histone modifications at promoters of *H2-Ab1*, *H2-DMb1* and *H2-Eb1* differentially modified epigenetic marks were identified, together with the observation of an increased expression in CECs. This renders the induction of MHC-II-dependent antigen presentation a further potential candidate for an epigenetically "memorized" inflammatory adaptation of CECs. Importantly, FACS-based confirmation of MHC-II expression (I-Ak and I-A/I-E, Figure 32) on CECs in the chronic and chronic remission conditions indeed show an enhanced percentage of MHC-II+ CECs. However, the percentage was surprisingly low given the previously observed transcriptional fold induction in bulk RNA-seq analysis. Thus, it is possible that the MHC-II-induction together with the accompanied epigenetic gene regulatory component is a special feature of only a subset of CECs rather than a general pan-population effect. Whether this notion even hints to a dedicated specialized IEC cell subset in the colon or e.g. is an adaptation of intestinal epithelial stem cells remains to be elucidated.

Coming back the questions initially placed in the beginning of this discussion section, the extensive analysis of the inflammatory and cellular immune responses mounted in context of DSS-induced colitis together with the molecular analyses of CECs allow to conclude that CECs indeed show some cellular inflammatory responses that seem to be epigenetically "memorized" over the course of the DSS model timeline. Biologically, these CEC responses are mainly related to immediate anti-microbial defense as well as to more complex mechanisms like the interaction with CD4+ T cells via MHC-II to indirectly suppress and counterbalance chronic colon inflammation by means of iTreg induction and/or T cell anergy. At the same time there are also indications for CECs simply sensing the current colon inflammation state at a given moment of the DSS model, shaped by other structural cells of the colon as well as by recruited immune cells.

5.3 Chronification of DSS Colitis is associated with an Accumulation of iTregs in the Colonic *Lamina Propria*

Epigenetic regulation of CECs caused the increased gene expression of MHC-II related genes. Therefore, to answer if CECs are expressing MHC-II related proteins to either expand Teff cells or Tregs, FACS analysis were performed to identify different CD4+ T cells subpopulations which are iTreg, nTreg and conventional T cells, including Th1, Th2 and Th17.

nTregs are characterized by FOXP3 and CD25 expression. In a pioneer study, Sagakuchi et al., showed that BALB/c athymic nude recipent mice developed multiorgan autoimmune disease following adoptive

transfer of CD25-depleted CD4+ T cells, indicating that CD4+CD25+ T cells are of crucially important for the maintenance of immunological self-tolerance (Sakaguchi et al., 1995). Interestingly, t-SNE analysis revealed that during chronic colitis stages and healthy state the majority of CD4+FOXP3+ Tregs within the colonic CD3+ T cell pool was CD25- (Figure 35). Curotto de Lafaille et al., showed that both CD4+CD25+ and CD4+CD25− splenic T cell populations include T lymphocytes that can suppress the hemagglutinin-specific IgE response (Curotto de Lafaille et al., 2001). Another report demonstrated that an integrin alpha-E+ CD4+CD25- T cell subpopulation exhibits regulatory function (Lehmann et al., 2002). Even though, Uhlig et al. documented that CD4+CD25+FOXP3+ Tregs are present in the colon of mice (Uhlig et al., 2006), marginal CD25 expression was found in CD4+FOXP3+ Tregs in this study (Figure 35). Moreover, t-SNE plots clearly represented that most of the CD4+FOXP3+ Tregs were in fact HELIOS-, indicating that these cells were iTregs, induced in the colon. This was expected, since the conversion of naive T cells recognizing microbiota-derived antigens into iTregs cells can be directed by commensal bacteria (Round and Mazmanian, 2010; Atarashi et al., 2011). Furthermore, the percentage of iTregs (NRP1−FOX3+) was shown to be increased in colon as well as small intestine compared to secondary lymphoid organs such as MLN and spleen (Weiss et al., 2012). Moreover, Karllson et al., showed that *in vitro* generated iTregs were remarkably more efficient than nTregs in attenuating preexisting chronic colitis (Karlsson et al., 2013).

Frequencies of iTregs and nTregs within the colonic CD4+ T cell population clearly showed that in healthy animals iTregs were more prominent than nTregs. Upon inflammation, this became even more relevant and the proportion of of iTregs increased to approximately 15 % of the total CD4+ T cell population, while the percentage of nTregs with ~ 4 % remained relatively low (Figure 36). This increase in iTreg fequencies might be the consequence of enhanced infiltration of bacteria and their products due to inflammation-related intestinal barrier breakdown, resulting in the conversion of naive CD4+ T cells into iTregs. Moreover, percentage of iTregs gradually increased during different stages of colitis and it was significantly enriched in the chronic remission phase. Even though not reaching statistical significance, absolute cell number of iTregs as well gradually increased with disease progression (Figure 36). The gradual increase of iTregs coincided with their increased proliferative activity as indicated by elevated KI67 expression, which however turned back to almost normal in the chronic remission phase.

With regard to the conventional CD4+ T cell composition in the colonic *lamina propria*, no obvious changes were observed in absolute cell numbers and percentages during the consecutive disease stages except for the frequency of RORγt+ Th17 cells that were increased in the remission phase of chronic DSS colitis (Figure 36). The low amount of Th17 cells in acute disease conditions is well in line with findings by Kim et al. who showed before that Th17 responses cannot be induced in acute stages of DSS colitis (Kim et al., 2011). Notably and although not reaching statistical significance, we observed an increase in Th17 cells both during chronic but as well during acute remission. To our knowledge, this

has not been described previously and may raise important questions regarding the role of this particular T cell subset during remission.

Due to the increase of IFN-γ, CD has been considered a Th1-mediated diseases, whereas UC is usually considered a Th2-type disease due to increased intestinal IL-5 expression (Fuss et al., 1996). Even though we as well observed increased IFN-γ concentrations during acute and chronic stages of disease (Figure 17B) in the gut, this finding does not sufficiently clarify the cellular source of the cytokine. Therefore, it is important to perform flow cytometry analysis in parallel to cytokine/chemokine profiling in tissues in order to figure out the contribution of specific immune cells to progression of inflammation (Figure 17, Figure 16). According to the FACS data, CD4+FOXP3+CD25-HELIOS- iTregs and/or the expansion of iTregs that might counterbalance the action of the as well expanding Th17 cells might play a more prominent role in intestinal immune regulation during disease chronification than Th1 and Th2 cells. The findings support the hypothesis that epigenetically regulated MHC-II gene expression in CECs represents a mechanism acting to prevent or retard the perpetuation of intestinal inflammation by the expansion of iTregs.

CD4+ T cells in the *lamina propria* interact with CECs by binding of their TCR to peptide-loaded MHC-II molecules. Indeed, RNA-Seq identified genes associated with MHC-II such as *H2-Aa*, *H2-Ab1* to be overexpressed in CECs during chronic intestinal inflammation. Upon inflammation, a small proportion of CECs upregulated MHC-II expression, however, MHC-II expression by no means reached a level observed for activated professional antigen presenting cells present in LPS-stimulated splenocytes (Figure 31). In order to efficiently activate naïve CD4+ T cells, CECs in addition to peptide-loaded MHC-II molecules would require the expression of costimulatory receptors on their surface. In the absence of costimulatory molecules, MHC-II-dependent TCR stimulation would favor the induction of T cell anergy (reviewed in (Appleman and Boussiotis, 2003)). Gene expression levels of costimulatory molecules in CECs were rather weak, which might suggest that T cell stimulation by CECs would result in T cell anergy. However, FACS analysis revealed that, a relatively large proportion of around 60 % and 40 % of CECs expressed CD86 and CD40, respectively while most of them were lacking CD80 expression (Figure 34). This observation was supported by another study showing that CD86 expression in CECs was more pronounced than CD80 expression and moreover, this study also showed that CECs did not induce anergy in T cells (Cruickshank et al., 2004). Together, these findings suggest that at least in the chronic stage of disease, costimulation-competent CECs would not cause T cell anergy. However, the pronounced drop in the expression of co-stimulatory molecules in CECs, which was most evident for CD86 in the chronic remission phase, implies enhanced capacity to induce T cell anergy in this particular disease state. Further functional studies are needed to prove or refute this hypothesis.

Another question was which further function costimulatory molecules (CD86 and CD40), that are strongly expressed on CECs might have, independent of promoting MHC-II based CD4+ T cell interaction. Given a strong expression of the MHC-I protein (H2Kb/H2-Db) on CECs, measured by

FACS, CECs may also interact with CD8+ T cells in the gut (data not shown). However, since this thesis mainly focuses on the interaction of CECs with CD4+ T cells, this was not further evaluated.

Since IECs fulfill important functions in maintenance of gut homeostasis (reviewed in (Okumura and Takeda, 2017)), and since iTregs accumulated in the colonic *lamina propria* during the chronic stage of disease (Figure 36), it was reasonable to consider that costimulation-competent CECs would contribute to expansion of iTregs and/or function.

There are contradictory data existing regarding the role of costimulatory molecules for Treg function. One study showed that antibody-mediated blockade of CD86 resulted in a strong increase in Treg inhibitory functions, while antibody-mediated blockade of CD80 disturbed Treg-dependent suppression of T cell reactions to alloantigens expressed by dendritic cells (Zheng et al., 2004). However, another study showed that even though both CD80 and CD86 were equally well capable to provide costimulation to induce proliferation of conventional CD4+ T cells, CD86 was more efficient in providing robust costimulation to Tregs (Halliday et al., 2020). It has been also demonstrated that CD40 or CD40L (CD154) deficient mice exhibit a strongly reduced frequency of FOXP3+ Tregs in the periphery as well as in the thymus compared to wild type mice (Spence and Green, 2008). Therefore, based on presented and published data, we suggest CD86- and CD40-mediated costimulation by CECs to play a more important role than CD80-mediated costimulation in Treg expansion in the inflamed gut.

Expansion of Tregs at sites of mucosal inflammation is not yet fully understood. Moreover, the question of which cells are mainly responsible for Treg expansion in the gut is still controversially discussed. Huang et al. demonstrated a dendritic cell subsets to play an important role in the transport of apoptotic IECs to the T cell areas of the MLN (Huang et al., 2000). Later, other studies documented that gut resident dendritic cells induce Tregs in the presence of retinoic acid and TGF-β (Coombes et al., 2007; Sun et al., 2007). However, pioneer work performed by Westendorf et al. revealed for the first time that IECs play a major role in induction of Treg expansion in the intestine (Westendorf et al., 2009). They showed that the peripheral expansion of Tregs was caused by antigen presentation by MHC-II on IECs, that was not dependent on dendritic cells (Westendorf et al., 2009). Furthermore, in contrast to dendritic cells, Treg expansion by IECs did not depend on TGF-β or retinoic acid (Westendorf et al., 2009). In their study, they used intestinal epithelial cells from the small intestine, and data from this thesis suggest that this mechanism might be also true for CECs.

Another mechanism to induce iTregs cells depend on IDO1, since IDO1 expression is associated with Treg induction (Fallarino et al., 2006; Mezrich et al., 2010) and IDO1 deficiency is associated with a decrease of Tregs in the colon (Takamatsu et al., 2013). In support of this, *Ido1* gene expression increased mainly in the chronic disease stage and FACS data revealed that IDO1 is constitutively expressed in CECs (Figure 21, Figure 32). In line with this, within the DSS model used in this thesis, in chronic and chronic remission conditions enhanced cell counts of HELIOS-negative CD4+ iTregs were

found. CECs from chronic DSS showed at the same time enhanced *Ido1* expression together with hypo-methylated histone marks at the *Ido1* promoter. It remains however unclear if the transcriptional *Ido1* enhancement alongside observed differential histone marks makes an effective impact on the capacity of CECs to convert CD4+ T cells into iTregs, as firstly FACS-based IDO1 protein expression on CECs was found to be steadily high in all tested DSS model conditions (Figure 32) and secondly further dedicated functional studies with focus on CEC/T cell interaction is required to practically confirm this. Moreover, it also needs to be considered to what extent iTregs expansion/induction might as well also occur in MLN or other secondary lymphatic compartments.

In summary, this thesis gave multi-approach insights into immunological, cellular, microbial and molecular aspects of perpetuating colon inflammation with a focus on colon epithelial cells, located directly at a sensitive mucosal interface. Next to indicators for disease progression of experimental ulcerative colon inflammation, presented data also provide clues to major immunological characteristics in different stages of the DSS disease model and their transition. Combined transcriptional and epigenetic analysis of CECs provided a deeper mechanistic understanding of the intestinal epithelial cell layer and its integration with the surrounding immune system. Thus, this thesis may help to improve experimental IBD animal models to enhance their clinical relevance, as well as to identify novel therapeutic targets to prevent disease progression and chronification of colitis in IBD patients.

6. References

Ahl, D., Liu, H., Schreiber, O., Roos, S., Phillipson, M., and Holm, L. (2016). Lactobacillus reuteri increases mucus thickness and ameliorates dextran sulphate sodium-induced colitis in mice. Acta physiologica (Oxford, England) *217*, 300-310. https://doi.org/10.1111/apha.12695.

Al Aboud, N.M., Tupper, C., and Jialal, I. (2022). StatPearls. Genetics, Epigenetic Mechanism (Treasure Island (FL)).

Alabert, C., Loos, C., Voelker-Albert, M., Graziano, S., Forné, I., Reveron-Gomez, N., Schuh, L., Hasenauer, J., Marr, C., and Imhof, A., et al. (2020). Domain Model Explains Propagation Dynamics and Stability of Histone H3K27 and H3K36 Methylation Landscapes. Cell reports *30*, 1223-1234.e8. https://doi.org/10.1016/j.celrep.2019.12.060.

Alam, M.T., Amos, G.C.A., Murphy, A.R.J., Murch, S., Wellington, E.M.H., and Arasaradnam, R.P. (2020). Microbial imbalance in inflammatory bowel disease patients at different taxonomic levels. Gut pathogens *12*, 1. https://doi.org/10.1186/s13099-019-0341-6.

Alex, P., Zachos, N.C., Nguyen, T., Gonzales, L., Chen, T.-E., Conklin, L.S., Centola, M., and Li, X. (2009). Distinct cytokine patterns identified from multiplex profiles of murine DSS and TNBS-induced colitis. Inflammatory bowel diseases *15*, 341-352. https://doi.org/10.1002/ibd.20753.

Altschul, S.F., Gish, W., Miller, W., Myers, E.W., and Lipman, D.J. (1990). Basic local alignment search tool. Journal of Molecular Biology *215*, 403-410. https://doi.org/10.1016/S0022-2836(05)80360-2.

Anderson, M.J. (2001). A new method for non-parametric multivariate analysis of variance. Austral Ecology *26*, 32-46. https://doi.org/10.1111/j.1442-9993.2001.01070.pp.x.

Andrews S. 2010. FastQC: a quality control tool for high throughput sequence data.

Appleman, L.J., and Boussiotis, V.A. (2003). T cell anergy and costimulation. Immunological reviews *192*, 161-180. https://doi.org/10.1034/j.1600-065X.2003.00009.x.

Araki, Y., and Mimura, T. (2017). The Histone Modification Code in the Pathogenesis of Autoimmune Diseases. Mediators of inflammation *2017*, 2608605. https://doi.org/10.1155/2017/2608605.

Arasaradnam, R.P., Khoo, K., Bradburn, M., Mathers, J.C., and Kelly, S.B. (2010). DNA methylation of ESR-1 and N-33 in colorectal mucosa of patients with ulcerative colitis (UC). Epigenetics *5*, 422-426. https://doi.org/10.4161/epi.5.5.11959.

Ardizzone, S., and Bianchi Porro, G. (2002). Inflammatory bowel disease: new insights into pathogenesis and treatment. Journal of internal medicine *252*, 475-496. https://doi.org/10.1046/j.1365-2796.2002.01067.x.

Asad, S., Wegler, C., Ahl, D., Bergström, C.A.S., Phillipson, M., Artursson, P., and Teleki, A. (2021). Proteomics-Informed Identification of Luminal Targets For In Situ Diagnosis of Inflammatory Bowel Disease. Journal of pharmaceutical sciences *110*, 239-250. https://doi.org/10.1016/j.xphs.2020.11.001.

Atarashi, K., Tanoue, T., Shima, T., Imaoka, A., Kuwahara, T., Momose, Y., Cheng, G., Yamasaki, S., Saito, T., and Ohba, Y., et al. (2011). Induction of colonic regulatory T cells by indigenous Clostridium species. Science (New York, N.Y.) *331*, 337-341. https://doi.org/10.1126/science.1198469.

Atreya, I., Atreya, R., and Neurath, M.F. (2008). NF-kappaB in inflammatory bowel disease. Journal of internal medicine *263*, 591-596. https://doi.org/10.1111/j.1365-2796.2008.01953.x.

Audia, J.E., and Campbell, R.M. (2016). Histone Modifications and Cancer. Cold Spring Harbor perspectives in biology *8*, a019521. https://doi.org/10.1101/cshperspect.a019521.

Axelsson, L.G., Landström, E., Goldschmidt, T.J., Grönberg, A., and Bylund-Fellenius, A.C. (1996). Dextran sulfate sodium (DSS) induced experimental colitis in immunodeficient mice: effects in CD4(+) -cell depleted, athymic and NK-cell depleted SCID mice. Inflammation research : official journal of the European Histamine Research Society … [et al.] *45*, 181-191. https://doi.org/10.1007/BF02285159.

Azarschab, P., Porschen, R., Gregor, M., Blin, N., and Holzmann, K. (2002). Epigenetic control of the E-cadherin gene (CDH1) by CpG methylation in colectomy samples of patients with ulcerative colitis. Genes, chromosomes & cancer *35*, 121-126. https://doi.org/10.1002/gcc.10101.

Azuma, M., Ito, D., Yagita, H., Okumura, K., Phillips, J.H., Lanier, L.L., and Somoza, C. (1993). B70 antigen is a second ligand for CTLA-4 and CD28. Nature *366*, 76-79. https://doi.org/10.1038/366076a0.

Bain, C.C., Scott, C.L., Uronen-Hansson, H., Gudjonsson, S., Jansson, O., Grip, O., Guilliams, M., Malissen, B., Agace, W.W., and Mowat, A.M. (2013). Resident and pro-inflammatory macrophages in the colon represent alternative context-dependent fates of the same Ly6Chi monocyte precursors. Mucosal immunology *6*, 498-510. https://doi.org/10.1038/mi.2012.89.

Bangia, N., and Watts, T.H. (1995). Evidence for invariant chain 85-101 (CLIP) binding in the antigen binding site of MHC class II molecules. International immunology *7*, 1585-1591. https://doi.org/10.1093/intimm/7.10.1585.

Bank, U., Deiser, K., Plaza-Sirvent, C., Osbelt, L., Witte, A., Knop, L., Labrenz, R., Jänsch, R., Richter, F., and Biswas, A., et al. (2020). c-FLIP is crucial for IL-7/IL-15-dependent NKp46+ ILC development and protection from intestinal inflammation in mice. Nature communications *11*, 1056. https://doi.org/10.1038/s41467-020-14782-3.

Bannister, A.J., and Kouzarides, T. (2011). Regulation of chromatin by histone modifications. Cell research *21*, 381-395. https://doi.org/10.1038/cr.2011.22.

Barker, N. (2014). Adult intestinal stem cells: critical drivers of epithelial homeostasis and regeneration. Nature reviews. Molecular cell biology *15*, 19-33. https://doi.org/10.1038/nrm3721.

Barker, N., van Es, J.H., Kuipers, J., Kujala, P., van den Born, M., Cozijnsen, M., Haegebarth, A., Korving, J., Begthel, H., and Peters, P.J., et al. (2007). Identification of stem cells in small intestine and colon by marker gene Lgr5. Nature *449*, 1003-1007. https://doi.org/10.1038/nature06196.

Barski, A., Cuddapah, S., Cui, K., Roh, T.-Y., Schones, D.E., Wang, Z., Wei, G., Chepelev, I., and Zhao, K. (2007). High-resolution profiling of histone methylations in the human genome. Cell *129*, 823-837. https://doi.org/10.1016/j.cell.2007.05.009.

Baydi, Z., Limami, Y., Khalki, L., Zaid, N., Naya, A., Mtairag, E.M., Oudghiri, M., and Zaid, Y. (2021). An Update of Research Animal Models of Inflammatory Bowel Disease. TheScientificWorldJournal *2021*, 7479540. https://doi.org/10.1155/2021/7479540.

Berin, M.C., Dwinell, M.B., Eckmann, L., and Kagnoff, M.F. (2001). Production of MDC/CCL22 by human intestinal epithelial cells. American journal of physiology. Gastrointestinal and liver physiology *280*, G1217-26. https://doi.org/10.1152/ajpgi.2001.280.6.G1217.

Bindea, G., Mlecnik, B., Hackl, H., Charoentong, P., Tosolini, M., Kirilovsky, A., Fridman, W.-H., Pagès, F., Trajanoski, Z., and Galon, J. (2009). ClueGO: a Cytoscape plug-in to decipher functionally grouped gene ontology and pathway annotation networks. Bioinformatics (Oxford, England) *25*, 1091-1093. https://doi.org/10.1093/bioinformatics/btp101.

Birchenough, G.M.H., Johansson, M.E.V., Gustafsson, J.K., Bergström, J.H., and Hansson, G.C. (2015). New developments in goblet cell mucus secretion and function. Mucosal immunology *8*, 712-719. https://doi.org/10.1038/mi.2015.32.

Bisping, G., Lügering, N., Lütke-Brintrup, S., Pauels, H.G., Schürmann, G., Domschke, W., and Kucharzik, T. (2001). Patients with inflammatory bowel disease (IBD) reveal increased induction capacity of intracellular interferon-gamma (IFN-gamma) in peripheral CD8+ lymphocytes co-cultured with intestinal epithelial cells. Clinical and experimental immunology *123*, 15-22. https://doi.org/10.1046/j.1365-2249.2001.01443.x.

Björnsson, S., and Jóhannsson, J.H. (2000). Inflammatory bowel disease in Iceland, 1990-1994: a prospective, nationwide, epidemiological study. European journal of gastroenterology & hepatology *12*, 31-38. https://doi.org/10.1097/00042737-200012010-00007.

Bloom, S., Simmons, D., and Jewell, D.P. (1995). Adhesion molecules intercellular adhesion molecule-1 (ICAM-1), ICAM-3 and B7 are not expressed by epithelium in normal or inflamed colon. Clinical and experimental immunology *101*, 157-163. https://doi.org/10.1111/j.1365-2249.1995.tb02292.x.

Boland, B.S., He, Z., Tsai, M.S., Olvera, J.G., Omilusik, K.D., Duong, H.G., Kim, E.S., Limary, A.E., Jin, W., and Milner, J.J., et al. (2020). Heterogeneity and clonal relationships of adaptive immune cells in ulcerative colitis revealed by single-cell analyses. Science immunology *5*. https://doi.org/10.1126/sciimmunol.abb4432.

Bruder, D., Probst-Kepper, M., Westendorf, A.M., Geffers, R., Beissert, S., Loser, K., Boehmer, H. von, Buer, J., and Hansen, W. (2004). Neuropilin-1: a surface marker of regulatory T cells. European journal of immunology *34*, 623-630. https://doi.org/10.1002/eji.200324799.

Brügger, M.D., Valenta, T., Fazilaty, H., Hausmann, G., and Basler, K. (2020). Distinct populations of crypt-associated fibroblasts act as signaling hubs to control colon homeostasis. PLoS biology *18*, e3001032. https://doi.org/10.1371/journal.pbio.3001032.

Burgueño, J.F., Fritsch, J., Santander, A.M., Brito, N., Fernández, I., Pignac-Kobinger, J., Conner, G.E., and Abreu, M.T. (2019). Intestinal Epithelial Cells Respond to Chronic Inflammation and Dysbiosis by Synthesizing H2O2. Frontiers in physiology *10*, 1484. https://doi.org/10.3389/fphys.2019.01484.

Burisch, J., Jess, T., Martinato, M., and Lakatos, P.L. (2013). The burden of inflammatory bowel disease in Europe. Journal of Crohn's & colitis *7*, 322-337. https://doi.org/10.1016/j.crohns.2013.01.010.

Byrne, B., Madrigal-Estebas, L., McEvoy, A., Carton, J., Doherty, D.G., Whelan, A., Feighery, C., O'Donoghue, D.P., and O'Farrelly, C. (2002). Human duodenal epithelial cells constitutively express molecular components of antigen presentation but not costimulatory molecules. Human Immunology *63*, 977-986. https://doi.org/10.1016/S0198-8859(02)00436-6.

Callahan, B.J., McMurdie, P.J., Rosen, M.J., Han, A.W., Johnson, A.J.A., and Holmes, S.P. (2016). DADA2: High-resolution sample inference from Illumina amplicon data. Nature methods *13*, 581-583. https://doi.org/10.1038/nmeth.3869.

Camarinha-Silva, A., Jáuregui, R., Chaves-Moreno, D., Oxley, A.P.A., Schaumburg, F., Becker, K., Wos-Oxley, M.L., and Pieper, D.H. (2014). Comparing the anterior nare bacterial community of two discrete human populations using Illumina amplicon sequencing. Environmental microbiology *16*, 2939-2952. https://doi.org/10.1111/1462-2920.12362.

Carlsen, H.S., Baekkevold, E.S., Johansen, F.-E., Haraldsen, G., and Brandtzaeg, P. (2002). B cell attracting chemokine 1 (CXCL13) and its receptor CXCR5 are expressed in normal and aberrant gut associated lymphoid tissue. Gut *51*, 364-371. https://doi.org/10.1136/gut.51.3.364.

Carter, M.J., Lobo, A.J., and Travis, S.P.L. (2004). Guidelines for the management of inflammatory bowel disease in adults. Gut *53 Suppl 5*, V1-16. https://doi.org/10.1136/gut.2004.043372.

Cash, H.L., Whitham, C.V., Behrendt, C.L., and Hooper, L.V. (2006). Symbiotic bacteria direct expression of an intestinal bactericidal lectin. Science (New York, N.Y.) *313*, 1126-1130. https://doi.org/10.1126/science.1127119.

Chaves-Moreno, D., Plumeier, I., Kahl, S., Krismer, B., Peschel, A., Oxley, A.P.A., Jauregui, R., and Pieper, D.H. (2015). The microbial community structure of the cotton rat nose. Environmental microbiology reports *7*, 929-935. https://doi.org/10.1111/1758-2229.12334.

Chelakkot, C., Ghim, J., Rajasekaran, N., Choi, J.-S., Kim, J.-H., Jang, M.H., Shin, Y.K., Suh, P.-G., and Ryu, S.H. (2017). Intestinal Epithelial Cell-Specific Deletion of PLD2 Alleviates DSS-Induced Colitis by Regulating Occludin. Scientific reports *7*, 1573. https://doi.org/10.1038/s41598-017-01797-y.

Chen, M., Li, Q., Cao, N., Deng, Y., Li, L., Zhao, Q., Wu, M., and Ye, M. (2019). Profiling of histone 3 lysine 27 acetylation reveals its role in a chronic DSS-induced colitis mouse model. Molecular omics *15*, 296-307. https://doi.org/10.1039/c9mo00070d.

Chen, Y., Chou, K., Fuchs, E., Havran, W.L., and Boismenu, R. (2002). Protection of the intestinal mucosa by intraepithelial gamma delta T cells. Proceedings of the National Academy of Sciences of the United States of America *99*, 14338-14343. https://doi.org/10.1073/pnas.212290499.

Chiba, M., Iizuka, M., and Masamune, O. (1988). Ubiquitous expression of HLA-DR antigens on human small intestinal epithelium. Gastroenterologia Japonica *23*, 109-116. https://doi.org/10.1007/BF02799021.

Chinen, T., Komai, K., Muto, G., Morita, R., Inoue, N., Yoshida, H., Sekiya, T., Yoshida, R., Nakamura, K., and Takayanagi, R., et al. (2011). Prostaglandin E2 and SOCS1 have a role in intestinal immune tolerance. Nature communications *2*, 190. https://doi.org/10.1038/ncomms1181.

Chruścik, A., Kauter, K., Windus, L., and Whiteside, E. (2021). Fundamentals of Anatomy and Physiology. 12.5 The Small and Large Intestines (University of Southern Queensland).

Ciurkiewicz, M., Herder, V., and Beineke, A. (2020). Beneficial and Detrimental Effects of Regulatory T Cells in Neurotropic Virus Infections. International journal of molecular sciences *21*. https://doi.org/10.3390/ijms21051705.

Clarke, K. (1993). Non-parametric multivariate analyses of changes in community structure. Austral Ecol *18*, 117-143. https://doi.org/10.1111/j.1442-9993.1993.tb00438.x.

Clarke, K., and Gorley, R. (2015). Primer V7: User Manual. (Prim Ltd.: Plymouth, UK).

Clemente, J.C., Pehrsson, E.C., Blaser, M.J., Sandhu, K., Gao, Z., Wang, B., Magris, M., Hidalgo, G., Contreras, M., and Noya-Alarcón, Ó., et al. (2015). The microbiome of uncontacted Amerindians. Science advances *1*. https://doi.org/10.1126/sciadv.1500183.

Colgan, S.P., Resnick, M.B., Parkos, C.A., Delp-Archer, C., McGuirk, D., Bacarra, A.E., Weller, P.F., and Madara, J.L. (1994). IL-4 directly modulates function of a model human intestinal epithelium. Journal of immunology (Baltimore, Md. : 1950) *153*, 2122-2129.

Coombes, J.L., Siddiqui, K.R.R., Arancibia-Cárcamo, C.V., Hall, J., Sun, C.-M., Belkaid, Y., and Powrie, F. (2007). A functionally specialized population of mucosal CD103+ DCs induces Foxp3+ regulatory T cells via a TGF-beta and retinoic acid-dependent mechanism. The Journal of experimental medicine *204*, 1757-1764. https://doi.org/10.1084/jem.20070590.

Cosovanu, C., and Neumann, C. (2020). The Many Functions of Foxp3+ Regulatory T Cells in the Intestine. Frontiers in immunology *11*, 600973. https://doi.org/10.3389/fimmu.2020.600973.

Creyghton, M.P., Cheng, A.W., Welstead, G.G., Kooistra, T., Carey, B.W., Steine, E.J., Hanna, J., Lodato, M.A., Frampton, G.M., and Sharp, P.A., et al. (2010). Histone H3K27ac separates active from poised enhancers and predicts developmental state. Proceedings of the National Academy of Sciences of the United States of America *107*, 21931-21936. https://doi.org/10.1073/pnas.1016071107.

Cruickshank, S.M., McVay, L.D., Baumgart, D.C., Felsburg, P.J., and Carding, S.R. (2004). Colonic epithelial cell mediated suppression of CD4 T cell activation. Gut *53*, 678-684. https://doi.org/10.1136/gut.2003.029967.

Curciarello, R., Canziani, K.E., Salto, I., Barbiera Romero, E., Rocca, A., Doldan, I., Peton, E., Brayer, S., Sambuelli, A.M., and Goncalves, S., et al. (2021). Probiotic Lactobacilli Isolated from Kefir Promote Down-Regulation of Inflammatory Lamina Propria T Cells from Patients with Active IBD. Frontiers in pharmacology *12*, 658026. https://doi.org/10.3389/fphar.2021.658026.

Curotto de Lafaille, M.A., Muriglan, S., Sunshine, M.J., Lei, Y., Kutchukhidze, N., Furtado, G.C., Wensky, A.K., Olivares-Villagómez, D., and Lafaille, J.J. (2001). Hyper immunoglobulin E response in mice with monoclonal populations of B and T lymphocytes. The Journal of experimental medicine *194*, 1349-1359. https://doi.org/10.1084/jem.194.9.1349.

Czarnewski, P., Parigi, S.M., Sorini, C., Diaz, O.E., Das, S., Gagliani, N., and Villablanca, E.J. (2019). Conserved transcriptomic profile between mouse and human colitis allows unsupervised patient stratification. Nature communications *10*, 2892. https://doi.org/10.1038/s41467-019-10769-x.

Daar, A.S., Fuggle, S.V., Ting, A., and Fabre, J.W. (1982). Anomolous expression of HLA-DR antigens on human colorectal cancer cells. Journal of immunology (Baltimore, Md. : 1950) *129*, 447-449.

(2016). Database resources of the National Center for Biotechnology Information. Nucleic acids research *44*, D7-19. https://doi.org/10.1093/NAR/GKV1290.

Dempsey, E., and Corr, S.C. (2022). Lactobacillus spp. for Gastrointestinal Health: Current and Future Perspectives. Frontiers in immunology *13*, 840245. https://doi.org/10.3389/fimmu.2022.840245.

Denzin, L.K., and Cresswell, P. (1995). HLA-DM induces clip dissociation from MHC class II αβ dimers and facilitates peptide loading. Cell *82*, 155-165. https://doi.org/10.1016/0092-8674(95)90061-6.

Dieleman, L.A., Palmen, M.J., Akol, H., Bloemena, E., Peña, A.S., Meuwissen, S.G., and van Rees, E.P. (1998). Chronic experimental colitis induced by dextran sulphate sodium (DSS) is characterized by Th1 and Th2 cytokines. Clinical and experimental immunology *114*, 385-391. https://doi.org/10.1046/j.1365-2249.1998.00728.x.

Dieleman, L.A., Ridwan, B.U., Tennyson, G.S., Beagley, K.W., Bucy, R.P., and Elson, C.O. (1994). Dextran sulfate sodium-induced colitis occurs in severe combined immunodeficient mice. Gastroenterology *107*, 1643-1652. https://doi.org/10.1016/0016-5085(94)90803-6.

Diny, N.L., Rose, N.R., and Čiháková, D. (2017). Eosinophils in Autoimmune Diseases. Frontiers in immunology *8*, 484. https://doi.org/10.3389/fimmu.2017.00484.

Dobin, A., Davis, C.A., Schlesinger, F., Drenkow, J., Zaleski, C., Jha, S., Batut, P., Chaisson, M., and Gingeras, T.R. (2013). STAR: ultrafast universal RNA-seq aligner. Bioinformatics (Oxford, England) *29*, 15-21. https://doi.org/10.1093/bioinformatics/bts635.

Dotan, I., Allez, M., Nakazawa, A., Brimnes, J., Schulder-Katz, M., and Mayer, L. (2007). Intestinal epithelial cells from inflammatory bowel disease patients preferentially stimulate CD4+ T cells to proliferate and secrete interferon-gamma.

American journal of physiology. Gastrointestinal and liver physiology *292*, G1630-40. https://doi.org/10.1152/ajpgi.00294.2006.

Durinck, S., Moreau, Y., Kasprzyk, A., Davis, S., Moor, B. de, Brazma, A., and Huber, W. (2005). BioMart and Bioconductor: a powerful link between biological databases and microarray data analysis. Bioinformatics (Oxford, England) *21*, 3439-3440. https://doi.org/10.1093/bioinformatics/bti525.

Dziarski, R., Park, S.Y., Des Kashyap, R., Dowd, S.E., and Gupta, D. (2016). Pglyrp-Regulated Gut Microflora Prevotella falsenii, Parabacteroides distasonis and Bacteroides eggerthii Enhance and Alistipes finegoldii Attenuates Colitis in Mice. PloS one *11*, e0146162. https://doi.org/10.1371/journal.pone.0146162.

El Hassani, R.A., Benfares, N., Caillou, B., Talbot, M., Sabourin, J.-C., Belotte, V., Morand, S., Gnidehou, S., Agnandji, D., and Ohayon, R., et al. (2005). Dual oxidase2 is expressed all along the digestive tract. American journal of physiology. Gastrointestinal and liver physiology *288*, G933-42. https://doi.org/10.1152/ajpgi.00198.2004.

Endharti, A.T., Okuno, Y., Shi, Z., Misawa, N., Toyokuni, S., Ito, M., Isobe, K.-i., and Suzuki, H. (2011). CD8+CD122+ regulatory T cells (Tregs) and CD4+ Tregs cooperatively prevent and cure CD4+ cell-induced colitis. Journal of immunology (Baltimore, Md. : 1950) *186*, 41-52. https://doi.org/10.4049/jimmunol.1000800.

Fallarino, F., Grohmann, U., You, S., McGrath, B.C., Cavener, D.R., Vacca, C., Orabona, C., Bianchi, R., Belladonna, M.L., and Volpi, C., et al. (2006). The combined effects of tryptophan starvation and tryptophan catabolites down-regulate T cell receptor zeta-chain and induce a regulatory phenotype in naive T cells. Journal of immunology (Baltimore, Md. : 1950) *176*, 6752-6761. https://doi.org/10.4049/jimmunol.176.11.6752.

Farnham, P.J. (2009). Insights from genomic profiling of transcription factors. Nature reviews. Genetics *10*, 605-616. https://doi.org/10.1038/nrg2636.

Feng, J., Liu, T., Qin, B., Zhang, Y., and Liu, X.S. (2012). Identifying ChIP-seq enrichment using MACS. Nature protocols *7*, 1728-1740. https://doi.org/10.1038/nprot.2012.101.

Finegold, S.M., Molitoris, D., Song, Y., Liu, C., Vaisanen, M.-L., Bolte, E., McTeague, M., Sandler, R., Wexler, H., and Marlowe, E.M., et al. (2002). Gastrointestinal microflora studies in late-onset autism. Clinical infectious diseases : an official publication of the Infectious Diseases Society of America *35*, S6-S16. https://doi.org/10.1086/341914.

Fontenot, J.D., Gavin, M.A., and Rudensky, A.Y. (2003). Foxp3 programs the development and function of CD4+CD25+ regulatory T cells. Nature immunology *4*, 330-336. https://doi.org/10.1038/ni904.

Fournier, B.M., and Parkos, C.A. (2012). The role of neutrophils during intestinal inflammation. Mucosal immunology *5*, 354-366. https://doi.org/10.1038/mi.2012.24.

Frank, D.N., St Amand, A.L., Feldman, R.A., Boedeker, E.C., Harpaz, N., and Pace, N.R. (2007). Molecular-phylogenetic characterization of microbial community imbalances in human inflammatory bowel diseases. Proceedings of the National Academy of Sciences of the United States of America *104*, 13780-13785. https://doi.org/10.1073/pnas.0706625104.

Fu, Y., Wang, Z., Yu, B., Lin, Y., Huang, E., Liu, R., Zhao, C., Lu, M., Xu, W., and Liu, H., et al. (2021). Intestinal CD11b+ B Cells Ameliorate Colitis by Secreting Immunoglobulin A. Frontiers in immunology *12*, 697725. https://doi.org/10.3389/fimmu.2021.697725.

Fuss, I.J., Neurath, M., Boirivant, M., Klein, J.S., La Motte, C. de, Strong, S.A., Fiocchi, C., and Strober, W. (1996). Disparate CD4+ lamina propria (LP) lymphokine secretion profiles in inflammatory bowel disease. Crohn's disease LP cells manifest increased secretion of IFN-gamma, whereas ulcerative colitis LP cells manifest increased secretion of IL-5. Journal of immunology (Baltimore, Md. : 1950) *157*, 1261-1270.

Garcia-Zepeda, E.A., Rothenberg, M.E., Ownbey, R.T., Celestin, J., Leder, P., and Luster, A.D. (1996). Human eotaxin is a specific chemoattractant for eosinophil cells and provides a new mechanism to explain tissue eosinophilia. Nature medicine *2*, 449-456. https://doi.org/10.1038/nm0496-449.

Gautam, A.M., Pearson, C., Quinn, V., McDevitt, H.O., and Milburn, P.J. (1995). Binding of an invariant-chain peptide, CLIP, to I-A major histocompatibility complex class II molecules. Proceedings of the National Academy of Sciences of the United States of America *92*, 335-339. https://doi.org/10.1073/pnas.92.1.335.

Gelmez, E., Lehr, K., Kershaw, O., Frentzel, S., Vilchez-Vargas, R., Bank, U., Link, A., Schüler, T., Jeron, A., and Bruder, D. (2022). Characterization of Maladaptive Processes in Acute, Chronic and Remission Phases of Experimental Colitis in C57BL/6 Mice. Biomedicines *10*, 1903. https://doi.org/10.3390/biomedicines10081903.

Gracz, A.D., Puthoff, B.J., and Magness, S.T. (2012). Identification, isolation, and culture of intestinal epithelial stem cells from murine intestine. Methods in molecular biology (Clifton, N.J.) *879*, 89-107. https://doi.org/10.1007/978-1-61779-815-3_6.

Grasberger, H., and Refetoff, S. (2006). Identification of the maturation factor for dual oxidase. Evolution of an eukaryotic operon equivalent. The Journal of biological chemistry *281*, 18269-18272. https://doi.org/10.1074/jbc.C600095200.

Gribble, F.M., and Reimann, F. (2019). Function and mechanisms of enteroendocrine cells and gut hormones in metabolism. Nature reviews. Endocrinology *15*, 226-237. https://doi.org/10.1038/s41574-019-0168-8.

Groux, H., O'Garra, A., Bigler, M., Rouleau, M., Antonenko, S., Vries, J.E. de, and Roncarolo, M.G. (1997). A CD4+ T-cell subset inhibits antigen-specific T-cell responses and prevents colitis. Nature *389*, 737-742. https://doi.org/10.1038/39614.

Gruening, B.A. (2014). Galaxy wrapper. https://github.com/bgruening/galaxytools.

Gryaznova, M.V., Solodskikh, S.A., Panevina, A.V., Syromyatnikov, M.Y., Dvoretskaya, Y.D., Sviridova, T.N., Popov, E.S., and Popov, V.N. (2021). Study of microbiome changes in patients with ulcerative colitis in the Central European part of Russia. Heliyon *7*, e06432. https://doi.org/10.1016/j.heliyon.2021.e06432.

Gunesh, S., Thomas, G.A.O., Williams, G.T., Roberts, A., and Hawthorne, A.B. (2008). The incidence of Crohn's disease in Cardiff over the last 75 years: an update for 1996-2005. Alimentary pharmacology & therapeutics *27*, 211-219. https://doi.org/10.1111/j.1365-2036.2007.03576.x.

Hall, L.J., Faivre, E., Quinlan, A., Shanahan, F., Nally, K., and Melgar, S. (2011). Induction and activation of adaptive immune populations during acute and chronic phases of a murine model of experimental colitis. Digestive diseases and sciences *56*, 79-89. https://doi.org/10.1007/s10620-010-1240-3.

Halliday, N., Williams, C., Kennedy, A., Waters, E., Pesenacker, A.M., Soskic, B., Hinze, C., Hou, T.Z., Rowshanravan, B., and Janman, D., et al. (2020). CD86 Is a Selective CD28 Ligand Supporting FoxP3+ Regulatory T Cell Homeostasis in the Presence of High Levels of CTLA-4. Frontiers in immunology *11*, 600000. https://doi.org/10.3389/fimmu.2020.600000.

He, L., Yu, W., Zhang, W., and Zhang, L. (2021). An optimized two-step chromatin immunoprecipitation protocol to quantify the associations of two separate proteins and their common target DNA. STAR protocols *2*, 100504. https://doi.org/10.1016/j.xpro.2021.100504.

Hendel, S.K., Kellermann, L., Hausmann, A., Bindslev, N., Jensen, K.B., and Nielsen, O.H. (2022). Tuft Cells and Their Role in Intestinal Diseases. Frontiers in immunology *13*, 822867. https://doi.org/10.3389/fimmu.2022.822867.

Herath, M., Hosie, S., Bornstein, J.C., Franks, A.E., and Hill-Yardin, E.L. (2020). The Role of the Gastrointestinal Mucus System in Intestinal Homeostasis: Implications for Neurological Disorders. Frontiers in cellular and infection microbiology *10*, 248. https://doi.org/10.3389/fcimb.2020.00248.

Hershberg, R.M., Framson, P.E., Cho, D.H., Lee, L.Y., Kovats, S., Beitz, J., Blum, J.S., and Nepom, G.T. (1997). Intestinal epithelial cells use two distinct pathways for HLA class II antigen processing. The Journal of clinical investigation *100*, 204-215. https://doi.org/10.1172/JCI119514.

Ho, J.W.K., Bishop, E., Karchenko, P.V., Nègre, N., White, K.P., and Park, P.J. (2011). ChIP-chip versus ChIP-seq: lessons for experimental design and data analysis. BMC genomics *12*, 134. https://doi.org/10.1186/1471-2164-12-134.

Hobart, M., Ramassar, V., Goes, N., Urmson, J., and Halloran, P.F. (1997). IFN regulatory factor-1 plays a central role in the regulation of the expression of class I and II MHC genes in vivo. Journal of immunology (Baltimore, Md. : 1950) *158*, 4260-4269.

Hochberg, Y., and Benjamini, Y. (1990). More powerful procedures for multiple significance testing. Statistics in medicine *9*, 811-818. https://doi.org/10.1002/sim.4780090710.

Hooper, L.V., Stappenbeck, T.S., Hong, C.V., and Gordon, J.I. (2003). Angiogenins: a new class of microbicidal proteins involved in innate immunity. Nature immunology *4*, 269-273. https://doi.org/10.1038/ni888.

Huang, F.P., Platt, N., Wykes, M., Major, J.R., Powell, T.J., Jenkins, C.D., and MacPherson, G.G. (2000). A discrete subpopulation of dendritic cells transports apoptotic intestinal epithelial cells to T cell areas of mesenteric lymph nodes. The Journal of experimental medicine *191*, 435-444. https://doi.org/10.1084/jem.191.3.435.

Hwu, P., Du, M.X., Lapointe, R., Do, M., Taylor, M.W., and Young, H.A. (2000). Indoleamine 2,3-dioxygenase production by human dendritic cells results in the inhibition of T cell proliferation. Journal of immunology (Baltimore, Md. : 1950) *164*, 3596-3599. https://doi.org/10.4049/jimmunol.164.7.3596.

Iborra, M., Bernuzzi, F., Correale, C., Vetrano, S., Fiorino, G., Beltrán, B., Marabita, F., Locati, M., Spinelli, A., and Nos, P., et al. (2013). Identification of serum and tissue micro-RNA expression profiles in different stages of inflammatory bowel disease. Clinical and experimental immunology *173*, 250-258. https://doi.org/10.1111/cei.12104.

Iljazovic, A., Roy, U., Gálvez, E.J.C., Lesker, T.R., Zhao, B., Gronow, A., Amend, L., Will, S.E., Hofmann, J.D., and Pils, M.C., et al. (2021). Perturbation of the gut microbiome by Prevotella spp. enhances host susceptibility to mucosal inflammation. Mucosal immunology *14*, 113-124. https://doi.org/10.1038/s41385-020-0296-4.

Ito, R., Shin-Ya, M., Kishida, T., Urano, A., Takada, R., Sakagami, J., Imanishi, J., Kita, M., Ueda, Y., and Iwakura, Y., et al. (2006). Interferon-gamma is causatively involved in experimental inflammatory bowel disease in mice. Clinical and experimental immunology *146*, 330-338. https://doi.org/10.1111/j.1365-2249.2006.03214.x.

Itoh, M., Takahashi, T., Sakaguchi, N., Kuniyasu, Y., Shimizu, J., Otsuka, F., and Sakaguchi, S. (1999). Thymus and autoimmunity: production of CD25+CD4+ naturally anergic and suppressive T cells as a key function of the thymus in maintaining immunologic self-tolerance. Journal of immunology (Baltimore, Md. : 1950) *162*, 5317-5326.

Johansson, M.E.V., Phillipson, M., Petersson, J., Velcich, A., Holm, L., and Hansson, G.C. (2008). The inner of the two Muc2 mucin-dependent mucus layers in colon is devoid of bacteria. Proceedings of the National Academy of Sciences of the United States of America *105*, 15064-15069. https://doi.org/10.1073/pnas.0803124105.

Johnson, D.S., Mortazavi, A., Myers, R.M., and Wold, B. (2007). Genome-wide mapping of in vivo protein-DNA interactions. Science (New York, N.Y.) *316*, 1497-1502. https://doi.org/10.1126/science.1141319.

Jordan, M.S., Boesteanu, A., Reed, A.J., Petrone, A.L., Holenbeck, A.E., Lerman, M.A., Naji, A., and Caton, A.J. (2001). Thymic selection of CD4+CD25+ regulatory T cells induced by an agonist self-peptide. Nature immunology *2*, 301-306. https://doi.org/10.1038/86302.

Kanehisa, M., Goto, S., Kawashima, S., Okuno, Y., and Hattori, M. (2004). The KEGG resource for deciphering the genome. Nucleic acids research *32*, D277-80. https://doi.org/10.1093/nar/gkh063.

Karlsson, F., Martinez, N.E., Gray, L., Zhang, S., Tsunoda, I., and Grisham, M.B. (2013). Therapeutic evaluation of ex vivo-generated versus natural regulatory T-cells in a mouse model of chronic gut inflammation. Inflammatory bowel diseases *19*, 2282-2294. https://doi.org/10.1097/MIB.0b013e31829c32dd.

KAUFMAN, J., AUFFRAY, C., KORMAN, A., SHACKELFORD, D., and STROMINGER, J. (1984). The class II molecules of the human and murine major histocompatibility complex. Cell *36*, 1-13. https://doi.org/10.1016/0092-8674(84)90068-0.

Kawamoto, A., Nagata, S., Anzai, S., Takahashi, J., Kawai, M., Hama, M., Nogawa, D., Yamamoto, K., Kuno, R., and Suzuki, K., et al. (2019). Ubiquitin D is Upregulated by Synergy of Notch Signalling and TNF-α in the Inflamed Intestinal Epithelia of IBD Patients. Journal of Crohn's & colitis *13*, 495-509. https://doi.org/10.1093/ecco-jcc/jjy180.

Kelly, D., Kotliar, M., Woo, V., Jagannathan, S., Whitt, J., Moncivaiz, J., Aronow, B.J., Dubinsky, M.C., Hyams, J.S., and Markowitz, J.F., et al. (2018). Microbiota-sensitive epigenetic signature predicts inflammation in Crohn's disease. JCI insight *3*. https://doi.org/10.1172/jci.insight.122104.

Kempski, J., Brockmann, L., Gagliani, N., and Huber, S. (2017). TH17 Cell and Epithelial Cell Crosstalk during Inflammatory Bowel Disease and Carcinogenesis. Frontiers in immunology *8*, 1373. https://doi.org/10.3389/fimmu.2017.01373.

Kim, B.-H., Shenoy, A.R., Kumar, P., Bradfield, C.J., and MacMicking, J.D. (2012). IFN-inducible GTPases in host cell defense. Cell host & microbe *12*, 432-444. https://doi.org/10.1016/j.chom.2012.09.007.

Kim, E.R., and Chang, D.K. (2014). Colorectal cancer in inflammatory bowel disease: the risk, pathogenesis, prevention and diagnosis. World journal of gastroenterology *20*, 9872-9881. https://doi.org/10.3748/wjg.v20.i29.9872.

Kim, J.J., Bridle, B.W., Ghia, J.-E., Wang, H., Syed, S.N., Manocha, M.M., Rengasamy, P., Shajib, M.S., Wan, Y., and Hedlund, P.B., et al. (2013). Targeted inhibition of serotonin type 7 (5-HT7) receptor function modulates immune responses and reduces the severity of intestinal inflammation. Journal of immunology (Baltimore, Md. : 1950) *190*, 4795-4804. https://doi.org/10.4049/jimmunol.1201887.

Kim, W.-K., Han, D.H., Jang, Y.J., Park, S., Jang, S.J., Lee, G., Han, H.S., and Ko, G. (2021). Alleviation of DSS-induced colitis via Lactobacillus acidophilus treatment in mice. Food & function *12*, 340-350. https://doi.org/10.1039/d0fo01724h.

Kim, Y.S., Lee, M.H., Ju, A.S., and Rhee, K.-J. (2011). Th17 responses are not induced in dextran sodium sulfate model of acute colitis. Immune network *11*, 416-419. https://doi.org/10.4110/in.2011.11.6.416.

Kita, H. (2011). Eosinophils: multifaceted biological properties and roles in health and disease. Immunological reviews *242*, 161-177. https://doi.org/10.1111/j.1600-065X.2011.01026.x.

Kluz, P.N., Kolb, R., Xie, Q., Borcherding, N., Liu, Q., Luo, Y., Kim, M.-C., Wang, L., Zhang, Y., and Li, W., et al. (2020). Cancer cell-intrinsic function of CD177 in attenuating β-catenin signaling. Oncogene *39*, 2877-2889. https://doi.org/10.1038/s41388-020-1203-x.

Komar, D.N., Mouriz, A., Jarillo, J.A., and Piñeiro, M. (2016). Chromatin Immunoprecipitation Assay for the Identification of Arabidopsis Protein-DNA Interactions In Vivo. Journal of visualized experiments : JoVE, e53422. https://doi.org/10.3791/53422.

Korolkova, O.Y., Myers, J.N., Pellom, S.T., Wang, L., and M'Koma, A.E. (2015). Characterization of Serum Cytokine Profile in Predominantly Colonic Inflammatory Bowel Disease to Delineate Ulcerative and Crohn's Colitides. Clinical medicine insights. Gastroenterology *8*, 29-44. https://doi.org/10.4137/CGast.S20612.

Kostic, M. (2010). Role of TH1 and TH17 Immune Responces in Pathogenesis of Multiple Sclerosis.

Kretschmer, K., Apostolou, I., Hawiger, D., Khazaie, K., Nussenzweig, M.C., and Boehmer, H. von (2005). Inducing and expanding regulatory T cell populations by foreign antigen. Nature immunology *6*, 1219-1227. https://doi.org/10.1038/ni1265.

Krueger F. 2012. Trim Galore!: A wrapper tool around Cutadapt and FastQC to consistently apply quality and adapter trimming to FastQ files, with some extra functionality for MspI-digested RRBS-type (Reduced Representation Bisufite-Seq) libraries.

Krych, L., Hansen, C.H.F., Hansen, A.K., van den Berg, F.W.J., and Nielsen, D.S. (2013). Quantitatively different, yet qualitatively alike: a meta-analysis of the mouse core gut microbiome with a view towards the human gut microbiome. PloS one *8*, e62578. https://doi.org/10.1371/journal.pone.0062578.

Kuenzig, M.E., Fung, S.G., Marderfeld, L., Mak, J.W.Y., Kaplan, G.G., Ng, S.C., Wilson, D.C., Cameron, F., Henderson, P., and Kotze, P.G., et al. (2022). Twenty-first Century Trends in the Global Epidemiology of Pediatric-Onset Inflammatory Bowel Disease: Systematic Review. Gastroenterology *162*, 1147-1159.e4. https://doi.org/10.1053/j.gastro.2021.12.282.

Kullberg, M.C., Andersen, J.F., Gorelick, P.L., Caspar, P., Suerbaum, S., Fox, J.G., Cheever, A.W., Jankovic, D., and Sher, A. (2003). Induction of colitis by a CD4+ T cell clone specific for a bacterial epitope. Proceedings of the National Academy of Sciences of the United States of America *100*, 15830-15835. https://doi.org/10.1073/pnas.2534546100.

Lamb, C.A., Yewdell, J.W., Bennink, J.R., and Cresswell, P. (1991). Invariant chain targets HLA class II molecules to acidic endosomes containing internalized influenza virus. Proceedings of the National Academy of Sciences of the United States of America *88*, 5998-6002. https://doi.org/10.1073/pnas.88.14.5998.

Landt, S.G., Marinov, G.K., Kundaje, A., Kheradpour, P., Pauli, F., Batzoglou, S., Bernstein, B.E., Bickel, P., Brown, J.B., and Cayting, P., et al. (2012). ChIP-seq guidelines and practices of the ENCODE and modENCODE consortia. Genome research *22*, 1813-1831. https://doi.org/10.1101/gr.136184.111.

Langmead, B., and Salzberg, S.L. (2012). Fast gapped-read alignment with Bowtie 2. Nature methods *9*, 357-359. https://doi.org/10.1038/nmeth.1923.

Langmead, B., Trapnell, C., Pop, M., and Salzberg, S.L. (2009). Ultrafast and memory-efficient alignment of short DNA sequences to the human genome. Genome biology *10*, R25. https://doi.org/10.1186/gb-2009-10-3-r25.

Laroui, H., Ingersoll, S.A., Liu, H.C., Baker, M.T., Ayyadurai, S., Charania, M.A., Laroui, F., Yan, Y., Sitaraman, S.V., and Merlin, D. (2012). Dextran sodium sulfate (DSS) induces colitis in mice by forming nano-lipocomplexes with medium-chain-length fatty acids in the colon. PloS one *7*, e32084. https://doi.org/10.1371/journal.pone.0032084.

Lehmann, J., Huehn, J., La Rosa, M. de, Maszyna, F., Kretschmer, U., Krenn, V., Brunner, M., Scheffold, A., and Hamann, A. (2002). Expression of the integrin alpha Ebeta 7 identifies unique subsets of CD25+ as well as CD25- regulatory T cells. Proceedings of the National Academy of Sciences of the United States of America *99*, 13031-13036. https://doi.org/10.1073/pnas.192162899.

Leppkes, M., Lindemann, A., Gößwein, S., Paulus, S., Roth, D., Hartung, A., Liebing, E., Zundler, S., Gonzalez-Acera, M., and Patankar, J.V., et al. (2021). Neutrophils prevent rectal bleeding in ulcerative colitis by peptidyl-arginine deiminase-4-dependent immunothrombosis. Gut. https://doi.org/10.1136/gutjnl-2021-324725.

Ley, R.E., Turnbaugh, P.J., Klein, S., and Gordon, J.I. (2006). Microbial ecology: human gut microbes associated with obesity. Nature *444*, 1022-1023. https://doi.org/10.1038/4441022a.

Li, H., and Durbin, R. (2009). Fast and accurate short read alignment with Burrows-Wheeler transform. Bioinformatics (Oxford, England) *25*, 1754-1760. https://doi.org/10.1093/bioinformatics/btp324.

Li, P., and Leonard, W.J. (2018). Chromatin Accessibility and Interactions in the Transcriptional Regulation of T Cells. Frontiers in immunology *9*, 2738. https://doi.org/10.3389/fimmu.2018.02738.

Li, Q., Brown, J.B., Huang, H., and Bickel, P.J. (2011). Measuring reproducibility of high-throughput experiments. Ann. Appl. Stat. *5*. https://doi.org/10.1214/11-AOAS466.

Li, Y., Chen, C.-Y., Kaye, A.M., and Wasserman, W.W. (2015). The identification of cis-regulatory elements: A review from a machine learning perspective. Bio Systems *138*, 6-17. https://doi.org/10.1016/j.biosystems.2015.10.002.

Li, Y., Jia, Y., Cui, T., and Zhang, J. (2021). IL-6/STAT3 signaling pathway regulates the proliferation and damage of intestinal epithelial cells in patients with ulcerative colitis via H3K27ac. Experimental and therapeutic medicine *22*, 890. https://doi.org/10.3892/etm.2021.10322.

Liao, Y., Smyth, G.K., and Shi, W. (2014). featureCounts: an efficient general purpose program for assigning sequence reads to genomic features. Bioinformatics (Oxford, England) *30*, 923-930. https://doi.org/10.1093/bioinformatics/btt656.

Lin, Y., Qiu, T., Wei, G., Que, Y., Wang, W., Kong, Y., Xie, T., and Chen, X. (2022). Role of Histone Post-Translational Modifications in Inflammatory Diseases. Frontiers in immunology *13*, 852272. https://doi.org/10.3389/fimmu.2022.852272.

Linsley, P.S., Clark, E.A., and Ledbetter, J.A. (1990). T-cell antigen CD28 mediates adhesion with B cells by interacting with activation antigen B7/BB-1. Proceedings of the National Academy of Sciences of the United States of America *87*, 5031-5035. https://doi.org/10.1073/pnas.87.13.5031.

Liu, A., Lv, H., Wang, H., Yang, H., Li, Y., and Qian, J. (2020). Aging Increases the Severity of Colitis and the Related Changes to the Gut Barrier and Gut Microbiota in Humans and Mice. The journals of gerontology. Series A, Biological sciences and medical sciences *75*, 1284-1292. https://doi.org/10.1093/gerona/glz263.

Lorenzen, J.M., Martino, F., and Thum, T. (2012). Epigenetic modifications in cardiovascular disease. Basic research in cardiology *107*, 245. https://doi.org/10.1007/s00395-012-0245-9.

Luger, K., Mäder, A.W., Richmond, R.K., Sargent, D.F., and Richmond, T.J. (1997). Crystal structure of the nucleosome core particle at 2.8 A resolution. Nature *389*, 251-260. https://doi.org/10.1038/38444.

MacFie, T.S., Poulsom, R., Parker, A., Warnes, G., Boitsova, T., Nijhuis, A., Suraweera, N., Poehlmann, A., Szary, J., and Feakins, R., et al. (2014). DUOX2 and DUOXA2 form the predominant enzyme system capable of producing the reactive oxygen species H2O2 in active ulcerative colitis and are modulated by 5-aminosalicylic acid. Inflammatory bowel diseases *20*, 514-524. https://doi.org/10.1097/01.MIB.0000442012.45038.0e.

Macpherson, A.J., Geuking, M.B., and McCoy, K.D. (2012). Innate and adaptive immunity in host-microbiota mutualism. Frontiers in bioscience (Scholar edition) *4*, 685-698. https://doi.org/10.2741/S293.

Madrigal, L., Lynch, S., Feighery, C., Weir, D., Kelleher, D., and O'Farelly, C. (1993). Flow cytometric analysis of surface major histocompatibility complex class II expression on human epithelial cells prepared from small intestinal biopsies. Journal of Immunological Methods *158*, 207-214. https://doi.org/10.1016/0022-1759(93)90216-T.

Mah, A.T., Yan, K.S., and Kuo, C.J. (2016). Wnt pathway regulation of intestinal stem cells. The Journal of physiology *594*, 4837-4847. https://doi.org/10.1113/JP271754.

Maidak, B.L., Olsen, G.J., Larsen, N., Overbeek, R., McCaughey, M.J., and Woese, C.R. (1997). The RDP (Ribosomal Database Project). Nucleic acids research *25*, 109-111. https://doi.org/10.1093/NAR/25.1.109.

Malmberg, E.K., Noaksson, K.A., Phillipson, M., Johansson, M.E.V., Hinojosa-Kurtzberg, M., Holm, L., Gendler, S.J., and Hansson, G.C. (2006). Increased levels of mucins in the cystic fibrosis mouse small intestine, and modulator effects of the Muc1 mucin expression. American journal of physiology. Gastrointestinal and liver physiology *291*, G203-10. https://doi.org/10.1152/ajpgi.00491.2005.

Marchesi, F., Martin, A.P., Thirunarayanan, N., Devany, E., Mayer, L., Grisotto, M.G., Furtado, G.C., and Lira, S.A. (2009). CXCL13 expression in the gut promotes accumulation of IL-22-producing lymphoid tissue-inducer cells, and formation of isolated lymphoid follicles. Mucosal immunology *2*, 486-494. https://doi.org/10.1038/mi.2009.113.

Martens, S., Parvanova, I., Zerrahn, J., Griffiths, G., Schell, G., Reichmann, G., and Howard, J.C. (2005). Disruption of Toxoplasma gondii parasitophorous vacuoles by the mouse p47-resistance GTPases. PLoS pathogens *1*, e24. https://doi.org/10.1371/journal.ppat.0010024.

Matthews, A.N., Friend, D.S., Zimmermann, N., Sarafi, M.N., Luster, A.D., Pearlman, E., Wert, S.E., and Rothenberg, M.E. (1998). Eotaxin is required for the baseline level of tissue eosinophils. Proceedings of the National Academy of Sciences of the United States of America *95*, 6273-6278. https://doi.org/10.1073/pnas.95.11.6273.

McDermott, E., Ryan, E.J., Tosetto, M., Gibson, D., Burrage, J., Keegan, D., Byrne, K., Crowe, E., Sexton, G., and Malone, K., et al. (2016). DNA Methylation Profiling in Inflammatory Bowel Disease Provides New Insights into Disease Pathogenesis. Journal of Crohn's & colitis *10*, 77-86. https://doi.org/10.1093/ecco-jcc/jjv176.

McMurdie, P.J., and Holmes, S. (2013). phyloseq: an R package for reproducible interactive analysis and graphics of microbiome census data. PloS one *8*, e61217. https://doi.org/10.1371/journal.pone.0061217.

Mehta, P., and Furuta, G.T. (2015). Eosinophils in Gastrointestinal Disorders: Eosinophilic Gastrointestinal Diseases, Celiac Disease, Inflammatory Bowel Diseases, and Parasitic Infections. Immunology and allergy clinics of North America *35*, 413-437. https://doi.org/10.1016/j.iac.2015.04.003.

Melgar, S., Karlsson, A., and Michaëlsson, E. (2005). Acute colitis induced by dextran sulfate sodium progresses to chronicity in C57BL/6 but not in BALB/c mice: correlation between symptoms and inflammation. American journal of physiology. Gastrointestinal and liver physiology *288*, G1328-38. https://doi.org/10.1152/ajpgi.00467.2004.

Mellor, A.L., Keskin, D.B., Johnson, T., Chandler, P., and Munn, D.H. (2002). Cells expressing indoleamine 2,3-dioxygenase inhibit T cell responses. Journal of immunology (Baltimore, Md. : 1950) *168*, 3771-3776. https://doi.org/10.4049/jimmunol.168.8.3771.

Ménager-Marcq, I., Pomié, C., Romagnoli, P., and van Meerwijk, J.P.M. (2006). CD8+CD28- regulatory T lymphocytes prevent experimental inflammatory bowel disease in mice. Gastroenterology *131*, 1775-1785. https://doi.org/10.1053/j.gastro.2006.09.008.

Mezrich, J.D., Fechner, J.H., Zhang, X., Johnson, B.P., Burlingham, W.J., and Bradfield, C.A. (2010). An interaction between kynurenine and the aryl hydrocarbon receptor can generate regulatory T cells. Journal of immunology (Baltimore, Md. : 1950) *185*, 3190-3198. https://doi.org/10.4049/jimmunol.0903670.

Molnar, C., and Gair, J. (2015). Concepts of Biology. 23.2. Adaptive Immune Response.

Munn, D.H., Shafizadeh, E., Attwood, J.T., Bondarev, I., Pashine, A., and Mellor, A.L. (1999). Inhibition of T cell proliferation by macrophage tryptophan catabolism. The Journal of experimental medicine *189*, 1363-1372. https://doi.org/10.1084/jem.189.9.1363.

Munyaka, P.M., Rabbi, M.F., Khafipour, E., and Ghia, J.-E. (2016). Acute dextran sulfate sodium (DSS)-induced colitis promotes gut microbial dysbiosis in mice. Journal of basic microbiology *56*, 986-998. https://doi.org/10.1002/jobm.201500726.

Muzaki, A.R.B.M., Tetlak, P., Sheng, J., Loh, S.C., Setiagani, Y.A., Poidinger, M., Zolezzi, F., Karjalainen, K., and Ruedl, C. (2016). Intestinal CD103(+)CD11b(-) dendritic cells restrain colitis via IFN-γ-induced anti-inflammatory response in epithelial cells. Mucosal immunology *9*, 336-351. https://doi.org/10.1038/mi.2015.64.

Nakazawa, A., Watanabe, M., Kanai, T., Yajima, T., Yamazaki, M., Ogata, H., Ishii, H., Azuma, M., and Hibi, T. (1999). Functional expression of costimulatory molecule CD86 on epithelial cells in the inflamed colonic mucosa. Gastroenterology *117*, 536-545. https://doi.org/10.1016/s0016-5085(99)70446-4.

Nancey, S., Holvöet, S., Graber, I., Joubert, G., Philippe, D., Martin, S., Nicolas, J.-F., Desreumaux, P., Flourié, B., and Kaiserlian, D. (2006). CD8+ cytotoxic T cells induce relapsing colitis in normal mice. Gastroenterology *131*, 485-496. https://doi.org/10.1053/j.gastro.2006.05.018.

Nguyen, T.L.A., Vieira-Silva, S., Liston, A., and Raes, J. (2015). How informative is the mouse for human gut microbiota research? Disease models & mechanisms *8*, 1-16. https://doi.org/10.1242/dmm.017400.

Oh, S.Y., Cho, K.-A., Kang, J.L., Kim, K.H., and Woo, S.-Y. (2014). Comparison of experimental mouse models of inflammatory bowel disease. International journal of molecular medicine *33*, 333-340. https://doi.org/10.3892/ijmm.2013.1569.

Okayasu, I., Hatakeyama, S., Yamada, M., Ohkusa, T., Inagaki, Y., and Nakaya, R. (1990). A novel method in the induction of reliable experimental acute and chronic ulcerative colitis in mice. Gastroenterology *98*, 694-702. https://doi.org/10.1016/0016-5085(90)90290-H.

Okumura, R., and Takeda, K. (2017). Roles of intestinal epithelial cells in the maintenance of gut homeostasis. Experimental & molecular medicine *49*, e338. https://doi.org/10.1038/emm.2017.20.

Online presence of ENCODE Consortium. Histone ChIP-seq Data Standards and Processing Pipeline. Target-specific Standards. https://www.encodeproject.org/chip-seq/histone/.

Ordovas-Montanes, J., Beyaz, S., Rakoff-Nahoum, S., and Shalek, A.K. (2020). Distribution and storage of inflammatory memory in barrier tissues. Nature reviews. Immunology *20*, 308-320. https://doi.org/10.1038/s41577-019-0263-z.

Pepke, S., Wold, B., and Mortazavi, A. (2009). Computation for ChIP-seq and RNA-seq studies. Nature methods *6*, S22-32. https://doi.org/10.1038/nmeth.1371.

Piseddu, I., Röhrle, N., Knott, M.M.L., Moder, S., Eiber, S., Schnell, K., Vetter, V., Meyer, B., Layritz, P., and Kühnemuth, B., et al. (2020). Constitutive Expression of CCL22 Is Mediated by T Cell-Derived GM-CSF. Journal of immunology (Baltimore, Md. : 1950) *205*, 2056-2065. https://doi.org/10.4049/jimmunol.2000004.

Ponath, P.D., Qin, S., Ringler, D.J., Clark-Lewis, I., Wang, J., Kassam, N., Smith, H., Shi, X., Gonzalo, J.A., and Newman, W., et al. (1996). Cloning of the human eosinophil chemoattractant, eotaxin. Expression, receptor binding, and functional properties suggest a mechanism for the selective recruitment of eosinophils. The Journal of clinical investigation *97*, 604-612. https://doi.org/10.1172/JCI118456.

Quinlan, A.R., and Hall, I.M. (2010). BEDTools: a flexible suite of utilities for comparing genomic features. Bioinformatics (Oxford, England) *26*, 841-842. https://doi.org/10.1093/bioinformatics/btq033.

R Core Team 2021. R: A language and environment for statistical.

Ramírez, F., Ryan, D.P., Grüning, B., Bhardwaj, V., Kilpert, F., Richter, A.S., Heyne, S., Dündar, F., and Manke, T. (2016). deepTools2: a next generation web server for deep-sequencing data analysis. Nucleic acids research *44*, W160-5. https://doi.org/10.1093/nar/gkw257.

Rapp, M., Wintergerst, M.W.M., Kunz, W.G., Vetter, V.K., Knott, M.M.L., Lisowski, D., Haubner, S., Moder, S., Thaler, R., and Eiber, S., et al. (2019). CCL22 controls immunity by promoting regulatory T cell communication with dendritic cells in lymph nodes. The Journal of experimental medicine *216*, 1170-1181. https://doi.org/10.1084/jem.20170277.

Read, S., Malmström, V., and Powrie, F. (2000). Cytotoxic T lymphocyte-associated antigen 4 plays an essential role in the function of CD25(+)CD4(+) regulatory cells that control intestinal inflammation. The Journal of experimental medicine *192*, 295-302. https://doi.org/10.1084/jem.192.2.295.

Ren, B., Robert, F., Wyrick, J.J., Aparicio, O., Jennings, E.G., Simon, I., Zeitlinger, J., Schreiber, J., Hannett, N., and Kanin, E., et al. (2000). Genome-wide location and function of DNA binding proteins. Science (New York, N.Y.) *290*, 2306-2309. https://doi.org/10.1126/science.290.5500.2306.

Robbins, G.R., Truax, A.D., Davis, B.K., Zhang, L., Brickey, W.J., and Ting, J.P.-Y. (2012). Regulation of class I major histocompatibility complex (MHC) by nucleotide-binding domain, leucine-rich repeat-containing (NLR) proteins. The Journal of biological chemistry *287*, 24294-24303. https://doi.org/10.1074/jbc.M112.364604.

Robertson, G., Hirst, M., Bainbridge, M., Bilenky, M., Zhao, Y., Zeng, T., Euskirchen, G., Bernier, B., Varhol, R., and Delaney, A., et al. (2007). Genome-wide profiles of STAT1 DNA association using chromatin immunoprecipitation and massively parallel sequencing. Nature methods *4*, 651-657. https://doi.org/10.1038/nmeth1068.

Robinson, M.D., McCarthy, D.J., and Smyth, G.K. (2010). edgeR: a Bioconductor package for differential expression analysis of digital gene expression data. Bioinformatics (Oxford, England) *26*, 139-140. https://doi.org/10.1093/bioinformatics/btp616.

Roche, P.A., and Cresswell, P. (1991). Proteolysis of the class II-associated invariant chain generates a peptide binding site in intracellular HLA-DR molecules. Proceedings of the National Academy of Sciences of the United States of America *88*, 3150-3154. https://doi.org/10.1073/pnas.88.8.3150.

Roche, P.A., Marks, M.S., and Cresswell, P. (1991). Formation of a nine-subunit complex by HLA class II glycoproteins and the invariant chain. Nature *354*, 392-394. https://doi.org/10.1038/354392a0.

Rogler, G. (2004). Update in inflammatory bowel disease pathogenesis. Current opinion in gastroenterology *20*, 311-317. https://doi.org/10.1097/00001574-200407000-00003.

Rosales, C., Demaurex, N., Lowell, C.A., and Uribe-Querol, E. (2016). Neutrophils: Their Role in Innate and Adaptive Immunity. Journal of immunology research *2016*, 1469780. https://doi.org/10.1155/2016/1469780.

Ross-Innes, C.S., Stark, R., Teschendorff, A.E., Holmes, K.A., Ali, H.R., Dunning, M.J., Brown, G.D., Gojis, O., Ellis, I.O., and Green, A.R., et al. (2012). Differential oestrogen receptor binding is associated with clinical outcome in breast cancer. Nature *481*, 389-393. https://doi.org/10.1038/nature10730.

Rothenberg, M.E., Nusse, Y., Kalisky, T., Lee, J.J., Dalerba, P., Scheeren, F., Lobo, N., Kulkarni, S., Sim, S., and Qian, D., et al. (2012). Identification of a cKit(+) colonic crypt base secretory cell that supports Lgr5(+) stem cells in mice. Gastroenterology *142*, 1195-1205.e6. https://doi.org/10.1053/j.gastro.2012.02.006.

Rothenberg, M.E., Ownbey, R., Mehlhop, P.D., Loiselle, P.M., van de Rijn, M., Bonventre, J.V., Oettgen, H.C., Leder, P., and Luster, A.D. (1996). Eotaxin triggers eosinophil-selective chemotaxis and calcium flux via a distinct receptor and induces pulmonary eosinophilia in the presence of interleukin 5 in mice. Molecular Medicine *2*, 334-348.

Round, J.L., and Mazmanian, S.K. (2010). Inducible Foxp3+ regulatory T-cell development by a commensal bacterium of the intestinal microbiota. Proceedings of the National Academy of Sciences of the United States of America *107*, 12204-12209. https://doi.org/10.1073/pnas.0909122107.

Rubin, D.C., Shaker, A., and Levin, M.S. (2012). Chronic intestinal inflammation: inflammatory bowel disease and colitis-associated colon cancer. Frontiers in immunology *3*, 107. https://doi.org/10.3389/fimmu.2012.00107.

Sæterstad, S., Østvik, A.E., Røyset, E.S., Bakke, I., Sandvik, A.K., and van Granlund, A.B. (2022). Profound gene expression changes in the epithelial monolayer of active ulcerative colitis and Crohn's disease. PloS one *17*, e0265189. https://doi.org/10.1371/journal.pone.0265189.

Sakaguchi, S., Sakaguchi, N., Asano, M., Itoh, M., and Toda, M. (1995). Immunologic self-tolerance maintained by activated T cells expressing IL-2 receptor alpha-chains (CD25). Breakdown of a single mechanism of self-tolerance causes various autoimmune diseases. Journal of immunology (Baltimore, Md. : 1950) *155*, 1151-1164.

Sanderson, I.R., Ouellette, A.J., Carter, E.A., Walker, W.A., and Harmatz, P.R. (1993). Differential regulation of B7 mRNA in enterocytes and lymphoid cells. Immunology *79*, 434-438.

Santos-Rosa, H., Schneider, R., Bannister, A.J., Sherriff, J., Bernstein, B.E., Emre, N.C.T., Schreiber, S.L., Mellor, J., and Kouzarides, T. (2002). Active genes are tri-methylated at K4 of histone H3. Nature *419*, 407-411. https://doi.org/10.1038/nature01080.

Sato, T., van Es, J.H., Snippert, H.J., Stange, D.E., Vries, R.G., van den Born, M., Barker, N., Shroyer, N.F., van de Wetering, M., and Clevers, H. (2011). Paneth cells constitute the niche for Lgr5 stem cells in intestinal crypts. Nature *469*, 415-418. https://doi.org/10.1038/nature09637.

Schewe, M., Franken, P.F., Sacchetti, A., Schmitt, M., Joosten, R., Böttcher, R., van Royen, M.E., Jeammet, L., Payré, C., and Scott, P.M., et al. (2016). Secreted Phospholipases A2 Are Intestinal Stem Cell Niche Factors with Distinct Roles in Homeostasis, Inflammation, and Cancer. Cell stem cell *19*, 38-51. https://doi.org/10.1016/j.stem.2016.05.023.

Scott, H., Solheim, B.G., Brandtzaeg, P., and Thorsby, E. (1980). HLA-DR-like antigens in the epithelium of the human small intestine. Scandinavian journal of immunology *12*, 77-82. https://doi.org/10.1111/j.1365-3083.1980.tb00043.x.

Selby, W.S., Janossy, G., Mason, D.Y., and Jewell, D.P. (1983). Expression of HLA-DR antigens by colonic epithelium in inflammatory bowel disease. Clinical and experimental immunology *53*, 614-618.

Seo, H., Seong, H., Kim, G.Y., Jo, Y.M., Cheon, S.W., Song, Y., Ryu, B.H., Kang, H., and Han, N.S. (2021). Development of Anti-inflammatory Probiotic Limosilactobacillus reuteri EFEL6901 as Kimchi Starter: in vitro and In vivo Evidence. Frontiers in microbiology *12*, 760476. https://doi.org/10.3389/fmicb.2021.760476.

Shang, L., Liu, H., Yu, H., Chen, M., Yang, T., Zeng, X., and Qiao, S. (2021). Core Altered Microorganisms in Colitis Mouse Model: A Comprehensive Time-Point and Fecal Microbiota Transplantation Analysis. Antibiotics (Basel, Switzerland) *10*. https://doi.org/10.3390/antibiotics10060643.

Simon, I., Barnett, J., Hannett, N., Harbison, C.T., Rinaldi, N.J., Volkert, T.L., Wyrick, J.J., Zeitlinger, J., Gifford, D.K., and Jaakkola, T.S., et al. (2001). Serial Regulation of Transcriptional Regulators in the Yeast Cell Cycle. Cell *106*, 697-708. https://doi.org/10.1016/S0092-8674(01)00494-9.

Siri, S., Zhao, Y., Maier, F., Pierce, D.M., and Feng, B. (2020). The Macro- and Micro-Mechanics of the Colon and Rectum I: Experimental Evidence. Bioengineering (Basel, Switzerland) *7*. https://doi.org/10.3390/bioengineering7040130.

Sloan, V.S., Cameron, P., Porter, G., Gammon, M., Amaya, M., Mellins, E., and Zaller, D.M. (1995). Mediation by HLA-DM of dissociation of peptides from HLA-DR. Nature *375*, 802-806. https://doi.org/10.1038/375802a0.

Snippert, H.J. (2016). Colonic Crypts: Safe Haven from Microbial Products. Cell *165*, 1564-1566. https://doi.org/10.1016/j.cell.2016.06.003.

Snoeck, V., Goddeeris, B., and Cox, E. (2005). The role of enterocytes in the intestinal barrier function and antigen uptake. Microbes and infection *7*, 997-1004. https://doi.org/10.1016/j.micinf.2005.04.003.

Spence, P.J., and Green, E.A. (2008). Foxp3+ regulatory T cells promiscuously accept thymic signals critical for their development. Proceedings of the National Academy of Sciences of the United States of America *105*, 973-978. https://doi.org/10.1073/pnas.0709071105.

Stark, R., Brown, G., and 2011 (2011). DiffBind: differential binding analysis of ChIP-Seq peak data. http://bioconductor.org/packages/release/bioc/vignettes/DiffBind/inst/doc/DiffBind.pdf.

Stelter, C., Käppeli, R., König, C., Krah, A., Hardt, W.-D., Stecher, B., and Bumann, D. (2011). Salmonella-induced mucosal lectin RegIIIβ kills competing gut microbiota. PloS one *6*, e20749. https://doi.org/10.1371/journal.pone.0020749.

Sturn, A., Quackenbush, J., and Trajanoski, Z. (2002). Genesis: cluster analysis of microarray data. Bioinformatics (Oxford, England) *18*, 207-208. https://doi.org/10.1093/bioinformatics/18.1.207.

Sun, C.-M., Hall, J.A., Blank, R.B., Bouladoux, N., Oukka, M., Mora, J.R., and Belkaid, Y. (2007). Small intestine lamina propria dendritic cells promote de novo generation of Foxp3 T reg cells via retinoic acid. The Journal of experimental medicine *204*, 1775-1785. https://doi.org/10.1084/jem.20070602.

Sun, M.-C., Zhang, F.-C., Yin, X., Cheng, B.-J., Zhao, C.-H., Wang, Y.-L., Zhang, Z.-Z., Hao, H.-W., Zhang, T.-H., and Ye, H.-Q. (2018). Lactobacillus reuteri F-9-35 Prevents DSS-Induced Colitis by Inhibiting Proinflammatory Gene Expression and Restoring the Gut Microbiota in Mice. Journal of food science *83*, 2645-2652. https://doi.org/10.1111/1750-3841.14326.

Takamatsu, M., Hirata, A., Ohtaki, H., Hoshi, M., Hatano, Y., Tomita, H., Kuno, T., Saito, K., and Hara, A. (2013). IDO1 plays an immunosuppressive role in 2,4,6-trinitrobenzene sulfate-induced colitis in mice. Journal of immunology (Baltimore, Md. : 1950) *191*, 3057-3064. https://doi.org/10.4049/jimmunol.1203306.

Takeshima, H., Ikegami, D., Wakabayashi, M., Niwa, T., Kim, Y.-J., and Ushijima, T. (2012). Induction of aberrant trimethylation of histone H3 lysine 27 by inflammation in mouse colonic epithelial cells. Carcinogenesis *33*, 2384-2390. https://doi.org/10.1093/carcin/bgs294.

Thankam, F.G., Boosani, C.S., Dilisio, M.F., and Agrawal, D.K. (2019). Epigenetic mechanisms and implications in tendon inflammation (Review). International journal of molecular medicine 43, 3-14. https://doi.org/10.3892/ijmm.2018.3961.

Thelemann, C., Eren, R.O., Coutaz, M., Brasseit, J., Bouzourene, H., Rosa, M., Duval, A., Lavanchy, C., Mack, V., and Mueller, C., et al. (2014). Interferon-γ induces expression of MHC class II on intestinal epithelial cells and protects mice from colitis. PloS one *9*, e86844. https://doi.org/10.1371/journal.pone.0086844.

Thia, K.T., Loftus, E.V., JR, Sandborn, W.J., and Yang, S.-K. (2008). An Update on the Epidemiology of Inflammatory Bowel Disease in Asia. Official journal of the American College of Gastroenterology | ACG *103*.

Thornton, A.M., Korty, P.E., Tran, D.Q., Wohlfert, E.A., Murray, P.E., Belkaid, Y., and Shevach, E.M. (2010). Expression of Helios, an Ikaros transcription factor family member, differentiates thymic-derived from peripherally induced Foxp3+ T regulatory cells. Journal of immunology (Baltimore, Md. : 1950) *184*, 3433-3441. https://doi.org/10.4049/jimmunol.0904028.

Tian, B., Yuan, Y., Yang, Y., Luo, Z., Sui, B., Zhou, M., Fu, Z.F., and Zhao, L. (2020). Interferon-Inducible GTPase 1 Impedes the Dimerization of Rabies Virus Phosphoprotein and Restricts Viral Replication. Journal of virology *94*. https://doi.org/10.1128/JVI.01203-20.

Turgeon, N., Blais, M., Gagné, J.-M., Tardif, V., Boudreau, F., Perreault, N., and Asselin, C. (2013). HDAC1 and HDAC2 restrain the intestinal inflammatory response by regulating intestinal epithelial cell differentiation. PloS one *8*, e73785. https://doi.org/10.1371/journal.pone.0073785.

Turgeon, N., Gagné, J.M., Blais, M., Gendron, F.-P., Boudreau, F., and Asselin, C. (2014). The acetylome regulators Hdac1 and Hdac2 differently modulate intestinal epithelial cell dependent homeostatic responses in experimental colitis. American journal of physiology. Gastrointestinal and liver physiology *306*, G594-605. https://doi.org/10.1152/ajpgi.00393.2013.

Turner, J.R. (2009). Intestinal mucosal barrier function in health and disease. Nature reviews. Immunology *9*, 799-809. https://doi.org/10.1038/nri2653.

Uhlig, H.H., Coombes, J., Mottet, C., Izcue, A., Thompson, C., Fanger, A., Tannapfel, A., Fontenot, J.D., Ramsdell, F., and Powrie, F. (2006). Characterization of Foxp3+CD4+CD25+ and IL-10-secreting CD4+CD25+ T cells during cure of colitis. Journal of immunology (Baltimore, Md. : 1950) *177*, 5852-5860. https://doi.org/10.4049/jimmunol.177.9.5852.

van der Merwe, P.A., Bodian, D.L., Daenke, S., Linsley, P., and Davis, S.J. (1997). CD80 (B7-1) binds both CD28 and CTLA-4 with a low affinity and very fast kinetics. The Journal of experimental medicine *185*, 393-403. https://doi.org/10.1084/jem.185.3.393.

van Kooten, C., and Banchereau, J. (2000). CD40-CD40 ligand. Journal of leukocyte biology *67*, 2-17. https://doi.org/10.1002/jlb.67.1.2.

Vancamelbeke, M., and Vermeire, S. (2017). The intestinal barrier: a fundamental role in health and disease. Expert review of gastroenterology & hepatology *11*, 821-834. https://doi.org/10.1080/17474124.2017.1343143.

Varol, C., Zigmond, E., and Jung, S. (2010). Securing the immune tightrope: mononuclear phagocytes in the intestinal lamina propria. Nature reviews. Immunology *10*, 415-426. https://doi.org/10.1038/nri2778.

Vieira, P.L., Christensen, J.R., Minaee, S., O'Neill, E.J., Barrat, F.J., Boonstra, A., Barthlott, T., Stockinger, B., Wraith, D.C., and O'Garra, A. (2004). IL-10-secreting regulatory T cells do not express Foxp3 but have comparable regulatory function to naturally occurring CD4+CD25+ regulatory T cells. Journal of immunology (Baltimore, Md. : 1950) *172*, 5986-5993. https://doi.org/10.4049/jimmunol.172.10.5986.

Vind, I., Riis, L., Jess, T., Knudsen, E., Pedersen, N., Elkjaer, M., Bak Andersen, I., Wewer, V., Nørregaard, P., and Moesgaard, F., et al. (2006). Increasing incidences of inflammatory bowel disease and decreasing surgery rates in Copenhagen City and County, 2003-2005: a population-based study from the Danish Crohn colitis database. The American journal of gastroenterology *101*, 1274-1282. https://doi.org/10.1111/j.1572-0241.2006.00552.x.

Wang, L., Ray, A., Jiang, X., Wang, J.-y., Basu, S., Liu, X., Qian, T., He, R., Dittel, B.N., and Chu, Y. (2015). T regulatory cells and B cells cooperate to form a regulatory loop that maintains gut homeostasis and suppresses dextran sulfate sodium-induced colitis. Mucosal immunology *8*, 1297-1312. https://doi.org/10.1038/mi.2015.20.

Wang, Q., Garrity, G.M., Tiedje, J.M., and Cole, J.R. (2007). Naive Bayesian classifier for rapid assignment of rRNA sequences into the new bacterial taxonomy. Applied and environmental microbiology *73*, 5261-5267. https://doi.org/10.1128/AEM.00062-07.

Weinhold, B. (2006). Epigenetics: the science of change. Environmental health perspectives *114*, A160-7. https://doi.org/10.1289/ehp.114-a160.

Weiss, J.M., Bilate, A.M., Gobert, M., Ding, Y., Curotto de Lafaille, M.A., Parkhurst, C.N., Xiong, H., Dolpady, J., Frey, A.B., and Ruocco, M.G., et al. (2012). Neuropilin 1 is expressed on thymus-derived natural regulatory T cells, but not mucosa-generated induced Foxp3+ T reg cells. The Journal of experimental medicine *209*, 1723-42, S1. https://doi.org/10.1084/jem.20120914.

Wen, L., Ley, R.E., Volchkov, P.Y., Stranges, P.B., Avanesyan, L., Stonebraker, A.C., Hu, C., Wong, F.S., Szot, G.L., and Bluestone, J.A., et al. (2008). Innate immunity and intestinal microbiota in the development of Type 1 diabetes. Nature *455*, 1109-1113. https://doi.org/10.1038/nature07336.

Wéra, O., Lancellotti, P., and Oury, C. (2016). The Dual Role of Neutrophils in Inflammatory Bowel Diseases. Journal of clinical medicine *5*. https://doi.org/10.3390/jcm5120118.

Westendorf, A.M., Fleissner, D., Deppenmeier, S., Gruber, A.D., Bruder, D., Hansen, W., Liblau, R., and Buer, J. (2006). Autoimmune-mediated intestinal inflammation-impact and regulation of antigen-specific CD8+ T cells. Gastroenterology *131*, 510-524. https://doi.org/10.1053/j.gastro.2006.05.015.

Westendorf, A.M., Fleissner, D., Groebe, L., Jung, S., Gruber, A.D., Hansen, W., and Buer, J. (2009). CD4+Foxp3+ regulatory T cell expansion induced by antigen-driven interaction with intestinal epithelial cells independent of local dendritic cells. Gut *58*, 211-219. https://doi.org/10.1136/gut.2008.151720.

Wirtz, S., Popp, V., Kindermann, M., Gerlach, K., Weigmann, B., Fichtner-Feigl, S., and Neurath, M.F. (2017). Chemically induced mouse models of acute and chronic intestinal inflammation. Nature protocols *12*, 1295-1309. https://doi.org/10.1038/nprot.2017.044.

Wu, F., Zhang, S., Dassopoulos, T., Harris, M.L., Bayless, T.M., Meltzer, S.J., Brant, S.R., and Kwon, J.H. (2010). Identification of microRNAs associated with ileal and colonic Crohn's disease. Inflammatory bowel diseases *16*, 1729-1738. https://doi.org/10.1002/ibd.21267.

Xu, H.-M., Huang, H.-L., Liu, Y.-D., Zhu, J.-Q., Zhou, Y.-L., Chen, H.-T., Xu, J., Zhao, H.-L., Guo, X., and Shi, W., et al. (2021). Selection strategy of dextran sulfate sodium-induced acute or chronic colitis mouse models based on gut microbial profile. BMC microbiology *21*, 279. https://doi.org/10.1186/s12866-021-02342-8.

Xu, Y., Zhang, S., Lin, S., Guo, Y., Deng, W., Zhang, Y., and Xue, Y. (2017). WERAM: a database of writers, erasers and readers of histone acetylation and methylation in eukaryotes. Nucleic acids research *45*, D264-D270. https://doi.org/10.1093/nar/gkw1011.

Yadav, M., Louvet, C., Davini, D., Gardner, J.M., Martinez-Llordella, M., Bailey-Bucktrout, S., Anthony, B.A., Sverdrup, F.M., Head, R., and Kuster, D.J., et al. (2012). Neuropilin-1 distinguishes natural and inducible regulatory T cells among regulatory T cell subsets in vivo. The Journal of experimental medicine *209*, 1713-22, S1-19. https://doi.org/10.1084/jem.20120822.

Yang, F., Wang, D., Li, Y., Sang, L., Zhu, J., Wang, J., Wei, B., Lu, C., and Sun, X. (2017). Th1/Th2 Balance and Th17/Treg-Mediated Immunity in relation to Murine Resistance to Dextran Sulfate-Induced Colitis. Journal of immunology research *2017*, 7047201. https://doi.org/10.1155/2017/7047201.

Yang, Y., and Wilson, M.J. (2018). Genome-wide analysis of H3K4me3 and H3K27me3 modifications throughout the mouse urogenital ridge at E11.5.

Yu, G., Wang, L.-G., and He, Q.-Y. (2015). ChIPseeker: an R/Bioconductor package for ChIP peak annotation, comparison and visualization. Bioinformatics (Oxford, England) *31*, 2382-2383. https://doi.org/10.1093/bioinformatics/btv145.

Yu, Y.-R.A., O'Koren, E.G., Hotten, D.F., Kan, M.J., Kopin, D., Nelson, E.R., Que, L., and Gunn, M.D. (2016). A Protocol for the Comprehensive Flow Cytometric Analysis of Immune Cells in Normal and Inflamed Murine Non-Lymphoid Tissues. PloS one *11*, e0150606. https://doi.org/10.1371/journal.pone.0150606.

Zerrahn, J., Schaible, U.E., Brinkmann, V., Guhlich, U., and Kaufmann, S.H.E. (2002). The IFN-inducible Golgi- and endoplasmic reticulum- associated 47-kDa GTPase IIGP is transiently expressed during listeriosis. Journal of immunology (Baltimore, Md. : 1950) *168*, 3428-3436. https://doi.org/10.4049/jimmunol.168.7.3428.

Zhang, Y., Liu, T., Meyer, C.A., Eeckhoute, J., Johnson, D.S., Bernstein, B.E., Nusbaum, C., Myers, R.M., Brown, M., and Li, W., et al. (2008). Model-based analysis of ChIP-Seq (MACS). Genome biology *9*, R137. https://doi.org/10.1186/gb-2008-9-9-r137.

Zheng, J., Wittouck, S., Salvetti, E., Franz, C.M.A.P., Harris, H.M.B., Mattarelli, P., O'Toole, P.W., Pot, B., Vandamme, P., and Walter, J., et al. (2020). A taxonomic note on the genus Lactobacillus: Description of 23 novel genera, emended description of the genus Lactobacillus Beijerinck 1901, and union of Lactobacillaceae and Leuconostocaceae. International journal of systematic and evolutionary microbiology *70*, 2782-2858. https://doi.org/10.1099/ijsem.0.004107.

Zheng, Y., Manzotti, C.N., Liu, M., Burke, F., Mead, K.I., and Sansom, D.M. (2004). CD86 and CD80 differentially modulate the suppressive function of human regulatory T cells. Journal of immunology (Baltimore, Md. : 1950) *172*, 2778-2784. https://doi.org/10.4049/jimmunol.172.5.2778.

Zhou, G., Peng, K., Song, Y., Yang, W., Shu, W., Yu, T., Yu, L., Lin, M., Wei, Q., and Chen, C., et al. (2018a). CD177+ neutrophils suppress epithelial cell tumourigenesis in colitis-associated cancer and predict good prognosis in colorectal cancer. Carcinogenesis *39*, 272-282. https://doi.org/10.1093/carcin/bgx142.

Zhou, G., Yu, L., Fang, L., Yang, W., Yu, T., Miao, Y., Chen, M., Wu, K., Chen, F., and Cong, Y., et al. (2018b). CD177+ neutrophils as functionally activated neutrophils negatively regulate IBD. Gut *67*, 1052-1063. https://doi.org/10.1136/gutjnl-2016-313535.

Zhu, L.J. (2013). Integrative analysis of ChIP-chip and ChIP-seq dataset. Methods in molecular biology (Clifton, N.J.) *1067*, 105-124. https://doi.org/10.1007/978-1-62703-607-8_8.

Zhu, L.J., Gazin, C., Lawson, N.D., Pagès, H., Lin, S.M., Lapointe, D.S., and Green, M.R. (2010). ChIPpeakAnno: a Bioconductor package to annotate ChIP-seq and ChIP-chip data. BMC bioinformatics *11*, 237. https://doi.org/10.1186/1471-2105-11-237.

Zhu, L.J., Ou, J., Yu, J., Pages, H., Gazin, C., Lawson, N., Thompson, R., Lin, S., and Green, D. (2017). ChIPpeakAnno (Bioconductor).

7. Appendix

ID	GoTerm	Nr. Genes	% Associated Genes	Term PValue Corrected with Bonferroni step down	Associated Genes Found
GO:0006959	humoral immune response	9	4.83871	6.72E-08	[Ang4, Cxcl2, H2-DMa, Mptx1, Mptx2, Reg3b, Reg3g, Slpi, Tac1]
GO:0016064	immunoglobulin mediated immune response	5	4.2735043	1.87E-04	[Cd74, H2-Ab1, H2-DMa, Mptx1, Mptx2]
GO:0019730	antimicrobial humoral response	6	5.769231	6.94E-06	[Ang4, Cxcl2, Reg3b, Reg3g, Slpi, Tac1]
GO:0019731	antibacterial humoral response	3	5.769231	7.94E-04	[Ang4, Slpi, Tac1]
GO:0019886	antigen processing and presentation of exogenous peptide antigen via MHC class II	6	40	3.40E-11	[Cd74, H2-Aa, H2-Ab1, H2-DMa, H2-DMb1, H2-Eb1]
GO:0035458	cellular response to interferon-beta	3	7.142857	6.29E-04	[Iigp1, Irf1, Irgm2]
GO:0042130	negative regulation of T cell proliferation	3	4.477612	8.39E-04	[H2-Aa, H2-Ab1, Ido1]
GO:0050832	defense response to fungus	3	7.5	9.05E-04	[Ang4, Pla2g5, Tac1]
GO:0050868	negative regulation of T cell activation	5	4.385965	1.89E-04	[Cd74, H2-Aa, H2-Ab1, Ido1, Irf1]
GO:0051085	chaperone cofactor-dependent protein refolding	3	10	4.54E-04	[Cd74, H2-DMa, H2-DMb1]
GO:0051702	biological process involved in interaction with symbiont	4	4.123711	7.34E-04	[Hpn, Mptx1, Mptx2, Reg3g]

Supplementary Table 1: Complete representation of Biological Process GO terms differentially expressed genes.

ID	Term	Nr. Genes	% Associated Genes	Term PValue Corrected with Bonferroni step down	Associated Genes Found
KEGG:04514	Cell adhesion molecules	5	4.2735043	6.46E-05	[H2-Aa, H2-Ab1, H2-DMa, H2-DMb1, H2-Eb1]
KEGG:04612	Antigen processing and presentation	6	10.909091	8.20E-07	[Cd74, H2-Aa, H2-Ab1, H2-DMa, H2-DMb1, H2-Eb1]
KEGG:04640	Hematopoietic cell lineage	5	7.246377	2.92E-05	[H2-Aa, H2-Ab1, H2-DMa, H2-DMb1, H2-Eb1]
KEGG:04658	Th1 and Th2 cell differentiation	5	6.756757	3.44E-05	[H2-Aa, H2-Ab1, H2-DMa, H2-DMb1, H2-Eb1]
KEGG:04659	Th17 cell differentiation	5	5.882353	4.10E-05	[H2-Aa, H2-Ab1, H2-DMa, H2-DMb1, H2-Eb1]
KEGG:04672	Intestinal immune network for IgA production	5	17.857143	7.96E-07	[H2-Aa, H2-Ab1, H2-DMa, H2-DMb1, H2-Eb1]
KEGG:04940	Type I diabetes mellitus	5	13.157895	2.34E-06	[H2-Aa, H2-Ab1, H2-DMa, H2-DMb1, H2-Eb1]
KEGG:05140	Leishmaniasis	6	10.344828	9.47E-07	[H2-Aa, H2-Ab1, H2-DMa, H2-DMb1, H2-Eb1, Nos2]
KEGG:05145	Toxoplasmosis	7	7.216495	9.81E-07	[H2-Aa, H2-Ab1, H2-DMa, H2-DMb1, H2-Eb1, Irgm2, Nos2]
KEGG:05150	Staphylococcus aureus infection	5	6.329114	3.81E-05	[H2-Aa, H2-Ab1, H2-DMa, H2-DMb1, H2-Eb1]
KEGG:05152	Tuberculosis	7	5	6.18E-06	[Cd74, H2-Aa, H2-Ab1, H2-DMa, H2-DMb1, H2-Eb1, Nos2]
KEGG:05310	Asthma	5	38.46154	1.21E-08	[H2-Aa, H2-Ab1, H2-DMa, H2-DMb1, H2-Eb1]
KEGG:05320	Autoimmune thyroid disease	5	14.285714	1.83E-06	[H2-Aa, H2-Ab1, H2-DMa, H2-DMb1, H2-Eb1]
KEGG:05321	Inflammatory bowel disease	5	11.111111	5.03E-06	[H2-Aa, H2-Ab1, H2-DMa, H2-DMb1, H2-Eb1]
KEGG:05322	Systemic lupus erythematosus	5	5.2083335	4.96E-05	[H2-Aa, H2-Ab1, H2-DMa, H2-DMb1, H2-Eb1]
KEGG:05323	Rheumatoid arthritis	6	8.823529	1.83E-06	[Cxcl2, H2-Aa, H2-Ab1, H2-DMa, H2-DMb1, H2-Eb1]
KEGG:05330	Allograft rejection	5	15.625	1.24E-06	[H2-Aa, H2-Ab1, H2-DMa, H2-DMb1, H2-Eb1]
KEGG:05332	Graft-versus-host disease	5	16.129032	1.13E-06	[H2-Aa, H2-Ab1, H2-DMa, H2-DMb1, H2-Eb1]
KEGG:05416	Viral myocarditis	5	9.090909	1.09E-05	[H2-Aa, H2-Ab1, H2-DMa, H2-DMb1, H2-Eb1]

Supplementary Table 2: Complete representation of KEGG terms differentially expressed genes.

Supplementary Figures

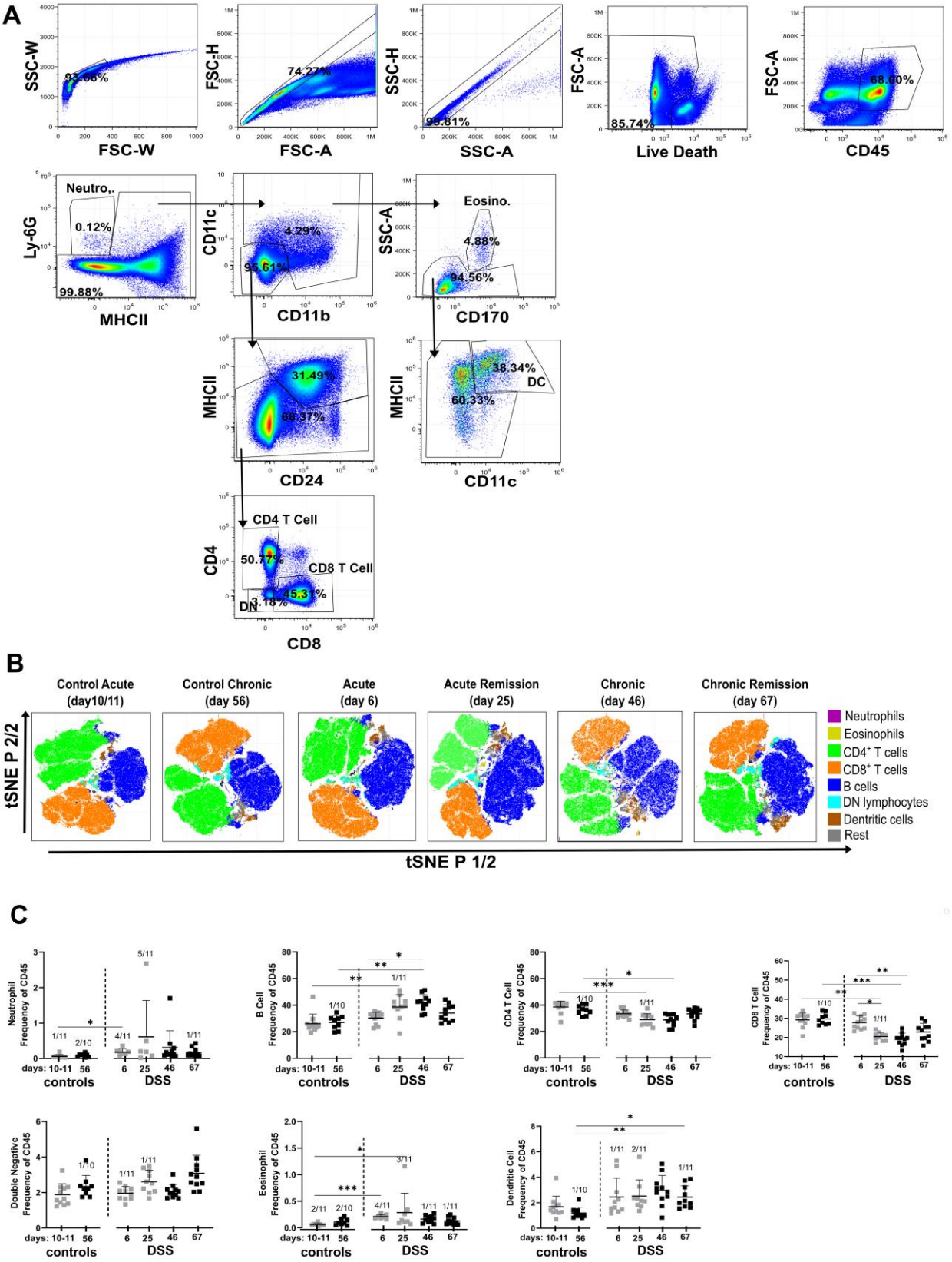

Supplementary Figure 1: Characterization of immune cell subsets in mesenteric lymph nodes during consecutive stages of colitis. DSS colitis and respective remission stages were induced as indicated in the main Figure 15A. At indicated time points, mice were sacrificed, and mesenteric lymph node (MLN) cells were isolated followed by antibody staining and FACS analysis. (A) Gating strategy used to identify the indicated cellular subsets. Cell debris and doublets were eliminated by sequential gating on FSC/SSC parameters (SSC-W vs FSC-W, FSC-H vs FSC-A, SSC-H vs SSC-A). Dead cells were excluded, and live leukocytes were determined by CD45 staining. Neutrophils were identified by Ly6G marker. CD11b and CD11c staining was used to differentiate the remaining myeloid cells from CD11b-CD11c- lymphoid immune cells. B and T lymphocytes subsets were determined by B cell-specific surface markers (MHCII and CD24). Next, CD4+ and CD8+ T cells were further determined by using CD4 and CD8 cell surface markers. Lymphoid cells negative for CD4 and CD8 lineage markers were considered as double negative (DN) lymphoid cells. Eosinophils were distinguished by CD170 marker expression within CD11b and CD11c positive myeloid cells. DCs were identified by MHCII+ and CD11c+ staining within the CD170- cell population. (B) Representative t-SNE plots. Unsupervised clustering of immune cell subsets was performed by t-distributed stochastic neighbor embedding (t-SNE) and clusters were subsequently identified and color-coded based on manual gating. (C) Frequency of indicated immune cell subsets within the CD45+ leukocyte pool. Data were obtained from 2 independent experiments (n = 10 - 11 mice). Grey squares represent control acute (day 10 - 11), acute (day 6) and acute remission (day 25) conditions and black squares represent control chronic (day 56), chronic (day 46) and chronic remission (day 67) groups. Data represent mean with error bars indicating standard deviation. Number of excluded samples is indicated on top of each condition (number of excluded sample/total sample number). Significance was calculated by Kruskal-Wallis test. All groups were compared with each other, significance is indicated only for relevant groups. *** $p < 0.001$, ** $p < 0.01$, * $p < 0.05$. Figure and figure legend have already been published in (Gelmez et al., 2022).

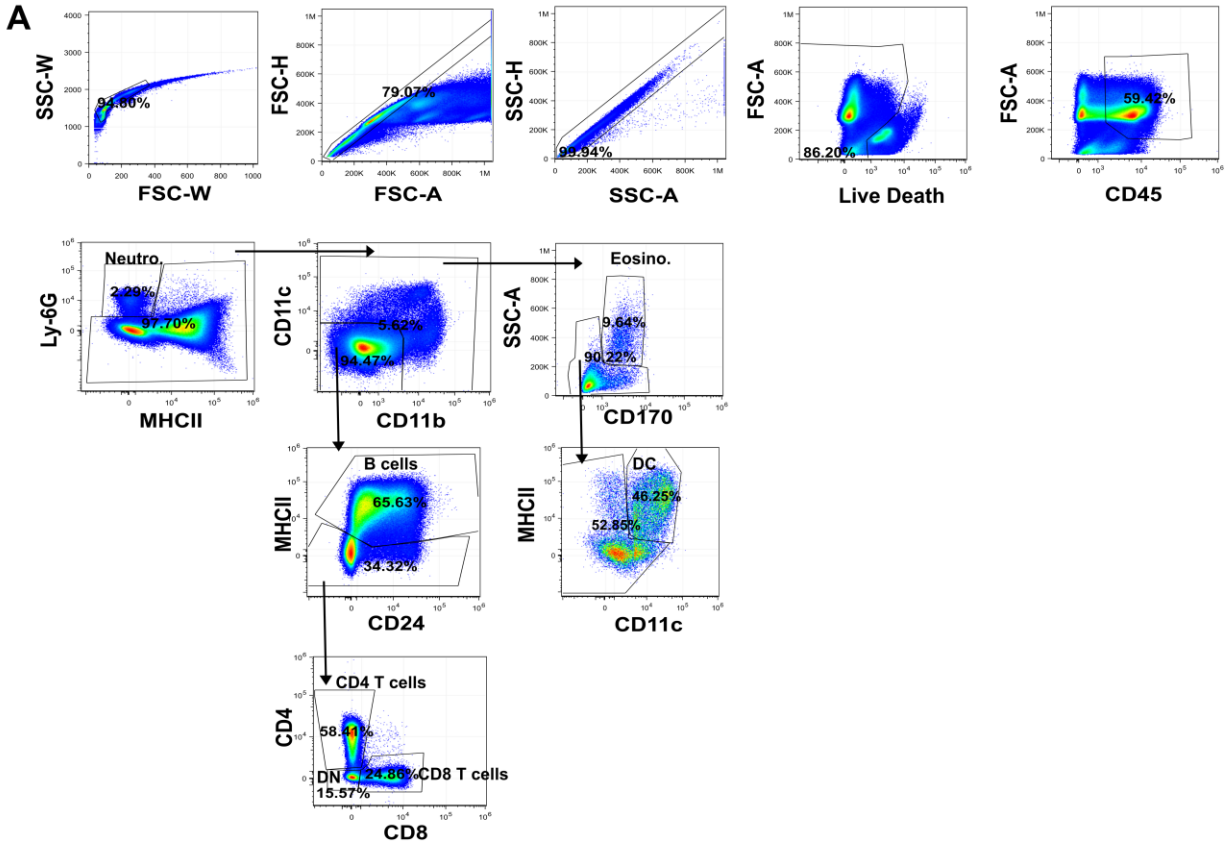
A
SSC-W
FSC-W
94.60%
FSC-H
FSC-A
79.07%
SSC-H
SSC-A
99.94%
FSC-A
Live Death
86.20%
FSC-A
CD45
59.42%
Ly-6G
MHCII
Neutro.
2.29%
97.70%
CD11c
CD11b
5.62%
94.47%
SSC-A
CD170
Eosino.
9.64%
90.22%
MHCII
CD24
B cells
65.63%
34.32%
MHCII
CD11c
DC
46.25%
52.85%
CD4
CD8
CD4 T cells
58.41%
DN
15.57%
24.86%
CD8 T cells

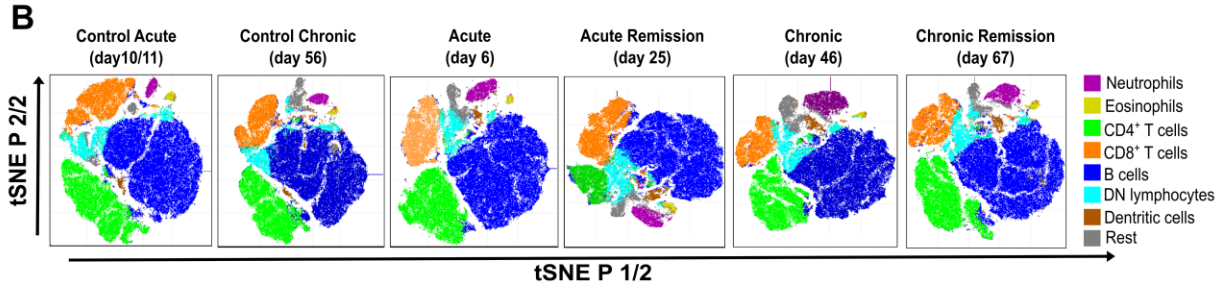
B
Control Acute (day10/11)
Control Chronic (day 56)
Acute (day 6)
Acute Remission (day 25)
Chronic (day 46)
Chronic Remission (day 67)
tSNE P 2/2
tSNE P 1/2
Neutrophils
Eosinophils
CD4+ T cells
CD8+ T cells
B cells
DN lymphocytes
Dentritic cells
Rest

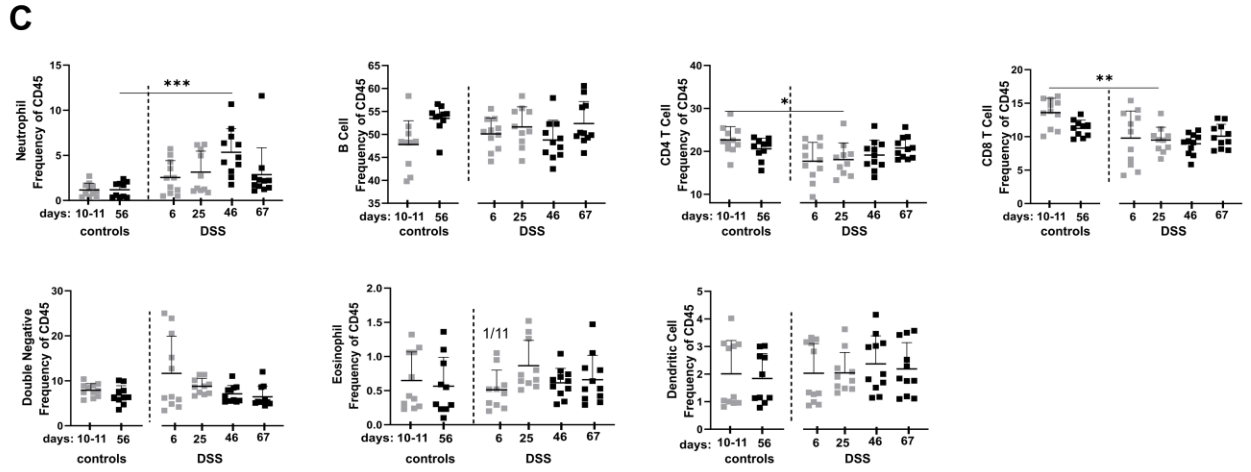
C
Neutrophil Frequency of CD45
B Cell Frequency of CD45
CD4 T Cell Frequency of CD45
CD8 T Cell Frequency of CD45
Double Negative Frequency of CD45
Eosinophil Frequency of CD45
Dendritic Cell Frequency of CD45
days: 10-11 56 6 25 46 67
controls
DSS
***
*
**
1/11

Supplementary Figure 2: Characterization of immune cell subsets in the spleen during consecutive stages of colitis. DSS colitis and respective remission stages were induced as indicated in the main Figure 15A. At indicated time points, mice were sacrificed, and splenocytes were isolated followed by antibody staining and FACS analysis. (A) Gating strategy used to identify the indicated cellular subsets. Cell debris and doublets were eliminated by sequential gating on FSC/SSC parameters (SSC-W vs FSC-W, FSC-H vs FSC-A, SSC-H vs SSC-A). Dead cells were excluded, and live leukocytes were determined by CD45 staining. Neutrophils were identified by Ly6G marker. CD11b and CD11c staining was used to differentiate the remaining myeloid cells from CD11b-CD11c- lymphoid immune cells. B and T lymphocytes subsets were determined by B cell-specific surface markers (MHCII and CD24). Next, CD4+ and CD8+ T cells were further determined by using CD4 and CD8 cell surface markers. Lymphoid cells negative for CD4 and CD8 lineage markers were considered as double negative (DN) lymphoid cells. Eosinophils were distinguished by CD170 marker expression within CD11b and CD11c positive myeloid cells. DCs were identified by MHCII+ and CD11c+ staining within the CD170- cell population. (B) Representative t-SNE plots. Unsupervised clustering of immune cell subsets was performed by t-distributed stochastic neighbor embedding (t-SNE) and clusters were subsequently identified and color-coded based on manual gating. (C) Frequency of indicated immune cell subsets within the CD45+ leukocyte pool. Data were obtained from 2 independent experiments (n = 10 - 11 mice). Grey squares represent control acute (day 10 - 11), acute (day 6) and acute remission (day 25) conditions and black squares represent control chronic (day 56), chronic (day 46) and chronic remission (day 67) groups. Data represent mean with error bars indicating standard deviation. Number of excluded samples is indicated on top of each condition (number of excluded sample/total sample number). Significance was calculated by Kruskal-Wallis test. All groups were compared with each other, significance is indicated only for relevant groups. *** $p < 0.001$, ** $p < 0.01$, * $p < 0.05$. Figure and figure legend have already been published in (Gelmez et al., 2022).

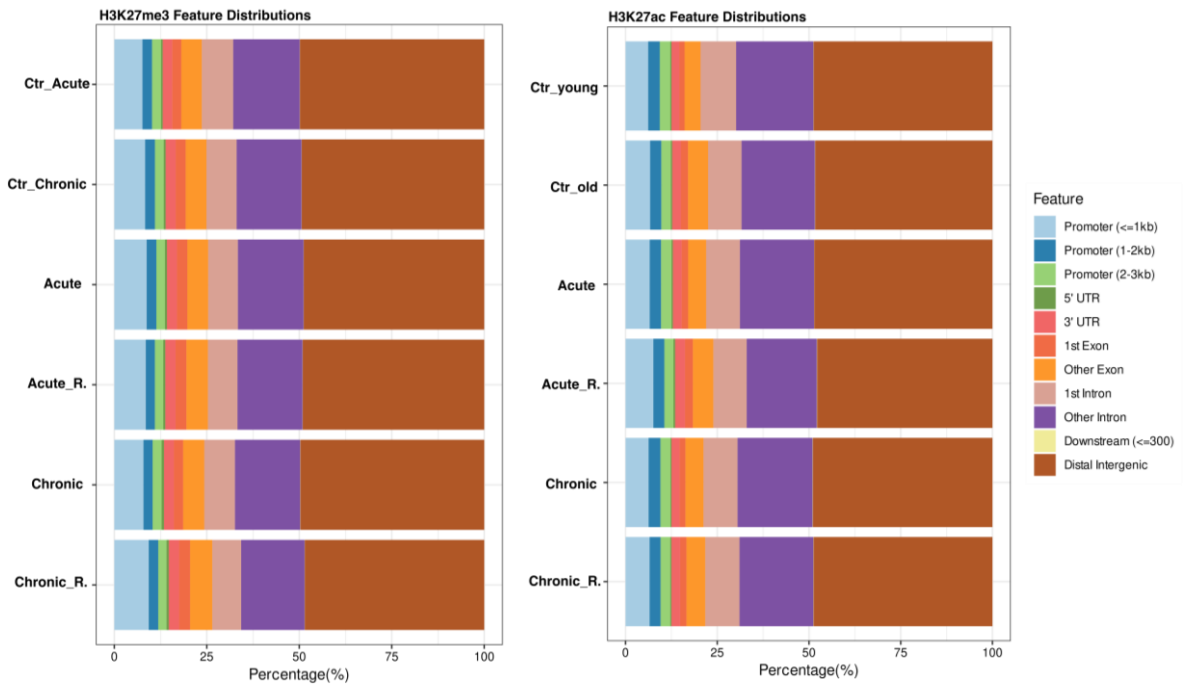

Supplementary Figure 3: ChIP-peak annotation distribution of randomly positioned genomic regions of H3K27me3 and H3K27ac. The high-confidence ChIP regions from all DSS model conditions were positionally permutated using the "ShuffleBed" function within the bedtool library, implemented in the online version of the Galaxy software suite (Gruening (2014), Galaxy wrapper; Quinlan and Hall, 2010). Randomized ChIP-peaks were annotated in terms of genomic features using the ChIPseeker package. Data represent relative abundances of stated genomic features, visualized with ChIPseeker's plotAnnoBar function. Promoter regions were defined as ranging from ±3 kb around TSS. If a ChIP region is adjacent to more than one gene locus the reported annotation only accounts for the closest one, with the following prioritization of genomic annotation: promoter region, 5' UTR, 3' UTR, exon, intron, downstream and intergenic. Ctr_Acute: untreated young mice, Ctr_Chronic: untreated old mice, Acute: one DSS cycle, Chronic: three DSS cycles, Acute_R: acute remission, Chronic_R: chronic remission.

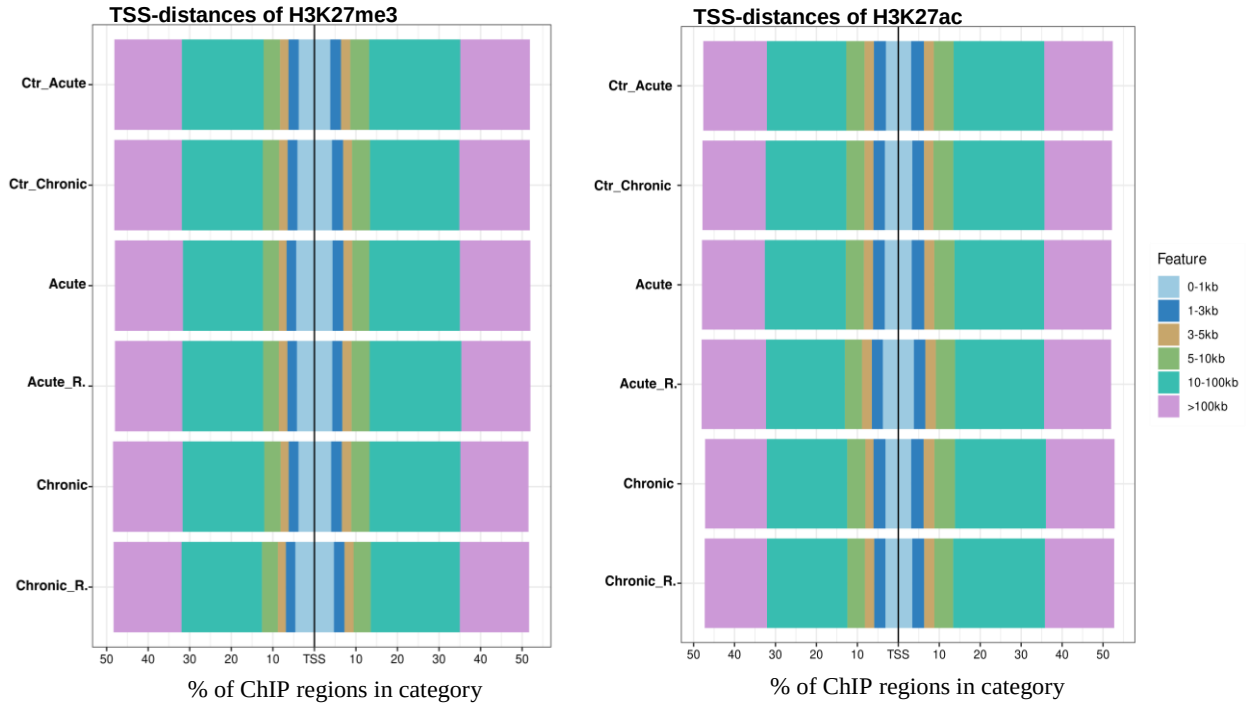

Supplementary Figure 4: Distance to TSS of randomly shuffled H3K27me3 and H3K27ac ChIP-peaks. The high-confidence ChIP regions from all DSS model conditions were positionally permutated using the "ShuffleBed" function within the bedtool library, implemented in the online version of the Galaxy software suite (Gruening (2014), Galaxy wrapper; Quinlan and Hall, 2010). Randomly shuffled ChIP-peak positioning in reference to TSS was analyzed by ChIPseeker's annotatePeak function. For each ChIP-peak only the closest TSS was reported. Distance to TSS was calculated in reference to peak start. Distances were plotted using the plotDistToTSS function. X-axis represents the percentage of ChIP-regions having a TSS-distance falling into one of the stated and color-coded distance categories. Ctr_Acute: untreated young mice, Ctr_Chronic: untreated old mice, Acute: one DSS cycle, Chronic: three DSS cycles, Acute_R: acute remission, Chronic_R: chronic remission.

Declaration of Honour

"I hereby declare that I prepared this thesis without the impermissible help of third parties and that none other than the aids indicated have been used; all sources of information are clearly marked, including my own publications.

In particular I have not consciously:
• fabricated data or rejected undesirable results,
• misused statistical methods with the aim of drawing other conclusions than those warranted by the available data,
• plagiarized external data or publications,
• presented the results of other researchers in a distorted way.

I am aware that violations of copyright may lead to injunction and damage claims by the author and also to prosecution by the law enforcement authorities.
I hereby agree that the thesis may be electronically reviewed with the aim of identifying plagiarism.

This work has not yet been submitted as a doctoral thesis in the same or a similar form in Germany, nor in any other country. It has not yet been published as a whole."

Magdeburg, 25.10.2022